Experimental and Thermodynamic Studies of Upper Mantle Phase Relations

by

Stephan Klemme

A thesis submitted for the degree of
Doctor of Philosophy
of the Australian National University

Canberra
December 1998

Declaration

This thesis contains the results of research done in the Research School of Earth Sciences, Australian National University between July 1995 and December 1998. Except where mentioned in the text or the acknowledgments, the research described in this thesis is my own. No part of this thesis has been submitted to any other University.

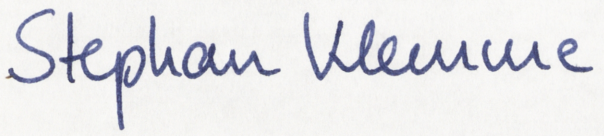

Stephan Klemme
Canberra, December 1998

ABSTRACT

The upper mantle predominantly consists of spinel lherzolite at lower pressures and of garnet lherzolite at higher pressures. The present study investigates the transition from spinel lherzolite to garnet lherzolite in the simple system CaO-MgO-Al_2O_3-SiO_2 (Chapter 1). High-pressure high-temperature experiments were performed at temperatures from 1200°C to 1500°C and pressures from 18 to 26 kb. A second set of reversal experiments were conducted to study the near-solidus solubility of alumina in pyroxenes at 23 kb pressure and temperatures between 1400°C to 1500°C. The transition from spinel to garnet lherzolite at elevated temperatures (T>1200°C) occurs at higher pressures than predicted by a straight extrapolation of previous studies, thus providing further insight in the region in pressure-temperature space relevant for mantle melting.

Although minor elements such as Fe and Cr have substantial effect on the position of the garnet-spinel transition, the overall position of the garnet-spinel lherzolite transition in nature will be significantly higher than previously estimated (e.g. Hirschmann and Stolper 1996). Implications for the genesis of mid-ocean-ridge basalts will be discussed.

Based on the experimental results in conjunction with experimental data from literature, a comprehensive thermodynamic model for subsolidus equilibria in the system CaO-MgO-Al_2O_3-SiO_2 has been developed (Chapter 5). A computer algorithm based on the thermodynamic model utilises free energy minimisation techniques and successfully reproduces the present results as well as data of several other reversal studies.

In the second chapter the thermodynamic properties of $MgCr_2O_4$ were determined by investigating the position of the reaction $MgCr_2O_4 + SiO_2 = MgSiO_3 + Cr_2O_3$ in P-T space. The reaction, which has a small positive slope in P-T space, has been bracketed at 100 K intervals between 1273 and 1773 K by reversal experiments. The reaction is extremely sluggish, and lengthy run times with a flux (H_2O, BaO-B_2O_3 or K_2O-B_2O_3) are needed to produce tight reversal brackets. The experimental results have been combined with literature values of the thermodynamic properties of $MgSiO_3$ (orthoenstatite) and SiO_2 (ß-quartz) from Holland and Powell (1990) and re-evaluated properties of Cr_2O_3 (eskolaite) from Holzheid and O'Neill (1995), to extract the enthalpy of formation and entropy of $MgCr_2O_4$. The results indicate that the existing calorimetrically derived value for the entropy of $MgCr_2O_4$ underestimates the true value

by ~14 J K^{-1} mol^{-1}, probably due to magnetic ordering of the Cr^{3+} ions at temperatures below which the existing low-temperature heat capacity measurements were made.

To investigate this further, the low-temperature heat capacity of $MgCr_2O_4$ was measured at temperatures between 1.5 and 340 K. The measurements indicate a large Cp-anomaly at 12.5 K, interpreted to be due to an antiferromagnetic transition. The entropy at 298.15 K was calculated from the Cp-data and resulted in S_{298} of 118.3 ± 1.2 J $mol^{-1}K^{-1}$ indicating a magnetic contribution to the entropy in the order of 12 J mol^{-1} K^{-1}. The resulting $S°_{298}$ for $MgCr_2O_4$ is in good agreement with the experimental results presented in Chapter 2 ($S°_{298}$ of 119.6 ± 0.9 J $mol^{-1}K^{-1}$ and $\Delta_fH°_{298}$ of -1762 ± 1.4 kJ mol^{-1}), taken into account the new thermochemical data for Cr_2O_3 (c.f. Chapter 3).

The low-temperature heat capacities of Cr_2O_3 and $FeCr_2O_4$ were also measured from 1.5 to 339 K and 2.4 K to 337 K, respectively. For $FeCr_2O_4$, three heat capacity anomalies are observed peaking at 36.5 ± 0.2 K, 68.7 ± 0.2 K and 124.1 ± 0.2 K. The anomalies are interpreted to correspond to a magnetic transition at the Néel temperature T_N = 36.5 ± 0.1 K, to a Curie-Weiss transition at T_{Curie} = 68.7 ± 0.1 K and to a phase transition due to the Jahn-Teller effect at T_D=124.1 ± 0.1 K.

The two Cp-anomalies at higher temperatures have been observed previously by a number of workers, but the Cp-anomaly at 36.5 K had not previously been measured calorimetrically, although the existence of such an anomaly was predicted by Shirane et al. (1964) and Sack and Ghiorso (1991a). Integration of the low-temperature Cp-data results in standard thermodynamic data for the entropy of $FeCr_2O_4$ at 298 K of 152.2 ± 1.5 J mol^{-1} K^{-1}. The estimate of S_{298} for $FeCr_2O_4$ is 6 J mol^{-1} K^{-1} higher than the previously published value of S_{298} = 146.1 ± 1.7 J mol^{-1} K^{-1} (Shomate 1944).

For Cr_2O_3, the measurements show a broad heat capacity anomaly peaking at the Néel temperature about 305.5 K, in good agreement with results of Bruce and Cannell (1977). The present heat capacity data lie considerably below the curve of Volger (1952) and higher than the curve of Anderson (1937). Integration of the low-temperature Cp data yields an entropy at 298.15 K for Cr_2O_3 = 82.8 ± 0.8 J mol^{-1} K^{-1}.

The partitioning of Cr and Al between co-existing spinel and orthopyroxene was investigated in the system MgO-Al_2O_3-SiO_2-Cr_2O_3 (Chapter 4). High-pressure high-temperature experiments were conducted at pressures from 5 to 54 kbar and temperatures between 1300°C and 1500°C. The experiments were conducted in the

spinel stability field only as the solubility of alumina in pyroxenes in equilibrium with spinel and olivine is much larger as in equilibrium with garnet and is, therefore, most sensitive to the influence of Cr. The experiments indicate that the amount of alumina dissolved in orthopyroxene is reduced with increasing Cr content of the system. The reduction of the alumina content of orthopyroxene is a function of temperature and also slightly depends on pressure. The partitioning of Cr and Al between coexisting pyroxenes and spinels, however, is virtually independent of pressure and temperature. Based on the present experiments and on experiments in the Cr-free systems MgO-Al_2O_3-SiO_2, CaO-MgO-Al_2O_3-SiO_2 and Na_2O-CaO-MgO-Al_2O_3-SiO_2, a thermodynamic model for Cr-bearing orthopyroxenes has been developed.

Based on the experimental and thermodynamic data in MASCr and the new thermodynamic properties for $MgCr_2O_4$, a thermodynamic model has been developed that enables calculations of phase equilibria in the system MASCr. Chapter 6 describes the calibration of the model and the argumentation for a solid solution model for binary garnets on the join $Mg_3Al_2Si_3O_{12}$ - $Mg_3Cr_2Si_3O_{12}$. Thermodynamic calculations in the system MASCr have been performed to investigate the transition from spinel to garnet peridotite as a function of the Cr-content of the bulk. Further calculations in MASCr show that the divariant field where garnet and spinel coexist is rather narrow at ratios of $Cr/(Cr+Al)<0.1$, but broadens non-linearly with increasing Cr content of the bulk. The calculations also indicate that present geothermobarometers (e.g. Nickel and Green 1985) may systematically overestimate equilibrium pressures derived from co-existing garnet and orthopyroxene.

ACKNOWLEDGMENTS

I would like to thank my supervisors Dr Hugh StC O'Neill and Professor David H. Green for guidance and support throughout the course of my studies.

Special thanks to the RSES high-pressure team Bill Hibberson, Paul Willis, Alan Major and Dean Scott for the introduction to the mystics of high-pressure experimental work.

Thanks to Martin and Ivana Cmíral, Steve Eggins, John and Sarah Mavrogenes and Andrew Berry for friendship. Also, thanks to my office mates Paul Hoskin, Sergey Matveev, Jörg Hermann and Alistair Hack who coped with my German accent and all the others that have contributed to my well being in Canberra: Uli and Nyssa (+ Georgia) Faul, Uli Troitzsch, Yax, the Delaney's, my housemate Marcel, Rommy, Chris Ballhaus and many more especially the group members of Petrochemistry and Experimental Petrology...

Many thanks also to Malcolm Sambridge and Paul Johnston for their patient help with the computer modelling and Walter Schnelle and Eberhard Gmelin (Max-Planck Institut für Festkörperphysik) for collaboration on the heat capacity measurements in Stuttgart. Thanks to Andrina and Paul Norden for sandwiches and Friday party pies. The present work was carried out under a ANU PhD scholarship. Finally, I would like to thank my parents and Jette Lamberth Nielsen for continuous support and encouragement during the last three years.

INTRODUCTION

0.1 Background

The Earth's upper mantle consists of plagioclase lherzolite at low pressure, spinel lherzolite at medium pressures and garnet lherzolite at high pressures.

Most natural samples of upper mantle material that have been transported to the surface as xenoliths in alkali-basalts and related magmas (basanites, nephelinites) are spinel- lherzolites (e.g. Nickel and Green 1984), although rarely garnet lherzolites (Ionov et al. 1993) also occur. Many of the latter also contain spinel (Ai 1992, Ionov et al. 1993). Garnet lherzolites are commonly found in kimberlites and lamproites, which sample deeper within the Earth's mantle.

The study of mantle xenoliths provide useful information on phase relations and compositions of phases at the pressure and temperature conditions of each individual rock fragment. These xenolitic rocks do not provide *a priori* information on the pressure and temperature of equilibration.

Experiments at high pressure and high temperatures have provided further insight into phase relations of mantle rocks as a function of pressure, temperature and composition. There are, in principle, two ways to investigate upper mantle processes experimentally.

Experiments can be conducted in complex multielement compositions intended to simulate natural compositions. For example, Green and Ringwood (1967) successfully demonstrated the relations between spinel and garnet lherzolite as a function of pressure and temperature. These experiments have the advantage of being close to compositions found in natural lherzolites, there are, however, disadvantages: With a complex chemical composition it is difficult to unravel chemical processes from these experiments that are caused by a particular element. It may also not be possible to extrapolate experimental results to different pressures, temperatures or compositions.

The other approach to experimental petrology consists of experiments in simplified compositions. These experiments have the advantage that the equilibria of interest are simple if not univariant, thus enabling rigorous tests of the attainment of equilibrium in the experiments. Simple system experiments can also be used to extract thermodynamic data for the participating mineral endmember components or information of solid solutions can be obtained. Assuming a good enough understanding of the derived thermodynamic properties of phases in a system, the

information may then, in principle, be used for rigorous extrapolation to different pressures, temperatures, and compositions. On the other hand, this approach has the disadvantage that chemical compositions of simple systems are sometimes too far removed from compositions of natural rocks, thus extrapolation from simple systems to natural rocks has the inherent danger of misinterpretation, especially when elements not present in the simple system, have a substantial effect on phase relations in nature.

This study follows, in principle, the simple system approach. Firstly experiments were conducted investigating the transition from spinel lherzolite to garnet lherzolite in the system CaO-MgO-Al_2O_3-SiO_2 (CMAS). The new experimental results on both the transition (which is univariant in CMAS) and on the solubility of alumina in pyroxenes were used in conjunction with selected data from the literature to develop an internally consistent thermodynamic model for equilibria in the part of CMAS relevant for the upper mantle. The thermodynamic dataset was used as input for a free-computer algorithm based on free energy minimisation techniques which enables calculation of phase equilibria at pressure, temperature and different compositions.

In order to understand the effects of additional components, the complexity of the simple system must then be increased. Consequently, the next chapters of this thesis investigate the influence of Cr on upper mantle phase relations.

Literature research indicated that thermodynamic properties of Cr-bearing spinels (i.e. $MgCr_2O_4$) might be in error, as calorimetric measurements, used to measure the heat capacity of phases and subsequently the entropy of a phase as a function of temperature, could have missed some substantial portion of the entropy of $MgCr_2O_4$ due to phase transitions at very low temperatures.

To investigate the thermodynamic properties of $MgCr_2O_4$, the univariant equilibrium $Cr_2O_3 + MgSiO_3 = MgCr_2O_4 + SiO_2$ was investigated at high pressures and high temperatures. The experimental results were used to extract thermodynamic data for $MgCr_2O_4$, assuming thermodynamic properties of the other three phases were sufficiently well known. Results indicate that, indeed, the previous results in the literature have underestimated the entropy of $MgCr_2O_4$ (at room temperature) by more than 12 J mol^{-1} K^{-1}, which is enough to significantly affect calculated phase relations in a thermodynamic model.

To further constrain the surprisingly large entropy differences between the present experimental results and the literature data, direct heat capacity measurements for $MgCr_2O_4$ and some other Cr-bearing phases were conducted at low temperatures.

These measurements indicate excellent agreement between the present experimental results and the calorimetry, confirming the new thermochemical data for $MgCr_2O_4$.

As a further step to investigate the influence of Cr on phase relations of the upper mantle, the partitioning of Cr and Al between spinels and orthopyroxenes was investigated in the system MgO-Al_2O_3-SiO_2-Cr_2O_3. High-pressure high-temperature experiments were conducted at pressures from 5 to 54 kbar and temperatures between 1300°C and 1500°C. Most experiments were conducted in the spinel stability field only as the solubility of alumina in pyroxenes is much larger as in equilibrium with garnet, the effects of Cr on the solubility of alumina in pyroxenes can, therefore be better studied in the spinel stability field. The experiments indicate a strong reduction of dissolved alumina in orthopyroxene with increasing Cr content of the bulk. This reduction depends on temperature and slightly, on pressure. Thermodynamic properties of Cr-bearing orthopyroxenes have been derived from these experiments.

The new thermochemical data for $MgCr_2O_4$ and the information on the thermodynamics of Cr-Al bearing pyroxenes were then used for thermodynamic calculations in Cr-bearing systems. These calculations were used to evaluate the influence of Cr on the transition from spinel to garnet peridotite and the widths of the divariant field where spinel and garnet co-exist. The calculations can also be used to assess the accuracy of geothermobarometers based on the solubility of alumina in orthopyroxene in equilibrium with either spinel or garnet peridotite.

0.2 Remarks on the structure of the thesis

The chapters of this thesis have been structured as separate scientific papers. Chapter 2 has been published, the others are about to be submitted. As a result, repetitions may occur especially in the introductory sections. The references were placed together at the end of the thesis. The most important results are summarised in Conclusions.

Table of Contents

CHAPTER 3.

The heat capacity of $MgCr_2O_4$, $FeCr_2O_4$ and Cr_2O_3 at low temperatures and derived thermodynamic properties

CHAPTER 4.

The partitioning of chromium and aluminium between orthopyroxene and spinel: Experiments and thermodynamics

CHAPTER 5.

Thermodynamic modelling in the system CaO-MgO-Al_2O_3-SiO_2

CHAPTER 1

The near-solidus transition from garnet lherzolite to spinel lherzolite: Experiments in the system $CaO-MgO-Al_2O_3-SiO_2$

1.1 INTRODUCTION

There is evidence that mid-ocean ridge basalts (MORB) are generated in the presence of garnet (Klein and Langmuir 1987, Hirschmann and Stolper 1996), e.g. depletion of heavier rare earth elements relative to lighter rare earth elements (Kay and Gast 1973), depletion in $^{177}Lu/^{176}Hf$ (Salters and Hart 1989) and elevated $^{230}Th/^{238}U$ ratios (Beattie 1993 a, Beattie 1993 b, La Tourette et al. 1993), generally referred to as the 'garnet signature' in MORB. If melting started in the garnet lherzolite stability field, simple melting models (e.g. Klein and Langmuir 1987, McKenzie and Bickle 1988, Iwamori et al. 1995) predict a thickness of the oceanic crust much greater than the average crust measured at 7±1 km by seismological studies (e.g. White et al. 1992).

Several possible solutions have been put forward to resolve this apparent conflict, including reduced melt productivity of upwelling peridotite (Asimov et al. 1995) or variations in depth of melting on the top of the melting zone beneath ridges (Shen and Forsyth 1995) or partial melting of small amounts of garnet assemblages in veins such as garnet pyroxenites or eclogites (among others: Wood 1979, Allègre et al. 1984).

However, in order to model the processes of mantle melting in the case of mid-ocean ridge basalts, reliable data on the exact position of the transition from spinel lherzolite to garnet lherzolite are indispensable.

Several studies have investigated the transition from garnet lherzolite to spinel lherzolite at lower temperatures i.e. from 800°C to 1100°C (e.g. O'Neill 1981, O'Hara et al. 1971, Jenkins and Newton 1979). However, there is only little and, unfortunately, controversial information available for the high temperature part of the univariant reaction close to the solidus, the pressure - temperature range where mid-ocean ridge magmas are likely to be generated.

The approach chosen here is to investigate the transition in a chemical system that contains all relevant mantle phases and closely approximates upper mantle composition.

The system CaO-MgO-Al_2O_3-SiO_2 (CMAS) is an excellent starting point because its composition represents more than 90% of the upper mantle's composition and it contains all major mineral phases olivine, garnet, spinel, orthopyroxene and clinopyroxene. In contrast to experiments in natural, complex compositions, the attainment of equilibrium in simple systems can be rigorously assessed and extraction of thermodynamic data for mineral endmembers is facilitated.

The equilibrium that defines the phase transition from spinel to garnet lherzolite in the system MgO-Al_2O_3-SiO_2 (MAS) may in essence be written as follows:

$2\ Mg_2Si_2O_6$ +	$MgAl_2O_4$ =	Mg_2SiO_4 +	$Mg_3Al_2Si_3O_{12}$
opx	spinel	olivine	garnet

This equilibrium is also univariant in the system CaO-MgO-Al_2O_3-SiO_2 (CMAS) if a calcium-containing phase, here clinopyroxene, is present to buffer the chemical potential of CaO.

The transition from spinel lherzolite to garnet lherzolite in CMAS is shown as the dashed line.

There are, in principle, two ways to investigate the aforementioned univariant equilibrium:

The transition may be investigated directly by performing reversal experiments with starting material containing both reactants and products of a reaction. These starting materials are equilibrated in divariant fields both above or below the univariant reaction. Analysis of coexisting phases with X-ray diffraction or electron microprobe show which phase assemblage is consumed and which is not.

A different approach investigates alumina isopleths in pyroxenes, that is, curves in pressure-temperature space of constant alumina content in orthopyroxene or

clinopyroxene.

The equilibrium that controls the alumina content in equilibrium with garnet (reaction B) has a positive slope in P-T space, whilst the equilibrium controlling the alumina content of pyroxenes in equilibrium with spinel (A) is almost independent of pressure. The position of the transition from garnet lherzolite to spinel lherzolite can be determined indirectly in pressure-temperature space, i.e. where equilibria A and B intersect.

This study investigates the transition of garnet to spinel lherzolite near the solidus using both approaches. The position of the univariant reaction in CMAS was directly reversed and the solubility of Al_2O_3 in pyroxenes near the solidus has been investigated.

The solubility of alumina in orthopyroxene in particular is important for the geothermobarometry of upper mantle rocks. This will be reviewed in the next section.

Pyroxene thermobarometry in the system CaO-MgO-Al_2O_3-SiO_2

Pyroxene compositions are very sensitive to varying pressure-temperature conditions. Thus, mineral assemblages containing orthopyroxene and clinopyroxene are widely used as indicators of pressure and temperature in ultramafic rocks such as in orogenic peridotites and mantle derived xenoliths, much effort has been put into investigation of the phase equilibria involving orthopyroxenes and clinopyroxenes.

The simplest system containing both orthopyroxene and clinopyroxene is the enstatite - diopside join in the system CaO-MgO-SiO_2 (CMS). Since firstly suggested for use for geothermometry by Leon Atlas (1952), numerous experimental studies have shown that the shape of the miscibility gap between enstatite and diopside is mainly a function of temperature and not of pressure. Phase relations and thermodynamic models of the diopside-enstatite system have been reviewed by Lindsley et al. (1981), Nickel and Brey (1984) or Carlson and Lindsley (1988).

Besides, there are equally important subsolidus equilibria important for geothermobarometry in ultramafic rocks that can be described with the following two equations.

$$MgAl_2O_4 + Mg_2Si_2O_6 = MgAl_2SiO_6 + Mg_2SiO_4 \quad (A),$$

$$Mg_3Al_2Si_3O_{12} = Mg_2Si_2O_6 + MgAl_2SiO_6 \quad (B).$$

The Al_2O_3 exchange between orthopyroxene and garnet (B) is sensitive to pressure as well as temperature and is commonly used for geothermobarometry (e.g. Wood and Banno 1973, Brey et al. 1986, Nickel and Green 1985). The exchange of Al_2O_3 between the orthopyroxene solid solution and spinel (A), however, is believed to be mainly sensitive to temperature and has found application in the geothermometry of ultramafic rocks (e.g. Gasparik and Newton 1984, Witt-Eickschen and Seck 1991). The alumina content of orthopyroxene coexisting with olivine and spinel has proven to be almost independent of pressure in the system MgO-Al_2O_3-SiO_2 (MAS) (e.g. Gasparik and Newton 1984, Dankwerth and Newton 1978) as well as in the system CaO-MgO-Al_2O_3-SiO_2 (CMAS) (Obata 1976, Fujii 1977). Gasparik (1984) claimed that the presence of Ca in the CMAS system appears to reduce the amount of Al_2O_3 in orthopyroxene (Gasparik 1984).

The presence of minor components such as Fe, Cr, Na and Ca can have an substantial effect on the subsolidus equilibria (e.g. O'Neill 1981). In order to extrapolate results from simple system experiments to the more complex compositions of natural occurring rocks thermodynamic models are needed to account for the influence of minor components on our results. For instance, the influence of chromium on thermodynamics of pyroxenes has previously been underestimated and will be discussed in subsequent chapters of this thesis.

1.2 EXPERIMENTS

This section gives a detailed description of how 'direct approach' and 'indirect approach' experiments were designed, what starting materials were used, how experimental run products were analysed and how the attainment of equilibration was assessed.

Equilibria in the system CMAS such as the transition from garnet lherzolite to spinel lherzolite are well known for their slow kinetics (O'Neill 1981, Nickel et al. 1985). In order to overcome this problem, lengthy experimental run duration were found to be necessary in our experiments (Table 2). However, conducting high-pressure experiments at high temperatures for many hours or days leads to another problem: Thermocouples that are used for temperature control in the high-pressure high-temperature experiments can drift to lower or higher temperatures due to contamination ("thermocouple poisoning"), or due to element migration within the thermocouple material itself. That has been a particular problem in the past with the usual types of thermocouples used in experimental petrology, namely type S (Pt-$Pt_{90}Rh_{10}$).

In order to prevent thermocouple contamination in the lengthy experiments of this study, care was taken to prepare a 'clean' assembly (c.f. *Experimental Techniques*). Most experiments were conducted with two different thermocouple wires to monitor possible thermocouple drift due to contamination. Details are given in the *'Experimental Techniques'* section.

"Direct Approach" Experiments

To directly investigate the transition from spinel lherzolite to garnet lherzolite, the position of the univariant equilibrium is 'bracketed'. Thus, samples containing both reactants and products of the reaction are equilibrated in divariant fields both above and below the univariant reaction. Analysis of coexisting phases with X-ray and electron microprobe techniques show which phase assembly is consumed and which phases grow.

"Indirect Approach" Experiments

A second series of experiments has been conducted at a pressure of 23 kbar and temperatures between 1400°C and 1500°C, again with rather lengthy run times. Experiments were duplicated with two different starting mixtures: One starting material contained pyroxenes with high Al_2O_3-content (10 wt.% Al_2O_3), the other with only half of the Al_2O_3-content. Equilibrium was, therefore, reversed in terms of the alumina content of the pyroxenes, i.e. approached from different sides.

The information derived from these reversal experiments in the spinel lherzolite stability field is used in conjunction with literature data to determine the position of alumina isopleths of orthopyroxene in pressure-temperature space and, therefore, to indirectly constrain the position of the boundary between garnet lherzolite and spinel lherzolite.

In the thermodynamic section of this thesis (PART II) a thermodynamic model has been developed that reproduces the experimental results presented here as well as results from other experimental studies. This model enables extrapolation and interpolation of experimental results and modelling of the position of the transition from garnet to spinel lherzolite in CMAS.

Starting Materials

All experiments were conducted with mixtures of crystalline starting materials. The choice of crystalline starting material in contrast to glass or gel as starting material circumvents nucleation problems of garnets and spinel and also prevents formation of pyroxenes, unrealistically high in Al_2O_3, known from unreversed synthesis experiments (c.f. Howells and O'Hara 1978 , Nickel et al. 1985).

Starting materials of the 'direct approach' experiments designed to bracket the position of the garnet-spinel boundary contained synthetic mineral mixtures consisting of all five phases, both minerals on the low pressure sides and the high pressure side of the reaction: Thus, the starting material contained olivine, clinopyroxene, orthopyroxene, garnet and spinel.

Starting materials were synthesised from sintered oxide mixes. $MgAl_2O_4$ was synthesised at 1200°C at atmospheric pressure and for 24 hours. Forsterite (Mg_2SiO_4) was synthesised at 1050°C at atmospheric pressure using a Li_2WO_4-flux. With a flux/oxide-mix ratio of 4/1 in a Pt-crucible, forsterite-syntheses were carried out for six days. Aluminous clinopyroxenes and orthopyroxenes were synthesised at 1200°C and

30 kb for 12 hours. These synthesis runs also contained minor amounts of olivine. Mixtures SM 6/9 and 15 are identical.

The "direct approach" experiments contained synthesized garnets with two different compositions: SM 3 consisted of garnets with 20 mol % grossular component and SM 4 garnets with 10 mol % grossular component. Five grams of each garnet for the starting mix were synthesised separately at 1400°C, 30 kb for 24 hours in a large capacity piston-cylinder apparatus at the Research School of Earth Sciences.

TABLE 1 STARTING MATERIAL

wt. %	SM 6/9/15	SM 25	SM 28
MgO	30.7	36.4	39.6
CaO	6.9	5.5	6.2
SiO_2	39.7	36.5	38.1
Al_2O_3	22.7	21.4	16.1

SM 6, SM 9 and SM 15 are of identical composition, consisting of $MgAl_2O_4$ (spinel), Mg_2SiO_4 (forsterite), SM1 (orthopyroxene and clinopyroxene), and two different garnet compositions (SM 3 and SM 4, see text). SM 25 and SM 28 consist of $MgAl_2O_4$, Mg_2SiO_4 and orthopyroxene and clinopyroxenes. Pyroxenes in SM 25 have twice the Al_2O_3 (ca. 10 wt.%) content compared to pyroxenes of SM 28 (ca 5 wt%).

The starting material of the 'near-solidus solubility' (indirect approach) experiments contained pure forsterite and spinel. These experiments also contained both orthopyroxenes and clinopyroxenes. Experiments were duplicated: Once with high alumina starting material orthopyroxenes and clinopyroxenes (SM 25) with approximately 10 % (wt.) Al_2O_3 in both pyroxenes, once with starting material pyroxenes (SM 28) that contained only ~ 5 % (wt.) Al_2O_3. SM 25 and SM 28 were synthesised at 1200°C, 30 kbar in a piston-cylinder apparatus. All starting materials were checked for composition and homogeneity with the electron microprobe (Ware 1991) and with X-ray diffraction techniques.

Attainment of equilibrium in the experiments

There are several lines of evidence for the attainment of equilibrium in the present experiments. Firstly, low standard deviations in mineral analyses indicate homogenous phase compositions providing evidence for chemical equilibration and also suggests that temperature gradients in the experimental charges were negligible. Secondly, two different garnet compositions were chosen as starting materials in the "direct approach" experiments, i.e. garnets with low and high contents of grossular component, respectively. Homogenous garnet compositions throughout the charge were taken as evidence that garnets reached equilibrium in the experiment. Equilibrium in the 'indirect approach' experiments is reversed in terms of the alumina content of the pyroxenes as explained above.

In order to obtain further evidence for the attainment of equilibrium in the run products we make use of Fick's second law, $h = \sqrt{D \cdot t}$ (Spear, 1993), where D is the diffusion coefficient at P and T, h the radius of the analysed mineral in an experimental charge and t the time. Assuming a diffusion coefficient D for Al diffusion in pyroxene of ca. 10^{-16} m^2/s needed to homogenise a crystal of 10 μm at 1400°C (Sautter et al. 1988), the equilibration time can be estimated to be in the order of a few days.

Experimental techniques

High-pressure, high-temperature experiments were carried out in a conventional piston-cylinder apparatus (Boyd and England 1960) using a 1/2″ diameter assembly. The assembly consists of two inner parts of MgO (66% density) surrounded by three concentric shells: a graphite heater, a glass tube (Pyrex) and an outermost sleeve of NaCl, pressed to >95% of the theoretical density. This low-friction assembly is thought not to require a pressure correction and pressures can therefore be controlled more accurately than in talc-pyrex assemblies (Green et al. 1966). High temperatures and long run durations should also ensure that any initial friction decays (Bose and Ganguly 1995). Starting materials were sealed in platinum capsules which were insulated from the graphite heater by a small Al_2O_3 sleeve and separated from the thermocouple tip by a 0.5 mm Al_2O_3 disc.

All experiments were performed using the 'piston-out' method, where the pressure was first raised to a few kilobars, then the temperature increased to ca. 450°C

to soften the pyrex, later the pressure was increased up to ca. 0.5 kbar higher than the desired pressure, the temperature increased to the nominal temperature of the run and the pressure lowered to the required pressure.

As a check on pressure calibration, the position of the univariant reaction $Fe_2SiO_4 + SiO_2 = 2\ FeSiO_3$ was reversed, as described in more detail in Chapter 2.

Temperatures were measured with $Pt_{94}Rh_6$-$Pt_{70}Rh_{30}$ thermocouples (type B) inserted axially into the assembly inside two- or four-bore high purity Al_2O_3 tubing. Type B thermocouples are much more resistant to contamination at high temperature than the more commonly used Pt-$Pt_{90}Rh_{10}$ (Type S) or Pt-$Pt_{87}Rh_{13}$ (Type R) thermocouples, although they are somewhat less sensitive. Nevertheless, because thermocouple drift due to contamination is always a potential hazard in piston-cylinder experiments at high temperatures (Holloway and Wood 1988), temperatures in some runs (particularly the higher temperature ones) were additionally monitored with a second thermocouple of $W_{75}Re_{25}$-$W_{97}Re_3$ (type C), using four-holed high purity Al_2O_3 thermocouple tubing. Temperatures as measured by the two thermocouples differed only by a maximum of 10°C. The sample was placed in the hot spot of the assembly which as found in previous calibrations in this laboratory (W.O. Hibberson, pers. comm.). This assembly has also previously been tested for temperature against the melting point of gold (cf Mirwald and Kennedy 1979). Possible pressure effects on the emf of thermocouple pairs was neglected. The temperature uncertainties are estimated to be less than ±10 °C at lower temperatures, increasing to about ±15 °C at 1500°C.

In order to minimise contamination of thermocouples in the lengthy runs it was found necessary to use high purity inner components in the run assemblies. In this study inner parts of the pressure assembly consisted of high purity Al_2O_3 thermocouple sleeves, believed to be superior to mullite sleeves because they reduce the possibility of thermocouple contamination (W.O. Hibberson, personal communication).

Analytical Techniques

Each experimental run product was cut with a diamond saw, one half of the capsule was mounted in epoxy and polished using a series of diamond pastes and a finish of 0.3 μm Al_2O_3 polishing powder (Linde B). Run products were carbon coated and analysed on a Cameca "Microbeam" electron microprobe at RSES, ANU and on a

JEOL 6400 scanning electron microprobe (SEM) in energy dispersive mode (EDS) at the Electron Microprobe Unit (EMU) at ANU. Analyses were performed using the quantitative mode. Accelerating voltage was 15 keV, ZAF correction was applied in all analyses (Ware, 1991). Starting material composition were also analysed using powder X-ray techniques. Standard materials for electron microprobe analyses were natural diopside, garnet and spinel as well as synthetic corundum crystals. Standards were analysed both with the SEM-EDS as well with the electron microprobe (EDS and WDS). Analytical results obtained with both techniques agree well with each other.

1.3 EXPERIMENTAL RESULTS

This study investigates the transition from garnet lherzolite to spinel lherzolite in the system CMAS. Table 2 compiles experimental conditions, start material information and results. Analytical results are presented in the end of this chapter (Table 3 - Analytical results). The direct approach experiments are listed on top of the table, followed by the indirect approach experiments.

TABLE 2 start materials, run conditions, results

run #	starting material	T [°C]	P [kbar]	duration [h]	phases present
C234-S 23	SM 9	1200	18	120	fo opx cpx spi, minor gnt
C276-S 29	SM 15	1200	20	360	fo opx cpx gnt, minor spi
C163-S 10	SM 6	1400	23	72	fo opx cpx spi, minor gnt
C246-S 26	SM 15	1400	24	72	fo opx cpx spi, minor gar
C231-S 21	SM 15	1400	25	72	fo opx cpx gnt, minor spi
C191-S 14	SM 9	1400	27	144	fo opx cpx gnt, minor spi
C418-S 75	SM 15	1475	25	48	opx spi & gnt
C332-S 54	SM 15	1500	27	24	fo opx cpx gnt, trace spi
C278-S 30	SM 9	1500	26	15	fo opx cpx spi, minor gnt
C470-S 89	SM 25	1400	23	44	fo opx cpx spi
C467-S 87	SM 25	1450	23	24	fo opx cpx spi
C468-S 88	SM 25	1475	23	24	fo opx spi quench
C473-S 90	SM 25	1500	23	12	fo spi quench
C478-S 92	SM 28	1400	23	44	fo opx cpx spi
C485-S 94	SM 28	1425	23	48	fo opx cpx spi
C483-S 93	SM 28	1450	23	24	fo opx cpx spi
C488-S 95	SM 28	1475	23	24	fo opx cpx spi
C477-S 91	SM 28	1500	23	12	opx spi quench

Abbreviations: T = temperature in [°C], P = pressure in [kb]. spi = spinel, cpx = clinopyroxene, opx = orthopyroxene, fo = forsterite, gnt = garnet, quench = melt. Starting material mixtures are explained in the text. Experiments C468-S 88, C473-S 90 and C477-S 91 contained partial melt. However, the position of the dry solidus as inferred by Walter and Presnall (1994) in a Na-bearing system (NCMAS) and by Gudfinnsson and Presnall (1996) in CMAS are in good agreement with results from this study.

1.4 COMPARISON WITH PREVIOUS STUDIES AND DISCUSSION

This section will briefly review experimental results from the literature, then compare new experimental results from the present study with literature data.

The transition form garnet lherzolite to spinel lherzolite was first investigated in CMAS by MacGregor (1965) in the temperature range from 1100°C to 1500°C. A similar study by Kushiro and Yoder (1966) (1175°C-1500°C) yielded only slightly differing results, probably due to the pressure correction applied. Both MacGregor (1965) and Kushiro and Yoder (1966) proposed a straight line of the univariant reaction in P-T space, in contrast to subsequent work. Detailed studies by Jenkins and Newton (1979) and O'Neill (1981) found in well reversed experiments a strong curvature below temperatures of 1300°C, resulting in a slope of the reaction that was nearly parallel to the temperature axis. That had the consequence that garnet lherzolite could never be stable at crustal pressures (c.f. O'Neill 1981). Patera (1982) presents a reversal at 1200°C and between 17 and 18.7 kb, corrected for the rigid talc-pyrex assembly used (as cited in Wood and Holloway 1984).

However, the information on the high-temperature part of the univariant reaction in CMAS is much less abundant and, unfortunately, controversial. MacGregor (1965) and O'Hara et al. (1971) performed bracketing experiments but microprobe analyses of the experimental charges were not possible so that the attainment of equilibrium could not be assessed. Kushiro and Yoder (1966) determined approximate stability fields of spinel and garnet lherzolite, respectively, but their experiments remained unreversed. Besides, uncertain pressure corrections in the different solid-media pressure devices further complicated inter-laboratory comparison of early experimental results (Koziol and Newton 1988).

The only experimental datum on the transition from spinel lherzolite to garnet lherzolite in the CMAS system at temperatures higher than 1200°C which is both reversed and analysed with electron microprobe stems from a study from Gasparik (1984). Recently, Milholland & Presnall (1998) reported a experimental datum at 1575°C and 30 kbar for the transition from garnet to spinel lherzolite exactly on the dry solidus.

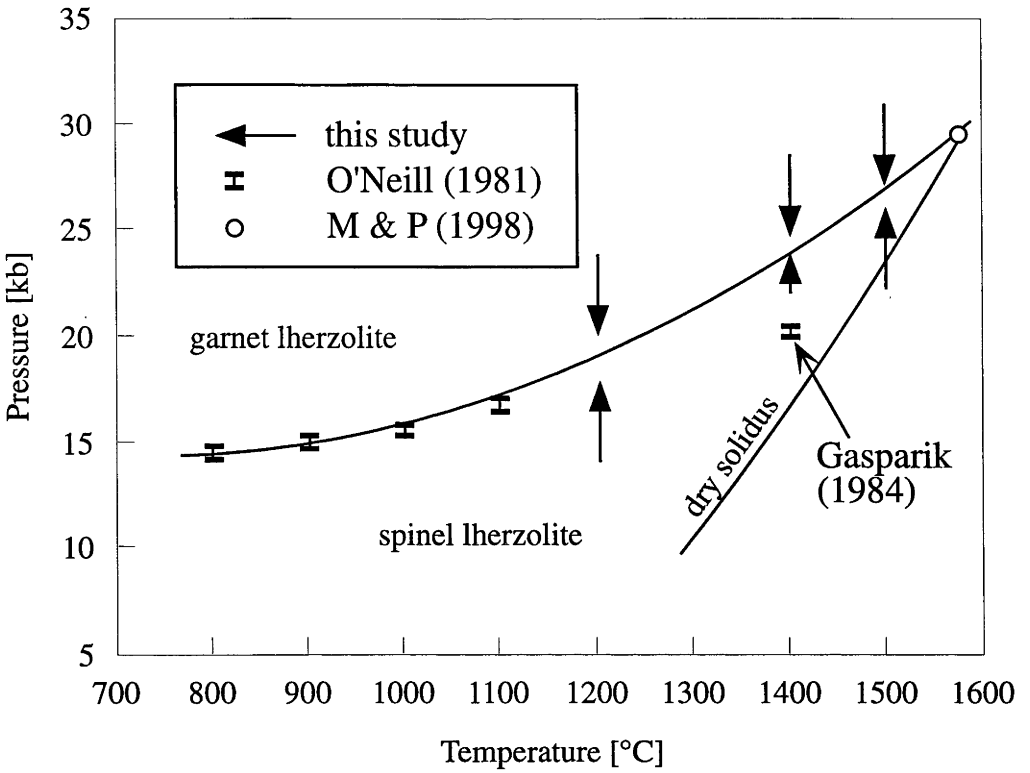

Figure 2 The transition from garnet lherzolite to spinel lherzolite in the system CMAS. Experimentally derived brackets from this study (arrows) are compared with results by O'Neill (1981) and one datum from Milholland & Presnall (M&P) (1998) and Gasparik (1984), respectively. The present results agree well with brackets (see text) in the low-temperature part of the diagram (800°C-1200°C) but for higher temperatures there are considerable differences between the present results and a published datum from Gasparik (1984). A recent datum by Milholland and Presnall (1998), however, is in perfect agreement with the position of the current univariant curve. The transition curve in this diagram is eye-fitted. The dry solidus is taken from Gudfinnsson and Presnall (1996) and Presnall et al. (1979).

As depicted in Figure 2, this study investigates the transition from spinel lherzolite to garnet lherzolite in proximity to the dry solidus, i.e. at temperatures between 1200°C and 1500°C. The present experimental brackets agree well with extrapolation of results from the studies in the low-temperature part (800°C - 1100°C) of the univariant reaction (c.f. O'Neill 1981, Jenkins and Newton 1979, Patera 1982) and results from Milholland and Presnall (1998). The studies in the low-temperature range from 800-1100°C agree well with each other, provided that a pressure correction of -10 % is applied to O'Neill's (1981) data because of the rigid talc-pyrex assembly he used (Green et al. 1966).

Results presented here confirm the datum from Milholland and Presnall (1998) but disagree considerably with the datum from Gasparik (1984). Gasparik used an

empirical pressure correction in his experiments, not found to be necessary for the assembly he used (Green et al. 1966). However, this does not fully explain the discrepancy between the results of Gasparik (1984) and this study. Gasparik's study focuses on the solubility of alumina in pyroxenes, the reversal of the garnet spinel boundary is only a minor part of the study (Gasparik 1984). Run durations of Gasparik's experiments might not have been long enough to reverse the reaction, whereas the reversals of the alumina content of pyroxenes are in good agreement with the results of our study (Figure 3).

The aforementioned 'indirect approach', has first been taken by Obata (1976) who used the experimentally determined isopleths of Al_2O_3 in orthopyroxene in the system (MAS), both in the garnet stability and the spinel lherzolite stability field, to deduce the position of reaction (1) from the intersection of the isopleths. Herzberg (1978) investigated in an analogous study the isopleths of alumina of clinopyroxene, coming to somewhat different conclusions. Both studies suffered from a lack of microprobe analyses in the original experimental studies and the experiments were not reversed.

Recently, Sen (1985) presented reversed experimental data in the spinel stability field, that are in good agreement with results presented here. All of his data, but one, compare well with the present results (Figure 3). An experimental study in the system Na_2O-CaO-MgO-Al_2O_3-SiO_2 (Walter and Presnall, 1994) presents results that are also in good agreement with the results of this study (Figure 3), indicating that the influence of sodium on the activity of alumina in orthopyroxene can neglected. However, Walter and Presnall's experiments remain unreversed, therefore their results should be regarded with caution.

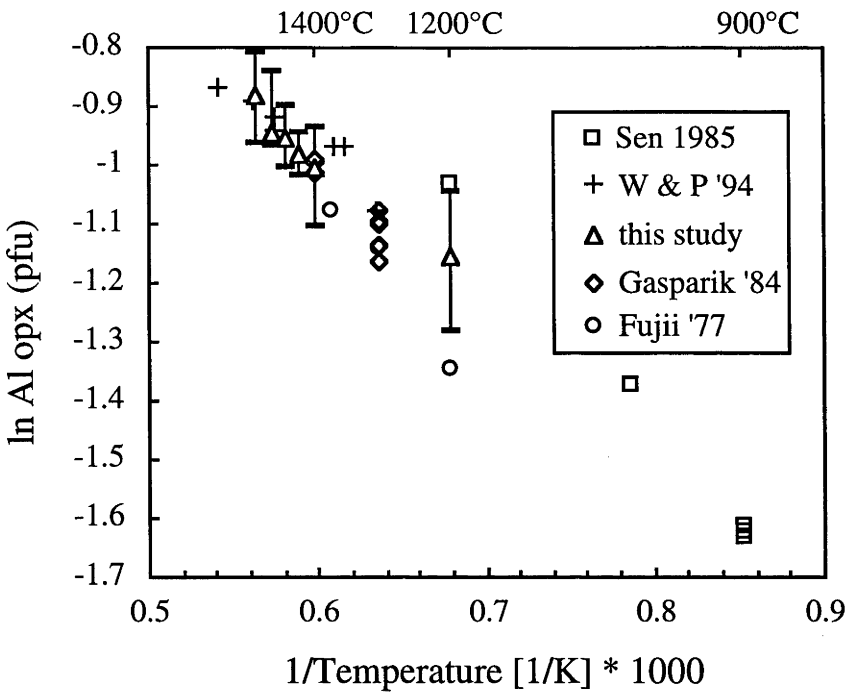

Figure 3 depicts the solubility of alumina in orthopyroxene (Al pfu: Al atoms calculated per formula unit of 6 oxygens) in equilibrium with spinel lherzolite in the system CMAS. Compared are experimental results from reversed studies of Gasparik (1984), Sen (1985) and this study. Also depicted are experimental results of an unreversed study of Walter and Presnall (1994) [W&P 94], that were derived from experiments in the system Na_2O-CaO-MgO-Al_2O_3-SiO_2. Walter and Presnall's (1994) results agree well with my experiments and with those of the other studies, indicating that there is only a minor influence of sodium on the solubility of alumina in orthopyroxene. Sen (1985) presents reversal experiments from 900°C - 1200°C. Good agreement is found between his results and experimental results of this study. One of Sen's data at 1200°C, however, considerably disagree with the results presented and with combined results from the other studies. Experiments depicted in this diagram were performed at a range of different pressures, thus indicating that the alumina solubility in orthopyroxene does not significantly depend on pressure.

Only experiments by Fujii (1977), Gasparik (1984) and Sen (1985) in the spinel lherzolite stability field were reversed and analysed with electron microprobe.

However, Gasparik (1984) presented results in the spinel stability field that apparently disagree with the study of Fujii (1977). Both studies are reversed and analysed with electron microprobe techniques, but do not state uncertainties in alumina content of the pyroxenes. However, Fujii's paper appears in an unreviewed annual

report (Carnegie Institution Yearbook) and does neither quote numbers nor uncertainties and might be in agreement with Gasparik's (1984) study, if errors had been quoted. If we compare one of my results at 1200°C, 18 kb (0.31 ± 0.04 N Al opx pfu = number of Al atoms in orthopyroxene based on a formula unit of six oxygens) with the datum of Fujii at 1200°C 15 kb (0.26 N Al opx pfu), one might find reasonable agreement assuming an error of approximate 0.02 (N Al pfu of 6 oxygens) for the datum of Fujii (1977). Note, however, on the large uncertainty of the present datum. However, run durations in Fujii's (1977) experiments are very short (a few hours). Comparing his run durations with the present experience with reaction rates in CMAS, a lack of complete equilibrium in his experiments remains possible.

As a further test for consistency, nominal experimental temperatures (this study) were compared to calculated temperatures based on the exchange of Ca and Mg between orthopyroxene and clinopyroxene, using the thermometric formulation of Nickel et al. (1985). Results of the thermometry (Table 3) indicate excellent agreement between the present experiments and Nickel et al.'s (1985) formulation.

As mentioned in the introduction, the aim of the following chapters of this thesis is to calibrate a thermodynamic model based on the new experimental results from this study as well as on literature data. The current experiments in both the spinel lherzolite stability field as well as reversals in the garnet lherzolite stability field (from the literature) will be used to calibrate a thermodynamic model for the system CMAS that reproduces the experimental data set presented here.

1.5 CONCLUSIONS AND IMPLICATIONS

This study presents new and reversed experimental results on the transition from garnet lherzolite to spinel lherzolite in a simplified system. The transition at temperatures close to the solidus is found to be substantially higher than previously estimated.

Minor elements like Cr and Fe^{2+} are known to have a substantial effect on the position of the transition. Cr is known to preferentially stabilise spinel bearing assemblages, whilst Fe^{2+} has the opposite effect, shifting the transition to lower pressures (e.g. MacGregor 1970, O'Neill 1981). Thus, rocks containing co-existing

almandine and fayalite ("eulysites") occur in regionally metamorphsed crustal rocks of the amphibolite facies (e.g. Woodland et al. 1995).
Chapter 2, 3, 4 and 6 investigate the influence of Cr on subsolidus equilibria and the reader is referred to these chapters for a more detailed discussion.

However, although Cr and Fe shift the reaction to higher or lower pressures, the relative position of the transition in natural compositions has to be substantially higher than in some recent estimates (e.g. Hirschmann and Stolper 1996) but consistent with other studies in natural compositions (Green and Falloon 1998).

The results of this study further complicate the interpretation of the so-called 'garnet signatures' in MORB, as the stability of garnet is shown here to be less than what has hitherto been assumed. Melting in the presence of garnet peridotite would begin even deeper, thus leading to an expected thickness of the oceanic crust even greater than previously predicted by melting models.

There are several apparent solutions to this conflict: either the rather simple melting models are in error, maybe because of the assumption of a linear increase in melt productivity or melting does indeed not start in the garnet lherzolite stability field, but in equilibrium with spinel lherzolite.

Indeed, recent trace element partitioning studies show that heavy rare earth elements (HREE) become increasingly compatible in clinopyroxene with increasing pressure (Wood and Blundy 1997, Wood et al. 1998), thus indicating that garnet needs not to be present to explain a relative HREE enrichment in mid ocean midge basalts.

1.6 TABLE 3 Analytical results

	1400°C 23 kb		1400°C 27 kb			1200°C 18 kb		1400°C 25 kb		
	S 10 OPX	S 10 CPX	S 14 OPX	S 14 CPX	S 14 GAR	S 23 OPX	S 23 CPX	S 21 OPX	S 21 CPX	S 21 GAR
SiO2	54.4(5)	51.5(2)	54.9(2)	53.4(9)	44.6(7)	54.2(9)	52.3(9)	54.2(3)	52.6(3)	44.8(9)
Al2O3	9.5(5)	9.5(1)	7.0(3)	6.9(5)	26.4(6)	7.9(11)	7.7(7)	8.8(4)	8.6(5)	25.4(8)
MgO	34.5(4)	22.2(2)	35.6(3)	23.9(3)	26.2(4)	34.6(5)	18.8(7)	34.5(2)	23.2(2)	25.9(3)
CaO	2.4(1)	16.6(3)	2.4(1)	16.6(2)	5.9(4)	2.1(4)	21.8(3)	2.2(1)	16.1(8)	5.6(3)
Total	100.8	99.8	99.9	100.8	103.1	98.8	100.6	99.7	100.5	101.7
Si	1.817(9)	1.811(6)	1.853(8)	1.859(5)	2.953(11)	1.846(22)	1.851(16)	1.830(8)	1.833(17)	3.001(7)
Al	0.373(14)	0.393(2)	0.278(9)	0.283(14)	2.06(7)	0.315(37)	0.321(19)	0.350(12)	0.353(13)	2.005(16)
Mg	1.718(6)	1.164(1)	1.791(0)	1.240(9)	2.586(10)	1.757(24)	0.991(11)	1.736(6)	1.205(7)	2.587(24)
Ca	0.087(4)	0.625(7)	0.087(2)	0.618(3)	0.418(21)	0.077(12)	0.826(9)	0.080(4)	0.600(21)	0.404(14)
total	3.996(2)	3.993(5)	4.008(3)	4.000(2)	8.017(7)	3.996(3)	3.989(6)	3.995(2)	3.991(10)	7.997(1)
SiO2	54.0(3)	51.6(2)	55.0(3)	53.0(1)	43.3(2)	54.9(7)	52.0(4)	54.4(3)	52.4(6)	44.0(1)
Al2O3	9.4(3)	9.5(0)	7.0(2)	6.8(4)	25.6(1)	7.9(9)	7.6(5)	8.8(3)	8.6(3)	25.0(2)
MgO	34.2(1)	22.2(0)	35.6(0)	23.7(2)	25.4(1)	35.0(5)	18.7(2)	34.6(1)	23.1(2)	25.5(2)
CaO	2.4(1)	16.6(2)	2.4(1)	16.4(1)	5.7(3)	2.1(3)	21.7(2)	2.2(1)	16.0(5)	5.5(2)
Total	100	100	100	100	100	100	100	100	100	100
T [°C] [NBK]	1424		1444			1187		1449		

	1400°C 24 kb		1200°C 20 kb			1500°C 27 kb			1475°C 25 kb	1500°C 26 kb
	S 26 OPX	S 26 CPX	S 29 OPX	S 29 CPX	S 29 GAR	S 54 OPX	S 54 CPX	S 54 GAR	S 75 OPX	S30 OPX
SiO2	55.3(13)	51.0(6)	54.5(9)	52.7(7)	44.2(9)	54.3(10)	51.8(11)	43.2(12)	54.0(13)	53.9(9)
Al2O3	9.7(22)	9.8(10)	7.8(11)	7.2(11)	24.8(7)	9.9(15)	9.7(2)	24.8(10)	9.9(21)	10.4(6)
MgO	34.9(9)	21.6(3)	35.4(5)	19.2(3)	25.9(9)	34.6(6)	24.5(6)	25.7(9)	34.2(9)	35.2(8)
CaO	2.3(2)	16.7(0)	1.9(4)	21.2(5)	5.7(3)	1.8(3)	15.0(8)	5.3(2)	2.0(2)	2.2(2)
Total	102.2	99.1	99.5	100.3	100.6	100.6	101.0	99.0	100.2	101.7
Si	1.823(38)	1.807(15)	1.843(22)	1.866(23)	2.998(16)	1.815(24)	1.793(6)	2.976(17)	1.814(35)	1.787(11)
Al	0.373(70)	0.409(32)	0.308(37)	0.301(39)	1.982(1)	0.388(45)	0.396(1)	2.013(14)	0.390(66)	0.406(12)
Mg	1.716(35)	1.138(8)	1.785(24)	1.013(10)	2.618(25)	1.724(27)	1.264(3)	2.639(8)	1.713(33)	1.739(2)
Ca	0.079(4)	0.635(10)	0.067(12)	0.804(4)	0.412(9)	0.064(8)	0.556(17)	0.389(4)	0.073(3)	0.078(7)
total	3.991(2)	3.989(1)	4.003(3)	3.984(3)	8.011(17)	3.991(2)	4.009(7)	8.017(10)	3.991(2)	4.010(5)
SiO2	54.2(12)	51.5(4)	54.8(7)	52.5(7)	44.0(3)	54.0(8)	51.3(3)	43.7(3)	54.0(11)	53.0(4)
Al2O3	9.4(18)	9.9(8)	7.8(9)	7.2(9)	24.7(0)	9.8(11)	9.6(0)	25.1(2)	9.9(17)	10.2(3)
MgO	34.2(7)	21.8(1)	35.6(5)	19.1(2)	25.7(2)	34.4(6)	24.3(1)	26.0(1)	34.2(7)	34.6(1)
CaO	2.2(1)	16.9(3)	1.9(3)	21.1(1)	5.6(1)	1.8(2)	14.8(4)	5.3(1)	2.0(1)	2.2(2)
Total	100	100	100	100	100	100.0	100	100	100	100
T [°C] [NBK]	1415		1227			1480				1475

	1500°C 26 kb S30 CPX	1400°C 23 kb S 89 OPX	S 89 CPX	1400°C 23 kb S 92 OPX	S 92 CPX	1425°C 23 kb S 94 OPX	S 94 CPX	1450°C 23 kb S 87 OPX	S 87 CPX	1450°C 23 kb S 93 OPX
SiO2	51.0(13)	54.3(4)	52.0(6)	53.8(5)	51.3(8)	53.6(5)	51.5(4)	53.6(5)	50.8(7)	54.0(5)
Al2O3	10.1(7)	9.6(5)	9.2(7)	8.9(8)	8.9(5)	9.3(5)	9.6(1)	9.7(6)	10.1(6)	9.6(5)
MgO	23.9(11)	34.6(5)	22.1(6)	34.1(4)	22.1(21)	33.6(2)	22.5(6)	33.5(3)	23.1(10)	34.0(3)
CaO	15.1(9)	2.2(2)	17.0(4)	2.1(1)	16.4(13)	2.2(1)	15.9(10)	2.2(1)	15.2(11)	2.3(1)
Total	100.1	100.7	100.3	98.9	98.7	98.8	99.5	99.0	99.2	99.9
Si	1.783(21)	1.816(13)	1.820(18)	1.830(15)	1.826(46)	1.826(6)	1.812(18)	1.822(10)	1.792(29)	1.818(7)
Al	0.416(13)	0.376(16)	0.379(19)	0.357(26)	0.371(4)	0.375(14)	0.398(1)	0.388(18)	0.418(12)	0.381(14)
Mg	1.245(11)	1.725(3)	1.153(8)	1.728(11)	1.168(64)	1.706(12)	1.180(13)	1.697(9)	1.214(16)	1.707(10)
Ca	0.565(11)	0.079(6)	0.637(0)	0.076(2)	0.624(23)	0.08(2)	0.599(26)	0.079(3)	0.574(24)	0.084(4)
total	4.009(14)	3.996(6)	3.990(9)	3.991(2)	3.989(44)	3.987(1)	3.989(19)	3.985(1)	3.999(23)	3.991(0)
SiO2	51.0(7)	54.0(5)	51.9(6)	54.4(5)	52.1(16)	54.3(2)	51.8(7)	54.2(3)	51.2(11)	54.0(2)
Al2O3	10.1(3)	9.5(4)	9.2(5)	9.0(7)	9.0(1)	9.4(4)	9.6(1)	9.8(4)	10.1(3)	9.6(4)
MgO	23.9(2)	34.4(1)	22.0(1)	34.5(2)	22.3(11)	34.9(2)	22.6(2)	33.9(2)	23.3(2)	34.0(2)
CaO	15.1(3)	2.2(2)	16.9(0)	2.1(1)	16.6(5)	2.2(1)	16.0(6)	2.2(1)	15.3(6)	2.3(1)
Total	100	100	100	100	100	100	100	100	100	100
T [°C] [NBK]		1415		1423		1440		1456		1440

	1450°C 23 kb S 93 CPX	1475°C 23 kb S 88 OPX	S 88 MELT	1475°C 23 kb S 95 OPX	S 95 CPX	1500°C 23 kb S 91 OPX
SiO2	51.5(4)	53.7(9)	49.3	53.8(4)	51.7(3)	53.7(6)
Al2O3	9.5(6)	10.0(12)	22.1	9.6(2)	9.2(6)	10.5(11)
MgO	21.9(7)	34.1(5)	15.6	33.6(2)	23.5(5)	33.7(5)
CaO	15.9(8)	2.0(2)	8.0	2.4(1)	15.0(6)	2.4(1)
Total	98.9	99.8	94.9	99.4	99.4	100.3
Si	1.822(26)	1.811(19)		1.822(2)	1.816(22)	1.804(20)
Al	0.398(16)	0.396(36)		0.382(3)	0.382(18)	0.414(32)
Mg	1.156(11)	1.712(21)		1.698(3)	1.230(3)	1.687(10)
Ca	0.604(17)	0.072(5)		0.086(2)	0.564(14)	0.085(1)
total	3.979(18)	3.991(1)		3.987(1)	3.993(13)	3.989(4)
SiO2	52.1(9)	53.9(6)		54.1(1)	52.0(8)	53.6(6)
Al2O3	9.6(4)	10.0(9)		9.6(1)	9.3(4)	10.4(8)
MgO	22.2(1)	34.1(4)		33.8(1)	23.6(0)	33.6(2)
CaO	16.1(4)	2.0(1)		2.4(1)	15.1(3)	2.4(0)
Total	100	100		100	100	100
T [°C] [NBK]				1471		

Electron microprobe analyses of experimental run products. All analyses represent averages of numerous analyses (at least ten per mineral per experiment). Numbers show element abundances in oxide components (wt.%) as well as recalculated on the basis of 6 or 4 oxygens, respectively. Numbers in brackets indicate the analytical uncertainties (e.g. 1.230(3) must be read 1.230±0.003 and 0.564(14) must be read as 0.564 ± 0.014). T[°C] [NBK] quotes temperature estimates [in °C] based on the formulation by Nickel et al. (1985).

CHAPTER 2

The reaction $MgCr_2O_4 + SiO_2 = Cr_2O_3 + MgSiO_3$ and the free energy of formation of magnesiochromite ($MgCr_2O_4$)[1]

2.1 INTRODUCTION

Cr_2O_3 is the sixth most abundant oxide component in the Earth's Upper Mantle (McDonough and Sun 1995). At lower and moderate mantle pressures Cr_2O_3 is largely contained in spinels i.e. as the end member component magnesiochromite ($MgCr_2O_4$). During partial melting in the mantle, the strong partitioning of Cr into spinel can greatly stabilise spinel relative to garnet or aluminous pyroxenes (Wood 1978; O'Neill 1981), and thus influence the trace element characteristics of melts as a function of the pressure of melt segregation. Thermodynamic modelling of the phase relations of Cr in mantle assemblages requires accurate thermodynamic data for $MgCr_2O_4$. These, however, are much less well known than what might be expected for such a key geological substance, which is also a commercially important refractory material and the sole commercially exploited ore for Chromium on Earth (Duke 1983; Pearce et al. 1984). Low-temperature heat capacity measurements for $MgCr_2O_4$ have only been performed down to 52K (Shomate, 1944), and the entropy at 298K (106 J K^{-1} mol^{-1}) was obtained by semi-empirical extrapolation of these measurements to 0 K without considering the magnetic or electronic ordering contributions to the entropy. Subsequent magnetic measurements at low temperature reveal that the Néel temperature, at which magnetic ordering of the Cr^{3+} ions in $MgCr_2O_4$ occurs, is at ~15K. Hence a substantial contribution to the entropy of $MgCr_2O_4$ has been missed.

In this study the thermodynamic properties of $MgCr_2O_4$ were determined by investigating the position of the univariant reaction $MgCr_2O_4 + SiO_2 = MgSiO_3 + Cr_2O_3$ in P-T space. The results

[1] This Chapter has been published in a similar form as: The reaction $MgCr_2O_4 + SiO_2 = Cr_2O_3 + MgSiO_3$ and the free energy of formation of magnesiochromite ($MgCr_2O_4$) Authors: Klemme and O'Neill (1997). Contributions to Mineralogy and Petrology 130, pp. 59-65

have been combined with literature values of the thermodynamic properties of $MgSiO_3$ (orthoenstatite) and SiO_2 (ß-quartz) from Holland and Powell (1990) and Cr_2O_3 (eskolaite) from Holzheid and O'Neill (1995), with heat capacities, molar volumes and thermal expansivity and compressibility data to extract the enthalpy of formation and entropy of $MgCr_2O_4$. The results indicate that the existing calorimetrically derived value for the entropy of $MgCr_2O_4$ underestimates the true value by ~16 J K^{-1} mol^{-1}.

2.2 SYMBOLS, ABBREVIATIONS AND CONSTANTS

T	Absolute temperature in Kelvin [K]
P	Pressure in [bar]
$S°_{298}$	Entropy at 1 bar and 298 K [J mol^{-1} K^{-1}]
$\Delta H°_{f,298}$	Enthalpy of formation from the elements at 1 bar and 298 K [J mol^{-1}]
$\Delta G°_T$	Gibbs free energy change for a reaction among pure end members at the pressure and temperature of interest [J mol^{-1}]
Chr	$MgCr_2O_4$ - magnesiochromite
Esk	Cr_2O_3 - eskolaite
En	$MgSiO_3$ - enstatite
Qz	SiO_2 - quartz
R	Gas constant 8.3143 [J K^{-1} mol^{-1}]
C_P	Heat capacity $C_P = a + bT + cT^{-2} + dT^{-0.5}$
V	Volume at 1 bar and 298 K [J $kbar^{-1}$ mol^{-1}]
a	Coefficient of thermal expansion [K^{-1}]
ß	Coefficient of isothermal compressibility [bar^{-1}]

2.3. EXPERIMENTAL AND ANALYTICAL TECHNIQUES

Experiments

High-pressure, high-temperature experiments were carried out in a conventional piston-cylinder apparatus (Boyd and England 1960) using a 1/2˝ diameter assembly. The assembly consists of two inner parts of MgO (66% density) surrounded by three concentric shells: a graphite heater, a glass tube (Pyrex) and an outermost sleeve of NaCl, pressed to >95% of the theoretical density. This low-friction assembly is thought not to require a pressure correction (Green et al. 1966). Starting materials were sealed in platinum capsules which were insulated from the graphite heater by a small Al_2O_3 sleeve and separated from the thermocouple tip by a 0.5 mm Al_2O_3 disc.

Runs were performed using the "piston-out" routine. First, a pressure of ~0.25 GPa was applied. Then the sample was heated up to 823 K to soften the glass. During the compression to the final run pressure temperatures did generally not exceed 1023 K to prevent deformation of the graphite heater. The pressure was then raised to approximately 0.1 GPa higher than the final run value, and then lowered to run value when the final run temperature was achieved. Pressure was kept constant during runs to within ±0.02 GPa, by manual adjustment if necessary.

As a check on the accuracy of the pressure of the runs, the position of the univariant reaction $Fe_2SiO_4 + SiO_2 = 2\ FeSiO_3$ has been reversed at 1323 K. The

reaction was bracketed between 1.60 and 1.65 (±0.03) GPa. This reaction has previously been determined by Bohlen et al. (1980) who report the bracket to lie between 1.48 and 1.50 GPa at this temperature, using a 1″ NaCl assembly and the "piston-in" technique. However, these results include a -6% correction for friction; without this correction, the bracket would be 1.57 and 1.59, in good agreement with the result from this study (taking into account our estimated uncertainty in pressure). More recent reversal experiments on the reaction $Fe_2SiO_4 + SiO_2 = 2\ FeSiO_3$ by Koch-Müller et al. (1992) between 1073 and 1273 K using a 26 mm NaCl cell and the "piston-in" technique, with no pressure correction, extrapolate to a pressure of 1.57 (probably ±0.03) at 1323K, also in agreement with the results of this study.

Temperatures were measured with $Pt_{94}Rh_6$-$Pt_{70}Rh_{30}$ thermocouples (type B) inserted axially into the assembly inside two- or four-bore high purity Al_2O_3 tubing. Type B thermocouples are much more resistant to contamination at high temperature than the more commonly used Pt-$Pt_{90}Rh_{10}$ (Type S) or Pt-$Pt_{87}Rh_{13}$ (Type R) thermocouples, although they are somewhat less sensitive. Nevertheless, because thermocouple drift due to contamination is always a potential hazard in piston-cylinder experiments at high temperatures (Holloway and Wood 1988), temperatures in some runs (particularly the higher temperature ones) were additionally monitored with a second thermocouple of $W_{75}Re_{25}$-$W_{97}Re_3$ (type C), using four-holed high purity Al_2O_3 thermocouple tubing. Temperatures as measured by the two thermocouples differed only by a maximum of 10K. The sample was placed in the hot spot of the assembly which was found in previous calibrations (Hibberson, pers. comm.). This assembly has also previously been calibrated for temperature against the melting point of gold (cf. Mirwald and Kennedy 1979). Possible pressure effects on the emf of thermocouple pairs were neglected. The temperature uncertainties are estimated to be less than ±10 K at lower temperatures, increasing to about ±15 K at 1773 K.

Starting materials

Starting mixtures were made from mechanical mixes of natural quartz, obtained from a gem quality single crystal of Brazilian quartz, finely ground in a agate mortar, ultra pure oxides (Cr_2O_3) sintered at 1373 K, and synthetic crystalline materials ($MgCr_2O_4$, $MgSiO_3$). $MgCr_2O_4$ was synthesised at 1773 K at atmospheric pressure under flowing CO_2 which produces a slightly reduced environment to prevent any oxidation of Cr^{3+} to Cr^{4+}. $MgSiO_3$ (clinoenstatite) was synthesised at 1373 K at

atmospheric pressure in air. This material, which transforms rapidly to orthoenstatite at high pressures, was used in the higher temperature runs (1473 - 1773 K). For lower temperature runs (< 1473 K), orthoenstatite was used in the starting mixture, synthesised from oxides at 1423 K and 2.0 GPa in a graphite capsule. Synthesis experiments were carried out for ~24 hours.

Preliminary experiments established that the reaction proceeds very sluggishly near the univariant reaction boundary. It was, therefore, considered necessary to enhance reaction rates with a flux. At low temperature (1173 to 1373 K), the flux was de-mineralised H_2O. Although H_2O is well known to greatly enhance reaction rates in experimental studies, here it proved rather ineffective. It was still not possible to establish the direction of reaction satisfactorily at 1173 K, despite run times of ~120 hours, and at 1273 K the extent of the reaction in run C 443-S 81 was only very slight. Adding excess H_2O to the system at temperatures higher than ~1373 K is undesirable due to the very high solubilities of SiO_2 and $MgSiO_3$, and the low melting point of the $MgSiO_3$-SiO_2-H_2O system. Therefore, at temperatures of 1373 - 1773 K, other fluxes were used: from 1473 - 1773 K, a mixture of BaO (78% wt.) and B_2O_3 (22% wt.) (Linares 1962; von Seckendorff and O'Neill 1993) was found to be effective. At 1373 K the BaO - B_2O_3 flux apparently failed to melt, and a K_2O-B_2O_3 flux was employed instead. BaO, K_2O and B_2O_3 enter into the solid phases present only in trace (ppm) levels; neither Ba nor K was detectable in any phase in the experimental run products with electron microprobe techniques, and a substantial body of previous work in the literature of the crystal growth of silicate and oxide phases with borate fluxes has failed to detect any significant substitution of B in these phases - e.g., Barks and Roy (1967) report 50 ppm B in bulk spectroscopic analyses of Cr_2O_3 grown from K_2O-B_2O_3-containing fluxes (this should be considered a maximum level of B substitution, as some of the analysed B may be incorporated in the crystals as flux inclusions). Such trace levels of Ba, K or B as may be present in the solid phases of the run products are insufficient to perturb the equilibrium subsolidus phase relations. A proportion of approximately 5% (wt.) flux was used in all experiments. For experiments at 1473 K a small amount of H_2O was added in order to enable melting of the BaO - B_2O_3 mixture.

The direction of the reaction in the low temperature (1173 to 1373 K) experiments, fluxed by H_2O, was assessed by powder XRD examination of the run products, using a Siemens K170 high-frequency generator and Philips PW 1050 goniometer, by comparing the intensity of reflections relative to those of the starting material. The direction of reaction in the higher temperature experiments, fluxed by

either K_2O-B_2O_3 or BaO - B_2O_3 fluxes was determined by examination by electron microscopy (see below). In all these cases, the direction could be determined unambiguously.

Analytical Procedures

Experimental run products from the higher temperature runs were cut into halves using a low speed diamond saw and mounted in epoxy resin for electron microscopy and microprobe analysis. Mounts were polished in several steps using sand paper and diamond paste of different grain sizes. The final polish was performed with 0.3 μm Linde B polishing powder.

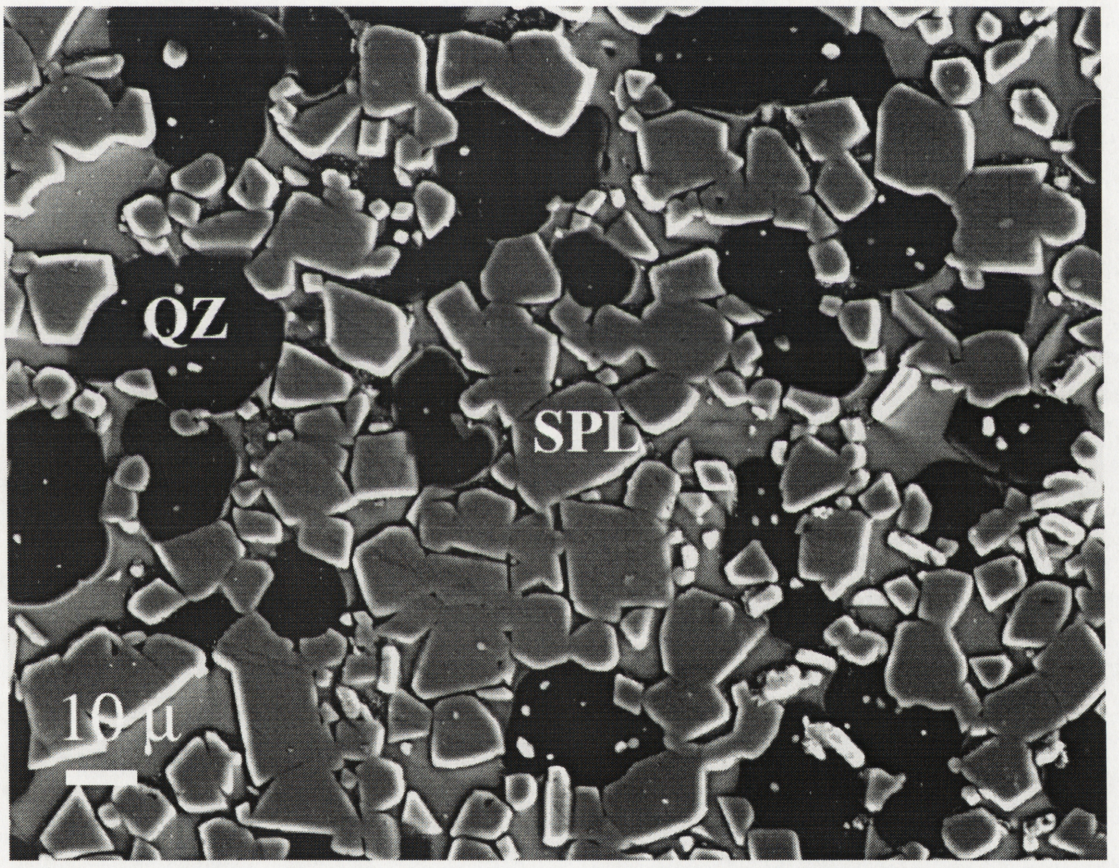

Figure 1: A typical experiment (S 52), characterized by well crystalline materials, dark grains are quartz, light grey grains are spinel, interstitial is flux. The scalebar measures 10 μm. Typical grainsize is 10-30 μm.

Energy and wavelength dispersive analysis were obtained with a Jeol 6400 Scanning Electron Microscope at the Electron Microscopy Unit (EMU) at the Australian National University and with a Cameca "Microbeam" electron microprobe at the Research School of Earth Sciences. All analyses were performed with a spot size of ca. 1 μm. Standards were synthetic Cr_2O_3, natural Cr-diopside and pyrope garnet (Ware, 1991).

2.4 EXPERIMENTAL RESULTS

The results of all experiments are given in Table 1 and the experiments which most closely bracket the equilibrium are shown graphically in Figure 2. The reaction $MgCr_2O_4 + SiO_2 = Cr_2O_3 + MgSiO_3$ has a small positive slope in pressure-temperature space. This nearly flat slope means that experimental errors in temperature measurement have almost negligible influence on the results.

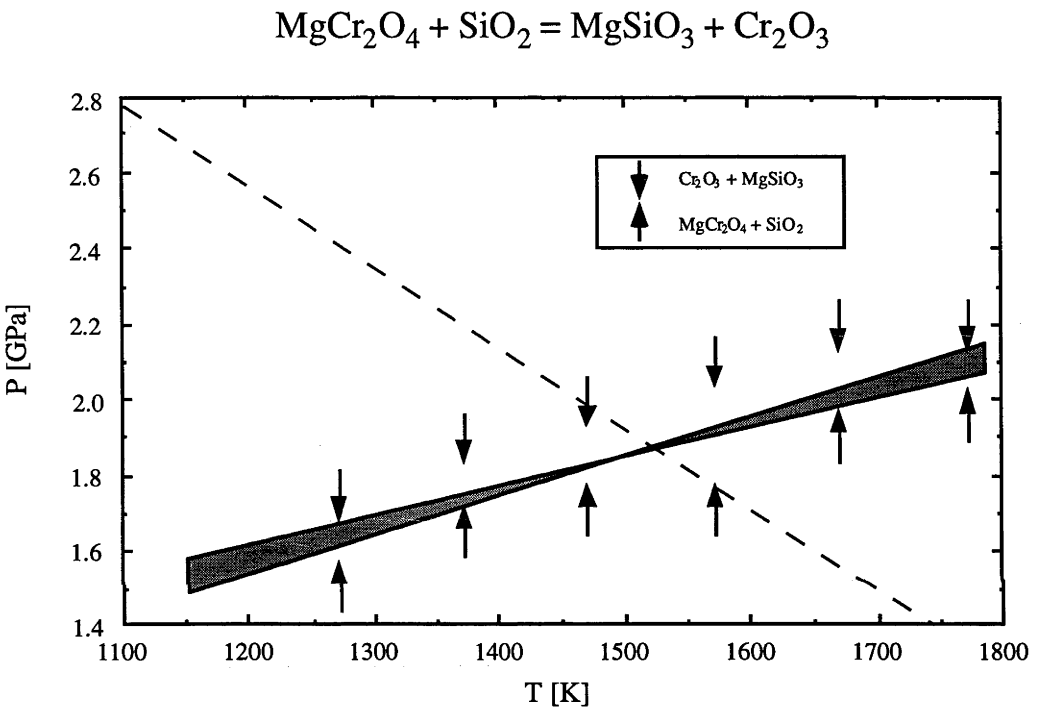

Figure 2 Defining brackets for the reaction $MgCr_2O_4 + SiO_2 = Cr_2O_3 + MgSiO_3$. To allow for experimental uncertainties in measure pressure, the defining high-pressure half-brackets were increased by 0.03 GPa, and the defining low-pressure half-brackets were decreased by 0.03 GPa. The shaded area shows the region allowed by the brackets if the reaction is linear in P-T space. The dashed line is the calculated position of the reaction using thermodynamic data for $MgSiO_3$, SiO_2 and Cr_2O_3 from the literature (see Table 3), with data for $MgCr_2O_4$ from Robie et al. (1979). The existing thermodynamic data cannot reproduce the experimental results.

TABLE 1 Results of Piston - Cylinder Experiments

Run #	T [K]	P [GPa]	t [h]	Result	Flux
C 374-S 64	1323	1.6	24	Ferrosilite	H_2O
C 375-S 65	1323	1.65	24	Fayalite + Quartz	H_2O
C 424-S 76	1173	1.5	120	no reaction	H_2O
C 425-S 77	1173	1.6	120	no reaction	H_2O
C 414-S 74	1273	1.6	48	CHR + QZ	H_2O
C 443-S 81	1273	1.65	135	slight increase of ESK + EN	H_2O
C 412-S 73	1273	1.7	48	ESK + EN, minor CHR	H_2O
C 397-S 69	1373	1.7	552	CHR + QZ	K_2O - B_2O_3
C 444-S 82	1373	1.75	48	growth of CHR + QZ	H_2O
C 394-S 70	1373	1.8	408	ESK + EN, minor CHR	K_2O - B_2O_3
C 245-S 25	1473	1.6	120	CHR + QZ	BaO - B_2O_3 + H_2O
C 304-S 39	1473	1.8	240	CHR + QZ, no EN	BaO - B_2O_3 + H_2O
C 359-S 57	1473	1.9	174	ESK + EN, no CHR	BaO - B_2O_3 + H_2O
C 322-S 46	1473	2.0	300	ESK + EN, minor CHR	BaO - B_2O_3 + H_2O
C 283-S 34	1573	1.8	120	CHR + QZ, no EN	BaO - B_2O_3
C 281-S 33	1573	2.0	120	ESK + EN, no CHR	BaO - B_2O_3
C 267-S 27	1673	2.0	120	CHR + QZ, no EN	BaO - B_2O_3
C 361-S 58	1673	2.1	30	ESK + EN, no CHR	BaO - B_2O_3
C 317-S 42	1673	2.2	120	ESK + EN, no CHR	BaO - B_2O_3
C 307-S 40	1673	2.4	150	ESK + EN, no CHR	BaO - B_2O_3
C 330-S 52	1773	2.0	24	CHR + QZ, no EN	BaO - B_2O_3
C 447-S 83	1773	2.05	24	CHR + QZ, minor EN	BaO - B_2O_3
C 365-S 59	1773	2.1	24	ESK + EN, no CHR	BaO - B_2O_3
C 318-S 43	1773	2.2	24	ESK + EN, no CHR	BaO - B_2O_3
C 319-S 44	1773	2.4	24	ESK + EN, no CHR	BaO - B_2O_3
C 320-S 45	1773	2.6	24	ESK + EN, no CHR	BaO - B_2O_3

CHR=magnesiochromite ($MgCr_2O_4$), ESK=eskolaite (Cr_2O_3), EN=enstatite ($MgSiO_3$), QZ=quartz (SiO_2), t [h]=run duration.

The electron microprobe analysis of the run products was severely hampered not only by the small grain size of the products in many runs, but more especially by the presence of numerous little inclusions, especially in the orthopyroxenes. Analyses of chromites and orthopyroxenes from a few selected runs in which this problem was least severe are given in Table 2. All four phases participating in the reaction are essentially pure, although in detail there is a small amount of substitution of Si in $MgCr_2O_4$ (presumably as Mg_2SiO_4, see Li et al. 1995) and of Cr in $MgSiO_3$. The latter substitution may either involve Cr^{2+} (e.g., as the $CrSiO_3$ component, Li et al. 1995), or perhaps Cr^{3+} in a vacancy-coupled substitution with an end-member of the type

$MgCr^{3+}_{2/3}\square_{1/3}O_6$, (or a combination). As far as can be judged, the amount of Si in the magnesiochromite is < 0.02 atoms per formula unit of 4 oxygens, implying a mole fraction of $MgCr_2O_4$ of > 0.98, while for the orthopyroxene, the mole atomic fraction of Cr/(Cr+Mg) is also ~0.02 (±0.01), implying a mole fraction of $MgSiO_3$ also of 0.98.

TABLE 2 Electron microprobe analyses of selected run products

Run #	SiO_2	Cr_2O_3	MgO	total	Si	Cr	Mg	total
C 320-S 45	59.2 (0.16)	1.87 (0.2)	38.1 (0.07)	99.5 (0.26)	2.00	0.05	1.92	3.97
C 322-S 46	59.3 (0.49)	1.42 (0.17)	38.8 (0.4)	99.5 (0.9)	2	0.04	1.95	3.98
C 330-S 52	0.46 (0.03))	79.5 (0.39)	19.9 (0.19)	99.8 (0.39)	0.01	2.01	0.95	2.98
C 319-S 44	58.3 (0.26)	1.76 (0.16)	38.1 (0.31)	98.7 (0.45)	1.98	0.05	1.96	3.99
C 318-S 43	59.3 (0.68)	1.39 (0.36)	38.5 (0.48)	99.2 (1.02)	2.00	0.04	1.94	3.98
C 359-S 57	58.2 (0.73)	1.77 (0.24)	39.54 (0.49)	99.6 (1.01)	1.96	0.05	1.99	4.0
C 361-S 58	59.1 (0.98)	2.1 (0.11)	38.1 (0.52)	99.3 (0.93)	2.00	0.06	1.92	3.97
C 365-S 59	59.7 (0.8)	1.95 (0.19)	38.3 (0.2)	99.5 (0.46)	2.00	0.05	1.92	3.97
C 281-S 33	60.3 (0.51)	1.27 (0.11)	39.6 (0.12)	101 (0.55)	2	0.03	1.96	3.99
C 307-S 40	59.3 (0.38)	2.30 (0.1)	38.9 (0.52)	100.5 (1.09)	1.98	0.06	1.94	3.99
C 317-S 42	59.5 (0.59)	2.37 (0.09)	38.8 (0.25)	101 (0.76)	1.99	0.06	1.93	3.98
C 267-S 27	0.51 (0.22)	79.2 (0.96)	20.3 (0.29)	100.1 (0.8)	0.02	2	0.97	2.99
C 304-S 39	0.51 (0.17)	76.53 (1.43)	22.56 (0.3)	99.6 (0.9)	0.05	1.93	1.07	3.01

Selected major-element analyses of orthopyroxenes and spinels in experimental run products. Pyroxene and spinel crystals were never bigger than 10 μm, resulting in overlap analyses with adjacent grains or flux, and, therefore, not satisfactory structural values. Pyroxenes usually contained numerous tiny spinel or eskolaite inclusions, so that the Cr_2O_3 contents of orthopyroxenes have to be considered as upper limits. Numbers show element abundances in oxide components (wt. %) as well as recalculated on the basis of 6 or 4 oxygens, respectively. Numbers in brackets show calculated standard deviations. All analyses represent averages of numerous analyses.

2.5 THERMODYNAMIC EVALUATION

The general condition of equilibrium can be expressed as:

$$\Delta_r G_{T,P} = 0 = \Delta_r G^\circ_{T,1bar} + \int_1^P \Delta V_T(P)dP + RT\ln K \qquad (1)$$

where $$K = \frac{a^{opx}_{MgSiO3} \cdot a^{esk}_{Cr2O3}}{a^{sp}_{MgCr2O4} \cdot a^{qz}_{SiO2}} \qquad (2)$$

The experimental half brackets define points in free energy - temperature - pressure space at which $\Delta_r G_{T,P} \geq 0$ (low pressure half-bracket) and $\Delta_r G_{T,P} \leq 0$ (high pressure half-bracket).

We assume $a^{qz}_{SiO2} = a^{esk}_{Cr2O3} = 1$ while (conveniently) $a^{opx}_{MgSiO3} = a^{sp}_{MgCr2O4} = 0.98$, and thus $K \cong 1$, in all runs, and that, therefore, the term in RT ln K is negligible.

Splitting $\Delta_r G^\circ_{T,1bar}$ into the entropy and the enthalpy terms gives:

$$\Delta_r G^\circ_{T,1bar} = \Delta_r H^\circ_T - T\Delta_r S^\circ_T. \qquad (3)$$

Inserting $$\Delta_r\left[H^\circ_T - H^\circ_{298}\right] = \int_{298}^T \Delta_r C^\circ_P(T)dT \qquad (4)$$

and $$\Delta_r S^\circ_T = \Delta_r S^\circ_{298} + \int_{298}^T \left[\frac{\Delta_r C^\circ_P(T)}{T}\right] dT \qquad (5),$$

we have

$$\Delta_r G^\circ_{T,1\,bar} = \Delta_r H^\circ_{298} + \int_{298}^T \Delta_r C^\circ_P(T)dT - T\Delta_r S^\circ_{298} - T\int_{298}^T \left[\frac{\Delta_r C^\circ_P(T)}{T}\right] dT. \qquad (6)$$

Using expressions for the thermal expansivity α and the compressibility β, for each phase we have:

$$\int_1^P V_T(P)\,dP = \left[V^\circ_{298} + \alpha V(T - 298)\right]P - \frac{\beta V}{2}P^2 \qquad (7)$$

Summarising, eqn. (1) can be expressed as:

$$\Delta_r H^\circ_{298,1} - T\Delta_r S^\circ_{298,1} = -\int_{298}^{T} \Delta_r Cp\, dT + T\int_{298}^{T}\left[\frac{\Delta_r Cp}{T}\right] dT - \sum\left[V^\circ_{298} + \alpha V(T-298) - \frac{\beta V}{2}P\right]P \quad (8)$$

Using available thermodynamic data for high temperature heat capacities, molar volumes, thermal expansivities and compressibilities (Table 3), the half brackets can then be considered as defining maximum and minimum values of the quantity ($\Delta_r H^\circ_{298,1} - T\Delta_r S^\circ_{298,1}$) at each experimental temperature. These are plotted in Figure 3.

To allow for experimental uncertainties in pressure, 0.03 GPa were subtracted from the low pressure half brackets and added 0.03 GPa to the high pressure half brackets.

As shown in Figure 3, the brackets constrain $\Delta_r S^\circ_{298,1}$ to lie between 11.76 and 13.77 J K^{-1} mol^{-1}, i.e., 12.77 ± 1.01 J K^{-1} mol^{-1}. The corresponding value of $\Delta_r H^\circ_{298,1}$ is -1504 ± 1364 J mol^{-1} (the uncertainty is highly correlated with the uncertainty in $\Delta_r S^\circ_{298,1}$).

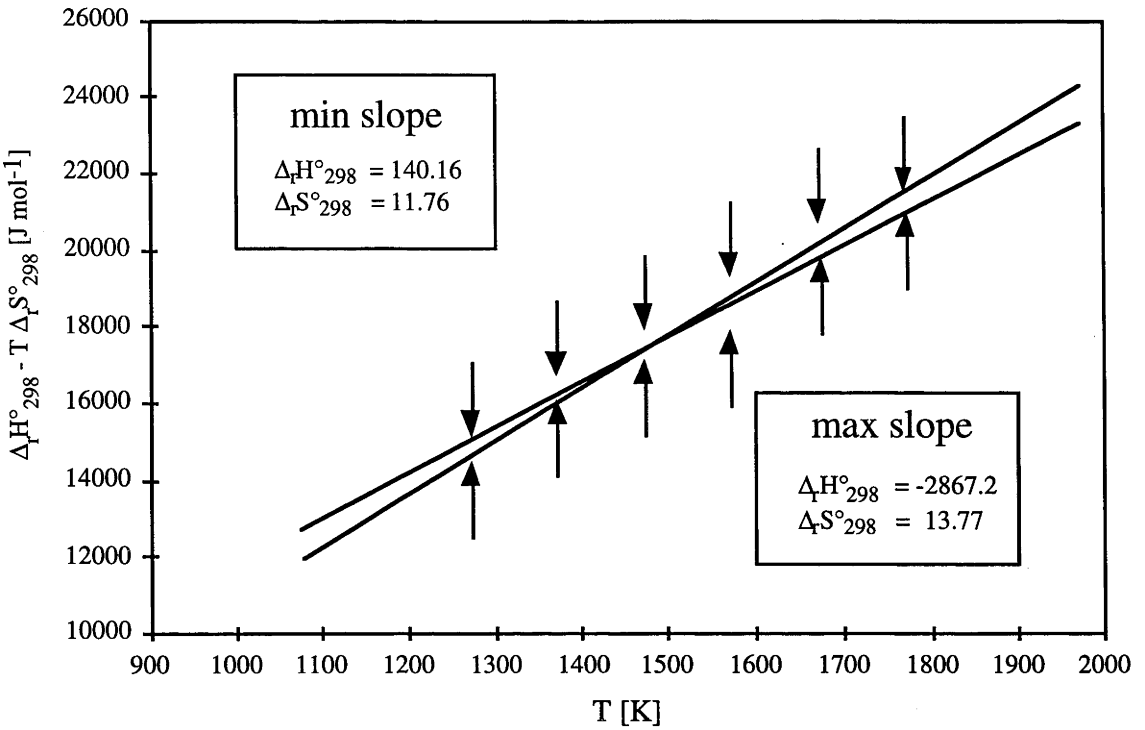

Figure 3 Constraints on the values of $\Delta_r H°_{298}$ - T $\Delta_r S°_{298}$ from the experimental half-brackets for the reaction $MgCr_2O_4 + SiO_2 = Cr_2O_3 + MgSiO_3$. The intercept gives the maximum and minimum value of $\Delta_r H°_{298}$ of the reaction, the slope gives the maximal and minimal entropy change ($\Delta_r S°_{298}$) of the reaction. Arrows correspond to constraining experiments (with ± 0.03 GPa added or subtracted, as appropriate, to allow for experimental uncertainty in pressure).

Using values of $\Delta_r H°_{298}$ and $S°_{298}$ data for eskolaite from Holzheid and O'Neill (1995), and for orthoenstatite and β-quartz from Holland and Powell (1990), $\Delta_r H°_{298}$ = -1759.2 ± 1.5 kJ mol^{-1} and $S°_{298}$ = 122.1 ± 1.0 J K^{-1} mol^{-1} are obtained for $MgCr_2O_4$. This is some 16 J K mol^{-1} more than the calorimetrically determined value of 106 J K^{-1} mol^{-1} (Shomate 1944). The thermodynamic data for $MgSiO_3$ and SiO_2 are well-known, but there remains some doubt regarding the data for Cr_2O_3, since the value of $S°_{298}$ recommended by Holzheid and O'Neill (1995) is 4.6 J K^{-1} mol^{-1} higher than that assessed from calorimetric data (Chase et al. 1985).

2.6 THE MAGNETIC CONTRIBUTION TO THE ENTROPY OF $MgCr_2O_4$

The low temperature heat capacity measurements for magnesiochromite from which the calorimetric entropy is derived only extend down to 53 K (Shomate 1944). Subsequently, magnetic susceptibility measurements have shown that $MgCr_2O_4$ undergoes a paramagnetic to antiferromagnetic transition at ~15 K, caused by ordering of the magnetic spins of the Cr^{3+} ions (Blasse and Fast 1963). The antiferromagnetic character of $MgCr_2O_4$ at 4.2 K was confirmed by Plumier (1968). Hartmann-Boutron et al. (1969) studied the transition using X-ray diffraction and Mössbauer, and concluded that the transition is first-order (i.e., is accompanied by a change in crystallographic symmetry). A similar magnetic transition has also been observed in $ZnCr_2O_4$ at ~10 K (Hartmann-Boutron et al. 1969; Kino and Lüthi 1971).

$MgCr_2O_4$ has the spinel crystal structure, which consists of a cubic close-packed array of anions with half of the octahedral interstices and one-eighth of the tetrahedral interstices occupied by cations. These are commonly referred to as the B and A sites, respectively. $MgCr_2O_4$ is a normal 2:3 cubic spinel with essentially all Mg^{2+} ions on A-sites and all Cr^{3+} on B-sites (O'Neill and Dollase 1994). Short range antiferromagnetic order between Cr^{3+} ions in B-sites is possible since their t_{2g} orbitals are directed towards each other (Dunitz and Orgel 1957).

The maximum contribution to the magnetic entropy of $MgCr_2O_4$ (S_{mag}) is given by 2R ln (2S+1), where S is the spin quantum number. Because Cr^{3+} has three unpaired d-electrons, S is 3/2, and the maximum magnetic contribution to the entropy is 2R ln 4, or 23.05 J K^{-1} mol^{-1}.

However, several spectroscopic studies (Dunitz and Orgel 1957; Baltzer and Wojtowicz 1959) show that the spin quantum number S in spinels is reduced with decreasing temperatures, resulting in some spin-quenching at very low temperatures. In the case of $MgCr_2O_4$, Vickerman (1970) has shown from magnetic susceptibility, and electron paramagnetic resonance and reflectance spectroscopy, that spin quenching does indeed occur in $MgCr_2O_4$, leading to an effective spin quantum number (S') of 1/2, and to a theoretical magnetic entropy (S_{mag}), for the two Cr^{3+} atoms in $MgCr_2O_4$, of 2R ln 2, i.e., 13.48 J K^{-1} mol^{-1}. This is very close to the missing entropy found in this study (the small extra amount found here, of 2.6 ± 1.1 J K^{-1} mol^{-1}, may be due to crystallographic changes accompanying the magnetic transition, or to failure of the structure to develop the full long-range magnetic order at low temperatures (McGuire et al. 1952).

2.7 COMPARISON WITH PREVIOUS MEASUREMENTS OF THE ENTHALPY AND FREE ENERGY OF FORMATION OF $MgCr_2O_4$

The value of $\Delta_r H°_{298}$ of -1504 ± 1364 J mol^{-1}, combined with the standard enthalpies of formation of $MgSiO_3$, SiO_2, Cr_2O_3 and MgO (Table 3) leads to a value of the standard enthalpy of formation of $MgCr_2O_4$ from the oxides ($\Delta_{f,ox} H°_{298,1}$) of -32.9 kJ mol^{-1}. This is considerably less negative than the value of -44.4 kJ mol^{-1}, from Müller and Kleppa (1973), obtained from oxide melt solution calorimetry at 1173 K ($\Delta_{f,ox} H°_{1173,1}$ = -46.3 ± 0.8 kJ mol^{-1}, corrected to 298 K using the heat capacities in Table 3). The reason for this discrepancy is not known.

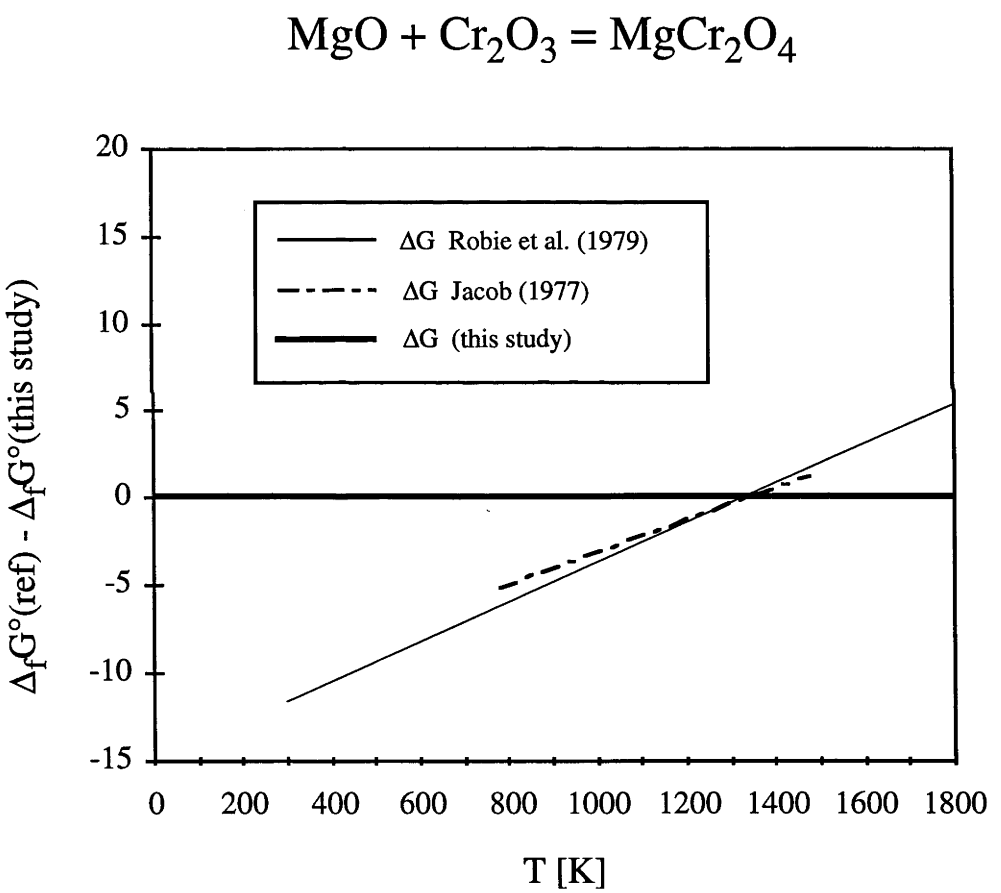

Figure 4 Comparison of previous estimates of the free energy of formation of $MgCr_2O_4$ relative to that of this study. Jacob (1977) used an electrochemical method with an yttria-doped thoria (YDT) solid electrolyte, over the temperature range indicated in the diagram.

The results of this study for the free energy of formation of $MgCr_2O_4$ are compared with the values tabulated by Robie et al. (1979), essentially from calorimetric data, in Figure 4. These tabulated data are clearly not compatible with the reversals of the $MgCr_2O_4 + SiO_2 = Cr_2O_3 + MgSiO_3$ equilibrium (as also illustrated in Figure 2).

TABLE 3 Thermodynamic data from the literature

	V [J bar^{-1}]	$S°_{298}$[J mol^{-1} K^{-1}]	$\Delta_fH°$ ($x10^3$) [KJ mol^{-1}]	
$MgSiO_3$	6.262	132.5	-3089.38	
SiO_2 (ß)	2.367	43.54	-909.07	
Cr_2O_3	2.905[1]	86.65	-1124.9 ♥	
$MgCr_2O_4$	4.356			
MgO			-601.41	
	a	b ($x10^{-2}$)	c ($x10^3$)	d
$MgSiO_3$	356.2	-0.299	-596.9	-3185.3
SiO_2 (ß)	97.9	-0.335	-636.2	-774
Cr_2O_3	108.73[4]	1.18[4]	-2348.5[4]	278.4[4]
$MgCr_2O_4$	196.14	0.54	-3126	-616.88
MgO				
	αV ($x10^{-5}$)	ßV ($x10^{-6}$)	source	
$MgSiO_3$	18	4.6	H&P ('90)	
SiO_2 (ß)	0	2.6	H&P ('90)	
Cr_2O_3	5.4[3]	0.9[2] *	H&ON ('95)	
$MgCr_2O_4$	7.2[3]	1.9[2] *	Rob ('79)	
MgO			H&P ('90)	

Data sources indicated in the right column unless further specified: [1] Chatterjee et al. (1982), [2] Holland & Powell (1990), [3] Fei (1995), [4] Robie et al. (1979). H&P ('90) = Holland & Powell (1990); H&ON ('95) = Holzheid & O'Neill (1995); Rob ('79)= Robie et al. (1979), * data for Al_2O_3 and $MgAl_2O_4$. ♥ based on $\Delta H°_f$=-1124.6 [kJ mol^{-1}], but adjusted to be used with a simple extrapolation of the Cp data to 298 K, ignoring the magnetic transition in Cr_2O_3 at ca. 300 K. V is the molar volume at 1 bar and 298K, $S°_{298}$ is the molar entropy [J mol^{-1} K^{-1}] at 1 bar and 298 K, $\Delta_fH°$ is the enthalpy of formation from the elements at 1 bar and 298 K. a,b,c and d are molar heat capacity polynomial coefficients, where the heat capacity is $Cp=a+b+cT^{-2}+dT^{-1/2}$. αV and ßV are the coefficients of thermal expansion and compressibility, respectively, multiplied by the molar volume.

The only direct measurement of the free energy of formation of $MgCr_2O_4$ is that of Jacob (1977), who used an emf method with yttria-doped thoria (YDT) to determine the chemical potential of oxygen defined by the reaction:

$$MgCr_2O_4 = MgO + 2\ Cr + 3/2\ O_2$$

over the temperature range 1073 to 1473 K. He did not use a flux, and his results are in poor agreement with those of the present study, although they do appear to be in good agreement with the old calorimetric data. In a previous attempt (Hugh O'Neill, personal communication) to perform a similar electrochemical study of this reaction, also using an YDT electrolyte, and no flux, the cell failed to reach a steady state even after several months of equilibration time at ~1220 K. The failure of the electrochemical method with unfluxed sample electrodes is perhaps not surprising, given the unreactive nature of $MgCr_2O_4$ evinced in the present work.

There remains a need for the heat capacity of magnesiochromite ($MgCr_2O_4$) to be measured to very low temperatures in order to confirm the contribution from magnetic ordering.

CHAPTER 3

The heat capacity of $MgCr_2O_4$, $FeCr_2O_4$ and Cr_2O_3 at low temperatures and derived thermodynamic properties.

3.1 INTRODUCTION

Spinels are constituents of many igneous and metamorphic rocks due to their stability over a wide range of pressures and temperatures. In ultramafic rocks spinels are typically chromium-rich (e.g. Meyer 1987).

Thermodynamic modelling of Cr-bearing mineral assemblages in the upper mantle requires accurate knowledge of the thermochemical and thermophysical properties of chromium spinels, chromium pyroxenes and chromium-bearing garnets. In particular, accurate, reliable thermodynamic data for Cr spinels are needed to "anchor" data for other Cr species in any thermodynamic model. The endmember properties of Cr-bearing mineral endmembers are, however, not well understood as recently demonstrated for magnesiochromite ($MgCr_2O_4$) (Chapter 2).

Thermochemical data for most mineral endmembers are usually derived from direct heat capacity measurements (e.g. Hemminger and Höhne 1979, Kleppa 1982, Robie et al. 1979). For temperatures below that of liquid nitrogen, there are no calorimeters commercially available (Gmelin 1985) so that Cp measurements of mineral samples at temperatures below 77 K are rare.

In practice, at least for geologically relevant substances, the heat capacity function was usually measured down to approximately 70 K, and then extrapolated to 0 K. Assuming that the entire heat capacity of the phase arises from the lattice vibrations, such extrapolations are made in accordance with Debye's Law, which predicts the heat capacity function of a mono-atomic solid near 0 K to be proportional to T^3 (Chatterjee 1991).

In the absence of Cp-measurements below the range of the calorimeter, any phase transition will go undetected. The calculation of $S°_{298}$, however, must take the entropy difference into account that is caused by any phase transition below 298.15 K.

The previous chapter describes high-pressure high-temperature experiments that were used to extract thermodynamic properties for $MgCr_2O_4$. These results considerably disagreed with previous estimates that were derived from calorimetry (Shomate 1944). As discussed in the previous chapter, it was assumed that the calorimetric measurements of Shomate (1944) missed a substantial magnetic contribution to the entropy at very low temperatures.

The present study intends to resolve the differences by performing low-temperature calorimetric measurements between 1.5 and 300 K. These measurements were performed at the Max-Planck-Institut für Festkörperphysik in Stuttgart, Germany (W. Schnelle, pers. comm.). Samples were prepared at the Research School of Earth Sciences, ANU. In addition to $MgCr_2O_4$, calorimetric measurements were also performed on $FeCr_2O_4$ and Cr_2O_3, intended to resolve the differences between previous calorimetric data for Cr_2O_3 and recent results obtained from electrochemical measurements (Holzheid and O'Neill 1995).

$MgCr_2O_4$ *magnesiochromite*

Previous heat capacity measurements of $MgCr_2O_4$ (magnesiochromite) were performed from 54 K to 296 K by Shomate (1944). The heat contents from 298 K - 1773 K were measured by Naylor (1944). The entropy at 298 K (J mol^{-1} K^{-1}) was obtained by extrapolation to 0 K without considering magnetic or electronic contributions to the entropy (Shomate 1944). There is, however, some evidence for magnetic ordering at lower temperatures with the Néel temperature at around 15 K: Shaked et al. (1970) investigated $MgCr_2O_4$ by neutron diffraction at low temperatures. They reported two distinct magnetically ordered states at 16 K and 13.5 K whilst Blasse and Fast (1963) reported a paramagnetic to antiferromagnetic transition at 15 K. Hartmann-Boutron et al. (1969) concluded in their investigation of the transition with Mössbauer spectroscopy and X-ray techniques that the transition was of first-order with a change in crystallographic symmetry. Thus a magnetic or electronic contribution to the entropy of $MgCr_2O_4$, associated with this transition has probably been missed in the calorimetric measurements of Shomate (1944).

A recent phase equilibrium study at high pressures and high temperatures (Klemme and O'Neill 1997, Chapter 2) investigated the thermodynamic

properties of magnesiochromite based on the univariant exchange reaction: $MgCr_2O_4 + SiO_2 = Cr_2O_3 + MgSiO_3$. These results are based on the assumption that the thermodynamic data for SiO_2 (quartz), Cr_2O_3 (eskolaite), and $MgSiO_3$ (enstatite) are sufficiently well known to extract the entropy at 298 K and the enthalpy of formation at 298 K for magnesiochromite. Klemme and O'Neill (1997) obtain $S°_{298} = 122 \pm 1$ JK^{-1} mol^{-1} for magnesiochromite, which is 16 J $mol^{-1}K^{-1}$ higher than the value of Shomate (1944), obtained calorimetrically.

Cr_2O_3 *eskolaite*

There is an ongoing debate about the thermochemical data for Cr_2O_3 (eskolaite) which could affect the conclusions drawn by Klemme and O'Neill (1997 and Chapter 2). Bruce and Cannell (1977), Anderson (1937) and Volger (1952) performed calorimetric measurements on Cr_2O_3 and all report an antiferromagnetic transition at around 300 K, resulting in a substantial contribution to the entropy at 298 K. Unfortunately, the
temperature of this transition is close to the customary join between low temperature adiabatic heat capacity measurements and high temperature heat contents measurements, resulting in difficulty in joining the low and high temperature data together.

Chase et al. (1985), based on heat capacity measurements by Anderson (1937) adopt a value for the entropy and enthalpy of formation of Cr_2O_3 of 81.1 ± 1.3 J mol^{-1} K^{-1} and -1134.7 ± 8.4 kJ mol^{-1}, respectively.

Mah (1954) reports $\Delta_f H°_{298}$ for Cr_2O_3 of -1141.7 ± 1.7 kJ mol^{-1} using oxygen bomb calorimetry, while a recent electrochemical study (Holzheid and O'Neill 1995) is in disagreement with the calorimetric measurements of Mah (1954), resulting in estimates of $S°_{298}$ (Cr_2O_3) of 85.74 ± 0.2 J $mol^{-1}K^{-1}$ and $\Delta_f H°_{298}$ (Cr_2O_3) of -1124.6 ± 2.5 kJ mol^{-1}. Holzheid and O'Neill's (1995) data are in good agreement with early results of Roth and Wolf (1940), however.

$FeCr_2O_4$ *chromite*

The low-temperature heat capacity of $FeCr_2O_4$ has been measured down to 53 K (Shomate 1944, 53-296 K) and the entropy and other functions were derived by

extrapolation to 0 K neglecting possible magnetic or electronic ordering contributions to the entropy at temperatures below 53 K. The high-temperature heat contents of $FeCr_2O_4$ were investigated by Naylor 1944 (386-1787 K).

The aforementioned heat capacity measurements report a lambda-like Cp-anomaly between 90 and 140 K, resulting in a contribution to the entropy of ca. 2.4 J mol^{-1} K^{-1}. The anomaly is believed to be related to a cubic to tetragonal phase transition (Shirane et al. 1964). A second Cp anomaly reported at around 75 K coincides with the measured Néel temperature at 80 K by Shirane et al. (1964). The contribution of this anomaly to the entropy of $FeCr_2O_4$, however, is only very small (ca. 0.75 J mol^{-1} K^{-1}).

Kose and Iida (1984) investigated the heat capacity of $FeCr_2O_4$ as a function of temperature from 80 K to 160 K, coming to the same conclusions. They report a Bragg-Williams type heat capacity anomaly peaking at 137 K for pure $FeCr_2O_4$, in good agreement with the observed cubic to tetragonal phase transition (Shirane et al. 1964).

Sack and Ghiorso (1991a) speculated that 'the majority of the magnetic entropy is either not developed at lower temperatures or is associated with the transformation from collinear to helicoidal spin' that has been found to occur at 35 K (Shirane et al. 1964). Sack and Ghiorso (1991a) estimated the entropy (298 K) of $FeCr_2O_4$ (142.7 J mol^{-1} K^{-1}) based on their formulation of the vibrational Gibbs energy of the spinel solid solution. Their estimate was, within errors, consistent with the old thermochemical data for $MgCr_2O_4$ (Shomate 1944).

In this study low-temperature heat capacity measurements from 1.5 K to 340 K are presented for magnesiochromite ($MgCr_2O_4$), chromite ($FeCr_2O_4$) and eskolaite (Cr_2O_3), intending to resolve the aforementioned uncertainties in the standard thermochemical data.

3.2 EXPERIMENTAL

Sample preparation and characterisation

$FeCr_2O_4$ and $MgCr_2O_4$ were prepared from ultrapure oxides (Cr_2O_3 - 99.99%, MgO and Fe_2O_3 - 99.9 %) at 1 atmosphere in high-temperature, controlled atmosphere furnaces at the Research School of Earth Sciences. The oxide mixes were mixed

manually in appropriate proportions in an agate mortar for at least three hours, and then pressed into pellets with a diameter of 0.5 inch.

$FeCr_2O_4$ was prepared from the oxide mixture at 1300°C for 72 hours, then slowly cooled to 950°C. The temperature was kept constant at 950°C for a further 20 hours, the sample was then quenched rapidly.

$MgCr_2O_4$ was synthesised from a pelletised mixture of MgO (dehydrated at 1100°C for 12 hours) and Cr_2O_3 by heating in an atmosphere of CO_2 at 1300°C for 24 hours. The mixture was rapidly quenched, reground and run in a 30 mm piston-cylinder apparatus at 1.0 GPa, 1300°C for 12 hours to minimise the pore space of the specimen. Cr_2O_3 was run in the piston-cylinder apparatus at 1300°C and 1.0 GPa for 12 hours. The high-pressure techniques are similar to those described in Chapter 2.

All synthesis products were checked for homogeneity and unreacted oxides using X-ray powder diffraction techniques. Electron microprobe analyses suggest that the spinels are homogenous and stoichiometric. No impurities or unreacted oxides could be detected by either electron microprobe analyses or X-ray diffraction. The pellets are grey-green and highly dense for $MgCr_2O_4$, dark green and highly dense for Cr_2O_3, and black and not very dense in the case of $FeCr_2O_4$ as the latter material has been synthesised at atmospheric pressure only.

Calorimetric methods

The heat capacities were measured in two vacuum calorimeters (Laboratory assignations Cal. I and Cal. III) at the Max-Planck Institut für Festkörperphysik in Stuttgart (Schnelle, pers comm., Schnelle and Gmelin 1995). The calorimeters are essentially identical except that III is specially designed for measurements in high magnetic fields. Calorimeter I is inserted into a bath cryostat and cooled by filling liquid helium. After vaporisation of the He bath the calorimeter is cooled by the cold helium gas and liquid nitrogen in the annular chamber around the He tank. Calorimeter III (1.5--100 K) is inserted into the 52 mm diameter bore of a 16 T superconducting solenoid and is always kept submerged in liquid helium.

Both calorimeters are equipped with exchangeable miniature sample holders. The holders consist of a frame and a platform made of a thin sapphire disc suspended by three threads from the frame. The platform carries the sample which can be heated by a thin film heater on the lower side of the platform. In Cal. I (for temperatures T >

20 K) a calibrated platinum miniature sensor (Pt-100 118MF; Rosemount) was used for thermometry. For measurements from 1.5 K (2.35 K for $FeCr_2O_4$) up to approximately 30 K a calibrated Cernox temperature sensor was used (CX-1050; Lake Shore). In high magnetic fields magnetoresistance corrections obtained by an in-situ calibration of the sensor, using a capacitance sensor (Oxford) as a transfer thermometer, were applied.

The samples are in the shape of small flat disks weighing 1.2224 g (Cr_2O_3; M = 151.9902 g/mol), 1.1389 g ($MgCr_2O_4$; M = 192.2946 g/mol), and 0.4846 g ($FeCr_2O_4$; M = 223.8366 g/mol), respectively. They are mounted on top of the sapphire sample platform with a small amount (maximal 10 mg) of Apiezon N high vacuum grease. The addenda contributions of the sample holder ensemble and of the Apiezon N grease (Schnelle et al. in press, Cryogenics) were determined in separate runs and subtracted from the raw data of each run.

For the measurements the quasi-adiabatic, isoperibol heat pulse method (Nernst's Method) was employed, using an isothermal shield control. The shield temperature was kept constant to within 0.5 mK (Cal. I) or better than 0.2 mK (Cal. III). The typical residual drift rates of the base line before the heat pulse were $\pm 2x10^{-3}$ mK/s. Typical heat pulse heights for T > 5 K are 2 % or less of the absolute temperature or maximal 1.0 K.

Due to the relatively small sample masses the heat leak of the sample ensemble to the isothermal shield resulted in external relaxation time constants τ^{ext} of 220 -- 4100 s, depending on the temperature range and sample ensemble heat capacity. Because of the excellent heat diffusivity of the Cr_2O_3 and the $MgCr_2O_4$ sample these short τ^{ext} caused no problems, except for the highest temperatures measured. The $FeCr_2O_4$ sample, however, had about half the mass of the two other samples and, in addition, displayed a much smaller thermal diffusivity. This resulted in longer internal equilibration times τ^{int} of this sample and comparatively short external relaxation times τ^{ext}.

The uncertainties of the Cp-data are estimated from previous measurements on Cu-standards (Schnelle, written communication). The estimated uncertainties are 0.6 % for Cp (200 K<T<300 K), 0.4 % for Cp (20 K<T<200.0K), and 0.7 % for Cp (T<20.0K) for the Cr_2O_3 and $MgCr_2O_4$ samples. It is estimated that the error margins for $FeCr_2O_4$ are twice as large for the aforementioned reasons, especially at elevated temperatures.

In order to investigate the very sharp phase transition in $MgCr_2O_4$ at approximately 12.5 K, heat pulses spanning temperature intervals as small as 15 mK were used. The magnetic field dependence of the transition temperature was tested in an applied field 14 T. To investigate whether this presumably first order transition shows temperature hysteresis, cooling curves of the sample holder ensemble were recorded. For that purpose the sample ensemble and the shield were heated to 30 K and then allowed to cool to the bath temperature (4.2 K).

3.3 RESULTS AND THERMODYNAMICS

Eskolaite Cr_2O_3

Figure 1 depicts the heat capacity of Cr_2O_3 determined in this study by low-temperature adiabatic calorimetry. The heat capacity was investigated as a function of temperature from 1.5 to 339 K and observed a broad heat capacity anomaly peaking at the Néel temperature at 305.5 K due to a magnetic transition.

There is good agreement between the present data and the results of Bruce and Cannell (1977) (Figure 1), whilst the present heat capacity data lie considerably below the curve of Volger (1952) and higher than the curve of Anderson (1937).

Integration of the low-temperature Cp data, having included a T^3 extrapolation to 0 K, yields an entropy at 298.15 K for Cr_2O_3 = 82.8 ± 0.8 J mol^{-1} K^{-1}.

As the Cp equation (at least in this study) will be most likely used to calculate equilibria well above room temperature, a heat capacity function was fitted to the data that ignores the Cp anomaly at about 300 K. In order to avoid the anomaly, the heat content data of Moore and Kelley (1944) were adjusted to 340 K, using H_{340}-$H_{298.15}$ = 4899 J. A combination of 5 Cp data (see Appenxix B) and 16 heat content data (Moore and Kelley 1944) were used to derive the following equation from least squares fits:

$$Cp = 227.25 - 0.02132*T + 3543029*T^{-2} - 2567.3*T^{-0.5} \qquad (1)$$

For use in conjunction with this expression, the "virtual" standard entropy at 298.15 K for Cr_2O_3 was estimated to be 83.63 J $mol^{-1}K^{-1}$.

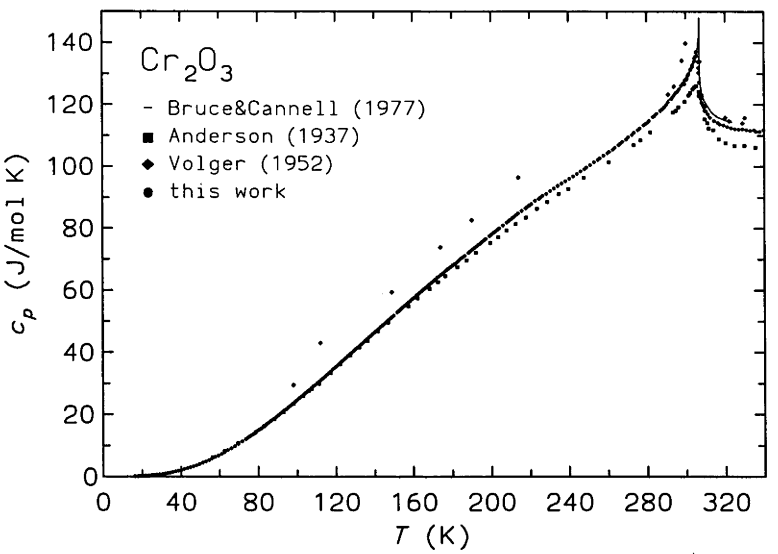

Figure 1 shows the heat capacity of polycrystalline Cr_2O_3 as investigated in this study between 1.5 K and 340 K. The broad heat capacity anomaly peaks at the Néel temperature T_N = 305.5 ± 0.2 K. Compared to this work are studies from Bruce and Cannell (1977), Volger (1952) and Anderson (1937). The standard state thermodynamic data at 298.15 K strongly depend on the position of the anomaly.

Re-evaluation of the EMF data of Holzheid and O'Neill (1995)

The free energy of formation of Cr_2O_3, defined by the reaction 2 Cr + 3/2 O_2 = Cr_2O_3 has recently been measured electrochemically (Holzheid and O'Neill 1995). Their results did not agree well with the literature data for Cr_2O_3 in Chase et al. 1985, which is based on Anderson (1937).

The present new calorimetric data for Cr_2O_3 are used here to re-evaluate Holzheid and O'Neill's (1995) EMF data. The calorimetric data for Cr metal and O_2 needed for third law analysis are listed in Table 1. All 74 EMF data of Holzheid and O'Neill (1995) were used, results of the third law analysis are depicted in Figure 2. In contrast to Holzheid and O'Neill (1995) it was opted to use all their data, although the high temperature data (T>1350K) show some systematic deviations from the trend established at temperatures between 900 and 1300 K.

Table 1 Calorimetric data

	$S°_{298}$ [J $mol^{-1}K^{-1}$]	a	b	c	d	e
O_2	205.15	47.255	-4.542E-4	0	-393.5	440223
Cr	25.24	-101.42	0.058012	-5.49845	2724.1	-5353833
Cr_2O_3	83.63*	227.25	-0.02132	0	-2567.3	3543029

Heat capacity and $S°_{298}$ data for Cr and O_2 from the JANAF tables (Chase et al. 1985). Cp data and $S°_{298}$ for Cr_2O_3 are from this study. * = "virtual entropy for Cr_2O_3, whilst the measured value is 82.8 ± 0.8 J mol^{-1} K^{-1}. $Cp = a + bT + cT^2 + dT^{-0.5} + eT^{-2}$ [J $mol^{-1}K^{-1}$].

Regression of the calculated values of $\Delta_r H°_{298}$ gives

$\Delta_f H°_{298}$ (±256) = -752206 (±230)+ 0.350 (±0.195) T J mol^{-1}, implying $\Delta(\Delta S°_{298})$ = 0.35. Hence, per mole of Cr_2O_3

$\Delta_f H°_{298}$ (Cr_2O_3) = 1128.2 ± 0.4 kJ mol^{-1} and $S°_{298}$ (Cr_2O_3) = 83.1 ± 0.3 J $mol^{-1}K^{-1}$.

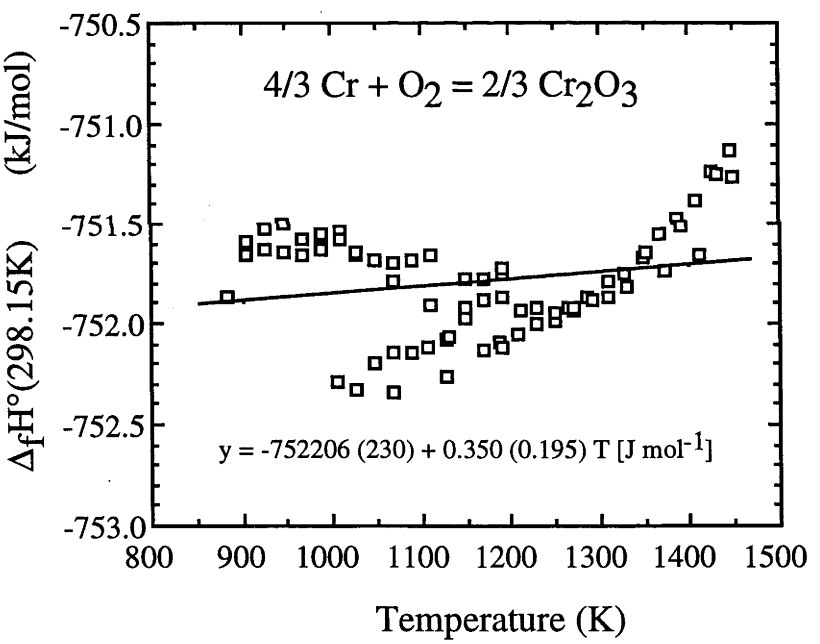

Figure 2: Values of $\Delta_f H°_{298}$ for Cr_2O_3 calculated from the third-law analysis of the EMF data (Holzheid and O'Neill 1995), using the calorimetric data listed in Table 1. Perfect agreement between electrochemical and calorimetric data would result in calculated values of $\Delta_f H°_{298}$ independent of temperature, or in other words, a horizontal array. The slightly positive slope of 0.35 J $mol^{-1}K^{-1}$ indicates a discrepancy between the calorimetric and electrochemical data of this magnitude.

As a next step, the experimental results on the reaction $MgCr_2O_4 + SiO_2 = Cr_2O_3 + MgSiO_3$ were re-evaluated, following the approach described in Chapter 2. Using the new estimates of $S°_{298.15}$= 83.1 J mol^{-1} K^{-1} (this chapter) and $\Delta_f H°_{298}$ = -1128.2 kJ mol^{-1} for Cr_2O_3 (this chapter), new standard thermochemical data for $MgCr_2O_4$ are derived ($S°_{298.15}$ = 119.6 ± 0.9 J mol^{-1} K^{-1} and $\Delta_f H°_{298}$ = -1762 ± 1.4 kJ mol^{-1}). These new estimates for $S°_{298}$ of $MgCr_2O_4$, based on the new calorimetric results for Cr_2O_3, are in even better agreement with the calorimetric measurements for $MgCr_2O_4$ of $S°_{298}$ = 118.3 ± 1.2 J $mol^{-1}K^{-1}$ (see below).

Magnesiochromite $MgCr_2O_4$

Figure 3 depicts the heat capacity measurements between 1.5 K and 340 K. At about 12.5 ± 0.2 K an extremely sharp peak is observed which is interpreted to coincide with the antiferromagnetic transition, previously observed by Shaked et al. (1970), Blasse and Fast (1963) and Hartmann-Boutron et al. (1969).

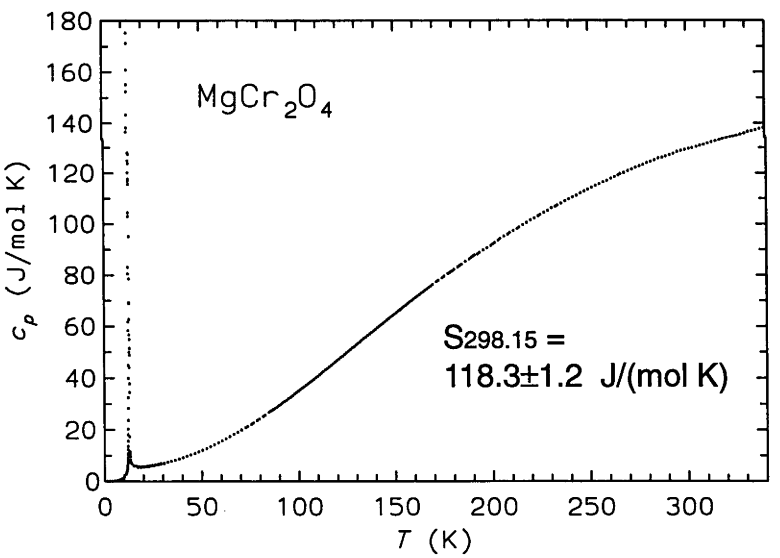

Figure 3 depicts the heat capacity of polycrystalline $MgCr_2O_4$ measured between 1.5 K and 340 K. An extremely sharp heat capacity anomaly is observed, peaking at the Néel temperature T_N = 12.5 ± 0.2 K.

In contrast to a detailed study by Shaked et al. (1970) who found two distinct transitions to magnetically ordered states at ~16 K and at ~13.5 K only one sharp peak was observed. The reason for this behaviour is unknown, but further investigations

using neutron diffraction methods are underway (W. Schnelle, written communication).

Some preliminary measurements were performed to investigate further the transition in a magnetic field of 0 Tesla as well as at 14 Tesla, both during heating as well as during cooling. These measurements resulted in only a small shift of the transition as depicted in Figure 4. A small hysteresis was observed during cooling, which is consistent with a first order phase transition (Hartmann-Boutron et al. 1969).

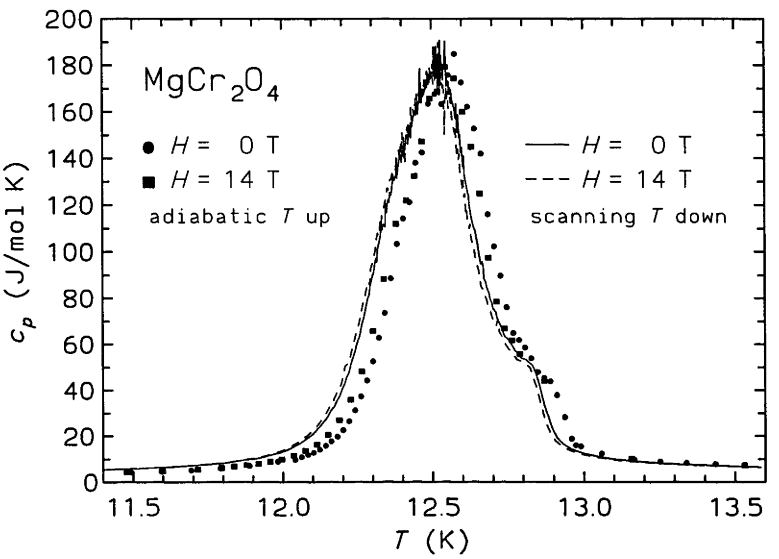

Figure 4: depicted is the heat capacity function of $MgCr_2O_4$ in magnetic fields of 14 Tesla as well in the zero-field. Depicted curves were measured both during heating as well as cooling.

The following equation represents the estimated heat capacity of $MgCr_2O_4$ as a function of temperature. The Cp-equation was fitted to the experimental Cp data from 250-338 (92 data points-see Appendix B) in conjunction with 13 heat content data (Naylor 1944) using a weighted least squares algorithm. The uncertainties in the Cp data (this study) were assumed to be 0.6% (T=200-300K), 0.4% (T=20-200K), 0.7% (T<20K) whilst the uncertainty of the heat content data is estimated at 0.2%.

$$Cp = 221.24 - 0.00102030*T - 1757210*T^{-2} - 1247.9*T^{-0.5} \qquad (2)$$

The entropy at 298.15 K was calculated from the Cp data and resulted in $S°_{298}$ of 118.3 ± 1.2 J $mol^{-1}K^{-1}$ indicating a magnetic contribution to the entropy in the order of 12 J $mol^{-1}K^{-1}$. The resulting $S°_{298}$ for $MgCr_2O_4$ is in good agreement with

experimental results (Chapter 2): ($S°_{298.15}$ = 119.6 ± 0.9 J $mol^{-1}K^{-1}$ and $\Delta_f H°_{298}$ = -1762 ± 1.4 kJ mol^{-1}), using the new calorimetric data for Cr_2O_3 as discussed above.

Ferrous Chromite $FeCr_2O_4$

The heat capacity function of $FeCr_2O_4$ was measured from 2.4 K to 337 K (Figure 5). Three heat capacity anomalies are observed peaking at 36.5 ± 0.2 K, 68.7 ± 0.2 K and 124.1 ± 0.2 K. The anomalies are interpreted to correspond to a magnetic transition at the Néel temperature T_N = 36.5 ± 0.1 K, to a Curie-Weiss transition at T_{Curie} = 68.7 ± 0.1 K and to a phase transition due to a Jahn-Teller effect at T_D=124.1 ± 0.1 K.

The Cp-anomalies at higher temperatures have been observed previously by a number of workers: Shomate (1944), Kose and Iida (1984). The Cp-anomaly at 36.5 K, however, has yet not been measured calorimetrically, although the existence of such an anomaly was predicted by Shirane et al. (1964) and Sack and Ghiorso (1991a).

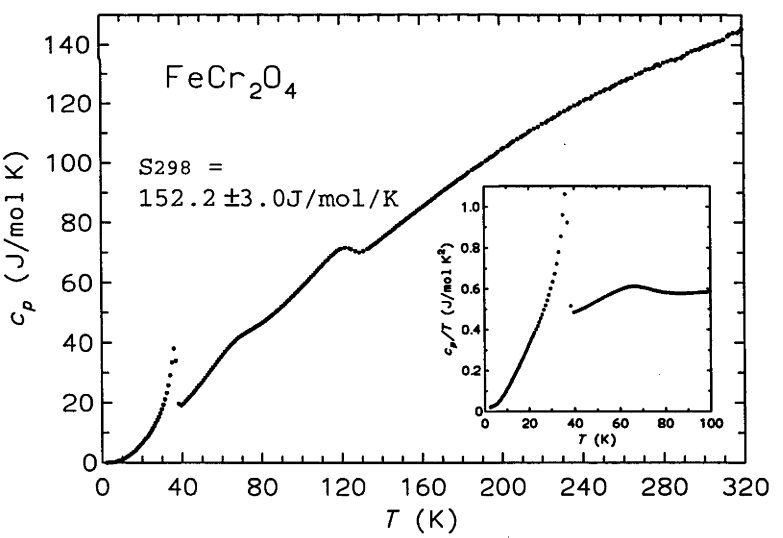

Figure 5 shows the heat capacity of polycrystalline $FeCr_2O_4$ as a function of temperature. T = temperature [K]. The smaller insert shows the sharp heat capacity anomaly peaking at the Néel temperature T_N = 36.5 ± 0.2 K in more detail.

In the absence of direct measurements at temperatures below 50 K, previous estimates of the entropy at 298 K and the enthalpy of formation at 298 K have neglected the magnetic contributions to the entropy at low temperatures (Shomate 1944). Integrating the present low-temperature Cp-data results in standard thermodynamic data for the entropy of $FeCr_2O_4$ at 298 K of 152.2 ± 3.0 J mol^{-1} K^{-1}, having included a T^3 extrapolation to zero K. The estimate of $S°_{298}$ for $FeCr_2O_4$ is some 6 J mol^{-1} K^{-1} higher than estimates by Shomate (1944: $S°_{298}$ = 146.1 ± 1.7 J mol^{-1} K^{-1}).

The quality of the Cp data is less good, mainly because the $FeCr_2O_4$ pellet was only synthesised at atmospheric pressure, resulting in less and more porous material than $MgCr_2O_4$ or Cr_2O_3. The uncertainties for the present Cp data are estimated to be 1.2% (T= 200-300 K), 0.8% (T= 20-200 K) and 1.4% (T<20 K). The heat content data (Shomate 1944) are also found to scatter substantially. The estimated uncertainties in the heat content data are 0.2% at T>600K and 2% at T<600K. Sixty nine heat capacity data (this study, 250-310K, see Appendix B) were used in conjunction with thirteen heat content data (Shomate 1944) to fit the following equation for the heat capacity as a function of temperature.

$$Cp = 139.75 + 0.029408 * T - 3359576 * T^{-2} + 474.8 * T^{-0.5} \quad (3)$$

The Cp data at temperatures higher than 310 K were excluded from the thermodynamic evaluation, because at these temperatures melting of the Apiezon N high vacuum grease occurred that is used for mounting of the sample on the sapphire sample holder. During the fitting procedure, one heat content datum at 386.2 K could not be fitted well, indicating too low values for the heat capacity.

3.4 CONCLUSIONS

This chapter presents new calorimetric measurements for minerals, $MgCr_2O_4$, $FeCr_2O_4$ and Cr_2O_3. Derived thermodynamic standard values for $MgCr_2O_4$ are in good agreement with a recent estimates presented in Chapter 2. The calorimetric measurements confirm a substantial magnetic contribution to the entropy of $MgCr_2O_4$. Furthermore, the agreement of the calorimetry with results from high-pressure high-temperature experiments indicates excellent pressure and temperature calibration of the piston-cylinder apparatus used in the latter study (Chapter 2).

New calorimetric results for Cr_2O_3 basically confirm the results of Bruce and Cannell (1977). The new calorimetric results for ferrous chromite ($FeCr_2O_4$) indicate that a substantial contribution to the entropy (6 J $mol^{-1}K^{-1}$) has been missed in previous studies.

Based on the heat capacity measurements presented in this chapter and heat content measurements from the literature, heat capacity functions were derived, needed for thermodynamic calculations in Cr-bearing systems. These heat capacity functions and the standard thermochemical data enable extension of the thermodynamic model developed in Chapter 5, to Cr-bearing compositions.

The results presented here suggest that basic thermodynamic data for many more Cr bearing phases might be in error, as similar heat capacity anomalies are expected for other Cr-bearing phases (e.g. $ZnCr_2O_4$) thus vindicating the need for more low-temperature calorimetric studies of geologically relevant phases.

CHAPTER 4

The partitioning of chromium and aluminium between orthopyroxene and spinel: Experiments and thermodynamics

4.1 INTRODUCTION

The upper mantle consists of rocks of peridotite composition (e.g. Ringwood 1975), which contain the minerals olivine, orthopyroxene, clinopyroxene and an aluminous phase, which, depending on pressure, is plagioclase (low pressure), spinel (intermediate pressure) or garnet (high pressure). Most natural samples of upper mantle material that have been transported to the surface as xenoliths in alkali-basalts and related magmas (basanites, nephelinites) are spinel- lherzolites (e.g. Nickel and Green 1984), although rarely garnet lherzolites (Ionov et al. 1993) also occur. Many of the latter also contain spinel (Ai 1992, Ionov et al. 1993). Garnet lherzolites are commonly found in kimberlites and lamproites, which sample deeper within the Earth's mantle.

In terms of chemical composition, the chemical components CaO, MgO, Al_2O_3, SiO_2 make up more than 90 % of these rocks. However, rigorous extrapolation of experimental and thermodynamic results in the system CaO-MgO-Al_2O_3-SiO_2 (c.f. Chapter 1 and 5) to multicomponent natural peridotites requires that the effects of minor elements are taken into account.

Most thermodynamic models based on internally consistent sets of thermodynamic data (e.g. Holland and Powell 1990, Berman 1988) were developed for calculations of metamorphic equilibria at crustal conditions. The influence of Cr was neglected in these thermodynamic databases, due to the fact that Cr behaves as a compatible element during melting of the upper mantle, resulting in low concentrations of Cr in the crust. Cr is therefore not an important constituent of most crustal rocks.

The situation is quite different, however, when upper mantle equilibria are considered: Natural spinel lherzolites and garnet lherzolites contain on average about 2600 ppm chromium (O'Neill and Palme 1998). Cr^{3+} is known to fractionate strongly among the major upper mantle phases, as illustrated in a 5-phase lherzolite (Table 1).

The presence of Cr and its preferred partitioning into spinel greatly stabilises spinel bearing assemblages relative to garnet bearing assemblages or plagioclase bearing peridotites (O'Neill 1981, Wood 1978).

Table 1 shows that spinel in this example contains ca. 18 % (wt.) Cr_2O_3, whereas the pyroxenes contain between 0.5 and 1.2 wt.% Cr_2O_3. Because of the differences in modal abundances of pyroxenes and spinel, however, quite a large percentage of bulk chromium is contained in the pyroxenes.

TABLE 1 spinel-garnet lherzolite - Ming-Xi (China)

	spinel	garnet	olivine	opx	cpx
MgO	20.1	20.7	49.1	32.8	15.9
Al_2O_3	49.9	23.1		4.6	6.0
Cr_2O_3	17.9	1.5		0.5	1.2
FeO	11.4	7.0	9.3	5.9	2.8
SiO_2		42.2	41.1	55.6	52.9
modal	0.7	7.3	64.5	15.8	11.9

Depicted are mineral analyses of a garnet-spinel bearing lherzolite from China (Ming-Xi, province (Ai, 1992). Cr is concentrated in the spinel phase, which is abundant in only minor modal amounts. Modal amounts were calculated from bulk rock analyses and mineral analyses (Ai, 1992).

Therefore, thermodynamic models of phase equilibria under upper mantle conditions should include thermodynamic formulations for both Cr-bearing spinels as well as Cr-bearing pyroxenes.

A recent study by Asimov et al. (1995) investigated melt productivity along the solidus of mantle peridotite. Their results indicated that melting may cease during adiabatic mantle upwelling as the boundary between garnet lherzolite and spinel lherzolite is crossed. Calculations were performed with the MELTS algorithm based on the internally consistent set of thermodynamic data designed by Sack and Ghiorso (1995). As the MELTS database incorporates thermodynamic properties of chromian spinels but not for these of Cr-bearing pyroxenes, the calculations were performed once with Cr in the composition and once without. Since the thermodynamic data for $MgCr_2O_4$ and $FeCr_2O_4$ in the MELTS database (Sack and Ghiorso 1991a, Ghiorso and Sack 1995) are in error, as indicated in Chapters 2 and 3 (a possibility foreshadowed by Sack and Ghiorso themselves), the calculated results from Asimov et al.'s (1995)

study should only be used qualitatively to illustrate the principles of how melt productivity may vary across the garnet - spinel transition; they cannot accurately compute phase equilibria or garnet -spinel relations. Figure 1 shows that the phase relations differ substantially between the Cr-free and the Cr-bearing model, not just in the position of the transition, but also in the width over which garnet and spinel coexist. It is this latter factor which is expected to influence melt productivity.

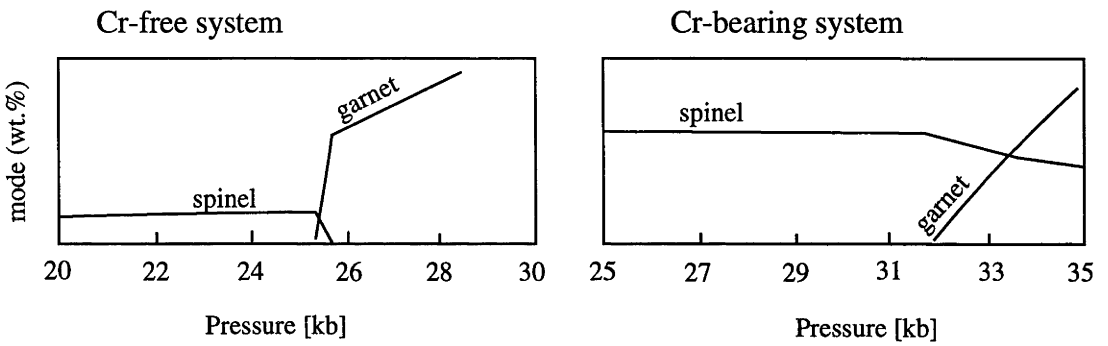

Figure 1 Calculated transition from spinel lherzolite to garnet lherzolite in complex compositions using the MELTS algorithm (Figure taken from Asimov et al. 1995). The left diagram depicts relations in a Cr-free system, the transition is quite sharp. In a Cr-bearing system, depicted on the right hand side, the spinel stability is overestimated due to the lack of Cr-bearing pyroxenes in the MELTS database (Ghiorso and Sack 1995).

In this study the partitioning of Cr and Al between spinel and orthopyroxene is investigated in the system MgO-Al_2O_3-SiO_2-Cr_2O_3 as a first step towards a better understanding of the influence of minor elements on upper mantle processes. A series of subsolidus experiments were conducted followed by thermodynamic analysis of the experimental results. Combining these data with results in the system CaO-MgO-Al_2O_3-SiO_2 (Chapter 5), an internally consistent thermodynamic model has been calibrated that enables calculation of phase relations in Cr-bearing systems.

The solubility of Al and Cr in orthopyroxene in equilibrium with olivine and spinel in the system MASCr may be described by two equilibria:

$$MgAl_2O_4 + Mg_2Si_2O_6 = MgAl_2SiO_6 + Mg_2SiO_4 \quad (1),$$

$$MgAl_2O_4 + MgCr_2SiO_6 = MgCr_2O_4 + MgAl_2SiO_6 \quad (2)$$

Equilibrium (1) describes the solubility of alumina in orthopyroxene in equilibrium with spinel and olivine while the exchange reaction (2) describes the exchange of Al and Cr between co-existing spinel and orthopyroxene.

Equilibrium (1) has been experimentally investigated in the systems MAS (e.g. Gasparik and Newton 1984), CMAS (e.g. Fujii 1977, Gasparik 1984, Sen 1985, this study) and Na_2O-CMAS (Walter and Presnall 1994). The addition of CaO to the MAS system should have negligible effect on this reaction, since substitution of CaO into the phases partaking in the reaction is minor (in orthopyroxene and tends to cancel out across the reaction) or negligible (in olivine and spinel). The addition of Na_2O to the system similarly has negligible effect.

Equilibrium (1) is used as a geothermometer in the spinel lherzolite facies (e.g. Gasparik and Newton 1984, Witt-Eickschen and Seck 1991). However, the replacement of Al by Cr in orthopyroxene probably exerts a large influence.

The alumina content of orthopyroxene should be most sensitive to the influence of Cr where it is greatest, i.e. in the spinel lherzolite facies rather than in the garnet lherzolite facies. For example, the solubility of Al_2O_3 in orthopyroxene (in the system CMAS) is >8 wt.% at 15 kbar and 1200°C, but only about 1.5 wt. % at 40 kbar at the same temperature. Hence experiments were conducted on reaction (1) rather than the equilibrium (3) that controls the solubility of alumina in orthopyroxene in equilibrium with garnet and olivine:

$$Mg_3Al_2Si_3O_{12} = MgAl_2SiO_6 + Mg_2Si_2O_6. \qquad (3)$$

However, the results of the present study should be applicable for garnet bearing equilibria provided the thermodynamics of Cr-bearing garnets are sufficiently well understood.

4.2 EXPERIMENTAL AND ANALYTICAL TECHNIQUES AND PROCEDURES

All high-pressure, high-temperature experiments but one were performed in a conventional piston-cylinder apparatus (Boyd and England 1960) at temperatures from 1300-1500°C and pressures between 0.5 to 4.0 GPa, using a 1/2″ diameter pressure assembly. The assembly consists of two inner parts of MgO (66% density) surrounded by three concentric shells: a graphite heater, a glass tube (Pyrex) and an outermost sleeve of NaCl, pressed to >95% of the theoretical density. This low-friction assembly is thought not to require a pressure correction (Green et al. 1966), especially given the high temperatures and long run times used here (see Bose and Ganguly 1995). Starting materials were sealed in platinum capsules which were insulated from the graphite heater by a small Al_2O_3 sleeve and separated from the thermocouple tip by a 0.5 mm Al_2O_3 disc.

Runs were performed using the "piston-out" routine. First, a pressure of ~2.5 kb was applied. Then the sample was heated up to 550°C to soften the glass. During the compression to the final run pressure temperatures did generally not exceed 750°C to prevent deformation of the graphite heater. The pressure was then raised to approximately 1 kb higher than the final run value, and then lowered to run value when the final run temperature was achieved. Pressure was kept constant during runs to within ±0.2 kb, by manual adjustment if necessary. Pressure calibration of the piston-cylinder apparatus has been reported in Chapter 2.

One experiment at a nominal pressure of 54 kb (S 54) was run in a newly designed 'Ultra High Pressure Piston Cylinder Apparatus'. This experiments is to be regarded as preliminary, as pressure calibration of the apparatus is incomplete.

Temperatures were measured with $Pt_{94}Rh_6$-$Pt_{70}Rh_{30}$ thermocouples (type B) inserted axially into the assembly inside two-bore high purity Al_2O_3 tubing. Type B thermocouples are much more resistant to contamination at high temperature than the more commonly used Pt-$Pt_{90}Rh_{10}$ (Type S) or Pt-$Pt_{87}Rh_{13}$ (Type R) thermocouples, although they are somewhat less sensitive. The sample was placed in the hot spot of the assembly, the location of which has been found in previous studies (W.O. Hibberson, personal communication). This assembly has also previously been calibrated for temperature against the melting point of gold (cf. Mirwald and Kennedy 1979). Possible pressure effects on the emf of thermocouples were neglected. The

temperature uncertainties are estimated to be less than ±15 °C in the temperature range of the present experiments.

To check whether Cr^{2+} was present in the experiments, a few runs were conducted with a Re-ReO_2 buffer to generate a high oxygen fugacity environment, approximately mid-way between the Ni-NiO and the Fe_3O_4-Fe_2O_3 buffers (Pownceby and O'Neill 1994b). The Re-ReO_2 buffer consisted of a fine-grained mixture of 50 mol % Re-metal with 50 mol % ReO_2. Neither Re nor ReO_2 reacted with the phases of interest in the experiments, hence the buffer mixture was mixed in with the starting materials. Results from the buffered runs were indistinguishable from unbuffered experiments, hence indicating no significant Cr^{2+} in the experiments. Another item of evidence against the presence of significant Cr^{2+} in all experiments is the lack of detectable Cr in olivine (detection limit ca. 600 ppm Cr with EDS and 150 ppm with WDS).

Starting materials

All experiments contained spinel, orthopyroxene and forsterite in the starting mixture, with the exception of SM 11 which contained no olivine. Starting mixtures were made from mechanical mixes of synthetic crystalline materials ($Mg(Cr,Al)_2O_4$, $Mg_2Si_2O_6$ and Mg_2SiO_4).

Spinels were synthesised at 1500°C at atmospheric pressure under flowing CO_2 which produces a slightly reduced environment to prevent any oxidation of Cr^{3+} to Cr^{4+}. $Mg_2Si_2O_6$ (clinoenstatite) was synthesised at 1100°C at atmospheric pressure in air. This material transforms rapidly to orthoenstatite at high pressures. Synthesis experiments were carried out for ~24 hours. Forsterite (Mg_2SiO_4) was synthesised at 1050°C at atmospheric pressure using a Li_2WO_4-flux. With a flux/oxide-mix ratio of 4/1 in a Pt-crucible, forsterite-syntheses were carried out for six days.

Most experiments were unreversed, approaching orthopyroxene equilibrium compositions from the Cr-and Al poor side. The attainment of equilibrium in such experiments can be assessed from homogeneity of the orthopyroxenes. Two reversal experiments were performed as to further confirm the achievement of equilibrium. The reversal experiments contained two different starting material pyroxenes, both in the same run. One of these consisted of pyroxenes with high Al_2O_3 and Cr_2O_3 contents, the other consisted of pure $Mg_2Si_2O_6$ (enstatite). Analyses of the run products indicated that both pyroxenes converge on the equilibrium value. Individual run

conditions are summarised in Table 3, whilst individual starting material compositions are listed in Table 2.

High-alumina and high-chromium orthopyroxene (in starting material SM 47) was crystallised from a melt at 19 kb in a 5/8″ piston cylinder apparatus at RSES. This synthesis experiment was conducted at 1700°C for 5 min, then cooled 2° per minute down to 1550°C. Crystallisation continued at 1550°C for 10 hours, the sample was then cooled at a rate of 1°/min down to 1300°C, resting at 1300°C for 24 hours before quenching.

Preliminary experiments established that the reaction proceeds very sluggishly. To evaluate the run durations needed for reasonable attainment of equilibrium in the experiments, time series of experiments were conducted with different run times. At 1400°C run durations of >120 hours were found to be sufficient to produce homogenous mineral compositions. Experiments at 1300°C had to be run for several weeks, but even then the mineral analyses showed larger scatter than at higher temperatures (Table 4 at the end of this chapter). Attempts at temperatures lower than 1300°C produced only inhomogenous pyroxenes.

TABLE 2 starting material

mixture	spinel	buffer
SM 11	$Mg(Cr_{0.5}Al_{0.5})_2O_4$	
SM 16	$Mg(Cr_{0.5}Al_{0.5})_2O_4$	
SM 34	$Mg(Cr_{0.46}Al_{0.54})_2O_4$	
SM 35	$Mg(Cr_{0.57}Al_{0.43})_2O_4$	
SM 41	$Mg(Cr_{0.8}Al_{0.2})_2O_4$	
SM 42	$Mg(Cr_{0.2}Al_{0.8})_2O_4$	
SM 47	$Mg(Cr_{0.46}Al_{0.54})_2O_4$	Re-ReO_2
SM 50	$Mg(Cr_{0.9}Al_{0.1})_2O_4$	

Starting materials: All starting material mixtures contained synthetic Mg_2SiO_4 as well as $Mg_2Si_2O_6$ with exception of SM 11 (no Mg_2SiO_4). SM 47 contained two starting pyroxenes: pure enstatite as well as an orthopyroxene with ca. 10 wt.% Al_2O_3 and 0.8 wt.% Cr_2O_3. See text for details and notes on the synthesis of the starting materials.

Analytical procedures

Experimental run products were cut into halves using a low speed diamond saw and mounted in epoxy resin for electron microscopy and microprobe analysis.

Mounts were polished in several steps using sand paper and diamond paste of different grain sizes. The final polish was performed with 0.3 μm Linde B polishing powder.

Energy and wavelength dispersive analyses were obtained with a JEOL 6400 Scanning Electron Microscope at the Electron Microscopy Unit (EMU) at the Australian National University and with a Cameca "Microbeam" electron microprobe at the Research School of Earth Sciences. All analyses were performed with a spot size of ca. 1 μm. Standards were synthetic Al_2O_3, natural Cr-diopside and pyrope garnet (Ware, 1991). Special care was to taken to avoid overlap of analyses of small spinel inclusions with orthopyroxenes.

TABLE 3 Experimental runs in the system MgO-Al_2O_3-SiO_2-Cr_2O_3

run no.	P [kb]	T [°C]	t [h]	start material	phases present
C 301-S 38	40	1300	244	11	spl, ol, opx
C 297-S 36	25	1300	260	11	spl, ol, opx
C 586-S 114 I	25	1300	360	41	spl, ol, opx
C 587-S 114 II	25	1300	360	42	spl, ol, opx
C 598-S 118 I	10	1300	400	42	spl, ol, opx
C 599-S 118 II	10	1300	400	41	spl, ol, opx
C 517-S101 I	10	1300	240	35	spl, ol, opx
UHP 28-S 126	54	1400	120	50	spl, ol, opx
C 543-S 104 I	40	1400	120	16	spl, ol, opx
C 544-S 104 II	40	1400	120	34	spl, ol, opx
C-545-S 104 III	40	1400	120	35	spl, ol, opx
C 299-S 37	35	1400	144	11	spl, ol, opx
C 576-S 111 I	35	1400	120	41	spl, ol, opx
C 577-S 111 II	35	1400	120	42	spl, ol, opx, gar
C 623-S 123 I	35	1400	120	47	spl, ol, opx
C 624-S 123 II	35	1400	120	50	spl, ol, opx
C 233-S 22	24	1400	24	11	spl, ol, opx
C 587-S 115 I	24	1400	120	42	spl, ol, opx
C 588-S 115 II	24	1400	120	41	spl, ol, opx
C 591-S 116 I	20	1400	150	41	spl, ol, opx
C 592-S 116 II	20	1400	150	42	spl, ol, opx
C 326-S 50	10	1400	120	16	spl, ol, opx
C 577-S 112 I	10	1400	120	42	spl, ol, opx
C 578-S 112 II	10	1400	120	41	spl, ol, opx
C 618-S 122 I	5	1400	120	41	spl, ol, opx
C 689-S 127 I	5	1400	122	50	spl, ol, opx
C 690-S 127 III	5	1400	122	47	spl, ol, opx
C 329-S 51	35	1500	24	11	spl, ol, opx
C 596-S 117 I	35	1500	24	42	spl, ol, opx, gar
C 597-S 117 II	35	1500	24	41	spl, ol, opx
C 323-S 47	25	1500	24	11	spl, ol, opx
C 578-S 113 I	25	1500	24	41	spl, ol, opx
C 579-S 113 II	25	1500	24	42	spl, ol, opx
C 685-S 124	15	1500	24	50	spl, ol, opx
C 325-S 49	10	1500	24	11	spl, ol, opx

experimental run conditions and starting material are listed for each experiment. See text for details. P=pressure [kb], T=temperature [°C], t=run duration [hours]. spl=spinel, ol=olivine, opx = orthopyroxene and gar = garnet.

4.3 EXPERIMENTAL RESULTS

Experiments in the system $MgO-Al_2O_3-SiO_2-Cr_2O_3$ were conducted at 1300°C-1500°C and pressures between 5 kb and 54 kb (Table 3). The solubility of alumina in orthopyroxene in equilibrium with spinel and olivine was described by equilibrium (1). As expected from this equilibrium, the addition of Cr to the MAS system lowers the amount of alumina dissolved in the orthopyroxene solid solution at a specified pressure and bulk composition (Figure 2). A similar trend is observed at pressures other than 24 kb. The experimental and thermodynamic results in the Cr-free system (e.g. Gasparik and Newton 1984) indicate that the solubility of alumina in orthopyroxene depends on temperature, resulting in increasing alumina in orthopyroxene with increasing temperature. The same trend is observed in the Cr-bearing system MASCr (Figure 2).

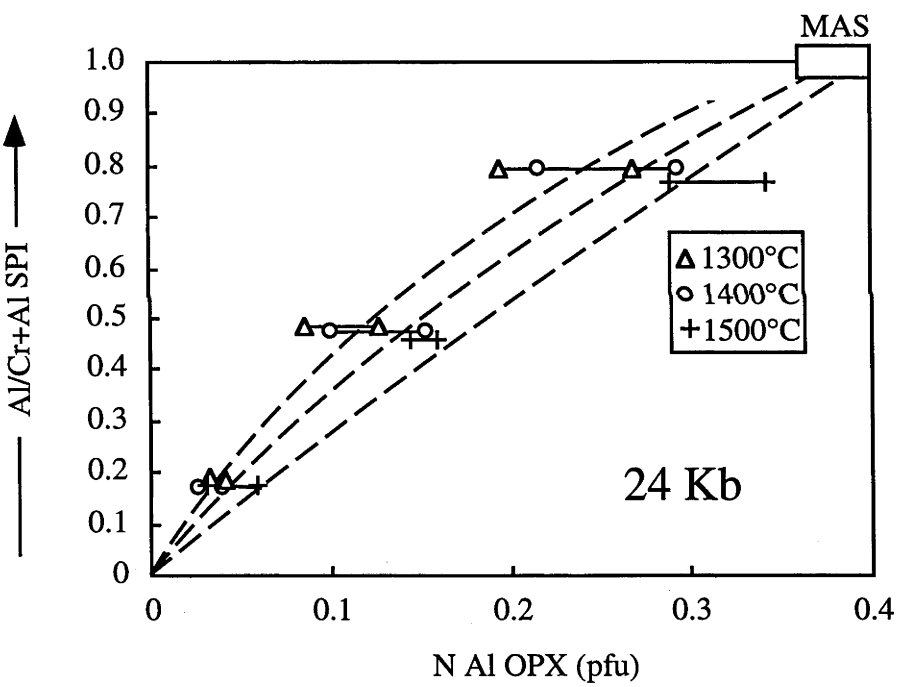

Figure 2 The solubility of alumina in orthopyroxene in equilibrium with spinel and olivine. Depicted are experimental results at 24 kb, experiments at other pressures show similar trends. The symbols indicate maximum and minimum alumina contents in orthopyroxene. Depicted are experiments between 1300°C and 1500°C. The box in the right upper corner indicates experiments in the Cr-free system (MAS) by Gasparik and Newton (1984). The lines are hand-drawn to illustrate the observed trends of the experimental results. (N Al (opx) = alumina content in orthopyroxene per formula unit of six oxygens). At 1300°C and 24 kb garnet is stable in the Cr-free system MAS.

Figure 3 shows results from experiments at 1400°C at pressures between 5 and 54 kb. As Figure 3 shows, however, the reduction of the alumina solubility in orthopyroxene also depends slightly on pressure. The higher the pressure at a constant bulk composition, the more Al_2O_3 is dissolved in the orthopyroxene at a given Al/(Al+Cr) ratio in spinel or, in other words, the lower the equilibrium pressure the higher the reduction of alumina in orthopyroxene at a constant spinel composition relative to the Cr-free system.

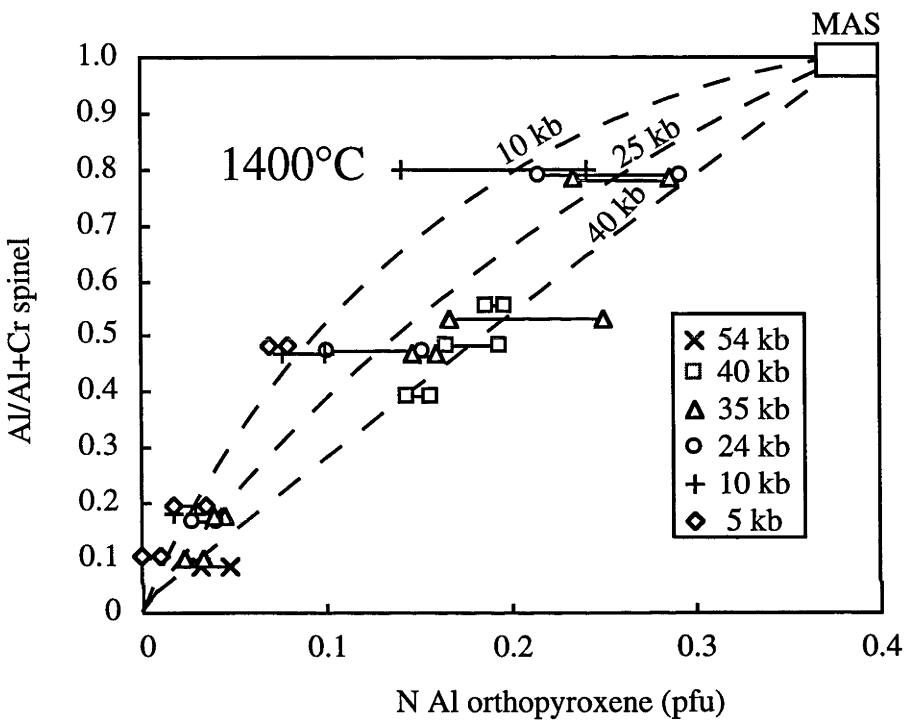

Figure 3 shows experiments in the system MASCr at 1400•C and pressures between 5 and 54 kb. Bars represent uncertainties in mineral composition as determined by electron microprobe. Experiments at other temperatures exhibit similar trends. The amount of alumina solved in orthopyroxene is a function of the coexisting spinel composition and of pressure. The depicted lines are hand-drawn to illustrate the pressure trends. (N Al orthopyroxene pfu = number of cations of Al in orthopyroxene per formula unit of 6 oxygens). The slight pressure effect on the solubility of alumina in orthopyroxene in the Cr-free system MAS is actually opposite to that observed in MASCr. This results in an inversion of the slightly positive slope of the alumina isopleths in orthopyroxene in MAS to a slightly negative slope of the isopleths in relatively Cr-rich compositions.

Equilibrium (2) describes the partitioning of Cr and Al between spinel and orthopyroxene in MASCr. Figures 4 and 5 depict experimental results in MASCr.

Figure 4 depicts the partitioning of Al and Cr between coexisting orthopyroxene and spinel as a function of temperature and a constant pressure. The results indicate the temperature effect on equilibrium (2) is negligible.

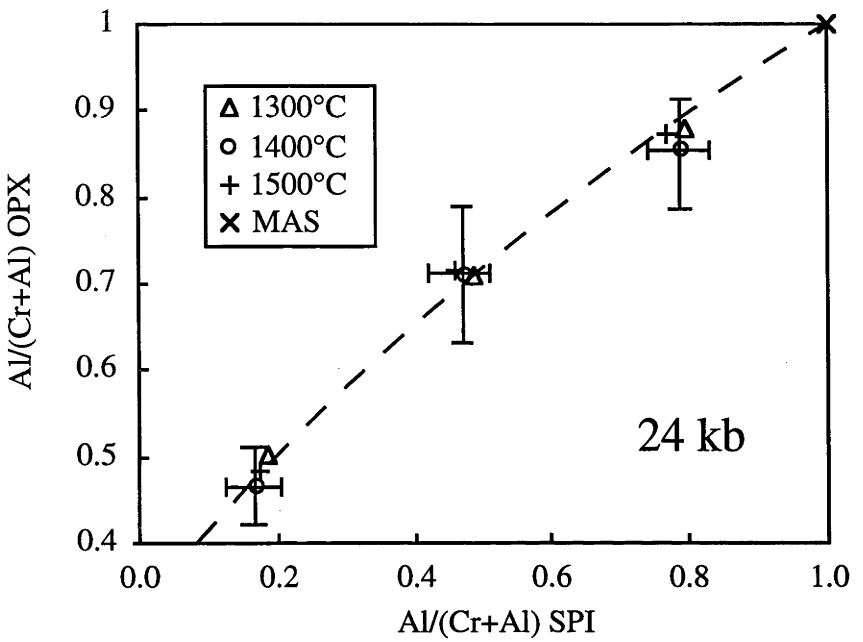

Figure 4: Experimental results at 24 kbars and different temperatures. The cross in the upper right corner depicts compositions in the Cr-free systems. For clarity, only uncertainties for the 1400°C experiments are shown. The line is hand-drawn.

Figure 5 depicts experimental results at a constant temperature, and pressures between 5 and 54 kbars. Within the error margins, no significant pressure effect on equilibrium (2) is observed.

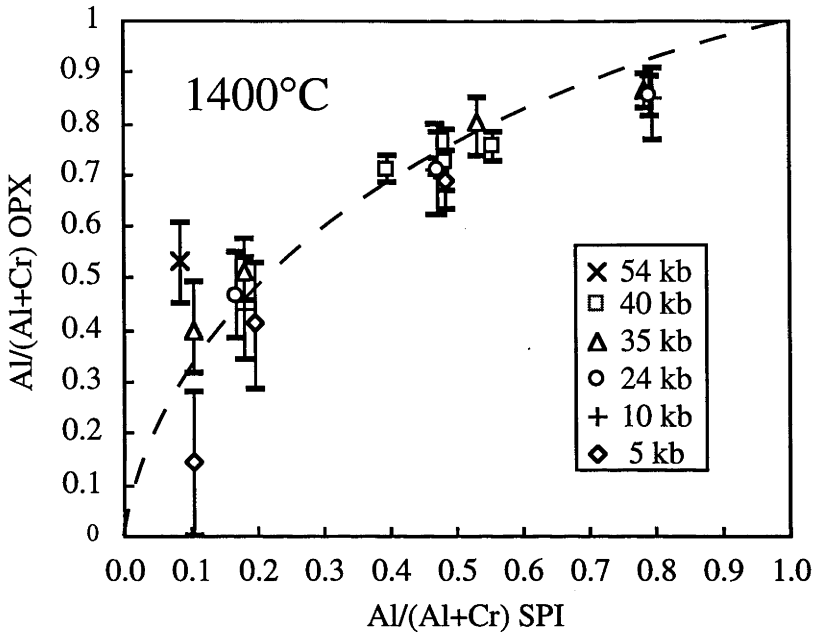

Figure 5: Depicted are experimental results in MASCr at 1400°C and pressures ranging from 5 to 54 kbars. The curve has been hand-drawn. Compositions in the Cr-free system (MAS) lie in the upper right corner. All experiments but two (at 5 and 54 kb) fall onto the curve.

Two experiments in relatively low bulk Cr/(Cr+Al) compositions yielded garnet (S-117-I and S-111-II at 35 kb, 1500°C and 1400°C, respectively). The garnet compositions exhibit a relative large scatter. Taking the uncertainties into account, the garnet composition in both experiments is virtually constant within the error margins with a Cr/(Cr+Al) (garnet) of 0.12 ± 0.03.

4.4 THERMODYNAMIC EVALUATION OF RESULTS

A number of solution models have been proposed to describe the mixing of $Mg_2Si_2O_6$-$MgAl_2SiO_6$ orthopyroxenes in the system MAS (e.g. Wood and Banno 1973; Ganguly and Ghose 1979; Lane and Ganguly 1980). In the most widely used model, Wood and Banno (1973) assumed that half the Al in the orthopyroxene formula unit substitutes for Mg on the M1 octahedral site, with the other half of the Al occupying an adjacent tetrahedral site. Since the substitution of the Al onto the tetrahedral site is completely specified by the octahedral Al, it contributes nothing to the configurational entropy of mixing, which therefore corresponds to one-site mixing. Hence

$a\ (Mg_2Si_2O_6) = 1\text{-}N_{Al}/2$

$a\ (MgAl_2SiO_6) = N_{Al}/2$

where N_{Al} is the number of Al cations per formula unit of 6 oxygens.

In the context of crystal-field theory, Cr^{3+} has the largest excess octahedral site preference energy of any first-row transition cation (Burns 1970; 1975), and is found exclusively in octahedral co-ordination in oxides and silicates (Burns and Burns 1975). Moreover, its ionic radius is considerably larger than that of Al^{3+}. Both these simple crystal-chemical considerations argue that Cr^{3+} should not substitute for Si on the tetrahedral sites of the orthopyroxene structure. Accordingly, a suitable end-member to describe the thermodynamics of Cr^{3+} in orthopyroxenes might, one would suppose, be $MgAlCrSiO_6$, and not $MgCr_2SiO_6$ (e.g., Chatterjee and Terhart 1985).

The results presented here, however, confound this expectation. The most obvious point is that in several runs $N_{Al} < N_{Cr}$ is observed, hence the hypothetical end-member $MgAlCrSiO_6$ cannot account for all the Cr^{3+}. Similarly, Canil and O'Neill (1996) have found $N_{Al} < (N_{Cr}+N_{Fe3+})$ in natural orthopyroxenes.

What is even more unexpected, is that an extremely good fit to the partitioning of Cr^{3+} and Al between orthopyroxene and spinel can be observed if the partitioning reaction is written as:

$$\underset{\text{opx}}{1/2\ MgAl_2SiO_6} + \underset{\text{sp}}{1/2\ MgCr_2O_4} = \underset{\text{opx}}{1/2\ MgCr_2SiO_6} + \underset{\text{sp}}{1/2\ MgAl_2O_4} \quad (2)$$

making the simplest possible assumption, that

$$a\ (MgAl_2SiO_6) = (N_{Al}/2)^2 \qquad \text{and} \qquad a\ MgCr_2SiO_6 = (N_{Cr}/2)^2$$

(i.e., ideal two site mixing of Al and Cr). For all the 37 data points, weighted according to the observed standard deviations, and using a symmetric model for the $Mg(Al,Cr)_2O_4$ solid solution (see below) with $W_{Al\text{-}Cr}$ (sp) = 9739 + 0.0096 P, the following results are obtained for this reaction:

$\Delta H = 19065 \pm 10351$ J mol^{-1}

$\Delta S = 17.1 \pm 5.9$ J mol^{-1}K^{-1}

$\Delta V = -0.154 \pm 0.047$ J bar^{-1}

with a reduced chi-squared for the regression of 0.76. Only two runs are not fitted within two standard deviations of their observed uncertainties (S 126 - 54 kb, S 127-

III 5 kb, see Figure 5). It was also tested to see if including non-ideal terms in the form of a ternary regular solution between $Mg_2Si_2O_6$, $MgAl_2SiO_6$ and $MgCr_2SiO_6$ could improve the fit. No improvement was observed, implying, W_{MC}=0, and W_{EM}=W_{EC} (M = $MgAl_2SiO_6$ MgTs, E = $Mg_2Si_2O_6$ Enstatite, C = $MgCr_2SiO_6$ CrTs).

Moreover, if $W_{Al\text{-}Cr}$ (spinel) is allowed to vary as a parameter in the regression, the $W_{Al\text{-}Cr}$ (spinel) ≈ 10.1 kJ mol^{-1} (on a 1-site basis) is obtained, i.e., in very good agreement with the experimentally determined value (Oka et al. 1984). This kind of agreement is surely indicative that the simple model, unlikely though it may appear from a crystal-chemical perspective, has real validity in a thermodynamic sense.

The next stage of the model-building process is to fit the experimental data along with literature data in the systems MAS, CMAS and NCMAS to a thermodynamic expression for reaction (1). However, here a paradox is encountered. The simple two-site model used so successfully for reaction 2 could not fit these data satisfactorily, even with more complicated excess models. If only the data from the Cr-free systems are to be considered, then although a fair fit, statistically speaking, can be obtained with the two-site model, this is only with an exceptionally large excess mixing term (W_{EM} ~ 200 kJ/mol). Such a large value is both physically unreasonable; more tangibly, it is also grossly inconsistent with the calorimetrically measured heats of mixing in the clinopyroxene join $CaMgSi_2O_6$-$CaAl_2SiO_6$ (Newton et al. 1977), expected to be somewhat similar to the $Mg_2Si_2O_6$-$MgAl_2SiO_6$ orthopyroxenes of interest here. This analogy implies that W_{EM} should be ~ 20 kJ/mol.

In any case, no satisfactory fit with two-site mixing at all could be found when the MAS-Cr data were included. The solution to this paradox is to invoke a model in which there is random mixing of Mg, Al and Cr^{3+} on the M1 site, with complete coupling of (Al+Cr^{3+}) on M1 with (Al+Cr^{3+}) on the tetrahedral sites (i.e., as postulated for one site mixing in the MAS system), but with random mixing of Al with Cr^{3+} on the "associated" tetrahedral site.

The configurational part of the activities are therefore:

$a\ Mg_2Si_2O_6 = (1\text{-}N_{Al}/2\text{-}N_{Cr}/2)$
$a\ MgAl_2SiO_6 = (N_{Al}/2)(N_{Al}/2/(N_{Al}/2+N_{Cr}/2))$
$a\ MgCr_2SiO_6 = (N_{Cr}/2)\ (N_{Al}/2/(N_{Al}/2+N_{Cr}/2))$

This formulation is equivalent to two-site mixing for the ratio a ($MgAl_2SiO_6$) / a ($MgCr_2SiO_6$) in modelling equilibrium (2), while reducing to one-site mixing in the Cr-free system, as required by the data for equilibrium (1). With this model it was possible to fit 97 data from the literature in the systems MAS, CMAS, Na-CMAS and MAS-Cr satisfactory to equilibrium (1) while also fitting the MAS-Cr data to equilibrium (2).

Note that in actuality, tetrahedral Cr^{3+} could be avoided if it is Mg^{2+} which occupies the tetrahedral site, with the Cr^{3+} replacing this Mg on the octahedral site:

$$2\ [6]Mg^{2+} + [4]Si^{4+} = [4]Mg^{2+} + 2\ [6]Cr^{3+}$$

A similar substitution mechanism has been proposed for the Cr^{3+} substitution into the wadsleyite structure (Gudfinnsson and Wood 1998).

4.5 DETAILS OF THE FITTING PROCEDURE

Precise activity-composition relations may in principle be determined from analysis of co-existing solid solutions. Such measurements can only accurately yield the difference in the activity-composition relations, the absolute values of one of the phases should be known independently.

In the present study, the evaluation of the orthopyroxene solid solution depends therefore, critically on the formulation of the spinel solid solution model. The spinel solid solution has been calibrated on the basis of the partitioning of Al and Cr between the $(Al,Cr)_2O_3$ solid solution and the $Mg(Al,Cr)_2O_4$ solid solution (Oka et al. 1984). Oka et al.'s (1984) results, therefore depend of the $(Al,Cr)_2O_3$ solid solution, which has been re-evaluated by Chatterjee et al. (1982) and Chatterjee et al.'s (1982) study is based on the experimental work of Jacob (1978). Appendix A presents a re-evaluation of Jacob's (1978) results, then re-evaluates the thermodynamics of the spinel solid solution. The results presented in Appendix A indicate that both the $(Al,Cr)_2O_3$ and the $Mg(Al,Cr)_2O_4$ solid solution are non-ideal. However, it is difficult to decide whether this non-ideality can be modelled assuming a symmetrical solution, or requires a more complicated, asymmetric approach. Accordingly, two possible models have been investigated:

A a symmetric model for both the $Mg(Al,Cr)_2O_4$ solid solution as well as the $(Al,Cr)_2O_3$ solid solution

B an asymmetric model for both the $Mg(Al,Cr)_2O_4$ solid solution as well as the $(Al,Cr)_2O_3$ solid solution.

Let us now consider the effects of these two differing models A and B for evaluation of equilibria (2) and (1) in the system MASCr.

Equilibrium (2) was fitted to the following equation using 37 data of the present study, weighting the data according to the uncertainties given in Table 4 (at the end of this chapter):

$$0 = \Delta H_2 - \Delta S_2 + \Delta V_2 P + RT \ln\left[\frac{X_{Al}^{sp}}{X_{Cr}^{sp}} \cdot \frac{X_{Cr}^{opx}}{X_{Al}^{opx}}\right] + RT \ln \gamma_{Cr}^{sp} - RT \ln \gamma_{Al}^{sp}$$

For equilibrium (2) and model A for the spinel solid solution (symmetric model) we derive

A ΔG_A (2) = 19065 (10351) - 17.1 (5.9) T - 0.154 (0.047) P

with a reduced chi-squared of 0.76, whilst model B (asymmetric model) for equilibrium (2) yields

B ΔG_B (2) = 21443 (10501) - 18.7 (6.0) T - 0.161 (0.048) P

with a reduced chi-squared of 0.72.

Numbers in brackets indicate the uncertainties of the individual parameters. It is obvious that both the asymmetric model and the symmetric model for the spinel solid solution give very similar results, therefore indicating no significant difference between the simpler symmetric model and the more complicated asymmetric model, the former of which was adopted in the present study.

Equilibrium (1) was also fitted with both the symmetric and the asymmetric model for the spinel solid solution. 97 data of the system MAS (Gasparik and Newton 1984, Dankwerth and Newton 1978), MASCr (this study), CMAS (Gasparik 1984,

Sen 1985, this study) and Na_2O-CMAS (Walter and Presnall 1994) were fitted to the following equation:

$$0 = \Delta H_1 - \Delta S_1 + \Delta V_1 P + T\left[\ln(1 - X_M - X_C) - 2\ln X_M + \ln(X_M + X_C) + 2\ln X_{Cr}^{sp}\right] + 2W_{sp}\left(1 - X_{Al}^{sp}\right)^2 + W^{opx}(X_M + X_C)$$

The data were weighted according to the published uncertainties in mineral compositions (Dankwerth and Newton 1978, Sen 1985, Walter and Presnall 1994, this study (Chapter 1). However, the uncertainties were not given by Gasparik and Newton (1984) and Gasparik (1984), so that uncertainties for N Al opx = 0.005 (Al atoms per formula unit of six oxygens) were assumed.

The two different models resulted in

A a symmetric model for the $MgAl_2O_4$-$MgCr_2O_4$ spinels in conjunction with a symmetric Al_2O_3-Cr_2O_3 model and a W_{Mg-Al}^{opx}= 20 KJ/mol, resulting in the following equation:

ΔG (1) = -19831 (308) - 4.5 (0.2) T - 0.018 (0.007) P

with a reduced chi-squared of 1.93. Numbers in brackets indicate the uncertainties of the individual parameters.

A less good fit was achieved with model B:

B an asymmetric spinel solid solution in conjunction with an asymmetric model for the Cr_2O_3-Al_2O_3 solid solution. With a W^{opx} = 21 KJ/mol the following fitted results were achieved

ΔG (1) = -19638 (299) -4.9 (0.2) T - 0.014 (0.0006)

with a reduced chi-squared of 2.21.

Model A (symmetric spinel and $(Al,Cr)_2O_3$ solid solution) was therefore adopted in the present study to describe both equilibrium (1) and (2).

Poor fits to the equilibrium (1) are S 126 (54 kb), S 127-III (5 kb) in the MASCr system, the same experiments that could not be well fitted with equilibrium (2). One datum of Sen (1985) in the system CMAS does not fit well either (15 kb, 1200°C). Also, the recent experimental results of Gudfinnsson and Presnall (1996) in the system CMAS could not be fitted within their stated uncertainties and were therefore excluded from the fitting procedure. These data differ from the earlier data from the same laboratory of Walter and Presnall (1994), which agree well with the other studies.

4.6 DISCUSSION

In an early experimental study, Dickey and Yoder (1971) investigated the distribution of Cr and Al between coexisting clinopyroxene and spinel in the system CMAS-Cr, focussing on the spinel compositions as a function of temperature above the solidus. Due to short run times spinels were only small (<3 μm) and there were numerous spinel inclusions in clinopyroxene. The experimental results, presented in the Carnegie Institution Yearbook, have not been published in a peer reviewed journal and must, therefore, be regarded as only preliminary results.

Wood (1978) investigated the influence of Cr on the transition from spinel to garnet peridotite in the system MASCr. Evaluation of his experiments lead him to the assumption of ideal two-site mixing of the $MgAl_2O_4$-$MgCr_2O_4$ solid solution. In a subsequent study on the transition in the system CMAS-Cr, O'Neill (1981) postulated a positive deviation from ideality on the binary $MgAl_2O_4$-$MgCr_2O_4$ join. Oka et al. (1984) investigated the partitioning between Cr and Al between the $(Al,Cr)_2O_3$ and the $Mg(Al,Cr)_2O_4$ solid solutions. Their results indeed indicate substantial positive deviations from ideality, in agreement with O'Neill's (1981) early predictions.

Carroll-Webb and Wood (1986) studied the partitioning of Cr and Al between coexisting spinel and sodic clinopyroxene. They performed reversal piston-cylinder experiments at 25 kb and 1100°C (two experiments at 1000°C) on the equilibrium $NaCrSi_2O_6 + 0.5\ MgAl_2O_4 = 0.5\ MgCr_2O_4 + NaAlSi_2O_6$. Caroll-Webb and Wood (1986) also found substantial positive, near symmetric non-ideal mixing in the binary $MgAl_2O_4$-$MgCr_2O_4$ solid solution. They also showed that mixing in $Na(Cr,Al)Si_2O_6$ was approximately ideal, which agrees well with the ideal mixing of the $MgAl_2SiO_6$ and $MgCr_2SiO_6$ components found in this study.

Nickel (1986) investigated equilibria in the system CaO-MgO-Al_2O_3-SiO_2-Cr_2O_3. He focussed on equilibria with coexisting garnet and spinel assemblages. Because of the influence of Ca on the garnet solid solution, his results cannot as yet be compared with results presented here. However, he finds a good positive correlation of the Al/(Al+Cr) ratios of orthopyroxene and spinel (Nickel 1983), indicating no significant pressure or temperature effect on the partitioning of Al and Cr between spinel and orthopyroxenes, in good agreement with results of the present study as illustrated by Figures 4 and 5 and the results from the least squares fitting of equilibrium (2).

The only experiments that could be directly compared with the results of this study are those reported in a recent paper by Doroshev et al. (1997). They investigated the partitioning of Cr and Al between coexisting spinel, orthopyroxene, olivine and garnet in the divariant field of the system MgO-Al_2O_3-SiO_2-Cr_2O_3 where garnet and spinel coexist with orthopyroxene and olivine.

An attempt to fit Doroshev et al.'s (1997) data in conjunction with the present experimental results was not successful. The reason for this might be the large scatter in the orthopyroxene compositions as indicated by Doroshev et al. (1997, p. 570), probably due to short run durations (e.g. only 24 hours at 1400°C as opposed to ca. 120 hours at 1400°C in the present study).

Further comparison of results presented here with data from Doroshev et al. (1997) will be presented in Chapter 6, when a thermodynamic model is calibrated and applied in the system MgO-Al_2O_3-SiO_2-Cr_2O_3.

Geothermometry based on the solubility of alumina in orthopyroxene

Sachtleben and Seck (1981) investigated the applicability of equilibrium (1) on a suite on mantle xenoliths from the West-Eifel, Germany. Their results indicated that apparent temperatures, based on the ideal solid solution model for multicomponent spinels, were correlated with the Cr/(Cr+Al) ratio of co-existing spinels. This observation lead Sachtleben and Seck (1981) to suggest substantial non-idealities for either the spinel or the orthopyroxene solid solution or both. Subsequently to Sachtleben and Seck (1981), experimental and thermodynamic studies (Oka et al. 1984, Carroll-Webb and Wood 1986) have established substantial positive deviation from ideality for spinels on the join $MgAl_2O_4$-$MgCr_2O_4$.

A recent study presents a geothermometric expression, based on equilibrium (1) (Witt-Eickschen and Seck 1991). This formulation (Witt-Eickschen and Seck 1991 - their equation [6]) is empirical, it relies on temperatures derived with the two-pyroxene geothermometer of Brey and Köhler (1990) for calibration of the Al in orthopyroxene temperatures.

A geothermobarometer is conventionally calibrated using high-pressure high-temperature experiments. As natural rocks rarely exhibit exactly the same P-T compositional conditions as the experiments, a rigorous geothermobarometer must enable interpolation between the individual experimental data points as well as extrapolation to different bulk compositions, temperatures and pressures. A *sine qua non* for a valid geothermobarometer is, therefore, the capability to reproduce experimental results in both simple and complex systems. The present experimental results were used to check the applicability of Witt-Eickschen and Seck's (1991) geothermometer in the simple system MASCr.

It is obvious from Figure 6, that Witt-Eickschen and Seck's (1991) formulation does not fulfil these requirements and temperature estimates with Witt-Eickschen and Seck (1991) must be regarded with caution.

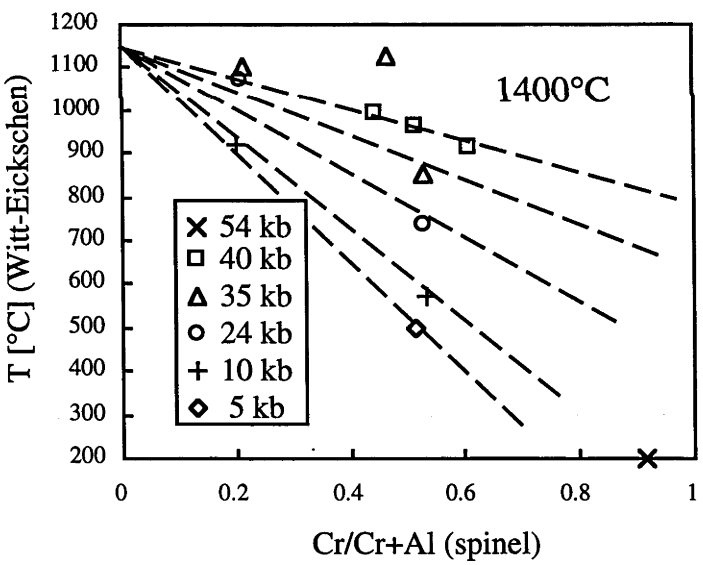

Figure 6: Depicted are experiments at 1400°C in MASCr of the present study, compared to temperature estimates using the empirical geothermometer of Witt-Eickschen and Seck (1991). Witt-Eickschen and Seck's (1991) thermometer does not reproduce experiments in MAS (Gasparik 1984), it also cannot reproduce the present experimental results. Especially at high Cr/(Cr+Al) ratios, Witt-Eickschen and Seck's geothermometer (1991) systematically underestimates the experimental temperatures by several hundred degrees.

Comparison to natural rocks

The present experiments in MASCr suggest that the spinel Cr/(Cr+Al) ratios are controlled by the bulk Cr /(Cr+Al). Natural spinels confirm that the spinel compositions in equilibrium with pyroxenes and olivine is independent of pressure and temperature, but is only controlled by the bulk composition. Figure 7 depicts both spinels in the system MASCr (this study) and spinels from several xenolith suites from alkali basalts. The natural xenoliths exhibit a range of temperatures, but fall onto a trend approximately parallel to the trend observed in the present experiments. The spinels from xenoliths are substantially higher in Cr than expected from the MASCr experiments (e.g. Nickel and Green 1984, Frey and Prinz 1978, Sachtleben and Seck 1981). Similar observations have also been made in massive peridotites (Green 1964, Rampone et al. 1993, Frey et al. 1991). Nickel (1986) observed a similar discrepancy between natural rocks and his experiments in the system CMASCr. He attributed the observed differences to the presence of Fe in natural systems. There are, however, other possible explanations for the observed differences between spinel compositions in the simple system MASCr and natural rocks.

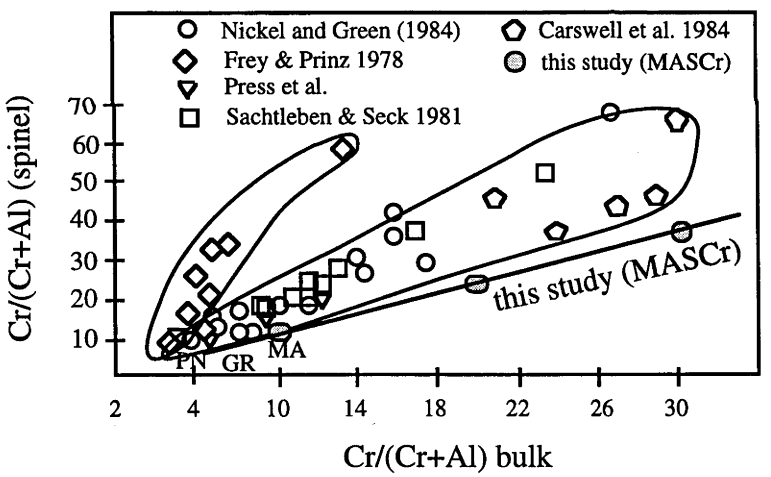

Figure 7: Depicted are spinel analyses from a number of xenoliths suites, compared with spinels of the present study. It is obvious that natural spinels have lower Cr/(Cr+Al) ratios than spinels in the system MgO-Al_2O_3-SiO_2-Cr_2O_3. Diagram drawn after Nickel 1986. Xenolith data are from Nickel and Green 1984, Frey and Prinz 1978, Press et al. 1986, Sachtleben and Seck 1981, Carswell et al. 1984. Also depicted Cr/(Cr+Al) ratios of different primitive mantle estimates (PN = Palme and Nickel 1985), average spinel lherzolite (MA = Maaloe and Aoki 1977) and pyrolite III (GR = Green and Ringwood 1967). San Carlos spinels (Arizona, USA - Frey and Prinz 1978) exhibit a different trend compared to the other xenolith suites presented here.

The presence of plagioclase, especially in orogenic peridotites, will result in more Cr-rich spinels as plagioclase contains virtually only aluminium and no chromium, thus increasing the effective Cr/(Cr+Al) ratio controlling the spinel composition. Amphibole is a common phase in spinel lherzolite, either present as pristine phases (Nickel and Green 1984) or melted during ascent of the xenoliths in the host basalt (Yaxley et al. 1997). Although amphibole is present only in minor modal amounts, the effect of increasing the effective Cr/(Cr+Al) could be substantial, especially if the amphiboles break down and melt during ascent of the xenolith. Recent melting experiments (Falloon et al. submitted, Niida and Green, in press) confirm this observation. These results indicate that with increasing temperature and increasing degree of melting the corresponding spinel becomes more chromium-rich, indicating that the effective Cr/(Cr+Al) ratio increased with the degree of melting.

4.7 CONCLUSIONS

The intention of this study was to derive a thermodynamic model for Cr-bearing pyroxene which could be incorporated into a thermodynamic database that allows calculation of upper mantle equilibria at high pressures and high temperatures. Experiments were conducted in the simple system MgO-Al_2O_3-SiO_2-Cr_2O_3 in the spinel stability field only. Two experiments in relatively low Cr compositions also produced garnet (S-117-I and S-111-II).

The experiments presented here have been used to extract thermodynamic data for Cr-Al bearing pyroxenes. The thermodynamic results are used in conjunction with results in the system MgO-Al_2O_3-SiO_2 (in Chapter 5) and with experimental results in the system MgO-SiO_2-Cr_2O_3 (Irifune et al. 1982) to calibrate a thermodynamic model that enables computation of phase equilibria in the system MgO-Al_2O_3-SiO_2-Cr_2O_3. Chapter 6 will further discuss the experimental results of this study and other studies, while calibrating a thermodynamic model for MASCr.

4.8 TABLE 4 Analytical results

P [kb]	40		25		25		25	
T [°C]	1300		1300		1300		1300	
Cr # (bulk)	50		50		80		20	
	OPX	SPI	OPX	SPI	OPX	SPI	OPX	SPI
	S 38	S 38	S 36	S 36	S 114-I	S 114-I	S 114-II	S 114-II
SiO2	57.1(4)	0.4(2)	57.7(4)	0.5(4)	59.4(7)	0.4(2)	56.6(7)	0.6(1)
Al2O3	3.2(2)	28.1(6)	2.7(5)	28.0(7)	0.9(1)	10.2(8)	5.9(9)	53.0(14)
Cr2O3	1.9(1)	45.8(9)	1.6(2)	45.9(8)	1.4(1)	66.0(7)	1.2(3)	20.5(17)
MgO	37.6(2)	22.8(3)	38.0(3)	22.8(2)	39.1(6)	20.9(3)	37.2(5)	25.8(4)
total	99.9	97.2	100.0	97.2	100.8	97.5	100.9	99.9
Si	1.923(4)	0.012(5)	1.937(14)	0.013(12)	1.976(4)	0.013(5)	1.881(21)	0.014(2)
Al	0.128(7)	0.954(19)	0.106(21)	0.950(23)	0.037(5)	0.374(28)	0.232(37)	1.584(34)
Cr	0.051(1)	1.043(20)	0.043(6)	1.046(19)	0.037(2)	1.626(25)	0.032(7)	0.412(34)
Mg	1.885(4)	0.981(9)	1.902(14)	0.980(6)	1.938(5)	0.974(7)	1.842(24)	0.977(6)
total	3.987(1)	2.990(3)	3.989(2)	2.989(3)	3.987(2)	2.987(2)	3.987(3)	2.988(3)

P [kb]	10		10		10		54	
T [°C]	1300		1300		1300		1400	
Cr # (bulk)	20		80		57		90	
	OPX	SPI	OPX	SPI	OPX	SPI	OPX	SPI
	S 118-I	S 118-I	S 118-II	S 118-II	S101-I	S101-I	S 126	S 126
SiO2	57.2(10)	0.5(1)	59.6(7)	0.4(0)	58.3(6)	0.3(1)	59.3(6)	0.6(1)
Al2O3	4.3(10)	50.6(6)	0.7(2)	11.0(7)	1.3(4)	22.7(30)	0.8(2)	4.6(1)
Cr2O3	1.1(3)	21.4(7)	1.3(2)	64.6(5)	1.2(3)	50.5(28)	1.3(1)	72.1(6)
MgO	38.0(6)	25.5(2)	39.6(5)	20.7(7)	38.5(6)	21.9(5)	39.2(4)	20.4(4)
total	100.5	98.0	101.3	96.8	99.3	95.4	100.6	97.7
Si	1.909(24)	0.013(1)	1.975(5)	0.012(2)	1.969(11)	0.010(2)	1.978(7)	0.020(2)
Al	0.168(40)	1.549(14)	0.027(7)	0.407(21)	0.053(16)	0.802(87)	0.040(8)	0.171(4)
Cr	0.028(7)	0.440(14)	0.035(6)	1.598(30)	0.032(7)	1.199(86)	0.035(4)	1.820(17)
Mg	1.887(27)	0.990(3)	1.957(13)	0.967(21)	1.936(16)	0.980(9)	1.947(13)	0.973(17)
total	3.993(7)	2.992(1)	3.994(5)	2.985(7)	3.989(6)	2.990(3)	3.990(6)	2.984(5)

P [kb]	40		40		40		35	
T [°C]	1400		1400		1400		1400	
Cr # (bulk)	50		46		57		50	
	OPX	SPI	OPX	SPI	OPX	SPI	OPX	SPI
	S 104-I	S 104-I	S 104-II	S 104-II	S 104-III	S 104-III	S 37	S 37
SiO2	57.1(11)	0.4(1)	55.7(4)	0.7(2)	56.6(7)	0.6(4)	56.7(15)	0.5(2)
Al2O3	4.6(4)	29.8(16)	4.9(2)	33.8(66)	3.8(2)	22.9(17)	3.9(1)	28.0(8)
Cr2O3	2.6(6)	47.2(16)	2.3(3)	39.8(70)	2.3(2)	52.4(18)	2.3(1)	47.0(11)
MgO	38.1(6)	23.9(2)	36.9(8)	23.9(10)	37.7(4)	22.3(6)	37.5(4)	23.2(3)
total	102.4	101.3	99.8	98.2	100.3	98.2	100.4	98.7
Si	1.878(21)	0.012(4)	1.879(8)	0.019(5)	1.896(7)	0.018(10)	1.901(15)	0.014(5)
Al	0.180(15)	0.968(45)	0.193(6)	1.103(176)	0.151(7)	0.788(47)	0.154(8)	0.937(26)
Cr	0.068(15)	1.028(39)	0.063(8)	0.880(176)	0.061(4)	1.208(57)	0.061(2)	1.055(25)
Mg	1.871(6)	0.981(5)	1.859(19)	0.988(9)	1.890(9)	0.970(12)	1.876(20)	0.984(7)
total	3.998(7)	2.990(2)	3.993(9)	2.990(3)	3.998(4)	2.984(6)	3.992(11)	2.990(2)

P [kb]	35		35			35		35	
T [°C]	1400		1400			1400		1400	
Cr # (bulk)	80		20			46		90	
	OPX	SPI	OPX	SPI	GAR	OPX	SPI	OPX	SPI
	S 111-I	S 111-I	S 111-II	S 111-II	S 111-II	S 123-I	S 123-I	S 123-II	S 123-II
SiO2	59.3(2)	0.5(0)	55.5(10)	0.6(1)	43.9(12)	55.9(7)	0.6(1)	59.7(6)	0.4(1)
Al2O3	1.0(1)	9.7(4)	6.6(7)	50.8(13)	23.1(5)	5.4(8)	32.1(7)	0.7(1)	5.6(3)
Cr2O3	1.5(3)	66.8(13)	1.5(3)	20.7(13)	4.0(8)	2.0(3)	42.2(6)	1.6(3)	72.8(25)
MgO	37.9(5)	20.4(4)	36.1(8)	24.9(4)	29.4(5)	38.7(56)	23.7(3)	39.8(5)	21.7(13)
total	99.7	97.3	99.8	97.1	100.3	101.9	98.6	101.8	100.5
Si	1.992(11)	0.014(1)	1.867(18)	0.016(2)	2.973(75)	1.853(74)	0.015(2)	1.969(9)	0.013(3)
Al	0.041(3)	0.358(15)	0.262(27)	1.567(27)	1.842(33)	0.209(33)	1.057(15)	0.028(5)	0.203(16)
Cr	0.040(7)	1.655(19)	0.041(8)	0.429(27)	0.215(43)	0.052(8)	0.933(19)	0.042(8)	1.780(26)
Mg	1.895(15)	0.951(11)	1.812(33)	0.973(2)	2.968(66)	1.902(164)	0.985(8)	1.956(8)	1.001(34)
total	3.968(8)	2.979(4)	3.982(12)	2.986(1)	7.999(47)	4.016(79)	2.990(3)	3.996(4)	2.996(12)

P [kb]	24		24		24		20	
T [°C]	1400		1400		1400		1400	
Cr # (bulk)	50		20		80		80	
	OPX	SPI	OPX	SPI	OPX	SPI	OPX	SPI
	S 22	S 22	S 115-I	S 115-I	S 115-II	S 115-II	S 116-I	S 116-I
SiO2	58.0(8)	0.7(3)	56.0(8)	0.7(1)	59.9(5)	0.4(1)	59.0(3)	0.4(0)
Al2O3	3.2(7)	28.0(3)	6.5(10)	51.8(15)	0.9(2)	9.4(4)	1.1(2)	10.1(2)
Cr2O3	2.0(3)	46.4(3)	1.6(3)	20.9(18)	1.5(2)	67.7(9)	1.6(2)	65.7(1)
MgO	37.9(4)	23.2(3)	36.5(4)	25.4(3)	38.8(6)	20.6(5)	38.6(3)	21.0(0)
total	101.1	98.4	100.7	98.9	101.1	98.2	100.3	97.1
Si	1.926(20)	0.021(10)	1.869(26)	0.017(1)	1.985(8)	0.012(3)	1.973(4)	0.013(1)
Al	0.127(26)	0.939(12)	0.255(38)	1.569(38)	0.034(6)	0.345(13)	0.042(9)	0.373(6)
Cr	0.052(9)	1.044(9)	0.043(7)	0.426(37)	0.039(6)	1.667(14)	0.042(4)	1.624(5)
Mg	1.879(17)	0.984(8)	1.814(19)	0.974(4)	1.920(14)	0.958(9)	1.927(11)	0.978(4)
total	3.984(6)	2.988(3)	3.982(5)	2.986(1)	3.978(6)	2.982(2)	3.985(2)	2.988(2)

P [kb]	20		10		10		10	
T [°C]	1400		1400		1400		1400	
Cr # (bulk)	20		50		20		80	
	OPX	SPI	OPX	SPI	OPX	SPI	OPX	SPI
	S 116-II	S 116-II	S 50	S 50	S 112-I	S 112-I	S 112-II	S 112-II
SiO2	56.1(7)	0.6(1)	58.7(7)	0.5(3)	56.4(13)	0.5(1)	57.6(7)	0.3(0)
Al2O3	5.7(9)	50.4(11)	2.2(3)	27.6(7)	4.8(12)	51.3(39)	0.5(2)	9.7(2)
Cr2O3	1.3(1)	22.2(17)	1.4(4)	46.9(7)	1.3(3)	19.4(43)	1.1(1)	65.3(5)
MgO	36.7(3)	25.4(2)	38.6(2)	23.1(2)	37.0(10)	24.5(6)	37.7(5)	19.9(1)
total	99.9	98.6	100.9	98.2	99.4	95.8	96.8	95.2
Si	1.885(20)	0.016(2)	1.950(14)	0.015(8)	1.901(32)	0.014(3)	1.990(7)	0.010(1)
Al	0.227(34)	1.539(32)	0.088(11)	0.929(20)	0.192(50)	1.597(93)	0.021(6)	0.367(4)
Cr	0.035(3)	0.454(35)	0.036(11)	1.061(20)	0.034(9)	0.407(94)	0.029(4)	1.653(3)
Mg	1.836(11)	0.979(3)	1.914(16)	0.984(4)	1.860(38)	0.966(7)	1.945(25)	0.950(6)
total	3.984(3)	2.988(1)	3.988(8)	2.99(3)	3.986(13)	2.984(3)	3.985(10)	2.980(2)

P [kb]	5		5		5		35	
T [°C]	1400		1400		1400		1500	
Cr # (bulk)	80		90		46		50	
	OPX	SPI	OPX	SPI	OPX	SPI	OPX	SPI
	S 122 I	S 122 I	S 127-I	S 127-I	S 127-III	S 127-III	S 51	S 51
SiO2	59.2(8)	0.4(0)	60.2(9)	0.4(1)	59.1(2)	0.4(1)	55.0(4)	0.5(1)
Al2O3	0.7(2)	10.7(2)	0.2(0)	5.7(3)	1.9(1)	28.7(13)	5.3(3)	29.4(7)
Cr2O3	1.4(2)	65.3(5)	1.1(1)	72.3(6)	1.3(2)	45.6(18)	2.9(2)	44.9(8)
MgO	39.2(5)	21.0(4)	39.8(6)	20.9(5)	39.3(3)	23.0(1)	36.9(1)	23.4(1)
total	100.5	97.4	101.3	99.4	101.6	97.8	100.0	98.2
Si	1.978(9)	0.012(1)	1.992(4)	0.013(4)	1.952(8)	0.012(2)	1.857(12)	0.015(2)
Al	0.026(9)	0.391(6)	0.005(5)	0.210(6)	0.075(4)	0.967(43)	0.211(12)	0.983(20)
Cr	0.037(6)	1.609(10)	0.029(3)	1.788(18)	0.033(6)	1.030(39)	0.076(6)	1.005(20)
Mg	1.949(7)	0.976(8)	1.964(5)	0.977(15)	1.934(8)	0.980(5)	1.856(8)	0.988(3)
total	3.990(4)	2.988(0)	3.991(2)	2.988(5)	3.994(5)	2.989(1)	4.000(5)	2.991(1)

P [kb]	35			35		25		25	
T [°C]	1500			1500		1500		1500	
Cr # (bulk)	20			80		50		80	
	OPX	SPI	GAR	OPX	SPI	OPX	SPI	OPX	SPI
	S 117-I	S 117-I	S 117-I	S 117-II	S 117-II	S 47	S 47	S 113-I	S 113-I
SiO2	55.4(7)	0.8(1)	43.7(1)	58.4(6)	0.6(1)	56.5(1)	0.7(1)	59.3(5)	0.5(1)
Al2O3	6.9(7)	47.0(34)	21.3(4)	1.2(3)	10.0(1)	3.9(2)	26.8(2)	1.2(4)	9.4(2)
Cr2O3	1.8(3)	24.9(38)	4.5(8)	2.0(5)	65.3(3)	2.3(1)	47.2(4)	1.8(3)	67.2(12)
MgO	36.0(3)	24.9(5)	29.6(8)	38.2(7)	21.0(2)	38.2(2)	23.4(1)	37.5(3)	20.3(8)
total	100.1	97.6	99.5	99.7	96.9	100.8	98.0	99.9	97.4
Si	1.859(19)	0.021(2)	3.004(17)	1.966(11)	0.019(2)	1.889(4)	0.020(3)	1.991(11)	0.016(3)
Al	0.271(28)	1.463(84)	1.728(20)	0.047(11)	0.368(4)	0.152(8)	0.904(10)	0.046(14)	0.349(7)
Cr	0.048(8)	0.522(86)	0.245(43)	0.053(13)	1.618(5)	0.061(2)	1.070(5)	0.049(8)	1.665(14)
Mg	1.803(14)	0.982(3)	3.034(56)	1.918(26)	0.982(6)	1.902(7)	0.999(1)	1.877(13)	0.948(21)
total	3.982(5)	2.987(1)	8.010(23)	3.984(10)	2.988(2)	4.004(3)	2.993(1)	3.962(3)	2.977(8)

P [kb]	25		15		10	
T [°C]	1500		1500		1500	
Cr # (bulk)	20		90		50	
	OPX	SPI	OPX	SPI	OPX	SPI
	S 113-II	S 113-II	S 124	S 124	S 49	S 49
SiO2	55.0(6)	0.7(1)	60.2(4)	0.4(0)	57.3(8)	0.6(1)
Al2O3	8.0(7)	49.6(7)	0.4(2)	5.2(4)	2.8(8)	27.4(13)
Cr2O3	1.7(2)	22.1(2)	1.6(2)	72.8(4)	2.0(4)	46.5(11)
MgO	35.1(5)	24.8(4)	39.5(2)	20.6(2)	38.5(5)	23.1(2)
total	99.8	97.2	101.6	99.0	100.6	97.6
Si	1.849(15)	0.019(2)	1.986(7)	0.014(1)	1.918(22)	0.017(4)
Al	0.316(27)	1.536(4)	0.014(7)	0.191(14)	0.111(32)	0.929(38)
Cr	0.045(5)	0.459(6)	0.041(5)	1.813(16)	0.052(10)	1.056(33)
Mg	1.759(18)	0.971(4)	1.946(7)	0.966(5)	1.919(21)	0.988(4)
total	3.970(4)	2.984(1)	3.987(3)	2.984(1)	4.000(4)	2.990(2)

Cr# [bulk] = Cr/(Cr+Al) in starting material. T=temperature in [°C]. P = pressure in [kb]. Numbers show average analyses for each phases, numbers in brackets indicate uncertainties. For example, 1.759(18) must be read as 1.759 ± 0.018). At least 10 analyses were done for each phase in every experiment. some notes on totals: Analyses of spinels yielded totals systematically lower than 100, although the structural values indicate high quality analyses. Low totals can be caused by beam current fluctations during the analyses. Another possibility to explain low totals in spinels might be lower conductivity of $Mg(Cr,Al)_2O_4$ spinels relative to orthopyroxene (Ware, pers. comm.) the latter of which yielded higher totals on average. Because of the strongly differing hardness of spinel, opx and olivine, polishing of the experimental specimens often resulted in proud spinel slightly sticking out of the surface. Proud minerals usually yield higher totals, as exited X-rays are less subject to attenuation on the way out of the sample into the detector. However, lower conductivity of the spinel would, in fact, counteract this effect, thus resulting in lower totals.

CHAPTER 5

Thermodynamic modelling in the system $CaO\text{-}MgO\text{-}Al_2O_3\text{-}SiO_2$

5.1 INTRODUCTION

This chapter describes the optimisation of an internally consistent set of thermodynamic data for compositions in the system $CaO\text{-}MgO\text{-}Al_2O_3\text{-}SiO_2$ using the new experimental results at high temperatures and high pressures described in the first chapter as well as experimental results from the literature. A computer algorithm, based on free energy minimisation techniques, is used for the computation of phase equilibria.

This chapter begins with an introduction, followed by a short summary of the thermodynamic background and the thermodynamic data required for phase equilibria calculation. Then the strategy of the calibration of the thermodynamic model will be presented, followed by a short section that briefly explains the principles of the numerical algorithm used for computing phase equilibria. A detailed description of the actual calibration procedure of the thermodynamic model is then presented. Finally, some tests of the thermodynamic model are presented, where equilibria were calculated that were not used for calibration.

Thermodynamic Modelling In Geologically Relevant Systems

To compare experimental results with other studies and to extrapolate experimental results in pressure-temperature-compositional space, thermodynamic modeling has found widespread application in geology.

The development of internally consistent databases (e.g. Berman 1988, Holland and Powell 1990, 1998; Gottschalk 1997 and most recently, Chatterjee et al. 1998) has been a major advance in thermodynamic modelling. These datasets are usually derived from a simultaneous treatment of numerous experimental results as well as results from calorimetric studies, using mathematical programming or least

squares techniques (Berman 1988, Holland and Powell 1990). Internal consistency is maintained by correcting either the entropy or enthalpy only or several parameters simultaneously. The main purpose of these internally consistent databases was to derive a internally consistent database for mineral endmembers, intended to facilitate equilibrium calculations for crustal rocks under moderate pressures and temperatures.

Contrastingly, this study intends to develop a model for subsolidus equilibria in the part of the system CaO-MgO-Al_2O_3-SiO_2 that is relevant for phase assemblages of the upper mantle. This has been done before (e.g. Wood and Holloway 1984), so the objective of this study was to use existing internally consistent data (here: Holland and Powell 1990) and investigate the applicability of these datasets at mantle conditions, but more importantly, investigate solid solutions of CMAS minerals that are consistent with experimental and thermodynamic results presented in the other chapters of this thesis.

As a starting point for the investigations in CMAS, the database of Holland and Powell (1990) was chosen. [1]

5.2 FREE ENERGY MINIMISATION

For computation of phase equilibria in pressure-temperature-compositional space a free energy minimisation algorithm is used in this study, which is outlined only briefly here. The objective is to perform calculations of several multi-site solid solutions and numerous end members. This is achieved by minimising the Gibbs free energy under mass balance and positivity constraints. Specifically we formulate the problem as the minimisation of,

$$G = \sum_{i,\alpha} \mu_i^{\alpha} n_i^{\alpha}$$

subject to mass balance constraints for each phase α (α=1,...)

$$\sum_{i} n_i^{\alpha} z_i^{\alpha} = N^{\alpha},$$

[1] A more recent version of this database (Holland and Powell 1998) which was only available on the internet when this chapter was written, includes more minerals and is based on more recent experiments. However, in the part of the system CMAS relevant for the upper mantle, the new database does not include significant changes to the 1990 database.

and positivity constraints,

$$n_i^\alpha \geq 0,$$

where μ_α^i is the chemical potential of component i in phase α, z_α^i are the stoichiometry factors, N^α is the total number of moles of phase α in the system, and n_i^α is the number of moles of component i in phase α. These are the unknowns whose values are sought such that G is minimised under the linear equality and inequality constraints. Many methods have previously been proposed for solving this problem. Usually they are based on simple gradient descent methods (e.g. Wood and Holloway 1984) or quasi-Newton methods (e.g. Ghiorso 1985). However these methods are not directly suited to non-linear (equality and inequality) constrained optimisation problems and so the problem is usually recast into a more suitable form. For example, the variables may be transformed to impose positivity constraints (as in, Wood and Holloway, 1984) or the problem may be reformulated into a coupled set of simpler optimisation problems (as in De Capitani and Brown 1987).

Constrained optimisation problems of this kind are much studied problems in the field of computational mathematics. All such transformations of the problem are avoided in this study by making use of a `Feasible iterate sequential quadratic programming' method (FFSQP) which is specifically designed for general constrained optimisation problems of this kind. The implementation of Zhou, Tits and Lawrence (1998) is used in this study, based on the algorithm of Panier and Tits (1993). The method is numerically robust, has super-linear convergence and makes use of modern automatic differentiation techniques, which means that it may be used with any type of expressions linking chemical potential, μ_α^i, to molar variables, n_i^α.

With FFSQP multiple minima in the Gibbs free energy can only be detected by re-starting from a different initial guess for the molar variables, however no multiple minima have been encountered in the cases considered here. Bina (1998) has presented a simulated annealing algorithm aimed at dealing with this case.

5.3 THERMODYNAMIC BACKGROUND

A chemical system may be described in terms of endmembers. Conventionally, for geologically relevant systems, a sufficient number of mineral endmember components are chosen to represent the entire chemical system. The stability of a mineral endmember component as a function of pressure, temperature and composition either as a pure phase or as a component in a solid solution can be entirely described with its chemical potential. The chemical potential of a component i in a phase α is defined as $\mu_i^{\alpha,*} \equiv \left[\frac{\partial (\ G)}{\partial n_i}\right]_{T,P,n_{j(j\neq i)}}$, where the * indicates conditions at elevated pressures and temperatures and n_j indicates the numbers of moles of all other components than i, $n_j \neq n_i$.

Considering mixing of several components in a solid solution, the chemical potential of the component i in phase α may be rewritten as

$$\mu_i^{\alpha,*} = \mu_i^{\alpha,0} + n\ RT \ln a_i = \mu_i^{\alpha,0} + n\ RT \ln X_i + n\ RT \ln \gamma_i \qquad (1)$$

ideal non-ideal

where the activity a_i of component i in phase α is defined as follows: $a_i \equiv X_i \cdot \gamma_i$. X_i denotes the molar fraction of component i in the phase and γ_i, the activity coefficient, corrects for interaction of the different components in the phase. This formulation can be seen as consisting of a pure component part, represented by the standard chemical potential $\mu_i^{\alpha,0}$, and a term that accounts for mixing of the components in a phase ($nRT\ln X_i + n\ RT\ln\gamma_i$). The $nRT\ln X_i$ term describes ideal mixing whilst the $n\ RT\ln\gamma_i$ term describes deviation from ideality.

The standard chemical potential $\mu_i^{\alpha,0}$, describing the pure component, may then be expanded into the following expression:

$$\mu_i^{\alpha,0} = \Delta_f H^0_{298} - T\ S^0_{298} + \int_{298}^{T} C_P^0(T)\,dT - \int_{298}^{T} \frac{C_P^0(T)}{T}\,dT + \int_{1}^{P} V_{T,i}(P)\ dP$$

where the latter term is approximated in the Holland and Powell (1990) model by:

$$\int_1^P V_{T,i}(P)\,dP = \left[V^0_{298} + \alpha V(T-298)\right] P - \frac{\beta V}{2} P^2$$

To characterise fully the chemical potential of a component in a chemical system at room temperature and atmospheric pressure, the standard thermodynamic data as $S°_{298}$, $\Delta_f H°_{298}$ and $V°_{298,1}$ must be known. To account for elevated temperatures and pressures, the heat capacity function (C_P (T)) as well as coefficients of thermal expansion α and thermal compressibility ß are also required. If a phase is not pure, suitable corrections for mixing (i.e. activity coefficients) of the components in a phase may be introduced.

Solid Solutions

Simple crystalline solid solutions (Chatterjee 1991) consist of a solid solution that contains as many components as mineral endmembers. The free energy of such a simple crystalline solution (Chatterjee 1991) is defined as

$$G = \underbrace{\sum_i X_i \mu_i^*}_{G^{mech}} + \underbrace{n\,RT \ln \sum_i X_i \ln X_i}_{G^{ideal}_{mix}} + \underbrace{n\,RT \ln \sum_i X_i \ln \gamma_i}_{G^{non-ideal\ (excess)}_{mix}} \qquad (4)$$

where n denotes the number of sites in the sublattice (site-multiplicity factor). The first term on the right hand side of the equation refers to the free energy of the endmembers (mechanical mixing), whereas the second and the third term refer to ideal and non-ideal chemical mixing, respectively.

For the predominantly ionic solutions of interest to this study, the excess mixing properties can be thought of as stemming from two effects,

1 mixing of different cations on the same crystallographic site, and
2 interactions between sites, or the "reciprocal solid solution effect".

Note that for simplicity order-disorder effects will not be considered here.

Mixing of different cations of the same site

The non-ideal G_{mix} term in equation (4) can be understood as the difference between the actual properties of the solid solution and the ideal solution. Classical

thermodynamics do not provide theoretical insight in the relation between ideal and observed solutions, but empirically formulated solution models have been very successful to reproduce experimental results. There are numerous ways of representing thermodynamic functions as power series (see e.g. Fei et al. 1986), the most popular among geochemist are the Margules-formulation (e.g. Margules 1895, Thompson 1967) and the Redlich-Kister model (Redlich and Kister 1948).

The *Redlich-Kister* model uses the following power series

$Z^{ex} = X_A^{ss}\left(1 - X_A^{ss}\right) \sum_{n=0}^{N} A_n^Z \left(2X_A^{ss} - 1\right)^n$, where Z^{ex} is any of the molar thermodynamic excess functions (G^{ex}, H^{ex}, V^{ex} etc), N the total number of adjustable parameters and X_A^{ss} is the mole fraction of of component A in the solid solution.

The expansion to partial molar quantities gives (e.g. Pownceby and O'Neill 1994 a) for component A:

$$RT \ln \gamma_A = \left(1 - X_A^{ss}\right)^2 \left[A_0^Z + A_1^Z \left(4X_A^{ss} - 1\right) + A_2^Z \left(2X_A^{ss} - 1\right)\left(6X_A^{ss} - 1\right) ...\right]$$

Note that the symmetric solution model corresponds to use of the first term only, whilst the asymmetric model corresponds to the first two terms (i.e. A_0 and A_1).

The *Margules model* uses the following truncated power series (Chatterjee 1991):

$Z^{ex} = (1\text{-}X_B)X_A\ [W_{Z,BA} + (W_{Z,AB}\text{-}W_{Z,BA})(X_2)]$.

The expansion to partial molar quantities gives (Chatterjee 1991) for component A

$$RT \ln \gamma_A = \left[W_{G,AB} + 2\left(W_{G,BA} - W_{G,AB}\right)X_A\right]\left(1 - X_A\right)^2$$

where the W_G's are the socalled Margules parameters. Solutions employing the two-parameter Margules equation are asymmetric solutions. Within the uncertainties of measurements, $W_{G,AB}$ and $W_{G,BA}$ are sometimes indistinguishable, resulting in $W_G = W_{G,AB} = W_{G,BA}$. The resulting one parameter Margules equations are called symmetric

solutions. The temperature and pressure dependency of the Margules parameter W_G is defined as follows: $W_G = W_H - TW_S + PW_V$

This study uses a general equation developed by Helffrich and Wood (1989), based on the Margules-model. This general equation expands to multicomponent solid solutions, but also reduces to simple binary symmetrical solutions.

The reciprocal solid solution effect

A different situation is encountered when a crystalline solid solution consists of more endmembers than necessary components (complex crystalline solutions). For example, in the crystalline solution $(A,B)^{n1}(X,Y)^{n2}$ R, cations A and B mix on lattice site 1 and cations X and Y mix independently on lattice site 2. R is the anionic rest of the chemical formula, and n1 and n2 are the site-multiplicity factors. This solid solution consists of four endmembers AX, AY, BX and BY, but only three of them are necessary to fully characterise the solid solution, because they are related to each other by the reciprocal reaction

$$AY + BX = BY + AX. \qquad (5)$$

Because of this relationship these complex crystalline solid solutions are also called 'reciprocal solid solutions' as described in detail by Wood and Nicholls (1978).

For example, following Wood and Nicholls (1978, p.391) the chemical potential for the component AX may be written as follows:

$$\mu_{AX} = \mu^*_{AX} + RT\left[(X_A)^{n1}(X_X)^{n2}\right] - X_B X_Y \Delta G^*_{rec} \qquad (6)$$

where the last term on the right hand side describes non-ideality of the reciprocal reaction (5) and ΔG_{rec} denotes the energy change of the reciprocal reaction (5). Comparison with equation (1) indicates the $RT\ln\gamma_{REC} = -X_B X_Y \Delta G^*_{REC}$. Expressions for the other components are described in Wood and Nicholls (1978, p.391).

Further non-ideality might arise due to non-ideal mixing on the individual sites in the lattice. These additional non-ideality might be introduced into equation (6) in the following manner:

$$\mu_{AX} = \mu^*_{AX} + RT\left[(X_A\gamma_A)^{n1}(X_X\gamma_X)^{n2}\right] - X_B X_Y \Delta G^*_{rec} \qquad (7)$$

Molar Volumes and Heat Capacities

Molar volumes of solid mineral endmember components are often well known from X-ray diffraction studies. The coefficients of thermal expansion α are also approximately known for many phases, and have been compiled with data for compressibility in the databases of Holland and Powell (1990) and Berman (1988). In this study thermal expansion coefficients (α) and compressibility coefficients (ß) were adopted from Holland and Powell (1990). It has to be noted, however, that the simple formulation of thermal expansivity α and compressibility ß is rather naive, but it will be shown later that the simple formulation used here is able to reproduce experimental results quite well.

Heat capacities are given in this chapter in the following general form:

$$C_P = a + bT + cT^{-2} + dT^{-½} + eT^{-3} + fT^3 + gT^{½}$$

The formulation presented here combines the conventional formulation by Haas and Fisher (1976) and the heat capacity functions proposed by Berman and Brown (1985). The extrapolation of heat capacities to higher temperatures than the calorimetric data is very problematic. Berman and Brown (1985) claim their formulation of the Cp-functions enables extrapolation for Cp-functions to higher temperatures, it does not, however, satisfactorily reproduce Cp-curves of phases that undergo a rapid increase in the heat capacity caused by a lambda transition. Berman and Brown's (1985) heat capacity functions also fails to reproduce the pre-melting behaviour of some minerals close to the melting point. In a conservative approach, this study uses a heat capacity function based on Holland and Powell (1990), using only the coefficients a, b, c and d. The Cp-data used here are listed in Table 3 at the end of this chapter.

5.4 CALIBRATION OF THE THERMODYNAMIC MODEL: CRITERIA AND PROCEDURES

For the calibration of the thermodynamic model, reversal experimental studies were preferred to synthesis experiments, as the attainment of equilibrium can only be rigorously assessed in the former studies. Well documented studies with detailed descriptions of the experimental procedures and with estimated analytical uncertainties were also preferred for calibration.

Starting the calibration procedure in a simple sub-system as e.g. CAS (CaO-Al_2O_3-SiO_2) simple univariant reactions were investigated establishing the endmember properties of mineral endmember components relative to each other. Doing that, care was taken not to violate calorimetric measurements for the individual mineral endmembers. In more complex systems such as MAS (MgO-Al_2O_3-SiO_2) and CMS (CaO-MgO-SiO_2), some mineral phases form solid solutions. The best models to account for these solid solutions were investigated on a trial and error basis aiming at finding a model that satisfactorily reproduces the selected experimental results. This procedure in not quite as elegant as e.g. linear programming techniques. It does, however, lead to the same results and the procedures itself provide detailed insight into the effects of thermodynamic properties on the stability of phases in P-T-compositional space.

TABLE 1 minerals and endmember components

mineral	endmember component	chemical formula
olivine	forsterite	Mg_2SiO_4
	monticellite	$CaMgSiO_4$
feldspar	anorthite	$CaAl_2Si_2O_8$
spinel	spinel	$MgAl_2O_4$
garnet	grossular	$Ca_3Al_2Si_3O_{12}$
	pyrope	$Mg_3Al_2Si_3O_{12}$
orthopyroxene	ortho-diopside (o-Di)	$CaMgSi_2O_6$
	enstatite (En)	$Mg_2Si_2O_6$
	magnesio-tschermak (MgTs)	$MgAl_2SiO_6$
	ortho-calcio-tschermak (o-CaTs)	$CaAl_2SiO_6$
clinopyroxene	diopside (o-Di)	$CaMgSi_2O_6$
	clino-enstatite (c-En)	$Mg_2Si_2O_6$
	clino-magnesio-tschermak (c-MgTs)	$MgAl_2SiO_6$
	calcio-tschermak (CaTs)	$CaAl_2SiO_6$
kyanite		Al_2SiO_5
sillimanite		Al_2SiO_5
α-quartz		SiO_2
ß-quartz		SiO_2
corundum		Al_2O_3

As a starting point in the calibration procedure endmember data from Holland and Powell (1990) were used. In the proceeding of the calibration some thermodynamic data for pure endmember phases had to be slightly adjusted (c.f. Table 3 in the end of this chapter). It was opted only to adjust $S°_{298}$ and $\Delta_f H°_{298}$, heat capacity functions, volumes and coefficients of thermal expansion and compressibility were left unchanged.

In a relative simple system such as CMAS, the endmember properties such as e.g. forsterite, enstatite, anorthite were readily derived from a few equilibria in simple systems. It was more problematic to determine a suitable solid solution model for mineral phases such as the garnet solid solution, and more complicatedly, the pyroxene solid solutions.

5.5 CALIBRATION OF THE THERMODYNAMIC MODEL

In the following section, the logical and chronological approach of the optimisation of the thermodynamic model will be described in detail. Following, in principle, the approach of Wood and Holloway (1984) first subsolidus equilibria in the system CaO-Al_2O_3-SiO_2 (CAS) were investigated.

5.5.1 The system CaO-Al_2O_3-SiO_2

The part of system CAS that is relevant for upper mantle compositions contains the phases clinopyroxene, anorthite, the Al_2SiO_5-polymorphs sillimanite and kyanite, α-quartz and ß-quartz, grossular and corundum. Other possible CAS phases such as e.g. andalusite are omitted from the modelling because of their limited stability field in pressure-temperature space or because these phases are known not to be stable under upper mantle conditions.

The univariant equilibrium $3\ CaAl_2Si_2O_8 = Ca_3Al_2Si_3O_{12} + 2\ Al_2SiO_5 + SiO_2$ (1) has been studied by Boyd and England (1961), Hays (1966), Hariya and Kennedy (1968), Wood (1978), Schmid et al. (1978), Goldsmith (1980), Gasparik (1984) and Koziol and Newton (1988). This equilibrium forms the basis of an important geobarometer for metamorphic rocks of pelitic composition (Koziol and Newton 1988).

As pointed out by Wood and Holloway (1984), Goldsmith's (1980) experiments are believed to be more reliable than experiments from Hays (1966) and Hariya and Kennedy (1968) because of the use of the frictionless NaCl-assembly as a pressure medium and the use W-Re thermocouples, which are less subject to drift from contamination relative to Type-S (Pt-$Pt_{90}Rh_{10}$) thermocouples. In a subsequent study to Wood and Holloway's paper, Gasparik (1984) re-examined reaction (1). His results are in excellent agreement with results from Goldsmith (1980), vindicating Wood and Holloway's interpretations. In a more recent study, Koziol and Newton (1988) extended the P-T range of the experiments to lower temperatures employing Li_2MoO_4 fluxes to enhance reaction rates. Figure 1 depicts the calculated results for reaction (1), depicted as lines, using the thermodynamic data listed in Table 3 (in the end of this chapter) which are based on the dataset by Holland and Powell (1990).

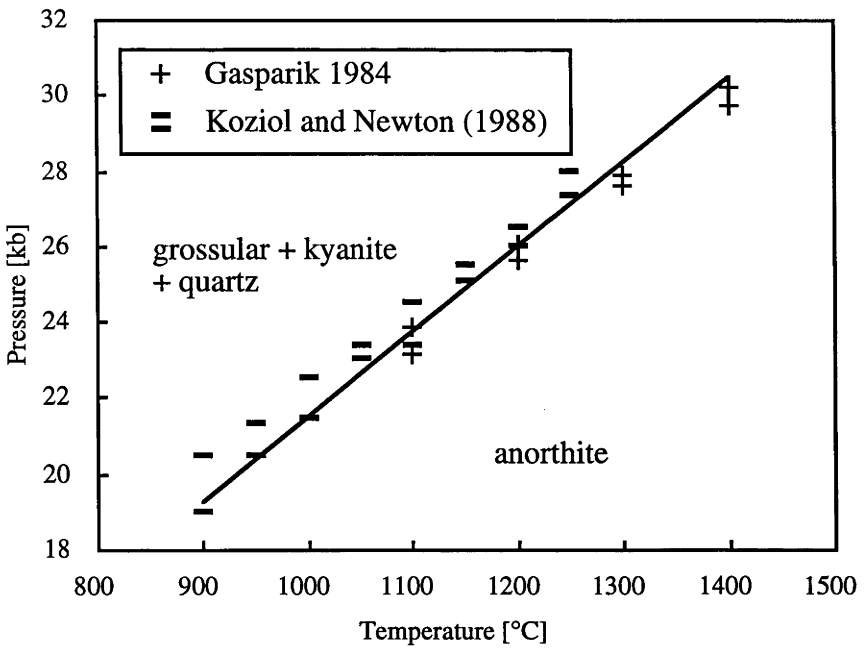

Figure 1 The univariant reaction 3 $CaAl_2Si_2O_8 = Ca_3Al_2Si_3O_{12} + 2$ $Al_2SiO_5 + SiO_2$ is successfully reproduced by the thermodynamic simulations. The calculations are depicted as the line, experimental brackets are from Gasparik (1984), and Koziol and Newton (1988). For clarity, experimental results by Goldsmith (1980) and others are not depicted. See text for details. Goldsmith's experiments are, however, in good agreement with results from Gasparik (1984).

Equilibrium (2): 3 $CaAl_2SiO_6 = Ca_3Al_2Si_3O_{12} + 2$ Al_2O_3 has been studied experimentally by Hays (1966) and Gasparik (1984). Following the same line of arguments as discussed above and by Wood and Holloway (1984), Gasparik's (1984) data were used for calibration of the thermodynamic model because of superior experimental methods.

TABLE 1 Equilibria

reactions in the system $CaO-Al_2O_3-SiO_2$	
1	3 $CaAl_2Si_2O_8 = Ca_3Al_2Si_3O_{12} + 2$ $Al_2SiO_5 + SiO_2$
2	3 $CaAl_2SiO_6 = Ca_3Al_2Si_3O_{12} + 2$ Al_2O_3
3	3 $CaAl_2Si_2O_8 + Al_2O_3 = Ca_3Al_2Si_3O_{12} + 3$ Al_2SiO_5 (Ky)
reactions in the system $CaO-MgO-SiO_2$	
4	$CaMgSi_2O_6^{OPX} + Mg_2Si_2O_6^{CPX} = CaMgSi_2O_6^{CPX} + Mg_2Si_2O_6^{OPX}$

reactions in the system $MgO-Al_2O_3-SiO_2$	
5	$2\ Mg_2Si_2O_6 + MgAl_2O_4 = Mg_2SiO_4 + Mg_3Al_2Si_3O_{12}$
6	$MgAl_2O_4 + Mg_2Si_2O_6 = MgAl_2SiO_6 + Mg_2SiO_4$
7	$3\ Mg_2Si_2O_6 + 2\ Al_2O_3 = 2\ Mg_3Al_2Si_3O_{12}$
8	$Mg_2Si_2O_6 + MgAl_2SiO_6 = Mg_3Al_2Si_3O_{12}$
9	$3\ Mg_2Si_2O_6 + 2\ Al_2SiO_5 = 2\ Mg_3Al_2Si_3O_{12} + 2\ SiO_2$
reactions in the system $CaO-MgO-Al_2O_3-SiO_2$	
10	$CaAl_2Si_2O_8 + 2\ Mg_2SiO_4 = MgAl_2O_4 + Mg_2Si_2O_6 + CaMgSi_2O_6$
11	$3\ CaAl_2Si_2O_8 + 9\ MgSiO_3 + Al_2SiO_5 = 3\ Mg_3Al_2Si_3O_{12} + Ca_3Al_2Si_3O_{12} + 4\ SiO_2$
12	$CaAl_2Si_2O_8 + 2\ Mg_2Si_2O_6 = Mg_3Al_2Si_3O_{12} + CaMgSi_2O_6 + SiO_2$
13	$3\ CaMgSi_2O_6 + Mg_2Si_2O_6 + 2\ MgAl_2O_4 = 2\ Mg_2SiO_4 + 2\ (Mg,Ca)_3Al_2Si_3O_{12}$

Equilibria in the systems CAS, CMS, MAS and CMAS. References are: CAS-1: Gasparik (1984), Koziol and Newton (1988), Hays (1966), Hariya and Kennedy (1968), Wood (1978), Goldsmith (1980), Schmid et al (1978). CAS-2: Hays (1966), Gasparik (1984). CAS-3: Gasparik (1984). CMS-4: Nehru and Wyllie (1974), Warner and Luth (1974), Mori and Green (1975), Lindsley and Dixon 1976, Finnerty (1977), Schweitzer (1982), Brey and Huth (1984), Nickel and Brey (1984). MAS-5 Perkins et al. (1981), Gasparik and Newton (1984), Dankwerth and Newton (1978), Staudigel and Schreyer (1977). MAS-6: Boyd and England (1964), Anastasiou and Seifert (1972), MacGregor (1974), Dankwerth and Newton (1978), Gasparik and Newton (1984). MAS-7: Gasparik and Newton (1984). MAS-8: Perkins et al. (1981), Lane and Ganguly (1980), MacGregor (1974). MAS-9: Hensen and Essene (1971), Hensen (1972), Perkins (1983), CMAS-10: Kushiro and Yoder (1966), Herzberg (1976), Green and Hibberson (1970), CMAS-11: Perkins (1983), CMAS-12: Hansen (1981), Perkins (1983), CMAS-13: Kushiro and Yoder (1966), Jenkins and Newton (1979), O'Neill (1981), O'Hara et al. (1971), Patera (1982), Gasparik (1984), Millholland and Presnall (1998), this study.

As Figures 1 and 2 indicate, equilibria (1) and (2) are accurately reproduced by the thermodynamic model. Therefore the endmember properties of anorthite, grossular, kyanite and ß-quartz are not to be altered any more during subsequent calibration of the database.

Equilibrium (3) $3\ CaAl_2Si_2O_8 + Al_2O_3 = Ca_3Al_2Si_3O_{12} + 3\ Al_2SiO_5$ has been studied by Gasparik (1984). Thermodynamic modelling results in good agreement between the database of the present study and the experimental brackets (Figure 3).

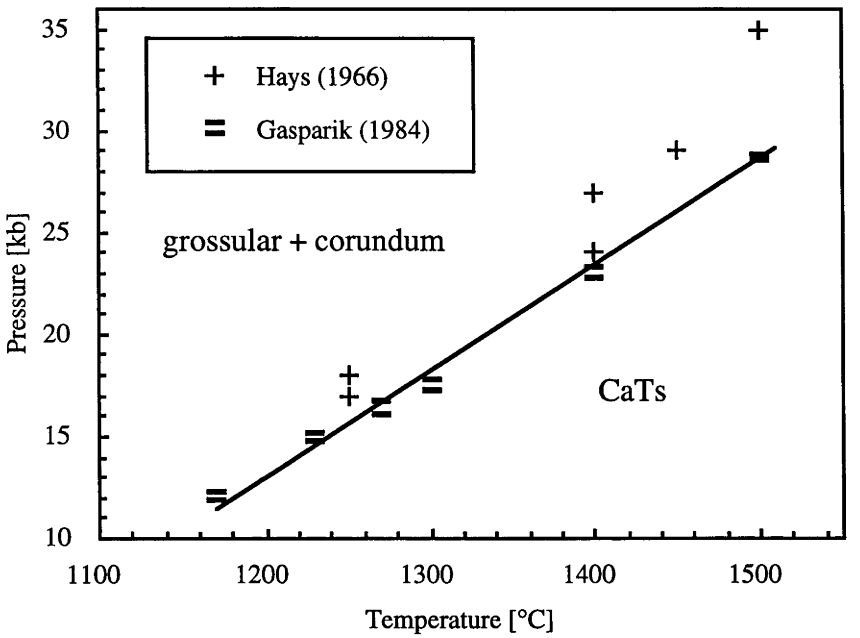

Figure 2 The univariant equilibrium (2): 3 $CaAl_2SiO_6$ = $Ca_3Al_2Si_3O_{12}$ + 2 Al_2O_3: Experimental brackets from Gasparik (1984) compared with thermodynamic calculations. There is good agreement between the calculations (line) and Gasparik's (1984) experiments.

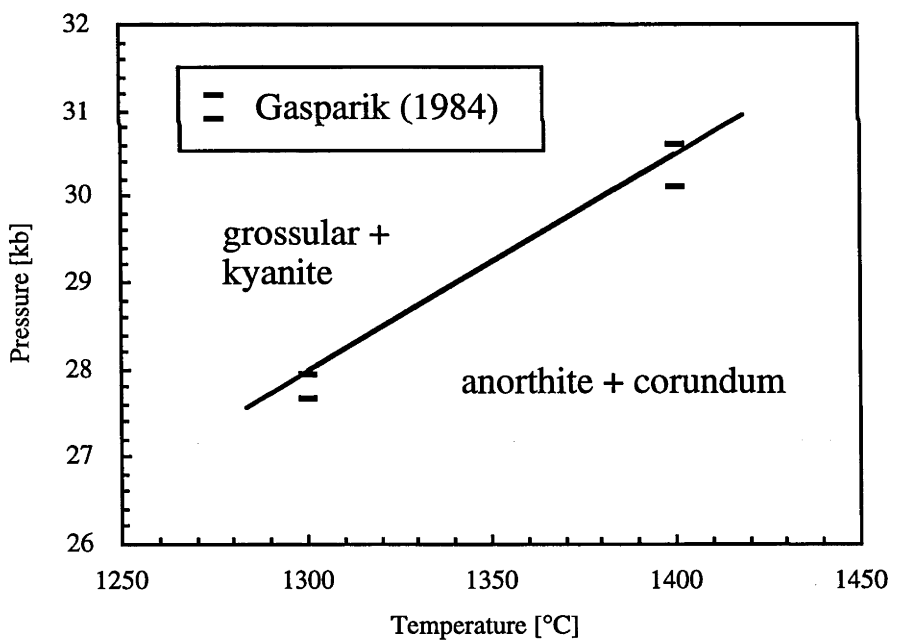

Figure 3 depicts the reaction 3 $CaAl_2Si_2O_8$ + Al_2O_3 = $Ca_3Al_2Si_3O_{12}$ + 3 Al_2SiO_5. Experimental brackets are from Gasparik (1984), compared to the thermodynamic calculations, depicted as the line.

Continuing in the same manner, the following equilibria in the simple systems $CaO\text{-}MgO\text{-}SiO_2$ (CMS) and $MgO\text{-}Al_2O_3\text{-}SiO_2$ (MAS) were analysed as indicated in Table 1.

5.5.2 The system $CaO\text{-}MgO\text{-}SiO_2$

The system $CaO\text{-}MgO\text{-}SiO_2$ (CMS) contains, among others phases, the upper mantle minerals enstatite and diopside. $Mg_2Si_2O_6$ (enstatite) and $CaMgSi_2O_6$ (diopside) exhibit limited solid solutions towards each other at lower temperatures. Atlas (1952) probably first recognised the potential of the miscibility gap for geothermometry. The temperature dependence of the miscibility gap at 30 kbar has been established experimentally by Davies and Boyd (1966) and has since then been re-investigated many times, as the miscibility gap between enstatite and diopside is probably the most important geothermometer for upper mantle rocks. Since Davies and Boyd (1966), later experimental studies have improved the understanding of the enstatite-diopside join by conducting reversal experiments that were analysed with the electron microprobe. Studies at a range of pressures and temperatures (Mori and Green 1975, Warner and Luth 1974, Nehru and Wyllie 1974, Lindsley and Dixon 1976, Finnerty 1977, Brey and Huth 1984, Nickel and Brey 1984) have provided further insight in the pressure dependence of the miscibility gap at elevated temperatures.

From a chemical point of view, the exchange of Ca and Mg between clinopyroxene and orthopyroxene in the system CMS can be described as follows:

$$CaMgSi_2O_6^{OPX} + Mg_2Si_2O_6^{CPX} = CaMgSi_2O_6^{CPX} + Mg_2Si_2O_6^{OPX} \qquad (4)$$

The join $Mg_2Si_2O_6$-$CaMgSi_2O_6$ join consists of C2/c clinopyroxene, Pbca orthopyroxene as well as a $P2_1/c$ pigeonitic clinopyroxene. To describe the solid solution thermodynamically, a model was chosen here that does not include a pigeonite component (Nickel and Brey 1984), mainly for simplicity and because the limited stability field of pigeonite under upper mantle conditions (Wood and Holloway 1984). For more detailed information about several other formulations of solid solutions, the reader is referred to papers by Lindsley et al. (1981), Nickel and Brey (1984) and Carlson and Lindsley (1988). The solid solution model of Nickel and Brey (1984) is found to successfully reproduce the miscibility gap between clinopyroxene and

orthopyroxene up to pressures of 50 kb, as shown in Figure 4. However, it has to be pointed out that Nickel and Brey's (1984) formulation of the excess volumes contradicts the calorimetric measurements of Newton et al. (1979) who found positive deviation from ideal mixing for volumes on the join Di-cEn.

However, the capability of the free energy minimisation algorithm to calculate miscibility gaps and solvi was investigated. After having duplicated the input clinopyroxene data, the algorithm computed a low-Ca clinopyroxene in the simple system CMS, in equilibrium with orthopyroxene and clinopyroxene at pressures lower than 15 kb and temperatures below 1450°C. For these computational tests the thermodynamic model of Carlson and Lindsley (1988) was employed.

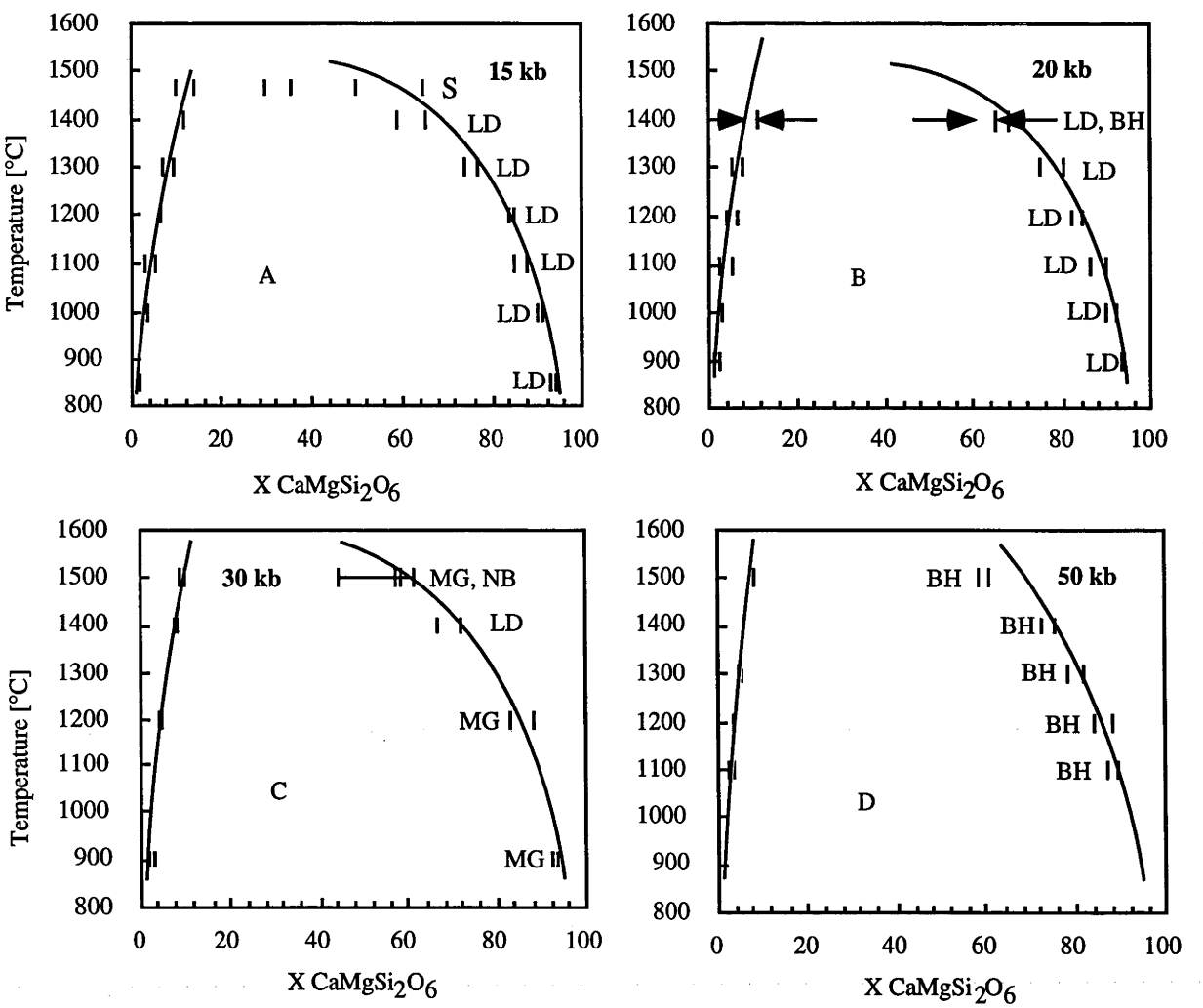

Figure 4 Thermodynamic calculations (lines) compared to experimental brackets from Brey and Huth (1984), Lindsley and Dixon (1976) Mori and Green (1975). 15 kb: Lindsley and Dixon (1976). 20 kb: Lindsley and Dixon (1976) and Brey and Huth (1984) at 1400°C. 30 kb: Mori and Green (1975) at 900°C, 1200°C, and 1500°C. 50 kb: Brey and Huth (1984).

5.5.3 The system $MgO-Al_2O_3-SiO_2$

The system $MgO-Al_2O_3-SiO_2$ contains several important upper mantle phases such as pyrope, spinel, forsterite, corundum, the Al_2SiO_5 polymorphs sillimanite and kyanite, and the orthopyroxene solid solution. Cordierite-bearing reactions were excluded from the calibration of the model, because of the uncertainties in the thermodynamic properties of cordierite (Holland and Powell 1990, Berman 1988, Gottschalk 1997).

The orthopyroxene solid solution in $MgO-Al_2O_3-SiO_2$

The solubility of alumina in orthopyroxene in equilibrium with either spinel or garnet bearing assemblages has been investigated in numerous experimental studies. The alumina content of orthopyroxene is both a function of pressure and temperature in the garnet stability field (e.g. Perkins et al. 1981, Lane and Ganguly 1980), it is virtually independent of pressure in the spinel stability field (e.g. Gasparik and Newton 1984).

The equilibrium describing the alumina solubility in the spinel stability field may be written as

$$MgAl_2O_4 + Mg_2Si_2O_6 = MgAl_2SiO_6 + Mg_2SiO_4 \qquad (6)$$

A number of solution models have been proposed to describe the mixing of $Mg_2Si_2O_6$-$MgAl_2SiO_6$ orthopyroxenes in the system MAS (e.g. Wood and Banno 1973; Lane and Ganguly 1980). In the most widely used model, Wood and Banno (1973) assumed that half the Al in the opx formula unit substitutes for Mg on the M1 octahedral site, with the other half of the Al occupying an adjacent tetrahedral site. Since the substitution of the Al onto the tetrahedral site is completely specified by the octahedral Al, it contributes nothing to the configurational the entropy of mixing, which therefore corresponds to one-site mixing. Hence

$$a\,(Mg_2Si_2O_6) = 1\text{-}N_{Al}/2$$

$$a\,(MgAl_2SiO_6) = N_{Al}/2$$

where NAl is the number of Al cations per formula unit of 6 oxygens.

In contrast to the simple model of Wood and Banno (1973) who assumed ideal mixing, Ganguly and Ghose (1979) proposed two different models (with and without Al-avoidance). However, the simple Wood and Banno (1973) model reproduces

experimental data (e.g. Perkins et al. (1981) for the garnet stability field) rather well, indicating that the experimental data, covering only a narrow range of compositions, are not sensitive enough for discrimination between simple ideal and more complex mixing models.

Based on experiments in the system $MgO-Al_2O_3-SiO_2-Cr_2O_3$, presented in Chapter 4 of this thesis, a solid solution model for Cr and Al bearing orthopyroxenes has been developed that is in good agreement with experimental results both in the system MAS (Gasparik and Newton 1984) as well as MASCr (Chapter 4). The formulation derived in Chapter 4 reduces to one-site mixing for Cr-free compositions. The advantage of the MASCr experiments is that these data can distinguish between alternative models for the orthopyroxene solid solution in the MAS system, strongly favouring the one-site model.

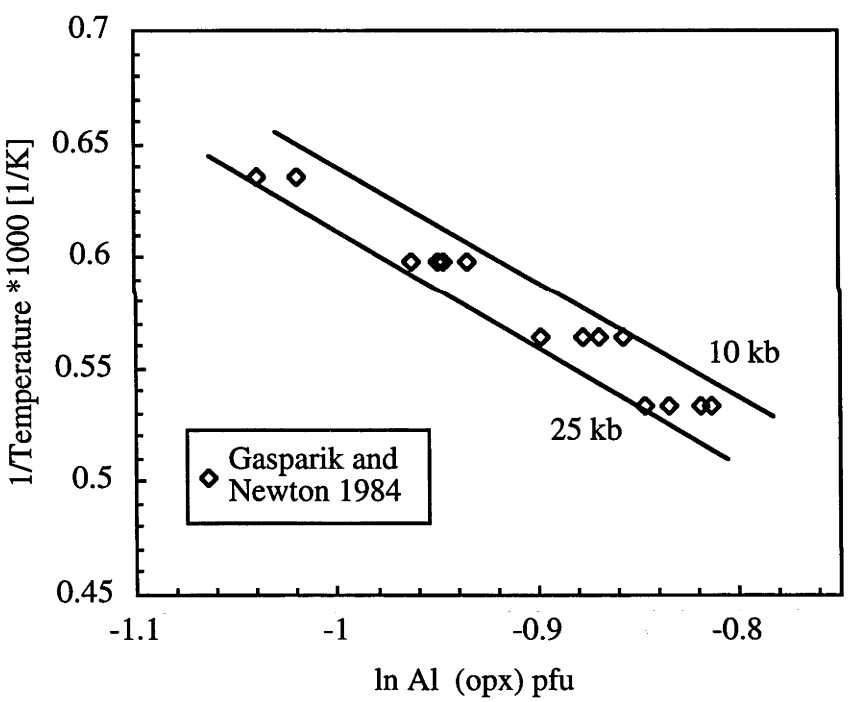

Figure 6 shows the alumina content of orthopyroxene in equilibrium with spinel and forsterite in the system $MgO-Al_2O_3-SiO_2$. Compared are experiments results from Gasparik and Newton (1984) [symbols] with the thermodynamic model [lines] calculated for 10 and 25 kbar. Al opx pfu = alumina in orthopyroxene per formula unit of six oxygens.

$MgAl_2O_4$ - spinel

Estimation of thermodynamic properties of $MgAl_2O_4$ spinel is hampered by the well known effect of Mg-Al disorder on octahedral and tetrahedral sites in the spinel structure (e.g. Navrotsky and Kleppa 1967, Wood et al. 1986). The cation configuration in $MgAl_2O_4$ depends on temperature with a Al^{3+} substituting into tetrahedral sites with increasing temperature. The kinetics of re-configuration are slow (Chamberlin et al. 1995) so that during quench from high temperatures reordering is often incomplete, depending of the thermal history of the specimen (Wood et al. 1986, Millard et al. 1992). Deriving thermodynamic properties directly from the calorimetric measurements (Bonnikson 1955, King 1955) without corrections for Mg-Al disorder would result in underestimations of the equilibrium entropy at high temperatures (see e.g. Robie et al. 1979).

The approach taken here (as in the internally consistent databases of e.g. Holland and Powell 1990) is to use reversal experimental data to indirectly constrain the thermodynamic properties of spinel ($MgAl_2O_4$) incorporating the contribution from disorder at standard conditions.

In order to satisfy the experimental results (Dankwerth and Newton 1978, Gasparik and Newton 1984) on the spinel-garnet transition in MAS, the stability of the spinel bearing assemblage had to be increased without violating the orthopyroxene mixing model for MAS derived from the MASCr and MAS experiments (Chapter 4). This was achieved by slightly increasing the entropy of $MgAl_2O_4$ (from 81.0 J mol^{-1} K^{-1}) in Holland and Powell (1990) to 81.8 J $mol^{-1}K^{-1}$) probably justified in light of the uncertainties in the calorimetrically determined standard values due to Mg-Al disorder. A recent study by Chamberlin et al. (1995) investigated the thermodynamic properties of $MgAl_2O_4$ using the palladium oxide equilibration technique (c.f. Chamberlin et al. 1994). They proposed $S°_{298}$ ($MgAl_2O_4$) = 81.1 ± 2.8 J $mol^{-1}K^{-1}$) and $\Delta_fH°(298.15)$ = -2302.9 ± 5.8 kJ mol^{-1}. The present estimates for the entropy and enthalpy at 298 K are in good agreement with their value, noting, however, the large errors in Chamberlin et al.'s (1995) data.

aluminous pyroxene in equilibrium with garnet and olivine in MAS

The orthopyroxene solid solution was derived by fitting equilibria in the spinel stability field both in MAS and MASCr (Chapter 4). An independent test for the aforementioned model is the calculation of phase equilibria in a system that was not used for calibration of the orthopyroxene solid solution model.

The equilibrium that controls the solubility of alumina in orthopyroxene in equilibrium with forsterite and garnet may be described as follows:

$$Mg_2Si_2O_6 + MgAl_2SiO_6 = Mg_3Al_2Si_3O_{12} \qquad (8)$$

This equilibrium has been examined experimentally by a number of workers (e.g. Boyd and England 1964, MacGregor 1974, Lane and Ganguly 1980, Perkins et al. (1981). Perkins et al. (1981) appears to be the most comprehensive of these studies, covering pressures from 20 to 40 kb and temperatures between 900 and 1600°C. The results for the calculated solubility of alumina in orthopyroxene in equilibrium with garnet harzburgite using the thermodynamic data for the orthopyroxene solid solution derived in the spinel stability field are depicted in Figure 8, compared to results from Perkins et al. (1981). Good agreement is observed with the endmember data for enstatite and magnesiotschermak ($MgAl_2SiO_6$) and the aforementioned orthopyroxene solid solution model derived from the calibrations in the spinel stability field (c.f. Chapter 4).

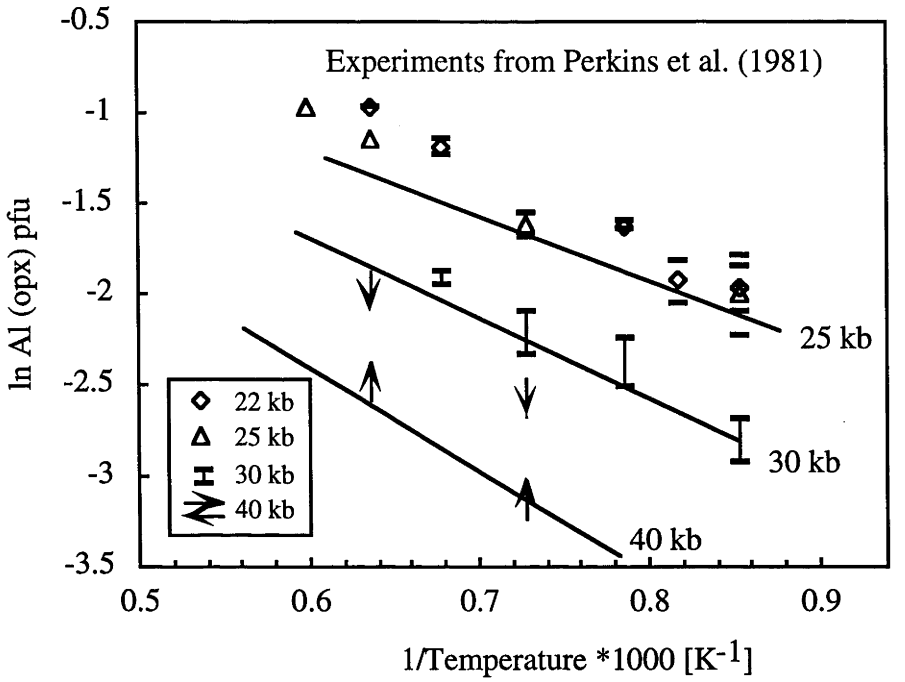

Figure 8 compares the solubility of alumina in orthopyroxene as a function of pressure and temperature in equilibrium with olivine and garnet in the system $MgO\text{-}Al_2O_3\text{-}SiO_2$. Depicted are experiments from Perkins et al. (1981) at 22, 25, 30 and 40 kbars, results of the thermodynamic model are shown as lines as a function of pressure at 25kb, 30 kb and 40 kb. Al opx pfu = alumina in orthopyroxene per formula unit of six oxygens. Bars and arrows indicate the widths of the individual experimental brackets.

The equilibrium that describes the transition from garnet harzburgite to spinel harzburgite in MAS, reaction (5) may be written as follows: $2\ Mg_2Si_2O_6 + MgAl_2O_4 = Mg_2SiO_4 + Mg_3Al_2Si_3O_{12}$. Figure 5 shows the results of the computed reaction compared with experimental brackets from Dankwerth & Newton (1978) and Gasparik & Newton (1984).

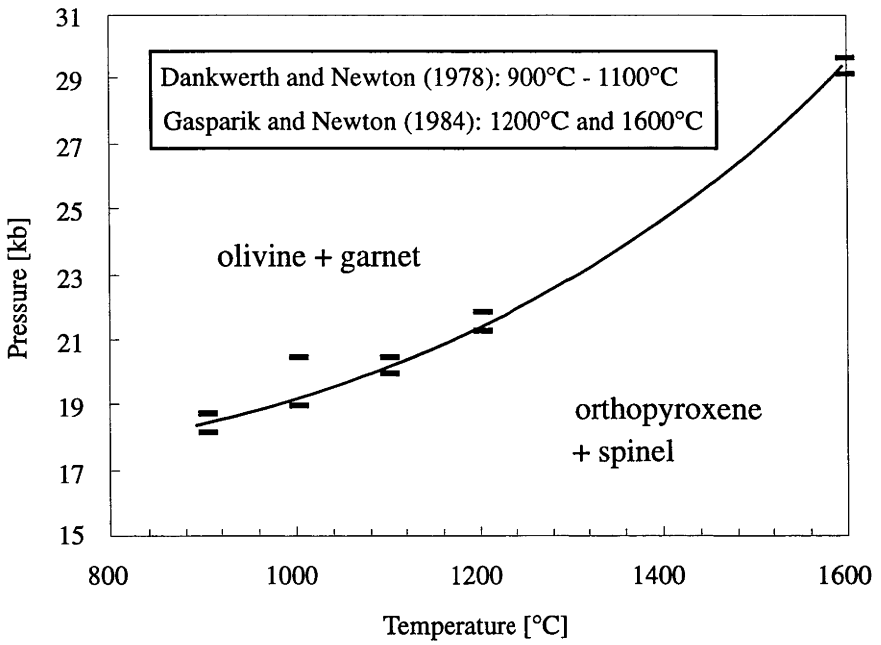

Figure 5 The equilibrium $Mg_2Si_2O_6+MgAl_2O_4=Mg_2SiO_4+-Mg_3Al_2Si_3O_{12}$ (5). Depicted are experimental brackets from Dankwerth & Newton (1978) at temperatures between 900°C and 1100°C and Gasparik & Newton (1984) at 1200°C and 1600°C. Both experimental studies agree well with each other and also with the calculations depicted as the curve.

It was again Gasparik and Newton (1984) who investigated the equilibrium

$$Mg_2Si_2O_6 + 2\ Al_2O_3 = 2\ Mg_3Al_2Si_3O_{12} \qquad (7)$$

at high pressures and high temperatures. They only performed reversal experiments at 850°C and bracketed the reaction between 16 and 16.5 kb. The results are in agreement with calorimetric studies by Newton et al. (1977) but disagree with results from Charlu et al. (1975) that are believed to be in error (Wood and Holloway 1984). The thermodynamic model presented here reproduces Gasparik and Newton's (1984) experiments within the experimental uncertainties. Equilibrium (7) is not shown graphically.

Concluding the discussion of garnet -spinel equilibria in the system MAS, the thermodynamic model calculates isopleths for orthopyroxene in equilibrium with garnet harzburgite and spinel harzburgite that are in accordance with experimental results from Gasparik and Newton (1984) in the spinel stability field and with experiments from Perkins et al. (1981) in the garnet stability field. Results of the

thermodynamic modelling in both the garnet stability field as well as in the spinel stability field are depicted in Figure 7. As the slope of the alumina isopleths of pyroxene in the spinel stability field are very different to the slope in the garnet stability field, the position of the transition from garnet harzburgite to spinel harzburgite in the system MAS can be inferred from where the isopleths bend in P-T space, as indicated in Figure 7.

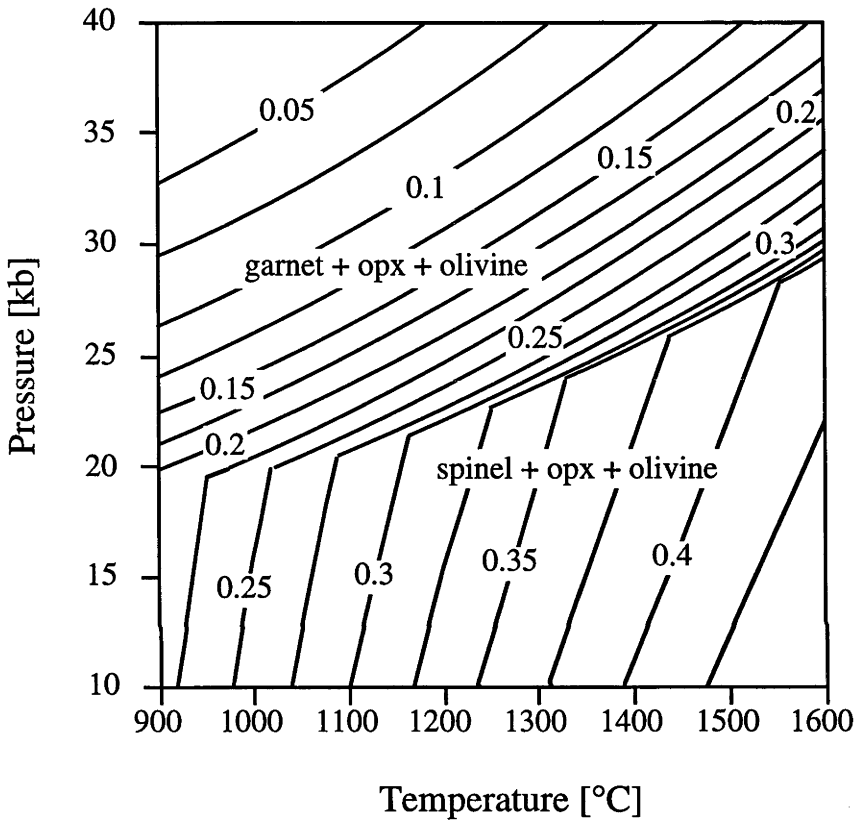

Figure 7 depicts the solubility of alumina in orthopyroxene in the system $MgO\text{-}Al_2O_3\text{-}SiO_2$, computed with the free energy minimisation algorithm. Isopleths depict the alumina content of orthopyroxenes recalculated on the basis of 6 oxygens per formula unit.

Equilibrium (9) has been investigated by Hensen and Essene (1971), Perkins (1983) and Hensen (1972). The latter two studies agree reasonably well with each other, Hensen and Essene's (1971) brackets lie at somewhat lower pressures, probably due to the different pressure corrections they used in the calibration of their high-pressure apparatus. Figure 9 compares computer simulations of the present study with the experimental brackets. Without further adjustments, the model reproduces the experiments of Perkins (1983) and Hensen (1972) quite well, only at 1000°C the

calculated curve differs somewhat from the experiments, the P-T region where kyanite becomes stable in our model. There is also some uncertainty associated with the thermodynamic properties of sillimanite, as sillimanite exhibits Al-Si disorder as spinel discussed above (Wood and Holloway 1984).

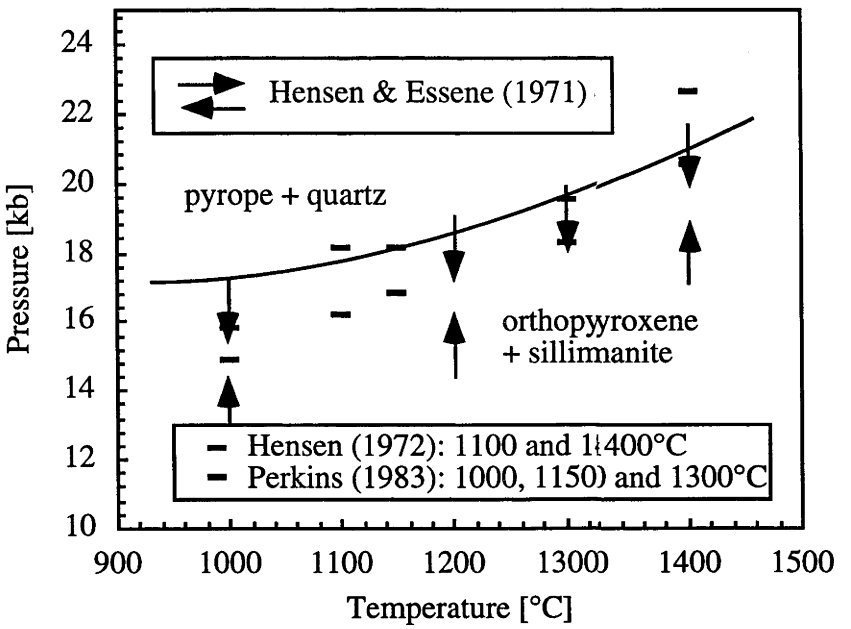

Figure 9 shows reaction (9): 3 $Mg_2Si_2O_6$ + 2 Al_2SiO_5 = 2 $Mg_3Al_2Si_3O_{12}$ + 2 SiO_2, as calculated with the free energy minimisation computer model. For comparison, experimental brackets are shown as performed by Hensen (1972) at 1100°C and 1400°C and by Perkins (1983) at 1000°C, 1150°C and 1300°C. Brackets from Hensen and Essene (1971) are depicted as arrows.

5.5.4 The system CaO-MgO-Al_2O_3-SiO_2

The system CaO-MgO-Al_2O_3-SiO_2 (CMAS) contains, next to some other possible phases, clinopyroxene, orthopyroxene, olivine, garnet and spinel, the major five mineral constituents of the upper mantle. Aiming at upper mantle conditions, the calibration of the thermodynamic model in this study only included experiments in SiO_2-undersaturated systems and also in systems with relatively low Al_2O_3-contents. Later, however, it will be shown that extrapolation into SiO_2-saturated compositions gives reasonable results for certain reactions.

Thermodynamic endmember properties of anorthite, diopside, Al_2SiO_5 and corundum and β-quartz have already been determined using equilibria in the system

CAS whilst endmember properties of enstatite, magnesio-tschermak, spinel and pyrope are fixed by calibration of experiments in the system MAS. Besides, the orthopyroxene solid solution has also been investigated in the system MAS. Therefore, reactions 10-14 in the system CMAS are used to test for internal consistency of the thermodynamic endmember properties derived from simpler sub-systems and to determine appropriate thermodynamic models for mineral solid solutions such as orthopyroxenes, clinopyroxenes and garnets.

Solid Solutions in CMAS

olivine

The olivine solid solution in the system CMAS may be represented by a symmetrical solid solution of the endmember components Mg_2SiO_4 (forsterite) and $CaMgSiO_4$ (monticellite). The partitioning of Ca and Mg between olivine and pyroxenes has been proposed as a geobarometer (e.g. Adams and Bishop 1982, 1986; Köhler and Brey 1990). Several studies have investigated the thermodynamics of Ca-bearing olivines (Davidson and Mukhopadhyay 1984, Davidson and Lindsley 1989 and Hirschmann 1991). In this study mixing properties for the forsterite -monticellite solid solution were adopted from Hirschmann (1991). However, consideration of Ca-bearing olivines in the database does not significantly effect phase relations in CMAS compared to initial modelling that was done with pure forsterite.

orthopyroxene and clinopyroxene

The orthopyroxene solid solution in the system $MgO-Al_2O_3-SiO_2$ may be described with the endmembers $Mg_2Si_2O_6$ and $MgAl_2SiO_6$ as discussed above. The solid solution between diopside and enstatite in the system $CaO-MgO-SiO_2$ may also be described by a binary solid solution consisting of the endmembers $Mg_2Si_2O_6$ and $CaMgSi_2O_6$. In the system $CaO-MgO-Al_2O_3-SiO_2$ the addition of these two binaries results in the reciprocal solid solution

$$MgAl_2SiO_6 + CaMgSi_2O_6 = Mg_2Si_2O_6 + CaAl_2SiO_6.$$

Following Wood and Holloway (1984, p. 167), the approach here is to treat the orthopyroxene and clinopyroxene solid solutions as mixing on each individual sites with additional reciprocal or 'cross-site' terms. Both the clinopyroxene and orthopyroxene solid solutions are in principle similar and may be described with the same set of endmember components, that is $Mg_2Si_2O_6$, $CaMgSi_2O_6$, $MgAl_2SiO_6$ and $CaAl_2SiO_6$.

Analysis of the MAS and MASCr experiments (Chapter 4) resulted in a solid solution model for the interaction on the M1 site (Mg^{2+}-Al^{3+}) of the orthopyroxene solid solution (see above), the interaction on the M2 site (Ca^{2+}-Mg^{2+}) in orthopyroxene has been calibrated from experiments in the system CaO-MgO-SiO_2 (c.f. Nickel and Brey 1984).

The clinopyroxene solid solution consists of interaction on the M2 sites (Ca^{2+}-Mg^{2+}) as well as the M1 sites (Mg^{2+}-Al^{3+}). The M2-site interaction has been calibrated by the CaO-MgO-SiO_2 experiments as described above, whilst the interaction on the M1-site is rather unconstrained (Wood and Holloway 1984). Newton et al. (1977) found positive excess enthalpies of mixing on the join $CaMgSi_2O_6$-$CaAl_2SiO_6$, whilst Gasparik and Lindsley (1980) proposed negative deviations from ideality. In order to reproduce the experimental results presented in Chapter 1 on the solubility of alumina in clinopyroxene in equilibrium with spinel lherzolite in CMAS, an empirical model was developed that reproduces the experiments presented in the first chapter as well as other experiments in the spinel lherzolite stability field (Table 2).

garnet

The garnet solid solution in CMAS may be described in terms of the endmembers $Mg_3Al_2Si_3O_{12}$ (pyrope) and $Ca_3Al_2Si_3O_{12}$ (grossular). The solid solution between these components has been investigated by several authors (e.g. Newton et al. 1977, Wood 1988, Ganguly et al. 1993 among others), the exact nature of this binary join is, nevertheless, still rather unconstrained. Many phase equilibria used for geothermobarometry, however, involve some sort of garnets. The most common geobarometer for garnet lherzolites is based on the exchange of aluminium between orthopyroxene and garnet (e.g. Nickel and Green 1985). Therefore, calibration of these equilibria requires a thorough understanding of the thermodynamics of complex garnet solid solutions.

Synthesis of homogenous garnet material at high pressures is difficult probably due to slow kinetics of garnet formation and to the fact that experiments intended to produce garnets of intermediate compositions, crystallised additional clinopyroxenes on the join $CaAl_2SiO_6$ - $CaMgSi_2O_6$. Because of these experimental problems, thermodynamic interpretations of several studies on the pyrope-grossular join differ substantially from each other. However, recent studies have reduced some uncertainties (Ganguly et al. 1993).

molar volumes of pyrope - grossular garnets

Newton et al. (1977), Haselton and Newton (1980), Wood (1988), Berman (1990), Ganguly et al. (1993) and Bosenick and Geiger (1997) analysed the excess molar volumes on the pyrope-grossular join using X-ray diffraction methods. The inferred results are substantially different, ranging from a description of the experimental results with an asymmetric solid solution model with positive excess volumes (Wood 1988) to an asymmetrical model with negative excess volumes at pyrope-rich compositions and positive excess volumes towards the grossular-end of the solution. Berman (1990) concluded in his analysis of the available volume data on the grossular-pyrope join that the scatter of the data was too large to justify any model but a simple non-ideal symmetrical model.

One of the problems associated with the excess volume function was that, until recently, no garnet could be synthesised at compositions between 0.5 and 0.8 grossular component. This gap is also present in the calorimetric measurements of Newton et al. (1977).

In a recent study, however, Ganguly et al. (1993) successfully synthesised homogenous garnets for a wide range of garnet compositions. Results from Ganguly et al. (1993) and another recent study by Bosenick and Geiger (1997) are in perfect agreement with each other. These studies are also in qualitative agreement with results of Wood (1988). In this study, Ganguly et al.'s (1993) expressions for the molar volumes were adopted, as this dataset is well documented and describes a wide range of garnet compositions.

excess enthalpy and entropy of pyrope -grossular garnets

The excess function for the enthalpy of the pyrope-grossular joint was determined by high-temperature lead borate solution calorimetry at 977 K (Newton et al. 1977), indicating positive and asymmetric deviation from ideality with largest deviation close to the pyrope rich end of the join.

Hensen et al. (1975) investigated the equilibrium ($3\ CaAl_2Si_2O_8 = Ca_3Al_2Si_3O_{12} + 2\ Al_2SiO_5 + SiO_2$) at pressure and temperature. The displacement of the reaction as a function of Ca-Mg ratio was used to determine mixing properties on the grossular-pyrope join, suggesting a W_{CaMg} of about 24000 J/mol (at 1000 K), assuming symmetric solution behaviour (Wood 1988).

Low-temperature adiabatic calorimetry (Haselton and Newton 1980) for one composition (X grossular = 0.4) also indicate large excess heat capacities of mixing, resulting in large positive excess entropies of mixing ($W_S^{CaMg} = 18.8$ J/molK). In an analysis of phase equilibria in CMAS, Wood and Holloway (1984) proposed a lower excess entropy than proposed by Haselton and Newton (1980), and Wood's (1988) evaluation of experimental results on the displacement of the anorthite breakdown reaction concluded in asymmetric excess entropy with lower W_S^{CaMg} at pyrope rich compositions and higher excess entropy at the grossular rich end of the binary join. The data taken together indicate that the excess entropy is asymmetric, the exact magnitude, however, remains rather unconstrained.

The present study presents new experimental data in the system CMAS, with the transition from garnet lherzolite to spinel lherzolite at higher pressures than in previous studies. The excess entropy function was empirically re-evaluated here, incorporating the new experimental results (Chapter 1). The excess enthalpy term determined by Newton et al. (1977) indicates positive deviation from ideality, the exact magnitude of the mixing is rather uncertain, due to large errors in the actual determinations. This study uses an asymmetric model according to the trends determined by Newton et al (1977) with the excess enthalpy term less positive as inferred by Newton et al (1977). The excess entropy, however, was found to be more asymmetric than the estimates by Haselton and Newton (1980) and Wood (1988). This is a result of the greater slope of the garnet-spinel transition in CMAS at temperatures higher than 1200°C as described in Chapter 1 of this thesis.

TABLE 2 Solid solutions

	solution type		W_H [J/mol]	W_S [J/mol/K]	W_V [cm^3/mol]	source
olivine	binary	W MgCa	34500			Hirschmann (1991)
		W CaMg	34500			
garnet	binary	W CaMg	7365	-9.6	0.013	W_H and W_S this study,
		W MgCa	2380	6.8	0.0577	W_V's from Ganguly et al. (1993)
orthopyroxene	two binaries	W CaMg	34022	0		Nickel and Brey (1984)
	and reciprocal	W MgAl	20000			this study (Chapter 4)
		ΔG_{rec}	0			
clinopyroxene	two binaries	W CaMg	21905	-4.431	-0.05229	Nickel and Brey (1984)
	and reciprocal	W MgAl	308	-4	0	this study
		ΔG_{rec}	0			

Thermodynamic mixing parameters used in this study. Sources are indicated in the right column. The binary solid solution was formulated after Helffrich and Wood (1989), the reciprocal solid solution following Wood and Nicholls (1978).

The transition from spinel lherzolite to garnet lherzolite

Experiments of this study were mainly conducted in the spinel lherzolite stability field, as discussed in Chapter 1. The pyroxene solid solutions have been calibrated using equilibria in the spinel lherzolite field. In the next step of the model building process, an appropriate garnet solid solution model was chosen (see above) that reproduces the transition from garnet lherzolite to spinel lherzolite in CMAS as well as garnet compositions along the transition.

Figure 13 depicts the transition from garnet to spinel lherzolite as calculated with the thermodynamic model (lines) in comparison with experimental brackets from O'Neill (1981), Jenkins and Newton (1979), Gasparik (1984), Patera (1982), Milholland and Presnall (1998) and from this study. The thermodynamic model reproduces the transition from garnet lherzolite to spinel lherzolite and is in excellent agreement with the experiments described in the first chapter of this thesis.

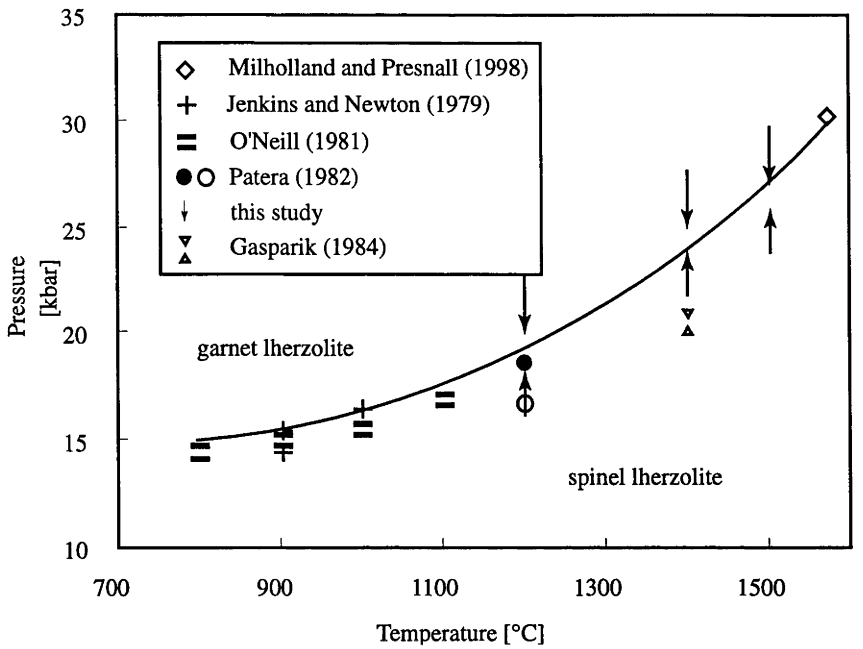

Figure 13 shows the calculated position of the transition from spinel lherzolite to garnet lherzolite in the system CMAS. The thermodynamic model presented here is compared with experimental studies from O'Neill (1981), Jenkins and Newton (1979), Gasparik (1984) and with experimental results of the present study (Chapter 1). Patera (1982) bracketed the reaction at 1200°C and 17-18.7 kb (as referred to by Wood and Holloway (1984)) which is in excellent agreement with the bracket at 1200°C (this study). Also shown is the invariant point on the solidus found by Milholland and Presnall (1998) which also is in good agreement with the calculations.

Comparing the calculated isopleths of alumina in orthopyroxene in CMAS with experimental results in the spinel lherzolite stability field, there is excellent agreement between the calculations and experimental results by Gasparik (1984) and the present study (Chapter 1). There is also good agreement with most of Sen's (1985) experiments (Figure 14), although some experiments at 1200°C (Sen 1985, Fujii 1977) do not agree very well, probably due to not fully equilibrated experiments at this relatively low temperature.

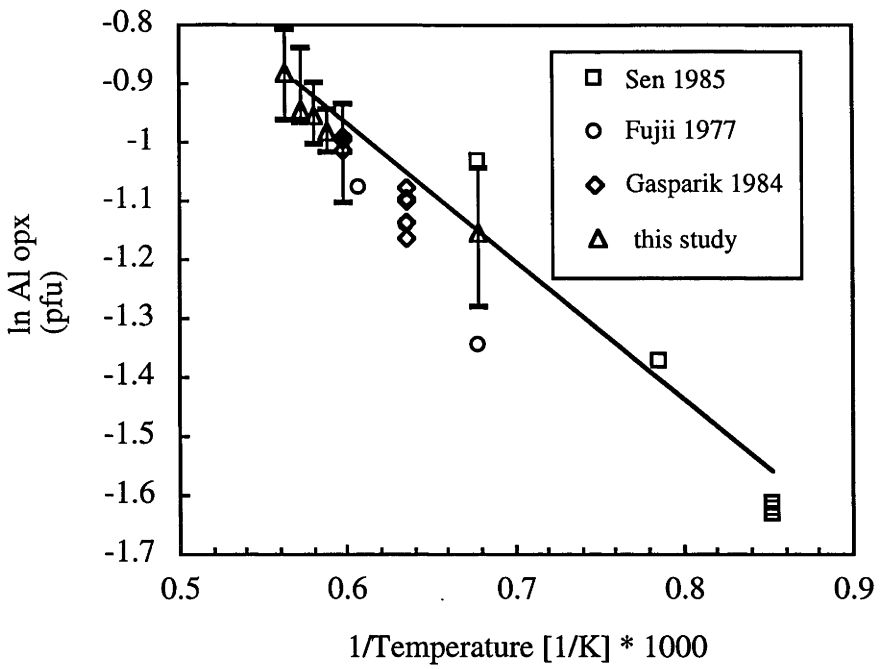

Figure 14 depicts the solubility of alumina in orthopyroxene in the equilibrium with spinel lherzolite as a function of temperature in the system CMAS. Calculated results (solid line, 15 kb) are in good agreement with experiments. Some experiments at 1200°C from Sen (1985) and Fujii (1977) appear to considerably disagree. However, no uncertainties are quoted for the studies of Fujii (1977) and Gasparik (1984). Assuming these studies exhibit similar uncertainties as the present study (note the large error bars for the 1200°C datum), reasonable agreement is observed within the error margins. The depicted experiments were performed at different pressures, thus indicating that the solubility of aluminium only slightly depends on pressure. pfu = per formula unit of six oxygens.

Figure 15 depicts the solubility of alumina in orthopyroxene in equilibrium with a garnet lherzolite assemblage. The present thermodynamic model agrees well with the high-pressure experiments (P>30 kb) and only reasonably well at 25 kb, as the model tends to slightly overestimate the alumina content of orthopyroxene at lower pressure. However, there is, in some cases, substantial overlap of the brackets between Perkins and Newton (1980) and Nickel et al. (1985). Perkins and Newton's (1980) experiments were performed at temperatures between 900 and 1100°C, whilst Nickel et al.'s (1985) experiments cover experiments at higher temperatures.

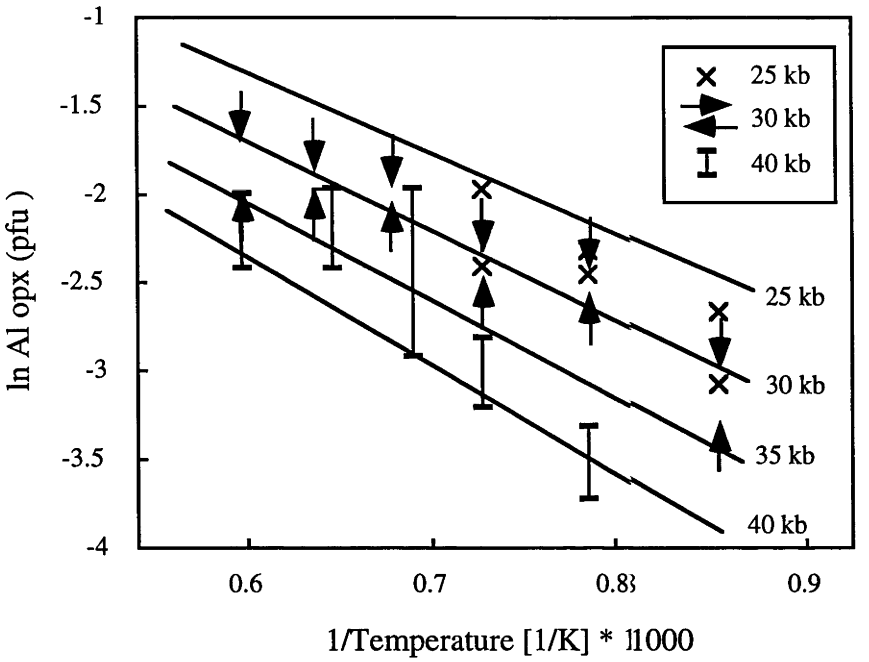

Figure 15 shows the solubility of alumina iin orthopyroxene as a function of temperature and of presssure. Depicted are experimental brackets of Perkins and Newtom (1980) and Nickel et al. (1985) Al pfu = alumina solved in orthopyroxene recalculated on basis of a formula unit of six oxygens.

The new experiments in CMAS (Chapter 1) present reversed garnet compositions at four different P-T conditions alomg the spinel to garnet lherzolite transition. The scatter of the analytical data is rellatively small (e.g. S 21, XPy = 86.5 ± 0.5) and the composition of the garnets stays viirtually constant over the (relatively small) P-T range of the experiments of this study.. According to experimental studies by Perkins and Newton (1980) and Brey et al. (1986) garnet in equilibrium with orthopyroxene, clinopyroxene and olivine becomes more Mg-rich with increasing pressure. The present thermodynamic model reproduces this trend (e.g. at 900°C, 20 kb XPy = 91.3 and at 900°C, 40 kb XPy = 93.1). However, the model also indicates that there might be a slight temperature effect causing garnets to become more pyrope-rich with increasing temperature (e.g. 30 kb, 900°C X Py=92.2 and 30 kb, 1400°C X Py=88.1).

To conclude, a summary plot is presentedl, depicting the isopleths of orthopyroxene in equilibrium with garnet lherzoliite and spinel lherzolite (Figure 16).

The transition from garnet lherzolite to spinel lherzolite can be estimated from where the alumina isopleths bend in P-T space.

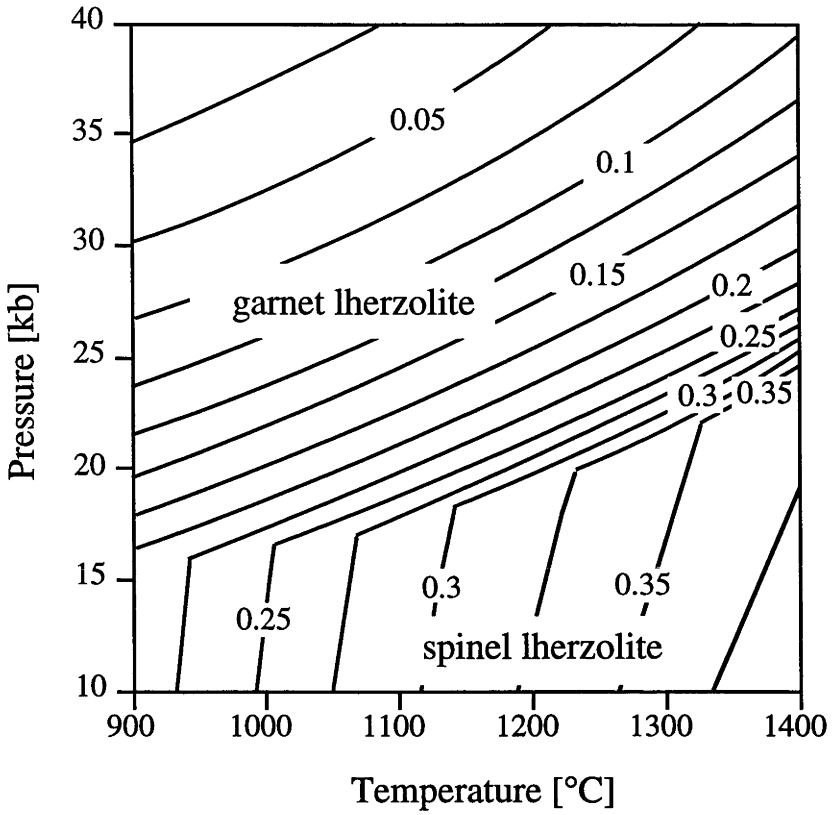

Figure 16 depicts the alumina contents of orthopyroxene in equilibrium with garnet lherzolite and spinel lherzolite, respectively. The transition from garnet lherzolite to spinel lherzolite is where the isopleths cross. The alumina content of orthopyroxene is depicted as isopleths, recalculated on the basis of an orthopyroxene formula unit of six oxygens (pfu).

5.6 TESTS OF THE THERMODYNAMIC MODEL

The equilibrium (10): $CaAl_2Si_2O_8 + 2\ Mg_2SiO_4 = MgAl_2O_4 + Mg_2Si_2O_6 + CaMgSi_2O_6$ has been investigated in early studies by Kushiro and Yoder (1966), Green and Hibberson (1970) and Herzberg (1976). These studies approximately determined the stability field of plagioclase lherzolite relative to spinel lherzolite. However, both Kushiro and Yoder's (1966) and Herzberg's (1976) experiments remained unreversed and rather large uncertainties in the pressures and temperatures have to be assumed, due to the choice of thermocouples and pressure media. Green and Hibberson's (1970) reversal bracket at 1250°C using seeded glass as starting

material is in excellent agreement with both the other two studies. Without any adjustments, the thermodynamic model predicts the transition from spinel lherzolite to plagioclase lherzolite at approximately the correct P-T range as indicated in Figure 10 only at temperatures below 1000°C the thermodynamic model predicts the transition at lower temperatures than observed in Herzberg's (1976) unreversed experiments.

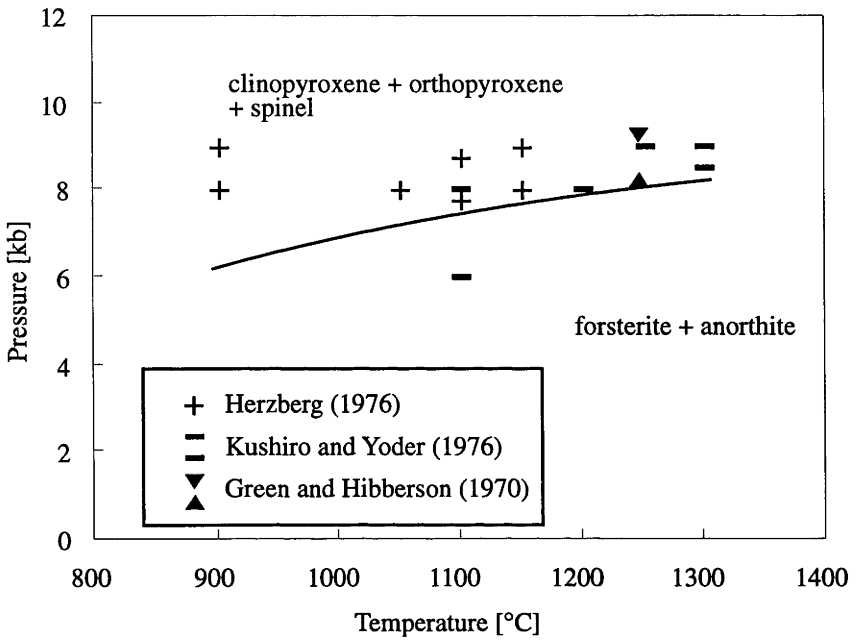

Figure 10 depicts modelling results (lines) compared with experimental brackets from unreversed synthesis experiments from Kushiro and Yoder (1966) and Herzberg (1976), the latter represented by crosses.

Figure 11 compares equilibrium (11) as calculated with the thermodynamic model with the experimental brackets by Perkins (1983). As noted by Wood and Holloway (1984), the reaction ought to be curved as a subsidiary reaction to equilibrium (9) in the system MAS: enstatite + sillimanite = pyrope + quartz. The results from the thermodynamic model disagree with the experimental results, but confirm Wood and Holloway (1984)'s calculations. As Perkins (1983) himself notes (p. 363), in fact at least one of the reversal brackets might be in error due to metastable phase assemblages.

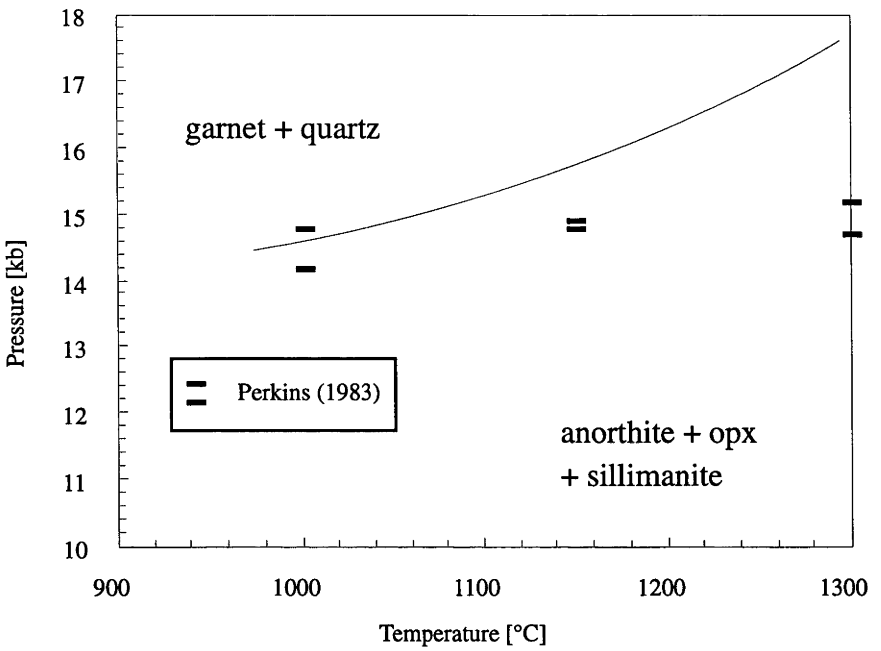

Figure 11 depicts results for the reaction anorthite + orthopyroxene + sillimanite = garnet + quartz. Experimental brackets are from Perkins (1983). As already noted by Wood and Holloway (1984) and Perkins (1983) at least one of the experimental brackets appears to be in error.

As a further test of the thermodynamic model, equilibrium (12) in a quartz-saturated part of the system CMAS has been investigated. Experiments were performed by Hansen (1981) and Perkins (1983). Both experimental studies agree well with each other. It is obvious from the Figure 12 that the computed equilibrium curve underestimates the stability field of the high pressure phase assemblage, if clinopyroxene is assumed to be stoichiometric. As pointed out by Wood and Holloway (1984) the presence of a small amount of non-stoichiometry in aluminous clinopyroxenes in SiO_2-saturated compositions results in stabilisation of garnet-clinopyroxene-quartz assemblages. This mechanism could well explain the observed discrepancy between the thermodynamic model and the experimental brackets from Hansen (1981) and Perkins (1983). The amount of non-stoichiometric clinopyroxene component appears to only small though, increasingly so at higher temperatures (Figure 12).

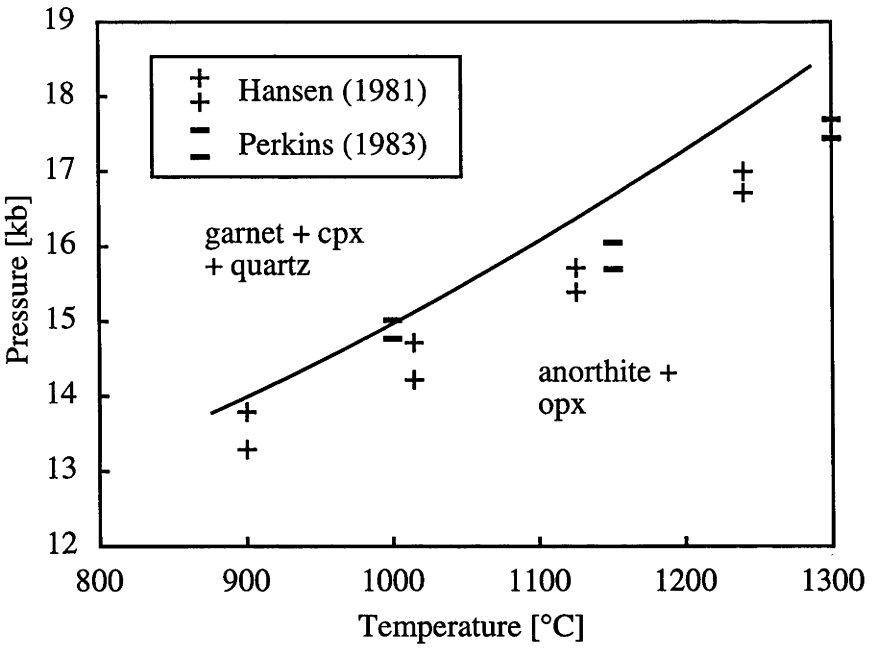

Figure 12: The univariant reaction $CaAl_2Si_2O_8$ + 2 $Mg_2Si_2O_6$ = $Mg_3Al_2Si_3O_{12}$ + $CaMgSi_2O_6$ + SiO_2. Results from our thermodynamic modelling are compared with experimental studies from Hansen (1981) and Perkins (1983). The solid line was calculated assuming stoichiometric clinopyroxenes. Small amounts of a non-stoichiometric clinopyroxene endmember ($Ca_{0.5}AlSi_2O_6$) would increase the garnet + clinopyroxene + quartz stability, bringing the results of the thermodynamic calculations in better agreement with the experimental brackets.

5.7 CONCLUSIONS

Based on high-pressure high-temperature experiments on the transition from garnet to spinel lherzolite (Chapter 1) and on several reversed experiments from the literature, a thermodynamic model has been calibrated that enables calculation of phase equilibria at pressures, temperatures and compositions that approximate upper mantle conditions. Using internally consistent databases as a starting point, thermodynamic properties of endmember phases and of solid solutions were refined to enable computation of high-pressure and high-temperature equilibria. This work may be seen as starting point for further investigations into phase relations of mantle minerals at high pressures and high temperatures and into more complex compositions.

TABLE 3 Thermodynamic data

	this study	H & P '90	B '88	this study	H & P '90	B '88		
endmember	H [J/mol]			S [J/(molK)			V [1/bar]	source
forsterite	-2171870	-2171870	-2174420	94.1	94.1	94.01	4.366	H&P
monticellite	-2250360	-2250360	-2250027	108.1	108.1	108.3	5.148	H&P
anorthite	-4231500	-4232740	-4228730	199.0	199.3	200.186	10.079	
spinel	-2303300	-2303570	-2300313	81.8	81	84.535	3.978	H&P
grossular	-6638300	-6638300	-6632859	256.0	256	255.15	12.535	H&P
pyrope	-6282900	-6283320	-6286548	266.4	266.3	266.359	11.318	H&P
o-diopside	-3187241	-3192790		151.2	148.5		6.782	
enstatite	-3089380	-3089380	-3091104	132.5	132.5	132.34	6.262	H&P
MATS	-3201000	-3192610		115.7	127		5.892	
o-CaTs	-3297136			134.5			6.408	
diopside	-3200150	-3200150	-3200583	142.7	142.7	142.5	6.619	H&P
c-enstatite	-3082380	-3083250	-3091852	136.5	135	132.65	6.324	
c-MATS	-3187870			131.8			6.061	
CaTs	-3305640	-3305640	-3298767	138.0	138	140.751	6.356	H&P
kyanite	-2595330	-2595330	-2594220	82.3	82.3	82.43	4.414	H&P
b-quartz	-909070		-908627	43.54	41.5	44.207	2.367	H&P
corundum	-1675730	-1675730	-1675700	50.9	50.9	50.82	2.558	H&P
coesite	-908170	-908170	-907604	39.0	39	39.424	2.064	H&P
a-quartz	-910800		-910700	41.5	41.5	41.46	2.269	H&P
sillimanite	-2587000	-2586670	-2586091	96.0	96	95.93	5.003	H&P

	a	b	c	d	source	α [1/K]	ß [1/bar]	source
forsterite	234.9	0.1069E-2	-542.9E3	-1906.4	H&P	3.66E-05	7.33E-07	H&P
monticellite	250.7	-1.0433E-2	-797.2E3	-1996.1	H&P	3.69E-05	8.55E-07	H&P
anorthite	391.4	1.2556E-2	-3036.2E3	-2583.2	H&P	1.42E-05	1.29E-06	H&P
spinel	222.9	0.6127E-2	-1685.7E3	-1551.2	H&P	2.59E-05	4.78E-07	H&P
grossular	728.6	-4.0986E-2	-3128.0E3	-6077.4	H&P	2.39E-05	6.30E-07	H&P
pyrope	545.0	2.068E-2	-8331.2E3	-2283.0	H&P	2.63E-05	5.57E-07	H&P
o-diopside	314.5	0.0041E-2	-2745.9E3	-2020.1	estimated	3.42E-05	8.56E-07	H&P
enstatite	356.2	-0.299E-2	-596.9E3	-3185.3	H&P	2.87E-05	7.34E-07	H&P
MATS	344.2	0.2068E-2	-1.74E6	-2830.0		2.89E-05	7.30E-07	H&P
o-CaTs	314.5	0.0041E-2	-2745.9E3	-2020.1	estimated	3.44E-05	8.52E-07	estimated
diopside	314.5	0.0041E-2	-2745.9E3	-2020.1	H&P	3.32E-05	8.31E-07	H&P
c-enstatite	356.2	-0.299E-2	-596.9E3	-3190.3	estimated	2.87E-05	7.35E-07	H&P
c-MATS	389.3	-0.01001	367400.0	-3922.7	estimated	2.16E-05	7.38E-07	estimated
CaTs	347.6	-0.6974E-2	-1781.6E3	-2757.5	H&P	2.61E-05	8.34E-07	H&P
kyanite	303.9	-1.339E-2	-895.2E3	-2904.0	H&P	2.54E-05	4.30E-07	H&P
b-quartz	97.9	-0.335E-2	-636.2E3	-774.0	RHF	0	2.50E-06	G
corundum	157.4	0.0719E-2	-1896.9E3	-988.0	H&P	2.50E-05	3.52E-07	H&P
coesite	108.7	-0.4387E-2	0.0	-1072.5	H&P	1.07E-05	9.69E-07	H&P
a-quartz	97.9	-0.335E-2	-636.2E3	-774.0	RHF	4.40E-05	2.50E-06	G
sillimanite	226.1	1.407E-2	-2440.0E3	-1376.0	H&P	1.44E-05	6.20E-07	H&P

Thermochemical data used in this study compared with data from other studies. Heat capacity function: $Cp = a + bT + cT^{-2} + dT^{-0.5} + eT^{-3}$. Sources: B 88 = Berman (1988), H&P = Holland and Powell (1990), G = Gottschalk (1997), RHF = Robie et al. (1979).

CHAPTER 6

Thermodynamic modelling in the System $MgO-Al_2O_3-SiO_2-Cr_2O_3$ with implications for the transition from spinel lherzolite to garnet lherzolite

6.1 INTRODUCTION

The transition from garnet lherzolite to spinel lherzolite in the system CaO-$MgO-Al_2O_3-SiO_2$ has been investigated experimentally and thermodynamically in the preceding chapters of this thesis. Aiming at an extension of the thermodynamic model into more complex compositions, the partitioning of Cr and Al between orthopyroxene and spinel was investigated in Chapter 4, whilst thermodynamic endmember properties of Cr-bearing spinels were investigated with high-pressure experiments and calorimetrically (Chapters 2 and 3, respectively).

Although Cr is a minor component in the upper mantle (ca. 2600 ppm, O'Neill and Palme 1998) it is well known to have significant effects on phase relations at upper mantle conditions. As Cr preferentially partitions into spinel, it stabilises spinel during partial melting and across the transition from the spinel lherzolite to the garnet lherzolite facies (Green and Ringwood 1967, Wood 1978, O'Neill 1981). The transition from spinel lherzolite to garnet lherzolite is univariant in the systems $MgO-Al_2O_3-SiO_2$ (MAS) and CaO- $MgO-Al_2O_3-SiO_2$ (CMAS), however, the addition of Cr to the system will broaden the P-T field over which the transition from spinel lherzolite to garnet lherzolite takes place (MacGregor 1970, O'Neill 1981, Caroll-Webb and Wood 1986).

Although Cr^{3+} mainly partitions into spinel, pyroxenes also contain a large proportion of the bulk chromium in upper mantle rocks as upper mantle xenoliths typically contain more than 30 % modal orthopyroxene compared to only a few percent of modal spinel. A thermodynamic model that does not account for the intake of Cr into the pyroxenes will result in overestimation of the stability field of spinel bearing assemblages (e.g. Asimov et al. 1995).

Present internally consistent thermodynamic databases (e.g. Holland and Powell 1990, Berman 1988, Gottschalk 1997) generally do not include Cr, probably

because these datasets were intended to calculate equilibria for conditions in the Earth's crust. Another reason for not considering Cr might be the previous uncertainties in the thermodynamic endmember properties of Cr-bearing minerals (c.f. Chapter 2 and 3).

The only thermodynamic model that includes Cr in its database is the software package MELTS (Ghiorso and Sack 1995). The MELTS database only incorporates Cr-spinels based on the mixing model for complex spinels (Sack and Ghiorso 1991). This database uses endmember properties for Cr-spinels that are in error as indicated in Chapter 2 and 3. This may be a reason for the over-complicated formulations for the spinel solid solutions in Sack and Ghiorso (1991 a, 1991 b).

The experimental study of Green and Ringwood (1967) indicated that in a natural composition the transition from garnet lherzolite to spinel lherzolite occurs with a very narrow divariant field of coexisting spinel and garnet lherzolite, at least for the composition studied, which had a bulk Cr/(Cr+Al) ratio of ≈0.08 (Green and Ringwood 1967). This may be consistent with the relative scarcity of lherzolitic mantle xenolitic inclusions in alkali basalts that contain both spinel and garnet (e.g. Ionov et al. 1993). But the scarcity of these xenoliths in alkali basalts could also indicate that alkali basalts only rarely erupt from depths within the Earth where garnet is stable.

In this study, a simple Cr-containing system will be used to exemplify compositional trends and the effect of chromium on the transition from garnet lherzolite to spinel lherzolite. This model must be understood as a first step towards a better understanding of the influence of minor elements on phase relations of the upper mantle.

6.2 THERMODYNAMIC DATABASE AND CALIBRATION OF THE MODEL

The part of the system MgO-Al_2O_3-SiO_2-Cr_2O_3 relevant for the upper mantle contains the following minerals: olivine, spinel, garnet and orthopyroxene.

Olivine

In the system MgO-Al_2O_3-SiO_2-Cr_2O_3 (MASCr) olivine may be described as the pure forsterite endmember. The thermodynamic properties of forsterite have been discussed in Chapter 5.

Spinel

Thermodynamic data for the endmembers $MgAl_2O_4$ and $MgCr_2O_4$ were discussed in Chapters 2, 3, and 5, respectively. The join $MgAl_2O_4$ - $MgCr_2O_4$, as part of the spinel solid solution, has been investigated in a detailed study by Oka et al. (1984). As described in Chapter 4, there is excellent agreement between the results of the thermodynamic evaluation of the current MASCr experiments, and the results of Oka et al. (1984).

Orthopyroxene

The orthopyroxene solid solution may be described in terms of the endmember components $Mg_2Si_2O_6$ (enstatite), $MgAl_2SiO_6$ (Mg-tschermak or MgTs) and $MgCr_2SiO_6$ (Cr-tschermak or CrTs). As part of the calibration of the thermodynamic model for the system CMAS the thermodynamic endmember properties of $Mg_2Si_2O_6$ and $MgAl_2SiO_6$ have been investigated and discussed in Chapters 4 and 5. The endmember properties of $MgCr_2SiO_6$ and information on the solid solution between the three endmember components were investigated in Chapter 4 and are used in the present study.

Garnets

The garnet solid solution may be described in terms of the endmember components $Mg_3Al_2Si_3O_{12}$ (pyrope) and $Mg_3Cr_2Si_3O_{12}$ (knorringite). Whilst internally

consistent thermodynamic properties of the endmember component pyrope have been calibrated in Chapter 5 (CMAS), the thermodynamics of the knorringite endmember are, unfortunately, rather unconstrained.

The knorringite ($Mg_3Cr_2Si_3O_{12}$) endmember

$Mg_3Cr_2Si_3O_{12}$ is only stable at very high pressures (probably greater than 80 kb at 1200°C, see below). Therefore, synthesis of a sufficient amount of knorringite for conventional calorimetry has not been possible yet, as most types of calorimeters require sample masses in the order of a few grams. Even if sufficient amounts of knorringite could be synthesised, low-temperature calorimetric measurements would also be required, as heat capacity-anomalies at very low temperatures are expected, similar to those reported for $MgCr_2O_4$ - spinel (Chapter 3).

A few experimental studies have tried to evaluate the position of a knorringite forming reaction in Temperature-Pressure space. Ringwood (1977), Turkin et al. (1983) and Irifune et al. (1982) investigated the reaction $2\ Cr_2O_3 + 3\ MgSiO_3 = Mg_3Cr_2Si_3O_{12}$ at high pressures and high temperatures.

Both Ringwood's (1977) and Turkin et al.'s (1983) studies agree qualitatively, indicating a negative slope for the reaction in T-P space (Figure 1). Their experiments, however, are not reversed, the interpretation of the reported results may be equivocal due to slow reaction kinetics. Ringwood's (1977) experiments were performed in a Bridgman-anvil high-pressure apparatus (Liebermann et al. 1976). Ringwood states that this high-pressure apparatus is well-suited for experiments below 1100°C, but that the apparatus did not possess pressure stability at T>1200°C. Calibration studies indicated that the pressure of the samples decreased with time due to relaxation of stress of the pressure gaskets. Therefore, Ringwood's quoted pressures are much less accurate than in modern multi-anvil apparatus (Alan Major, pers. comm.) which are routinely calibrated on phase transitions *in situ* at high pressures and high temperatures. Turkin et al.'s (1983) experiments were performed in a split-sphere apparatus, calibrated for pressures at room temperature and at high temperatures. However, their paper appears in a non-peer reviewed journal (in Russian), so that their result should be regarded with reserve.

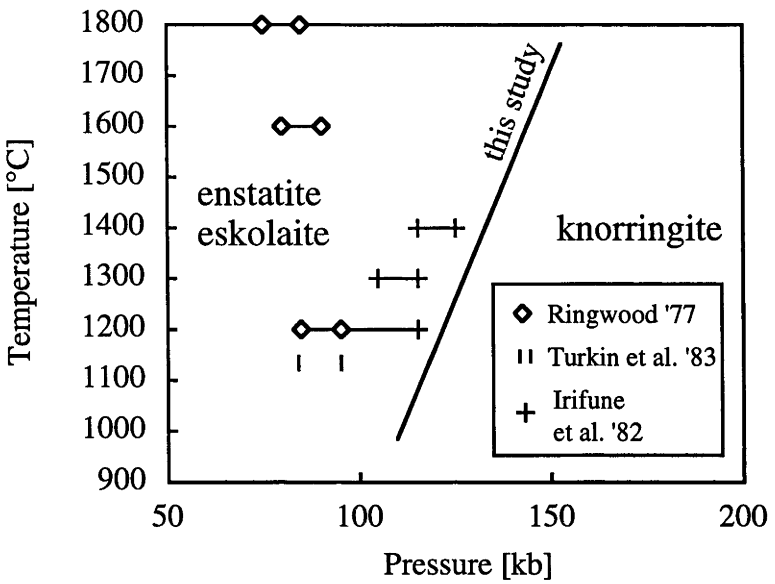

Figure 1 Depicted are experimental results for the equilibrium 2 Cr_2O_3 + 3 $MgSiO_3$ = $Mg_3Cr_2Si_3O_{12}$. Experiments by Ringwood (1977) and Turkin et al. (1983) qualitatively agree, indicating a negative slope for the equilibrium. Experimental results of Irifune et al. (1982) define a positive slope in T-P space. Also depicted are calculations of the present study, using thermodynamic data for knorringite, derived later in this chapter.

In a more recent study, Irifune et al. (1982) and, subsequently, Irifune and Hariya (1983), determined a positive slope for the same equilibrium positioned at considerably higher pressures than the studies of Ringwood (1977) and Turkin et al. (1983). The uncertainties of Irifune et al.'s (1982) experiments may, however, be as large as in Ringwood's (1977) study, as the multi-anvil apparatus used by Irifune et al. (1982) and Irifune and Hariya (1983) in the same laboratory, has only been calibrated at room temperature. As temperature substantially reduces the friction of the pressure-assembly of a multi-anvil apparatus, the pressure estimates of Irifune et al.'s (1982) experiments could be in error. Correction of the calibration curve for high temperatures is expected to bring Irifune et al.'s (1982) experiments closer to Ringwood's (1977) results.

Thermodynamic evaluation of Ringwood's (1977) experiments yields $S°_{298}$ ($Mg_3Cr_2Si_3O_{12}$) = 313 J mol^{-1} K^{-1} and $\Delta_fH°_{298}$ = -5670 kJ mol^{-1}, assuming the thermodynamic properties of Cr_2O_3 and $Mg_2Si_2O_6$ are well known. The heat capacities for Cr_2O_3 and $Mg_2Si_2O_6$ were taken from Chapter 3 and 5, the heat capacities of $Mg_3Cr_2Si_3O_{12}$ are unknown and were estimated as Cp ($Mg_3Cr_2Si_3O_{12}$) = Cp

($Mg_3Al_2Si_3O_{12}$) - Cp (Al_2O_3) + Cp (Cr_2O_3) (c.f. Table 1). The analysis of Irifune et al. (1982) experiments results in approximately $S°_{298}$ = 276 J mol^{-1} K^{-1} and $\Delta_f H°_{298}$ = -5718 kJ mol^{-1}. It has to be pointed out that these estimates have large uncertainties, due to rather wide experimental brackets. It was attempted to find thermodynamic arguments for or against one of the studies, by computing $\Delta_r S_T$ for the following exchange reaction: $Al_2O_3 + Mg_3Cr_2Si_3O_{12} = Cr_2O_3 + Mg_3Al_2Si_3O_{12}$. The thermodynamic data for corundum, eskolaite and pyrope were taken from Chapter 3 and 5, respectively), resulting in $\Delta_r S_{1673K}$ = -20 J $mol^{-1}K^{-1}$ for Irifune et al. (1982) and $\Delta_r S_{1673}$ = +17 J mol^{-1} K^{-1} for Ringwood's (1977) results. As $\Delta S(T)$ is expected to be close to zero, neither of the experimental studies appears to be favourable.

Concluding, the slope of the garnet forming reaction 2 Cr_2O_3 + 3 $MgSiO_3$ = $Mg_3Cr_2Si_3O_{12}$, and thus the thermodynamic properties of knorringite garnet, are not well constrained by either of the experimental studies because of the large experimental uncertainties. The following section investigates other lines of evidence for the thermodynamics of garnets on the join $Mg_3Cr_2Si_3O_{12}$- $Mg_3Al_2Si_3O_{12}$.

Doroshev et al. (1997)

A recent experimental study in the system MgO-Al_2O_3-SiO_2-Cr_2O_3 (Doroshev et al. 1997) investigated the partitioning of Cr and Al between coexisting spinel, garnet, orthopyroxene and olivine. Doroshev et al. (1997) also report experimental results for the equilibrium between garnet, spinel and the Al_2O_3-Cr_2O_3 solid solution. They observed that garnets become Cr-richer with increasing temperature, whilst coexisting spinels tend to become more aluminous with increasing temperature, a trend also observed in a study by the same authors in an Fe-bearing system (FeO-Al_2O_3-MgO-SiO_2-Cr_2O_3) (Brey et al. 1998, in press and Girnis and Brey, in press 1998).

Doroshev et al. (1997) have conducted reversal experiments, using crystalline starting materials. The reversal experiments were aimed at approaching equilibrium from different compositional sides. Doroshev et al.'s (1997) reversals are reported to overshoot the inferred equilibrium composition: i.e. in the case of garnet, the low Cr starting material yields higher Cr garnets after the run, whilst the high-Cr starting material yields lower Cr garnets than the low Cr -starting mixture. This phenomenon has been reported before (Perkins and Newton 1980) and is believed to be caused by overstepping of the equilibrium resulting in crystallisation of minerals of metastable composition. Conventionally, the zone of overlapping compositions is interpreted as the experimental bracket (e.g. Carlson and Lindsley 1988).

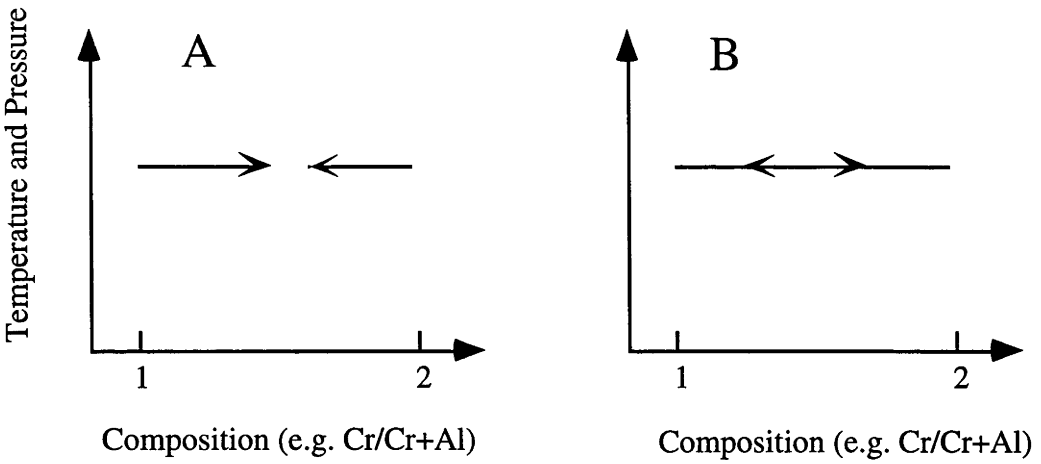

Figure 2: A: At specified pressure and temperature, reversal experiments are conducted using two starting materials with different compositions (1 and 2). The experimental results shown here as arrows approach an intermediate composition from the two compositional directions. The inferred equilibrium composition lies somewhere in between the arrows. B: The socalled 'path-looping' phenomenon: the low composition starting material (1) yields higher compositions after the run than the high composition starting material (2).

However, the true equilibrium composition is not constrained by the overlapping experiments. These experiments do not constitute true brackets, as the 'rate of overstepping' may not necessarily be the same for the different starting materials. In fact, reaction rates starting from a high and low Cr composition are expected to be rather different.

Initial modelling

Nevertheless, initial modelling was done with the garnet solid solution formulated following Doroshev et al. (1997). This formulation is in accordance with Ringwood's (1977) experiments on the knorringite-forming reaction $2\ Cr_2O_3 + 3\ Mg_2Si_2O_6 = 2\ Mg_3Cr_2Si_3O_{12}$ (i.e. negative slope of the reaction in T-P space). Ideal solid solution behaviour was assumed for the garnet solid solution, similar to that found by Mattioli and Bishop (1984) and Wood and Kleppa (1984) for $Ca_3Al_2Si_3O_{12}$ - $Ca_3Cr_2Si_3O_{12}$ garnets (albeit with considerable uncertainty).

The model then reproduced the compositional trends observed by Doroshev et al. (1997) at Cr/(Cr+Al) ratio of more than 0.3. However, at lower Cr/(Cr+Al) ratios this model overestimated the stability of garnet-bearing assemblages relative to spinel

bearing assemblages, so that the transition from spinel harzburgite to garnet harzburgite appeared at a (bulk) Cr/(Cr+Al) = 0.1 at substantially lower pressures than in the Cr-free system $MgO-Al_2O_3-SiO_2$ (MAS), which grossly violates experiments by Wood (1978), O'Neill (1981) and Nickel (1986).

If the assumption of an almost ideal solid solution for the join $Mg_3Al_2Si_3O_{12}$ and $Mg_3Cr_2Si_3O_{12}$ is correct, the experiments by Doroshev et al. (1997) must, therefore, be incorrect in terms of the reported garnet compositions (whilst their spinel data appear to be correct). Doroshev et al. (1997) reported a rather large scatter in their data which may actually be too large to elucidate a pressure or temperature effect on the garnet compositions coexisting with spinel, orthopyroxene and olivine. As mentioned in Chapter 4, an attempt made to fit Doroshev et al.'s (1997) data to the experimental results presented in this study was not successful.

Experiments of this study

The experiments presented in Chapter 4 include two experiments in relatively low Cr/(Cr+Al) bulk compositions (S117-I, S111-II, Cr/(Cr+Al) = 0.2) that yielded garnets coexisting with spinel, orthopyroxene and forsterite. The experiments are not reversed in terms of the garnet compositions. Nevertheless, taking the quoted uncertainties (Table 4 in Chapter 4) into account, these two experiments do not show the compositional trend observed by Doroshev et al. (1997), they rather indicate no dramatic temperature effect on the knorringite solubility in the garnets.

Based on the experimental uncertainties in Doroshev et al.'s (1997) experiments (path-looping) and on the two experiments of the present study, only a very slight temperature effect is proposed here, i.e slightly decreasing Cr-content of garnets in the divariant field with increasing temperatures, combined with lower Cr-content of spinels with increasing temperature (c.f. Figure 3).

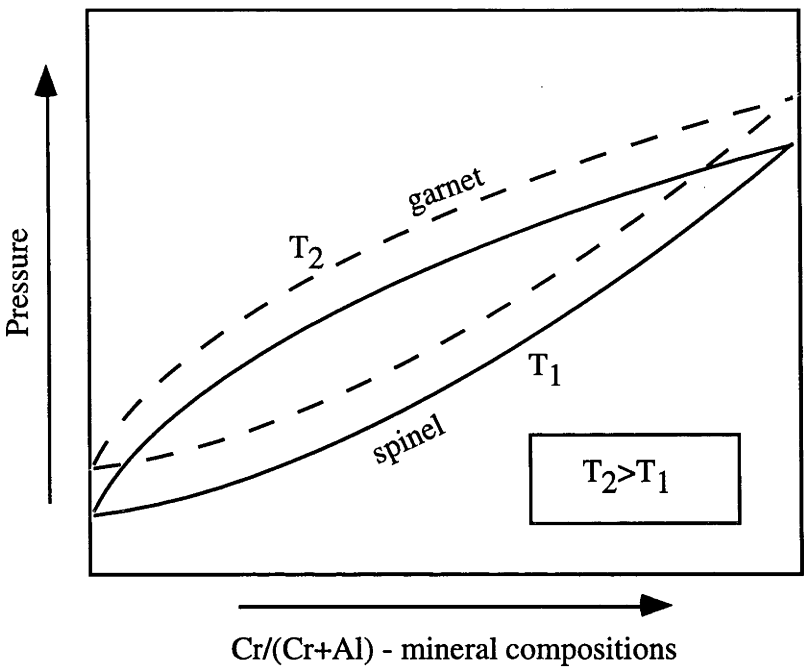

Figure 3: A prediction of the temperature effect on the composition of coexisting garnet and spinel in the divariant field in the system MASCr (*not to scale*). At constant pressure and bulk composition garnets should become Cr-poorer with increasing temperature. The trends shown here are predictions, in disagreement with trends inferred by Doroshev et al. (1997).

Volumes of pyrope - knorringite garnets

The molar volume of pure knorringite has been measured by Ringwood (1977) and Irifune et al. (1982). The molar volumes of garnets on the knorringite-pyrope join have been investigated by Irifune and Hariya (1983) and Doroshev et al. (1997). Compared to the uncertainties in other thermodynamic properties, the molar volumes are reasonably well known. Here the endmember molar volume for knorringite is taken from Irifune et al. (1982). Thermodynamic analysis of the molar volumes indicate a slight non-ideality on the join (Doroshev et al. 1997, Chatterjee and Terhart 1985). Chatterjee and Terhart's (1985) data were chosen to model the volumes of the garnet join, although the results from Doroshev et al. (1997) are also in good agreement.

Modelling strategy for MASCr garnets

In the absence of any direct calorimetric measurements or reliable high-pressure high-temperature experiments on the thermodynamic endmember properties of knorringite, the approach chosen here is to initially assume almost ideal solid solution (with non-ideality only for the volumes) on the pyrope - knorringite join, based on Cr-Al mixing studies on the join $Ca_3Cr_2Si_3O_{12}$- $Ca_3Cr_2Si_3O_{12}$ (Mattioli and Bishop 1984, Wood and Kleppa 1984). The garnet solid solution will be modelled so that the Cr content of the garnet stays virtually constant or slightly decreases with increasing temperature (see above). This trend requires thermodynamic properties of endmember knorringite that are in agreement with a positive slope of the reaction $2\ Cr_2O_3 + 3\ Mg_2Si_2O_6 = 2\ Mg_3Cr_2Si_3O_{12}$ in T-P space, as found experimentally by Irifune et al. (1982). As discussed above, the exact position of this reaction in T-P space is not well known, the thermodynamic endmember properties have, therefore, to be estimated from other observations.

For calibration of the model, the thermodynamic endmember properties of knorringite will be adjusted to satisfy the constraints set by the two experiments presented in this study and the constraints of near-ideal Cr-Al mixing in garnet (Mattioli and Bishop 1984, Wood and Kleppa 1984).

The present two experiments at 35 kb in MASCr (Chapter 4) indicate that garnet becomes stable between 24 and 35 kbar at at bulk Cr/(Cr+Al) = 0.2. According to these experiments, compositions of the garnets at 35 kb, 1673 and 1773 K must be around $X_{Mg3Cr2Si3O12} = 0.12 \pm 0.03$.

In a next step, modelling assumed non-ideal mixing only in the molar volumes and thermodynamic properties for the endmember knorringite derived from the reaction $2\ Cr_2O_3 + 3\ Mg_2Si_2O_6 = 2\ Mg_3Cr_2Si_3O_{12}$ after Irifune et al. (1982). A problem was then encountered as the stability of the garnet solid solution was found to be too high at low bulk Cr/(Cr+Al), resulting in the transition from spinel to garnet harzburgite at lower pressures than in the Cr-free system. Also, the solubility of knorringite in the garnets was found too high at P-T-conditions of the two experiments in MASCr (S117-I and S111-II, c.f. Chapter 4).

There were two possibilities: Firstly to keep the assumption of ideal mixing in the garnet solid solution and violate Irifune et al. (1982) experiments to a rather large extent (knorringite-in at P>150 kb and 1473 K), or alternatively to accept Irifune et

al.'s (1982) experiments and to assume substantial non-ideality in the garnet solid solution.

As a compromise, a W_H=9000 J/mol (in conjunction with W_V=0.1145 J/bar mol) after Chatterjee and Terhart 1985), and thermodynamic endmember properties of knorringite that approximately reproduce Irifune et al.'s (1982) experiments but shifted to higher pressures (by ≈ 5-10 kbar), were chosen (as depicted in Figure 1).

Concluding, there are large uncertainties associated with the thermodynamics of both the garnet solid solution between knorringite and pyrope, as well as with the thermodynamic properties of the endmember knorringite ($Mg_3Cr_2Si_3O_{12}$). It must be stated that all conclusions and applications that involve Cr-bearing garnets are uncertain and will need revision once calorimetric data for $Mg_3Cr_2Si_3O_{12}$ or better experiments involving Mg-Cr garnets become available.

TABLE 1 Thermodynamic data in MgO-Al_2O_3-SiO_2-Cr_2O_3

endmember	formula	$\Delta_fH°_{298}$	$S°_{298}$	V (J/bar)	source
Cr-Ts	$MgCr_2SiO_6$	-2637.8	169.3	6.116	Chapter 4
Mg-Ts	$MgAl_2SiO_6$	-3201.0	115.7	5.892	Chapter 4
enstatite	$Mg_2Si_2O_6$	-3089.4	132.5	6.262	Chapter 5
eskolaite	Cr_2O_3	-1128.2	83.6	2.909	Chapter 3
corundum	Al_2O_3	-1675.7	50.9	2.558	Chapter 5
picrochromite	$MgCr_2O_4$	-1762.0	119.6	4.356	Chapter 2,3
spinel	$MgAl_2O_4$	-2303.3	81.8	3.978	Chapter 5
knorringite *	$Mg_3Cr_2Si_3O_{12}$	-5710.0	275.0	11.738	this study
pyrope	$Mg_3Al_2Si_3O_{12}$	-6282.9	266.4	11.318	Chapter 5
	a	b	c	d	
Cr-Ts	342.5	-5.08E-03	-1.81E+06	-2526.8	Chapter 4
Mg-Ts	344.2	2.07E-03	-1.74E+06	-2830.1	Chapter 4
enstatite	356.2	-2.99E-03	-5.97E+05	-3185.3	H&P
eskolaite	227.3	-2.13E-02	3.54E+06	-2567.3	Chapter 3
corundum	157.4	7.19E-04	-1.90E+06	-988	H&P
picrochromite	221.2	-1.02E-03	-1.76E+06	-1247.9	Chapter 3
spinel	222.9	6.13E-03	-1.69E+06	-1551.2	H&P
knorringite	614.9	-1.36E-03	-2.89E+06	-3862.3	py-cor+es
pyrope	545.0	2.07E-02	-8.33E+06	-2283	H&P

Internally consistent thermodynamic data used in this chapter. The heat capacity function is $Cp = a + bT + cT^{-2} + dT^{-0.5}$. units: $S°_{298}$ [$Jmol^{-1}K^{-1}$], Δ_fH_{298} [kJ mol^{-1}]. H&P= Holland and Powell (1990). * thermodynamics of knorringite are discussed in Chapter 6.

6.3 APPLICATIONS

A computer algorithm based on free energy minimisation techniques was used to compute equilibria at high pressures and high temperatures (c.f. Chapter 5).

6.3.1 The transition from spinel peridotite to garnet peridotite

The effect of Cr on the position of the spinel-garnet transition as a function of pressure and temperature (Figure 4) was investigated. In the Cr-free systems MAS and CMAS the transition can be described by univariant equilibria (c.f. Chapter 5). In more complex systems, however, the garnet forming equilibria are multivariant, resulting in a broadened P-T field where garnett and spinel co-exist.
There are three major effects in the model system MgO-Al_2O_3-SiO_2-Cr_2O_3, which influence the position of the transition in P-T space.

1 Cr strongly partitions into the spinel phase relative to the other phases, thus stabilising the spinel-lherzolite assemblage and shifting the garnet-in boundary to higher pressures.
2 In the thermodynamic model developed here garnets are predicted to become slightly less chromian with increasing temperature at constant pressure and bulk composition (Figure 3) thus, with increasing temperature, slightly de-stabilising the garnet-bearing assemblage relative to the spinell-bearing assemblage.
3 Pyroxenes contain only a small amount of Cr relative to spinel, but the modal abundance of pyroxene is much greater than that of spinel. Therefore the shift of the transition to higher pressures will depend on the amount of pyroxene present, i.e. a mineral assemblage with a higher pyroxene/spinel ratio will be stable to higher pressures than an assemblage with smaller amounts of modal pyroxene present.

As Figure 4 shows, the first mechanism dominates, resulting in a shift of the transition to higher pressures as a function of the bulk Cr/(Cr+Al). At higher temperatures the shift is greater with high Cr/(Cr+Al), interpreted to be caused by lower solubility of Cr in the garnet solid solution at higher temperatures.

Fe^{2+} is known to shift the transition to lower pressures (O'Neill 1981). As the partitioning of Fe^{2+} between the phases is closer to 1 than in the case of chromium, Fe^{2+} is expected to influence the transition to a much lesser extent. Fe^{3+} behaves like Cr^{3+}, and may be expected to have a similar effect (MacGregor 1970).

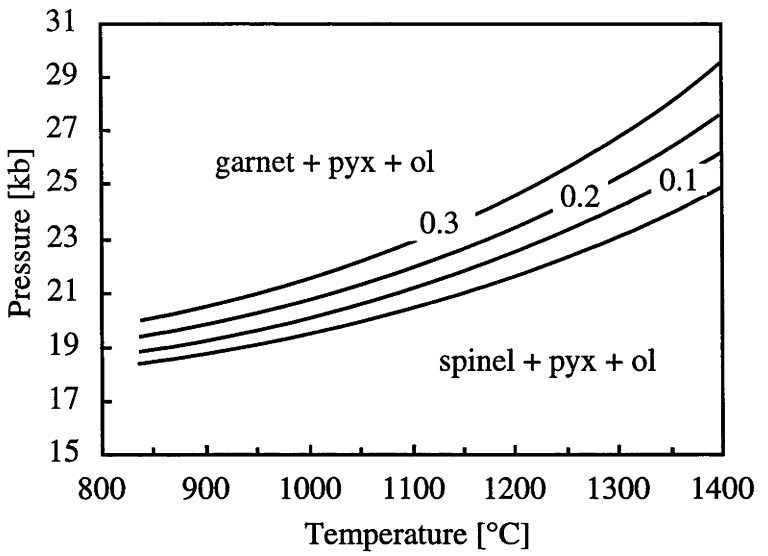

Figure 4 depicts the garnet-in boundary in the system MASCr. Lines are calculated with different bulk Cr/(Cr+Al) ratios ranging from 0 (MAS) to Cr/(Cr+Al) = 0.3. The transition is shifted to higher pressures as more Cr substitutes for Al in the spinel. The garnets become less chromium rich with increasing temperature. Calculations were done with a Mg/Si ratio = 1.5.

In an early study, Wood (1978) investigated the effect of Cr on the garnet-in boundary in the system MASCr. His results (Wood 1978, p.80) show similar trends as the calculations depicted in Figure 4. Comparison between the present results (Figure 4) and results from Wood (1978) is difficult as the latter study does not present experimental and analytical details as e.g. bulk Cr/(Cr+Al), orthopyroxene compositions and Mg/Si ratios of the bulk.

Nickel (1986) investigated the influence of Cr on the garnet-in reaction in the system CMASCr. Nickel (1986) suggested that, in contrast to studies by O'Neill (1981) and Caroll-Webb and Wood (1986), the influence of Cr on the pressure required for the stability of garnet is far from linear. He suggested that the presence of minor amounts of Cr shifts the garnet boundary to higher pressures, whilst at higher Cr/(Cr+Al) in the bulk the pressure increase (relative to the CMAS system) is rather small (Figure 5).

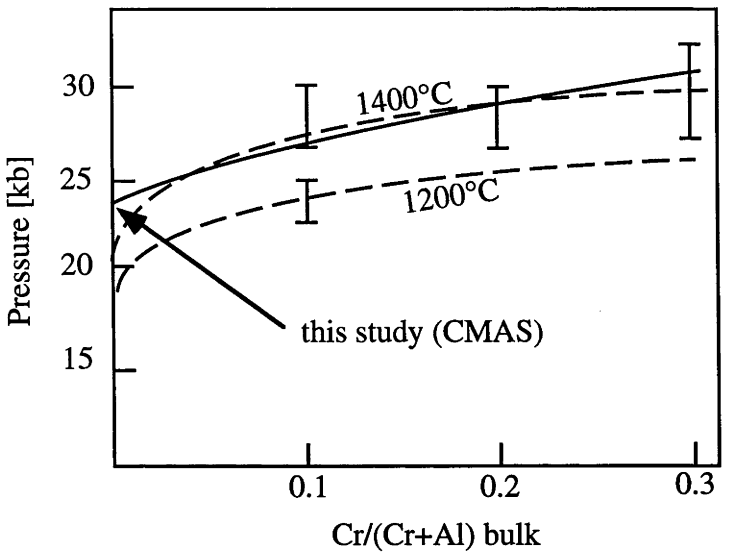

Figure 5: The position of the garnet-in reaction as a function of the Cr/(Cr+Al) ratio of the bulk. Depicted are experimental brackets of Nickel (1986) in the system CMASCr at 1200°C and 1400°C. Also shown are experimental results in the Cr-free system CMAS (Gasparik 1984 and from this study at 1400°C). The diagram has been adopted from Nickel (1986). The dashed line is drawn after Nickel, the strong curvature at Cr/(Cr+Al)<0.1 is mainly caused by Gasparik's (1984) data in CMAS. The present results in CMAS (Chapter 1) on the garnet-in reaction indicate significantly higher pressures for the garnet-spinel transition: The present results, in conjunction with Nickel's (1986) data indicate, at least at 1400°C, an almost linear influence of Cr on the garnet-in reaction.

Nickel's (1986) interpretation, however, depends critically on the position of the garnet-in reaction in CMAS (as discussed by Harley and Carswell 1990). New experiments in CMAS (Chapter 1) determined the garnet-in boundary at substantially higher pressures (24-25 kb at 1400°C) than previous estimates (Gasparik 1984) so that the influence of Cr on the garnet-in reaction is not far from linear.

6.3.2 The width of the field where spinel and garnet co-exist

Green and Ringwood (1967) have investigated the transition from spinel lherzolite to garnet lherzolite in natural compositions. Their pyrolite III composition was simulated in the present calculations, depicted in Figure 6. There is good agreement between Green and Ringwood's (1967) observations of a very narrow P-T

area where spinel and garnet coexist. In the present model a divariant field of about 2.5 kb is observed at a bulk Cr/(Cr+Al) of 0.08 (as in pyrolite III), in perfect agreement with observations by Green and Ringwood (1967), indicating that chromium only can account for the observed broadening of the transition from spinel lherzolite to garnet lherzolite.

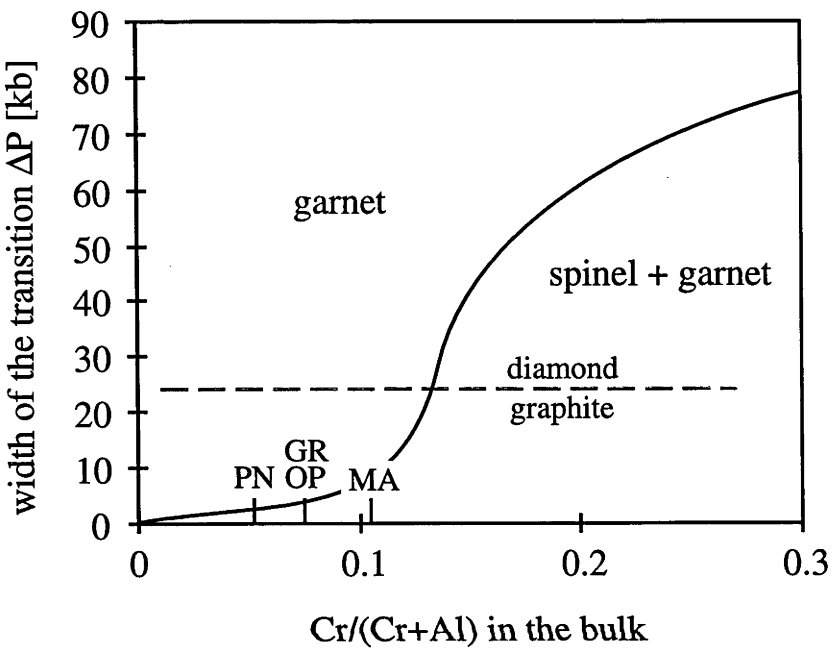

Figure 6: The width of the coexistence of garnet and spinel in the system MASCr as a function of Cr/(Cr+Al) in the bulk. The divariant field is narrow at lower Cr contents of the system. At Cr/(Cr+Al) ratios greater than 0.1 the width of the divariant field increases dramatically due to the drastic decrease in modal spinel which becomes more and more chromium rich. Calculations were done with a Mg/Si ratio of 1.5, very close to the pyrolite III composition of Green and Ringwood (1967) with a (Mg+Ca+Fe)/Si = 1.46. Calculations were performed at 1100°C. Similar trends are observed at other temperatures. Also depicted are estimates for primitive mantle compositions: Maaloe and Aoki 1977, Palme and Nickel 1985, O'Neill and Palme 1998 and Green and Ringwood's (1967) pyrolite III. Also depicted is the diamond-graphite transition. It is obvious that diamond can only be stable together with spinel if the bulk composition is fairly depleted (i.e. Cr/(Cr+Al) > 0.15).

Cr-rich spinels are often used as indicator minerals in diamond exploration. Figure 6 indicates the relationship between depleted and fertile mantle. From Figure 6 it is obvious that only with increasing depletion of the rock (i.e. increasing Cr/(Cr+Al)

of the bulk) spinel becomes stable. Thus spinel + garnet + diamond bearing rocks are expected top be depleted, whilst diamond-bearing garnet lherzolites are more fertile and are spinel-free.

6.3.3 Garnet - orthopyroxene geothermobarometry

Geothermobarometry in the garnet lherzolite stability field is based on the equilibrium

$$Mg_2Si_2O_6 + MgAl_2SiO_6 = Mg_3Al_2Si_3O_{12} \qquad (3)$$
enstatite MgTs pyrope

Geothermobarometers have been developed (Harley and Green 1982, Nickel and Green 1985, Wood 1974, Brey and Köhler 1990) that are based on experimental results in simple systems (CMAS, MAS, CMAS-FeO, CMASCr). Using the present thermodynamic model in the system MASCr, we have the possibility of exploring the influence of Cr on the solubility of alumina in orthopyroxene coexisting with garnet. It has to be pointed out, however, that the present calculations have to be regarded as preliminary due to the uncertainties associated with the pyrope-knorringite solid solution. Nevertheless, even these preliminary calculations should indicate trends in P-T compositional space. Choosing a pressure of 30 kb and 1100°C we then calculate equilibria with garnet and orthopyroxene and compare them to pressure-estimates with the commonly used geothermobarometer of Nickel and Green (1985).

Nickel and Green's (1985) formulation is based on CMAS and CMASCr experiments. This formulation incorporates an empirical correction for the Cr-content of garnets (Nickel 1986), it also only empirically accounts for the reduction of alumina in orthopyroxene.

The geothermobarometer of Nickel and Green (1985) systematically overestimates pressures as a function of bulk Cr/(Cr+Al) (Figure 7). Due to the uncertainties in the garnet solid solution (see above) it is not possible in this study to rigorously assess the magnitude of the Cr-effect of geobarometry.

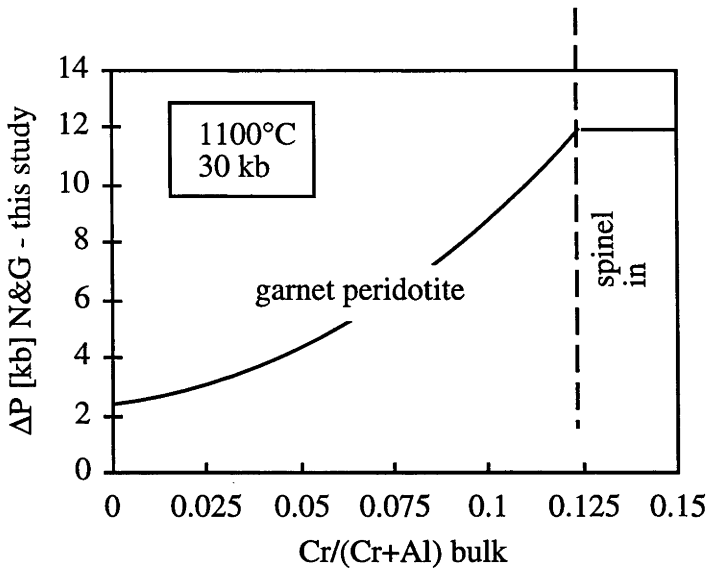

Figure 7: Calculated equilibria of coexisting garnet, orthopyroxene and olivine, compared with geobarometric estimates using the formulation of Nickel and Green (1985). Calculations were done with a Mg/Si ratio of 1.5. Note that Nickel and Green (1985) slightly overestimate pressures in the MAS system (2.3 kb) due to their choice of data in the Cr-free CMAS system. With increasing Cr/(Cr+Al) of the bulk, Nickel and Green (1985) increasingly overestimate pressure. At a Cr/(Cr+Al) of ca. 0.125 spinel becomes stable, then spinel, garnet and orthopyroxene compositions are independent of the bulk.

Part of the discrepancy may be due to the effect of Ca, which is implicitly taken into account in the empirical formulation of Nickel and Green (1985), for clinopyroxene saturated compositions. Clearly, however, the Nickel and Green (1985) formulation cannot be used for clinopyroxene undersaturated compositions (e.g. harzburgites).

6.4 CONCLUSIONS AND FUTURE WORK

The present study presents a thermodynamic model for compositions in the system MASCr. The thermodynamic analysis of Cr bearing experiments presented here clearly indicates that thermodynamics of Cr-bearing garnets involving pyrope and knorringite are virtually unconstrained. Previous experimental studies are contradictory, probably due to uncertain pressure calibrations of the high-pressure

apparatus and due to kinetic problems with the experiments resulting in metastable garnet compositions (c.f. "path-looping").

In this chapter thermodynamic properties for the garnet solid solution on the join knorringite - pyrope are suggested that are compatible with the present (admittingly limited) experimental results in the P-T region of the system MASCr where garnet is stable. The results roughly agree with results on the Cr-Al mixing in garnets on the uvarovite-grossular join (Mattioli and Bishop 1984, Wood and Kleppa (1984). The present suggestions also qualitatively agree (positive slope in T-P space, Figure 1) with experiments from Irifune et al. (1982) on the knorringite forming reaction $2\ Cr_2O_3 + 3\ Mg_2Si_2O_6 = 2\ Mg_3Cr_2Si_3O_{12}$, although the stability of knorringite is predicted to be somewhat less than previously envisaged (Irifune et al. 1982).

There is a need to investigate knorringite bearing phase relations in a better calibrated high-pressure apparatus. These experiments should be reversed, and probably need to employ some sort of flux to speed up reaction rates. The recent development of a 1/2" 'ultra-high-pressure' piston-cylinder (UHPPC) apparatus at RSES is certainly a step in the right direction, as the calibration of this particular apparatus will, in the near future, be more accurate than the Belt apparatus or multi-anvil systems. The UHPPC has so far reached pressures of about 65 kbar routinely, although pressure calibration is still underway and further development is needed.

Recent development in calorimetry indicates that measurements of small sample sizes might be possible in the nearer future. Schnelle and Gmelin (1995) developed a micro-calorimeter that enabled measurements of Cp-curves both at low-temperatures and with sample sizes of less than 100 mg. Application of this technique to high-pressure phases would be rewarding for phase equilibria calculations at high pressures, especially if sufficient amounts if Cr-Al garnets could be synthesised in a 1/2" piston-cylinder apparatus at pressures of more than 80 kbars.

Future calibrations of the aluminous orthopyroxene-garnet geothermobarometer need to incorporate appropriate corrections for the influence of Cr on the solubility of alumina in orthopyroxene. That, however, depends critically on a better understanding of the Cr and Ca bearing garnet solid solutions.

Conclusions and Future Work

The transition from spinel lherzolite to garnet lherzolite

This study presents new and reversed experimental results on the transition from garnet lherzolite to spinel lherzolite in the simplified system CaO-MgO-Al_2O_3-SiO_2. The transition at temperatures close to the solidus is found to be substantially higher than previously estimated.

Although Cr and Fe^{2+} shift the reaction to higher or lower pressures, the relative position of the transition in natural compositions has to be substantially higher than in some recent estimates (e.g. Hirschmann and Stolper 1996). The current results further complicate the interpretation of the so-called 'garnet signatures' in MORB, as the stability of garnet is shown here to be less than what has previously been assumed. Melting in the presence of garnet peridotite would begin even at greater depths, thus leading to an expected thickness of the oceanic crust even greater than previously predicted by simple melting models (e.g. McKenzie and Bickle 1988).

The present results indicate that either the rather simple melting models are in error, maybe because of the assumption of a linear increase in melt productivity or melting does indeed not start in the garnet lherzolite stability field, but in equilibrium with spinel lherzolite. The latter suggestion is supported by recent trace element partitioning studies showing that heavy rare earth elements (HREE) become increasingly compatible in clinopyroxene with increasing pressure (Wood and Blundy 1997, Wood et al. 1998), thus indicating that garnet may not be needed to explain a relative HREE depletion in mid ocean midge basalts.

Based on the experimental results in conjunction with experimental data from literature, a comprehensive thermodynamic model for subsolidus equilibria in the system CaO-MgO-Al_2O_3-SiO_2 has been developed (Chapter 5). A computer algorithm based on the thermodynamic model utilises free energy minimisation techniques and successfully reproduces the present results on the transition from spinel lherzolite to garnet lherzolite as well as data of several other reversal studies.

Thermodynamics of Cr-bearing phases

The present study investigates the position of the near-univariant reaction $MgCr_2O_4 + SiO_2 = MgSiO_3 + Cr_2O_3$. The results, combined with assessed thermodynamic data for $MgSiO_3$ and SiO_2 and with new data for Cr_2O_3 (Chapter 3), give the entropy and enthalpy of formation of $MgCr_2O_4$ spinel: $\Delta_fH°_{298} = -1762.0 \pm 1.4$ kJ mol^{-1} and $S°_{298} = 119.6 \pm 0.9$ J $K^{-1}mol^{-1}$. This entropy is some 14 J K mol^{-1} more than the calorimetrically determined value, and implies a value for the magnetic entropy of $MgCr_2O_4$ consistent with an effective spin quantum number (S') for Cr^{3+} of 1/2 rather than the theoretical 3/2, indicating, as in other spinels, spin quenching.

The present study also presents new results obtained from low-temperature heat capacity measurements of $MgCr_2O_4$, basically confirming the results from the high-pressure experiments, with $S°_{298} = 118.3 \pm 1.2$ J $K^{-1}mol^{-1}$. The good agreement between calorimetry and high-pressure high-temperature experiments also indicate a valid pressure and temperature calibration of the piston-cylinder high-pressure apparatus used in the present study.

Additional low-temperature heat capacity measurements for Cr_2O_3 and $FeCr_2O_4$ have been performed to further investigate the thermodynamics of Cr-bearing minerals. New standard thermodynamic data are presented for $FeCr_2O_4$ with $S°_{298} = 152.2 \pm 3.0$ J mol^{-1} K^{-1}. This estimate of $S°_{298}$ for $FeCr_2O_4$ is some 6 J mol^{-1} K^{-1} higher than previous estimates by Shomate (1944: $S°_{298} = 146.1 \pm 1.7$ J mol^{-1} K^{-1}), due to a heat capacity anomaly at $T_N = 36.5 \pm 0.1$ K, interpreted to correspond to a magnetic transition. The heat capacity of Cr_2O_3 was investigated from 1.5 to 339 K and a broad heat capacity anomaly was observed, peaking at the Néel temperature at 305.5 K due to a magnetic transition. The present data basically confirm the results of Bruce and Cannell (1977) whilst the present heat capacity data lie considerably below the curve of Volger (1952) and higher than the curve of Anderson (1937). The present results indicate an entropy at 298.15 K for $Cr_2O_3 = 82.8 \pm 0.8$ J mol^{-1} K^{-1}.

The present calorimetric results indicate that basic thermodynamic data for many more Cr-bearing phases may be in error, as previous heat capacity measurements could have missed Cp-anomalies at temperatures below the range of conventional calorimeters.

The partitioning of Al and Cr between orthopyroxene and spinel

High-pressure high-temperature experiments have been performed to investigate the partitioning of Cr and Al between co-existing spinel and orthopyroxene was investigated in the system MgO-Al_2O_3-SiO_2-Cr_2O_3 (Chapter 4) aimed at developing a thermodynamic model for Cr-bearing pyroxenes. The experiments were conducted in the spinel stability field only as the solubility of alumina in pyroxenes in equilibrium with spinel and olivine is much larger as in equilibrium with garnet and is, therefore, most sensitive to the influence of Cr. Two experiments in relatively low Cr compositions also produced garnet. The experiments indicate that the amount of alumina dissolved in orthopyroxene is reduced with increasing Cr content of the system. The reduction of alumina content is a function of temperature and also slightly depends on pressure. The partitioning of Cr and Al between coexisting pyroxenes and spinels, however, is virtually independent of pressure and temperature. Thermodynamic evaluation of the experiments confirms substantial non-idealities in the spinel solution, whilst the Cr-Al mixing is suggested to be ideal in orthopyroxenes. An additional advantage of the MASCr experiments is that these data can distinguish between alternative models for the orthopyroxene solid solution in the MAS system, strongly favouring the one-site model.

Combining the thermodynamic information on Cr-bearing pyroxenes with the new thermodynamic properties for $MgCr_2O_4$, a thermodynamic model has been developed that enables calculations of sub-solidus phase equilibria in the system MASCr. Chapter 6 describes the calibration of the model and the argumentation for a solid solution model for binary garnets on the join $Mg_3Al_2Si_3O_{12}$ - $Mg_3Cr_2Si_3O_{12}$. The thermodynamic properties of the Cr-bearing garnets are shown to be virtually unconstrained, there is a need for better experiments involving Cr-bearing garnets. Recent trends in calorimetry should, in the nearer future, allow calorimetric measurements of high-pressure Cr-bearing garnets, as sample sizes required for some calorimeters are only in the order of 100 mg.

Thermodynamic calculations in the system MASCr have been performed to investigate the transition from spinel to garnet peridotite as a function of the Cr-content of the bulk. Further calculations in MASCr show that the divariant field where garnet and spinel coexist is rather narrow at ratios of $Cr/(Cr+Al)<0.1$, but broadens non-linearly with increasing Cr content of the bulk. The calculations also indicate that

present empirical geothermobarometers (e.g. Nickel and Green 1985) may, at least for harzburgites, systematically overestimate equilibrium pressures derived from co-existing garnet and orthopyroxene.

7. Appendix A:

Activity-composition relations in Al-Cr solid solutions.

Cr^{3+} can replace Al in octahedral co-ordination in many minerals, and complete solid solution exists between, for example, the oxides Al_2O_3-Cr_2O_3 (albeit with a solvus below ~ 950°C (Roy and Barks 1972), spinels M Al_2O_4-M Cr_2O_4, where M is Mg, Fe^{2+}, Zn etc. (O'Neill and Navrotsky 1984), garnets $Ca_3Al_2Si_3O_{12}$-$Ca_3Cr_2Si_3O_{12}$ (Huckenholz and Knittel 1975) and $Mg_3Al_2Si_3O_{12}$-$Mg_3Cr_2Si_3O_{12}$ (Irifune and Hariya 1983, Doroshev et al. 1997) and clinopyroxenes $NaAlSi_2O_6$-$NaCrSi_2O_6$ (Carroll-Webb and Wood 1986). However, Cr^{3+} generally does not replace Al on tetrahedral sites. For example, the amounts of Cr substituting in $CaAl_2Si_2O_8$ (anorthite), are generally too small to be reported even when the anorthite-rich plagioclase is in equilibrium with Cr-rich spinel (e.g. Deer et al. 1992).

Approximate activity-composition relations in $Ca_3Al_2Si_3O_{12}$-$Ca_3Cr_2Si_3O_{12}$ garnet solutions were determined by Mattioli and Bishop (1984), by displacement of the univariant reaction:

$$Ca_3Al_2Si_3O_{12} = CaAl_2Si_3O_8 + Al_2SiO_5 + SiO_2$$

They found the solution to be nearly ideal, in agreement with the almost negligible excess enthalpies of solution found by Wood and Kleppa (1984) from oxide melt solution calorimetry.

More precise activity-composition relations in Al-Cr oxide and silicate solid solutions may in principle be determined from analysis of co-existing solid solutions. However, as has been shown for Fe^{2+}-Mg solid solutions, such measurements can only accurately yield the difference in the activity-composition relations of the two phases (e.g., Matsui and Nihizawa 1974; von Seckendorff and O'Neill 1993): it is necessary for absolute values of one of the phases to be known independently. Fortunately, such measurements exist for the Al_2O_3-Cr_2O_3 solid solution. Jacob (1978) determined the mixing properties of this solution from the displacement of the reaction:

$$2\ Cr + 1.5\ O_2 = Cr_2O_3$$

in fO_2-T space, using an reversible electromotive force (EMF) method with YDT (yttria-doped thoria) solid oxygen-specific electrolytes. The low fO_2 of the Cr- Cr_2O_3 equilibrium is beyond the useful range of zirconia-based electrolytes. The thoria-based electrolytes are difficult to obtain (they appear to be no longer manufactured

commercially), and are also extremely expensive. Consequently, it is unlikely that Jacob's (1978) experiments will be repeated.

Jacob's experimental results were re-interpreted by Chatterjee et al. (1982), who fitted them to a sub-regular (asymmetric) solution model. Chatterjee et al (1982) also reported molar volumes for the $(Al,Cr)_2O_3$ solution. This modelling was then used by Oka et al. (1984) in conjunction with their experimental partitioning data on co-existing $(Al,Cr)_2O_3$ - $Mg(Al,Cr)_2O_4$ solid solutions at 25 kb, to derive activity-composition relations for the latter solution. They found that the $Mg(Al,Cr)_2O_4$ spinel solid solution shows slightly asymmetric positive deviations from ideality. However, the uncertainties (i.e., standard deviations) were not given by Chatterjee et al. (1982) or by Oka et al. (1984); indeed, nor were the details of the regression method they used. In view of the importance of the solution properties of $Mg(Al,Cr)_2O_4$ spinels to the interpretation of the experimental data of this study, the data fitting of these studies have been re-examined in detail.

Activity-compositions in $(Al,Cr)_2O_3$ solutions

Jacob (1978) studied seven compositions (nominal X_{Cr} from 0.1 to 0.9 using cells of the type:

Pt, $(Al,Cr)_2O_3$+Cr | YDT | Cr_2O_3+Cr,Pt

The temperature range was 800 to 1320 °C. Results are given in the form of an equation for the EMF of the cell, E (in millivolts). Data fitting was accomplished as follows. The EMF at 1173 K (a temperature near the middle of the range studied, and close to the optimum for this type of experiment, according to Pownceby and O'Neill, 1994 a) was fitted to an equation of the form

$$3FE = \Delta G(mix) = RT \ln X_{Cr} + [AG_0 + AG_1(4X-1).....]$$

where the terms in AG_0 etc. are the terms in the Redlich-Kister expansion, F is the Faraday constant (96484.56 J/C), and R the gas constant. The data were weighted assuming an uncertainty, one standard deviation, of 0.4 to 0.7 mV in E (Jacob 1978, his Table 1), and of ±0.01 in X_{Cr}. The latter is assumed, as no uncertainty in composition is given by Jacob (1978). This is unfortunate, as in these type of experiments, it is the uncertainties in composition which generally predominate.

For a one-term model (i.e., a symmetric or regular solution, AG_0=19390 ± 690 J/mol with a reduced chi-squared (χ^2_ν) of 2.57. For the two term model (asymmetric or subregular), AG_0=20200 ±700 and AG_1 = -2880 ±1100 J/mol, with χ^2_ν = 1.48,

i.e., seemingly a significantly better fit. Calculated values of X_{Cr} from these two fits are compared to their nominal values in Table A-1.

Table A-1

X_{Cr} nom	X_{Cr} calc 1-term	X_{Cr} calc 2-term
0.1	0.1132	0.0968
0.24	0.2463	0.2386
0.37	0.3707	0.3751
0.5	0.4982	0.5094
0.64	0.6057	0.6181
0.77	0.7707	0.7774
0.9	0.9017	0.9032

It may be seen that the better fit of the two-term (subregular) model is entirely due to one composition, that at X_{Cr}=0.64 (nominal).

The calculated values of X_{Cr} for each model were then used as the input values in the regression to determine the temperature dependence of the mixing parameters AG_0 ($\pm AG_1$), i.e., the excess entropies of mixing, from the slopes dE/dT of the EMF of the cells. The uncertainty in the slopes was assumed to be the uncertainty in the EMF for each cell as given by Jacob (1978), divided by 400 K, the typical temperature range over which the cells were studied. For the one-term model, $AS_0 = 1.53 \pm 0.4$ $Jmol^{-1}K^{-1}$, while for the two term model, $AS_0 = 2.10 \pm 0.39$ and $AS_1 = 1.09 \pm 0.60$ $Jmol^{-1}K^{-1}$.

The molar volumes of $(Al,Cr)_2O_3$ solutions measured by Chatterjee et al. (1982) were fitted to quadratic and cubic expressions in X_{Cr}, corresponding to the symmetric (regular) and asymmetric (subregular) solution models respectively, weighting the data according to the uncertainties in volume given by Chatterjee et al. (1982: their Table 1). However, Chatterjee et al. (1982) report their uncertainties in composition as standard errors of the mean, rather than as standard deviations. Standard errors of the mean tend to underestimate the true uncertainties in composition, probably because it is doubtful whether the parent population of compositions being sampled by a set of analyses is really completely homogenous. It is therefore preferable to use standard deviations, which were assumed to be three times the reported standard errors of the mean (as would be the case if the latter were based on ten analyses).

With this weighting,

$V/cm^3 = 25.578 + 3.634X_{Cr} - 0.158X_{Cr}^2$ $= 2.16$

or

$$V/cm^3 = 25.578 + 3.795X_{Cr} - 0.629\ X_{Cr}^2 - 0.311\ X_{Cr}^3 \qquad = 1.13$$

Hence for each g-atom of Al,Cr mixing, $AV_0 = 0.0079$ J/bar (symmetric model) or $AV_0 = 0.0081$ and $AV_1 = -0.0078$ J/bar. These numbers are slightly different from those given by Chatterjee et al. (1982), because the latter used a simplified regression method with unweighted data.

In summary: for a one-term, regular (symmetric) solution model:

AG_0 (=W) = 17300 + 1.53 T + 7.9 P

with an uncertainty of ~ 700 J/mol.

For a two-term, subregular (asymmetric) model:

$AG_0 = 17320 + 2.10\ T + 8.1\ P$

$AG_1 = -1380 - 1.09\ T - 7.8\ P$

where P is in kbar. The effect of pressure is obviously quite minor.

Activity-compositions in $Mg(Al,Cr)_2O_4$ spinel solutions

Oka et al. (1984) measured the partitioning of Al and Cr between $(Al,Cr)_2O_3$ and $Mg(Al,Cr)_2O_4$ solutions at 796, 1050 and 1250°C. Compositions were determined from lattice parameters (see below). The uncertainties in X_{Cr} for the $Mg(Al,Cr)_2O_4$ solid solutions are quoted as 0.0091, 0.0022 and 0.0015 at 796, 1050 and 1250°C respectively, while those for X_{Cr} in the $(Al,Cr)_2O_3$ solution are 0.0200, 0.0172 and 0.0028. Thus the composition of the $(Al,Cr)_2O_3$ oxide solution is quoted as being nearly an order of magnitude more precise at 1250°C than at the other two compositions. The scatter of the data at 1250°C shows that this level of precision is over-optimistic. Therefore, to lessen the domination of these data in the regression analysis, their uncertainty in X_{Cr} was doubled to 0.0056.

With these uncertainties, the results of Oka et al. (1984) were fit by least squares regression in two ways, according to which model (symmetric or asymmetric) was assumed for the $(Al,Cr)_2O_3$ solution. For the asymmetric model, the regression gives:

$\Delta H = 1015 \pm 710$ J/mol

$\Delta S = 0.341 \pm 0.460$ J/mol

$AG_0 = 12400 \pm 260$ J/mol

$AG_1 = -4963 \pm 450$ J/mol

with $\chi^2_\nu = 1.72$. The entropy of the exchange reaction is thus predicted to be approximately zero. No improvement to the fit was observed if the excess mixing parameters were allowed to vary as a function of temperature. For the symmetric model:

$\Delta H = -6992 \pm 1524$ J/mol

$\Delta S = -4.101 \pm 0.985$ J/mol

$AG_0 = 9980 \pm 275$ J/mol

with $\chi^2_\nu = 1.07$, i.e., a significantly better fit to the data. In principle, the difference in standard entropies of the exchange reaction between the two models could also be used to discriminate between them, but at the moment the uncertainty in the entropy of $MgAl_2O_4$ (due to the configurational entropy of $MgAl_2O_4$) is too large for this to be practical.

$Mg(Al,Cr)_2O_4$ lattice parameters and molar volumes of mixing

Oka et al. (1984) also measured the lattice parameters across the $MgAl_2O_4$-$MgCr_2O_4$ solid solution, and hence derived molar volumes of mixing at room temperature. The interpretation of their data is complicated by the fact that the lattice parameter of $MgAl_2O_4$ depends on the amount of Mg/Al order-disorder, as well as the exact stoichiometry (i.e., bulk Mg/Al ratio), which can vary widely in this spinel. (By contrast, $MgCr_2O_4$ spinel shows negligible Mg/Cr order-disorder, and does not deviate significantly from the ideal stoichiometry, provided that the sample is synthesised somewhere within the broad range of oxygen fugacities where neither Cr^{2+} or Cr^{4+} is stable: O'Neill and Dollase (1994). Oka et al. (1984) thus found that samples quenched from different temperatures have slightly different lattice parameters, which they ascribed to differing degrees of Mg/Al order. However, it is doubtful whether the difference between the equilibrium cation distributions at 1250°C or 1050°C and 796°C would be preserved during the quench (O'Neill 1997). It is therefore probable that the low value of the lattice parameter which they observed is instead due to the Mg/Al ratio in their $MgAl_2O_4$-rich spinels being slightly less than unity. This asymmetry appears to be largely due to a slightly low value for the lattice parameter of $MgAl_2O_4$, e.g., 8.0810 (1) Å at 1250°C, as compared to that given by O'Neill (1997):

$$ao = 7.9829 + 0.1052\ (X_{MgO}/X_{Al2O3}) - 4.01 * 10^{-6}\ T/K$$

where T is the temperature from which the sample was quenched (all values refer to room temperature measurements. (The value of the lattice parameter of $MgCr_2O_4$ measured by Chatterjee et al. (1982) is identical to that given by O'Neill and Dollase (1994), so there seems to be no interlaboratory bias). Hence stoichiometric $MgAl_2O_4$ quenched from 1250°C should have a lattice parameter of 8.0820 Å. However, as mentioned above, slightly non-stoichiometric $MgAl_2O_4$ re-orders extremely rapidly on quenching, such that it is likely that the sample synthesised by Chatterjee et al. (1982) at 1250°C has a cation distribution corresponding to an equilibration temperature of ~800°C. The lattice parameter of stoichiometric $MgAl_2O_4$ at 800°C is 8.0837 Å.

Because of these problems, the molar volume data of Chatterjee et al. (1982) was fitted without the datum for pure $MgAl_2O_4$ (although it may seem that cation ordering may also be important in the more Al-rich members of the solid solution series, thermodynamic modelling indicates that it becomes rapidly less so as Cr replaces Al). A satisfactory fit to a quadratic equation was obtained, with:

$$V\ (J/bar) = 3.9780 + 0.3983\ X_{Cr} - 0.01919\ (X_{Cr})^2$$

with chi-squared = 2.31. Hence W_V Al-Cr (sp) = 0.0096 J/bar per mole of Al-Cr. A slightly better fit is obtained using a cubic (i.e., asymmetric fit), with chi-squared = 1.95. However, examination of the fit shows that this is probably an artefact of the slightly lower lattice parameters of the most Al-rich data, as discussed above.

Hence Wsp = 9739 + 9.6 P

where P is in kb.

8. Appendix B

Results from low-temperature calorimetry

Heat capacity measurements were performed at the Max-Planck-Institut für Festkörperphysik, Stuttgart (W. Schnelle, pers comm).

Cr_2O_3 T [K]	Cp [J/mol/K]	$MgCr_2O_4$ T [K]	Cp [J/mol/K]	$FeCr_2O_4$ T [K]	Cp [J/mol/K]
1.481	5.836E-4	1.462	1.658E-2	2.350	4.700E-2
1.500	5.635E-4	1.483	1.701E-2	2.365	4.711E-2
1.505	5.602E-4	1.507	1.744E-2	2.379	4.781E-2
1.547	5.913E-4	1.530	1.780E-2	2.392	4.820E-2
1.561	6.023E-4	1.553	1.820E-2	2.406	4.912E-2
1.607	5.987E-4	1.580	1.868E-2	2.420	4.942E-2
1.839	7.167E-4	1.614	1.932E-2	2.435	5.043E-2
1.944	7.898E-4	1.640	1.983E-2	2.451	5.052E-2
2.356	1.064E-3	1.669	2.055E-2	2.465	5.146E-2
2.360	1.080E-3	1.701	2.090E-2	2.479	5.236E-2
2.361	1.071E-3	1.736	2.154E-2	2.492	5.293E-2
2.362	1.070E-3	1.769	2.214E-2	2.507	5.312E-2
2.364	1.024E-3	1.808	2.289E-2	2.520	5.392E-2
2.368	1.082E-3	1.845	2.362E-2	2.533	5.467E-2
2.371	1.059E-3	1.891	2.452E-2	2.547	5.520E-2
2.392	1.080E-3	1.934	2.540E-2	2.560	5.582E-2
2.398	1.126E-3	1.979	2.631E-2	2.574	5.658E-2
2.407	1.215E-3	2.023	2.713E-2	2.592	5.741E-2
2.423	1.143E-3	2.074	2.815E-2	2.634	5.649E-2
2.532	1.208E-3	2.121	2.908E-2	2.647	5.744E-2
2.547	1.165E-3	2.172	3.012E-2	2.663	5.802E-2
2.557	1.238E-3	2.223	3.113E-2	2.677	5.880E-2
2.602	1.261E-3	2.284	3.235E-2	2.691	5.963E-2
2.628	1.346E-3	2.342	3.357E-2	2.707	6.010E-2
2.695	1.377E-3	2.399	3.472E-2	2.727	6.079E-2
2.724	1.405E-3	2.458	3.592E-2	2.739	6.162E-2
2.762	1.400E-3	2.522	3.722E-2	2.750	6.182E-2
2.781	1.482E-3	2.589	3.859E-2	2.759	6.216E-2
2.815	1.505E-3	2.662	4.010E-2	2.768	6.238E-2
2.839	1.485E-3	2.735	4.168E-2	2.779	6.249E-2
2.911	1.602E-3	2.812	4.334E-2	2.789	6.276E-2
2.957	1.621E-3	2.882	4.489E-2	2.797	6.317E-2
2.991	1.667E-3	2.952	4.646E-2	2.806	6.336E-2
3.032	1.718E-3	3.025	4.809E-2	2.817	6.364E-2
3.081	1.763E-3	3.111	5.013E-2	2.827	6.391E-2
3.121	1.813E-3	3.202	5.233E-2	2.836	6.416E-2
3.161	1.863E-3	3.295	5.471E-2	2.844	6.474E-2
3.200	1.888E-3	3.394	5.723E-2	2.854	6.483E-2
3.778	2.638E-3	3.489	5.986E-2	2.862	6.504E-2
3.817	2.674E-3	3.566	6.210E-2	2.870	6.547E-2
3.858	2.746E-3	3.645	6.421E-2	2.880	6.565E-2
4.250	3.294E-3	3.720	6.649E-2	2.888	6.571E-2

4.331	3.394E-3	3.806	6.917E-2	2.897	6.624E-2
4.377	3.426E-3	3.894	7.219E-2	2.904	6.631E-2
4.427	3.543E-3	4.010	7.617E-2	2.911	6.657E-2
4.495	3.575E-3	4.083	7.887E-2	2.921	6.687E-2
4.534	3.717E-3	4.170	8.231E-2	2.929	6.703E-2
4.578	3.808E-3	4.202	8.294E-2	2.936	6.718E-2
4.611	3.835E-3	4.236	8.487E-2	2.944	6.784E-2
4.666	3.959E-3	4.242	8.246E-2	2.952	6.788E-2
4.783	4.306E-3	4.250	8.554E-2	2.959	6.807E-2
4.821	4.306E-3	4.300	8.488E-2	2.967	6.831E-2
4.870	4.372E-3	4.307	8.785E-2	2.974	6.838E-2
4.906	4.547E-3	4.330	8.915E-2	2.982	6.920E-2
4.955	4.615E-3	4.387	8.864E-2	2.990	6.944E-2
5.006	4.763E-3	4.392	9.169E-2	2.997	6.970E-2
5.060	4.863E-3	4.428	9.372E-2	3.004	6.971E-2
5.114	4.993E-3	4.476	9.282E-2	3.011	6.994E-2
5.166	5.126E-3	4.480	9.597E-2	3.019	7.021E-2
5.226	5.300E-3	4.568	9.899E-2	3.025	7.034E-2
5.288	5.444E-3	4.659	1.040E-1	3.033	7.070E-2
5.341	5.612E-3	4.752	1.093E-1	3.039	7.070E-2
5.410	5.848E-3	4.848	1.151E-1	3.047	7.097E-2
5.465	5.950E-3	4.945	1.198E-1	3.054	7.121E-2
5.529	6.125E-3	4.949	1.237E-1	3.062	7.148E-2
5.582	6.267E-3	5.045	1.269E-1	3.067	7.152E-2
5.638	6.462E-3	5.049	1.309E-1	3.074	7.162E-2
5.718	6.691E-3	5.145	1.342E-1	3.081	7.189E-2
5.780	6.887E-3	5.152	1.390E-1	3.087	7.206E-2
5.852	7.144E-3	5.246	1.427E-1	3.094	7.219E-2
5.949	7.469E-3	5.259	1.481E-1	3.099	7.233E-2
5.990	7.713E-3	5.355	1.520E-1	3.107	7.262E-2
6.028	7.746E-3	5.368	1.580E-1	3.112	7.280E-2
6.090	7.985E-3	5.462	1.620E-1	3.119	7.293E-2
6.138	8.160E-3	5.480	1.689E-1	3.126	7.308E-2
6.183	8.264E-3	5.567	1.726E-1	3.132	7.334E-2
6.272	8.762E-3	5.597	1.811E-1	3.140	7.358E-2
6.359	8.872E-3	5.676	1.842E-1	3.144	7.367E-2
6.420	9.137E-3	5.715	1.944E-1	3.151	7.394E-2
6.472	9.380E-3	5.785	1.965E-1	3.156	7.402E-2
6.547	9.798E-3	5.838	2.094E-1	3.163	7.427E-2
6.647	1.008E-2	5.903	2.111E-1	3.170	7.441E-2
6.668	1.017E-2	5.964	2.258E-1	3.175	7.465E-2
6.733	1.044E-2	6.025	2.272E-1	3.180	7.469E-2
6.782	1.064E-2	6.144	2.421E-1	3.187	7.493E-2
6.847	1.099E-2	6.277	2.664E-1	3.192	7.502E-2
6.914	1.135E-2	6.412	2.875E-1	3.199	7.524E-2
6.971	1.150E-2	6.545	3.108E-1	3.205	7.535E-2
7.042	1.182E-2	6.678	3.363E-1	3.213	7.512E-2
7.171	1.236E-2	6.813	3.636E-1	3.225	7.738E-2
7.212	1.272E-2	6.951	3.934E-1	3.244	7.831E-2
7.266	1.285E-2	7.092	4.256E-1	3.261	7.938E-2
7.327	1.307E-2	7.235	4.613E-1	3.282	8.021E-2
7.375	1.348E-2	7.381	4.998E-1	3.305	8.131E-2
7.433	1.369E-2	7.530	5.416E-1	3.329	8.262E-2
7.486	1.414E-2	7.683	5.868E-1	3.358	8.387E-2
7.539	1.442E-2	7.837	6.357E-1	3.382	8.466E-2
7.598	1.473E-2	7.995	6.896E-1	3.536	8.840E-2
7.658	1.510E-2	8.156	7.471E-1	3.570	9.115E-2
7.716	1.541E-2	8.320	8.100E-1	3.602	9.337E-2
7.778	1.577E-2	8.488	8.770E-1	3.629	9.521E-2

7.837	1.618E-2	8.658	9.511E-1	3.766	9.867E-2
7.898	1.654E-2	8.833	1.031E+0	3.801	1.016E-1
8.026	1.737E-2	9.010	1.117E+0	3.937	1.058E-1
8.091	1.777E-2	9.191	1.213E+0	3.978	1.093E-1
8.156	1.825E-2	9.376	1.315E+0	4.143	1.148E-1
8.225	1.866E-2	9.564	1.429E+0	4.188	1.187E-1
8.291	1.917E-2	9.757	1.551E+0	4.215	1.097E-1
8.362	1.968E-2	9.953	1.687E+0	4.231	1.220E-1
8.434	2.022E-2	10.150	1.837E+0	4.260	1.128E-1
8.503	2.069E-2	10.349	2.014E+0	4.325	1.167E-1
8.573	2.128E-2	10.547	2.218E+0	4.389	1.210E-1
8.684	2.209E-2	10.745	2.450E+0	4.455	1.252E-1
8.746	2.254E-2	10.943	2.740E+0	4.517	1.304E-1
8.950	2.426E-2	11.092	3.002E+0	4.589	1.333E-1
9.016	2.476E-2	11.194	3.229E+0	4.660	1.375E-1
9.132	2.550E-2	11.296	3.485E+0	4.733	1.421E-1
9.212	2.635E-2	11.396	3.781E+0	4.802	1.469E-1
9.285	2.706E-2	11.496	4.133E+0	4.872	1.516E-1
9.353	2.773E-2	11.595	4.563E+0	4.941	1.565E-1
9.420	2.829E-2	11.693	5.130E+0	5.007	1.617E-1
9.488	2.884E-2	11.791	5.916E+0	5.080	1.667E-1
9.606	2.981E-2	11.888	7.066E+0	5.164	1.733E-1
9.629	3.025E-2	11.983	8.865E+0	5.255	1.806E-1
9.738	3.121E-2	12.041	9.765E+0	5.349	1.885E-1
9.775	3.165E-2	12.062	1.086E+1	5.442	1.963E-1
9.885	3.262E-2	12.083	1.184E+1	5.528	2.046E-1
9.977	3.368E-2	12.103	1.294E+1	5.629	2.138E-1
10.049	3.439E-2	12.123	1.407E+1	5.727	2.231E-1
10.119	3.512E-2	12.143	1.575E+1	5.816	2.323E-1
10.234	3.621E-2	12.163	1.763E+1	5.913	2.425E-1
10.330	3.733E-2	12.182	1.975E+1	6.004	2.521E-1
10.402	3.809E-2	12.201	2.269E+1	6.101	2.633E-1
10.472	3.881E-2	12.221	2.650E+1	6.206	2.788E-1
10.589	4.024E-2	12.241	3.122E+1	6.299	2.890E-1
10.683	4.126E-2	12.262	3.721E+1	6.390	2.982E-1
10.754	4.202E-2	12.282	4.430E+1	6.492	3.106E-1
10.874	4.355E-2	12.303	5.256E+1	6.588	3.240E-1
10.972	4.461E-2	12.323	6.274E+1	6.700	3.383E-1
11.045	4.555E-2	12.343	7.362E+1	6.800	3.534E-1
11.166	4.697E-2	12.363	8.857E+1	6.932	3.718E-1
11.264	4.834E-2	12.383	1.034E+2	7.038	3.884E-1
11.385	4.990E-2	12.405	1.142E+2	7.177	4.092E-1
11.472	5.087E-2	12.426	1.211E+2	7.291	4.275E-1
11.599	5.263E-2	12.447	1.380E+2	7.442	4.529E-1
11.693	5.369E-2	12.468	1.425E+2	7.562	4.746E-1
11.822	5.561E-2	12.490	1.635E+2	7.719	5.027E-1
11.963	5.762E-2	12.512	1.677E+2	7.842	5.271E-1
12.066	5.900E-2	12.534	1.634E+2	8.007	5.590E-1
12.196	6.096E-2	12.555	1.758E+2	8.139	5.867E-1
12.284	6.206E-2	12.576	1.849E+2	8.310	6.226E-1
12.418	6.413E-2	12.599	1.726E+2	8.448	6.537E-1
12.564	6.641E-2	12.619	1.620E+2	8.602	6.887E-1
12.655	6.761E-2	12.641	1.527E+2	8.799	7.351E-1
12.790	6.981E-2	12.663	1.420E+2	8.962	7.759E-1
12.934	7.199E-2	12.685	1.160E+2	9.133	8.193E-1
13.080	7.451E-2	12.705	1.022E+2	9.319	8.686E-1
13.184	7.595E-2	12.726	8.963E+1	9.442	9.010E-1
13.317	7.836E-2	12.746	7.599E+1	9.670	9.644E-1
13.462	8.084E-2	12.767	6.482E+1	9.794	1.002E+0

13.562	8.243E-2	12.786	6.185E+1	9.993	1.060E+0
13.696	8.496E-2	12.806	5.851E+1	10.195	1.122E+0
13.842	8.773E-2	12.827	5.388E+1	10.395	1.186E+0
13.992	9.032E-2	12.849	4.788E+1	10.610	1.258E+0
14.101	9.241E-2	12.870	4.545E+1	10.831	1.332E+0
14.238	9.511E-2	12.890	4.392E+1	11.056	1.411E+0
14.384	9.798E-2	12.913	3.781E+1	11.277	1.489E+0
14.534	1.010E-1	12.938	2.822E+1	11.509	1.576E+0
14.645	1.030E-1	12.960	1.884E+1	11.758	1.671E+0
14.782	1.056E-1	12.974	1.600E+1	12.002	1.765E+0
14.929	1.090E-1	12.989	1.554E+1	12.256	1.870E+0
15.083	1.123E-1	13.059	1.231E+1	12.511	1.974E+0
15.238	1.157E-1	13.166	9.689E+0	12.759	2.084E+0
15.351	1.176E-1	13.252	8.823E+0	13.017	2.196E+0
15.491	1.212E-1	13.339	8.289E+0	13.285	2.317E+0
15.642	1.249E-1	13.434	7.834E+0	13.548	2.439E+0
15.798	1.282E-1	13.532	7.477E+0	13.803	2.562E+0
15.916	1.306E-1	13.629	7.227E+0	14.070	2.692E+0
16.054	1.345E-1	13.728	6.991E+0	14.338	2.827E+0
16.204	1.378E-1	13.826	6.824E+0	14.595	2.964E+0
16.690	1.501E-1	13.925	6.690E+0	14.868	3.108E+0
16.816	1.534E-1	14.075	6.529E+0	15.140	3.252E+0
16.956	1.574E-1	14.276	6.341E+0	15.402	3.400E+0
17.110	1.617E-1	14.476	6.197E+0	15.672	3.555E+0
17.270	1.662E-1	14.674	6.132E+0	15.946	3.712E+0
17.411	1.706E-1	14.874	6.039E+0	16.217	3.876E+0
17.566	1.743E-1	15.075	5.972E+0	16.487	4.039E+0
17.728	1.796E-1	15.273	5.922E+0	16.760	4.207E+0
17.892	1.838E-1	15.472	5.876E+0	17.035	4.381E+0
18.044	1.886E-1	15.674	5.851E+0	17.312	4.568E+0
18.204	1.939E-1	15.876	5.792E+0	17.588	4.747E+0
18.339	1.972E-1	16.077	5.761E+0	17.863	4.934E+0
18.483	2.021E-1	16.285	5.745E+0	18.139	5.125E+0
18.645	2.087E-1	16.486	5.693E+0	18.410	5.318E+0
18.825	2.132E-1	16.679	5.698E+0	18.688	5.517E+0
18.986	2.191E-1	16.880	5.669E+0	18.744	5.463E+0
19.125	2.231E-1	17.079	5.662E+0	18.972	5.728E+0
19.273	2.284E-1	17.281	5.656E+0	19.253	5.818E+0
19.431	2.343E-1	17.481	5.644E+0	19.254	5.938E+0
19.596	2.400E-1	17.681	5.624E+0	19.535	6.148E+0
19.768	2.466E-1	17.881	5.632E+0	19.788	6.221E+0
19.922	2.515E-1	18.082	5.623E+0	19.811	6.364E+0
20.073	2.573E-1	18.281	5.599E+0	20.089	6.596E+0
20.235	2.640E-1	18.481	5.607E+0	20.317	6.634E+0
21.061	2.961E-1	18.679	5.606E+0	20.381	6.822E+0
21.221	3.032E-1	18.877	5.620E+0	20.670	7.057E+0
21.388	3.104E-1	19.076	5.617E+0	20.882	7.079E+0
21.562	3.185E-1	19.278	5.619E+0	20.949	7.300E+0
21.721	3.243E-1	19.477	5.622E+0	21.230	7.533E+0
21.879	3.324E-1	19.674	5.641E+0	21.453	7.570E+0
22.048	3.402E-1	19.873	5.649E+0	21.512	7.780E+0
22.223	3.483E-1	20.071	5.653E+0	21.793	8.031E+0
22.405	3.569E-1	20.268	5.655E+0	22.041	8.103E+0
22.578	3.640E-1	20.466	5.660E+0	22.076	8.294E+0
22.742	3.726E-1	20.664	5.675E+0	22.371	8.555E+0
22.915	3.818E-1	20.860	5.691E+0	22.656	8.681E+0
23.096	3.901E-1	21.059	5.720E+0	23.288	9.292E+0
23.269	3.981E-1	21.257	5.725E+0	23.933	9.922E+0
23.434	4.076E-1	21.456	5.738E+0	24.602	1.066E+1

23.608	4.167E-1	21.653	5.745E+0	25.285	1.144E+1
23.794	4.264E-1	21.850	5.779E+0	25.991	1.227E+1
23.974	4.350E-1	22.050	5.797E+0	26.718	1.320E+1
24.142	4.449E-1	22.248	5.811E+0	27.463	1.419E+1
24.320	4.555E-1	22.447	5.825E+0	28.230	1.528E+1
25.050	4.974E-1	22.645	5.840E+0	29.018	1.651E+1
25.243	5.088E-1	22.841	5.876E+0	29.828	1.786E+1
25.434	5.210E-1	23.039	5.884E+0	30.654	1.938E+1
25.615	5.313E-1	23.236	5.904E+0	31.505	2.116E+1
25.791	5.415E-1	23.433	5.926E+0	32.372	2.327E+1
25.963	5.544E-1	23.629	5.948E+0	33.253	2.585E+1
26.145	5.660E-1	23.825	5.986E+0	34.150	2.918E+1
26.339	5.785E-1	24.025	5.999E+0	35.060	3.357E+1
26.533	5.909E-1	24.222	6.022E+0	35.975	3.815E+1
26.719	6.030E-1	24.419	6.041E+0	37.014	3.407E+1
26.912	6.168E-1	24.616	6.076E+0	38.396	1.973E+1
27.108	6.293E-1	24.813	6.096E+0	39.745	1.915E+1
27.296	6.407E-1	25.012	6.123E+0	40.773	1.979E+1
27.490	6.575E-1	25.764	6.152E+0	41.769	2.046E+1
27.686	6.701E-1	26.512	6.265E+0	42.756	2.116E+1
27.876	6.856E-1	27.289	6.391E+0	43.746	2.189E+1
28.066	6.984E-1	28.086	6.524E+0	44.733	2.264E+1
28.249	7.158E-1	28.900	6.665E+0	45.719	2.341E+1
28.444	7.289E-1	29.739	6.813E+0	46.705	2.419E+1
28.651	7.457E-1	30.600	6.975E+0	47.701	2.499E+1
28.860	7.617E-1	31.486	7.144E+0	48.698	2.582E+1
29.056	7.770E-1	32.398	7.321E+0	49.696	2.665E+1
29.241	7.936E-1	33.337	7.518E+0	50.695	2.749E+1
29.435	8.100E-1	34.301	7.720E+0	51.695	2.836E+1
30.222	8.794E-1	35.293	7.937E+0	52.693	2.922E+1
30.424	8.982E-1	36.297	8.163E+0	53.692	3.008E+1
30.635	9.162E-1	37.303	8.395E+0	54.692	3.097E+1
30.836	9.349E-1	38.316	8.632E+0	55.690	3.185E+1
31.030	9.540E-1	39.332	8.883E+0	56.690	3.272E+1
31.230	9.744E-1	40.334	9.136E+0	57.689	3.359E+1
31.438	9.943E-1	41.335	9.393E+0	58.691	3.448E+1
31.645	1.016E+0	42.334	9.660E+0	59.693	3.535E+1
31.856	1.034E+0	43.334	9.935E+0	60.691	3.620E+1
32.455	1.095E+0	44.329	1.021E+1	61.691	3.704E+1
32.667	1.117E+0	45.327	1.049E+1	62.695	3.785E+1
33.199	1.165E+0	46.341	1.079E+1	63.699	3.864E+1
33.841	1.238E+0	47.358	1.110E+1	64.705	3.938E+1
34.498	1.317E+0	48.372	1.141E+1	65.710	4.007E+1
35.170	1.399E+0	49.381	1.172E+1	66.715	4.070E+1
35.852	1.486E+0	50.390	1.204E+1	67.727	4.129E+1
36.551	1.580E+0	51.396	1.237E+1	68.729	4.182E+1
37.262	1.679E+0	52.403	1.271E+1	69.741	4.228E+1
37.986	1.784E+0	53.412	1.305E+1	70.750	4.273E+1
38.727	1.897E+0	54.423	1.340E+1	71.753	4.314E+1
39.482	2.015E+0	55.437	1.376E+1	72.757	4.355E+1
40.178	2.131E+0	56.458	1.413E+1	73.756	4.391E+1
40.971	2.264E+0	57.469	1.450E+1	74.766	4.431E+1
41.742	2.400E+0	58.482	1.487E+1	75.769	4.473E+1
42.530	2.544E+0	59.489	1.525E+1	76.774	4.510E+1
43.315	2.694E+0	60.494	1.565E+1	77.776	4.551E+1
44.099	2.848E+0	61.497	1.604E+1	78.787	4.595E+1
44.892	3.008E+0	62.504	1.644E+1	79.802	4.639E+1
45.683	3.174E+0	63.515	1.685E+1	80.819	4.685E+1
46.476	3.344E+0	64.527	1.726E+1	81.830	4.735E+1

47.270	3.523E+0	65.531	1.768E+1	82.840	4.787E+1
48.064	3.705E+0	66.535	1.810E+1	83.848	4.841E+1
48.861	3.892E+0	67.544	1.853E+1	84.857	4.893E+1
49.656	4.086E+0	68.550	1.897E+1	85.865	4.949E+1
50.451	4.284E+0	69.553	1.941E+1	86.871	5.008E+1
51.251	4.487E+0	70.565	1.986E+1	87.879	5.067E+1
52.048	4.698E+0	71.566	2.030E+1	88.885	5.119E+1
52.847	4.911E+0	72.585	2.077E+1	89.895	5.192E+1
53.648	5.132E+0	73.592	2.124E+1	90.899	5.252E+1
54.450	5.358E+0	74.604	2.172E+1	91.902	5.314E+1
55.251	5.586E+0	75.616	2.219E+1	92.911	5.383E+1
56.052	5.824E+0	76.621	2.266E+1	93.916	5.436E+1
56.856	6.065E+0	77.624	2.315E+1	94.919	5.512E+1
57.658	6.308E+0	78.628	2.363E+1	95.916	5.580E+1
58.455	6.557E+0	79.634	2.412E+1	96.917	5.648E+1
59.254	6.811E+0	80.640	2.461E+1	97.916	5.711E+1
60.058	7.072E+0	81.647	2.513E+1	98.921	5.784E+1
60.871	7.344E+0	82.651	2.564E+1	99.924	5.854E+1
61.696	7.619E+0	83.661	2.614E+1	100.927	5.922E+1
62.532	7.905E+0	84.675	2.668E+1	101.928	5.986E+1
63.376	8.196E+0	85.682	2.718E+1	102.931	6.059E+1
64.235	8.500E+0	86.688	2.771E+1	103.931	6.132E+1
65.101	8.813E+0	87.692	2.824E+1	104.930	6.202E+1
65.980	9.130E+0	88.698	2.873E+1	105.930	6.274E+1
66.873	9.463E+0	89.706	2.930E+1	106.929	6.345E+1
67.778	9.803E+0	90.709	2.984E+1	107.929	6.416E+1
68.695	1.015E+1	91.715	3.040E+1	108.934	6.491E+1
69.626	1.052E+1	92.717	3.095E+1	109.938	6.559E+1
70.567	1.088E+1	93.728	3.149E+1	110.941	6.627E+1
71.524	1.127E+1	94.735	3.205E+1	111.942	6.701E+1
72.484	1.166E+1	95.738	3.260E+1	112.942	6.762E+1
73.459	1.206E+1	96.749	3.317E+1	113.942	6.834E+1
74.445	1.247E+1	97.759	3.375E+1	114.944	6.897E+1
75.434	1.289E+1	98.761	3.430E+1	115.944	6.956E+1
76.425	1.331E+1	99.761	3.487E+1	116.945	7.010E+1
77.419	1.374E+1	100.761	3.544E+1	117.945	7.065E+1
78.412	1.417E+1	101.762	3.602E+1	118.944	7.105E+1
79.405	1.460E+1	102.760	3.659E+1	119.945	7.143E+1
80.399	1.504E+1	103.762	3.716E+1	120.944	7.170E+1
81.393	1.550E+1	104.761	3.776E+1	121.949	7.176E+1
82.390	1.595E+1	105.760	3.833E+1	122.950	7.169E+1
83.384	1.641E+1	106.754	3.891E+1	123.950	7.154E+1
84.380	1.687E+1	107.754	3.949E+1	124.957	7.120E+1
85.378	1.734E+1	108.753	4.008E+1	125.958	7.088E+1
86.372	1.782E+1	109.748	4.066E+1	126.962	7.052E+1
87.358	1.828E+1	110.748	4.127E+1	127.966	7.025E+1
88.350	1.873E+1	111.742	4.189E+1	128.969	7.013E+1
89.352	1.924E+1	112.741	4.246E+1	129.973	7.024E+1
90.351	1.973E+1	113.741	4.306E+1	130.967	7.055E+1
91.350	2.023E+1	114.739	4.365E+1	131.965	7.086E+1
92.346	2.071E+1	115.735	4.427E+1	132.960	7.128E+1
93.342	2.120E+1	116.731	4.484E+1	133.956	7.167E+1
94.338	2.171E+1	117.727	4.546E+1	134.949	7.214E+1
95.332	2.220E+1	118.722	4.605E+1	135.942	7.272E+1
96.331	2.271E+1	119.718	4.668E+1	136.943	7.314E+1
97.333	2.323E+1	120.713	4.728E+1	137.935	7.361E+1
98.331	2.375E+1	121.709	4.790E+1	138.933	7.420E+1
99.327	2.425E+1	122.705	4.848E+1	139.927	7.464E+1
100.324	2.476E+1	123.700	4.909E+1	140.922	7.524E+1

101.322	2.527E+1	124.694	4.968E+1	141.916	7.570E+1
102.317	2.580E+1	125.691	5.030E+1	142.911	7.623E+1
103.313	2.633E+1	126.680	5.091E+1	143.901	7.672E+1
104.309	2.686E+1	127.673	5.151E+1	144.895	7.721E+1
105.302	2.736E+1	128.670	5.210E+1	145.887	7.775E+1
106.298	2.790E+1	129.665	5.272E+1	146.875	7.827E+1
107.291	2.843E+1	130.658	5.332E+1	147.857	7.886E+1
108.286	2.897E+1	131.651	5.394E+1	148.847	7.934E+1
109.281	2.949E+1	132.642	5.454E+1	149.835	7.989E+1
110.278	3.003E+1	133.634	5.509E+1	150.826	8.030E+1
111.272	3.056E+1	134.627	5.574E+1	151.815	8.084E+1
112.263	3.108E+1	135.616	5.634E+1	152.806	8.144E+1
113.257	3.165E+1	136.611	5.698E+1	153.803	8.187E+1
114.251	3.216E+1	137.601	5.756E+1	154.791	8.244E+1
115.244	3.271E+1	138.591	5.816E+1	155.781	8.294E+1
116.238	3.326E+1	139.580	5.880E+1	156.775	8.337E+1
117.233	3.381E+1	140.570	5.935E+1	157.767	8.396E+1
118.226	3.436E+1	141.558	5.994E+1	158.756	8.449E+1
119.218	3.492E+1	142.549	6.053E+1	159.749	8.499E+1
120.212	3.546E+1	143.537	6.117E+1	160.743	8.545E+1
121.205	3.599E+1	144.525	6.174E+1	161.733	8.593E+1
122.198	3.651E+1	145.516	6.236E+1	162.724	8.645E+1
123.189	3.708E+1	146.502	6.295E+1	163.709	8.694E+1
124.183	3.762E+1	147.492	6.354E+1	164.700	8.742E+1
125.177	3.818E+1	148.483	6.416E+1	165.689	8.798E+1
126.169	3.873E+1	149.469	6.475E+1	166.677	8.851E+1
127.163	3.927E+1	150.462	6.534E+1	167.655	8.910E+1
128.153	3.981E+1	151.447	6.596E+1	168.647	8.950E+1
129.145	4.036E+1	152.436	6.647E+1	169.636	8.999E+1
130.136	4.094E+1	153.425	6.705E+1	170.618	9.049E+1
131.129	4.149E+1	154.410	6.765E+1	171.602	9.100E+1
132.122	4.201E+1	155.401	6.825E+1	172.590	9.148E+1
133.114	4.259E+1	156.386	6.885E+1	173.579	9.195E+1
134.105	4.315E+1	157.373	6.942E+1	174.571	9.238E+1
135.096	4.370E+1	158.360	6.996E+1	175.556	9.294E+1
136.083	4.423E+1	159.346	7.056E+1	176.548	9.341E+1
137.063	4.481E+1	160.333	7.116E+1	177.542	9.391E+1
138.050	4.532E+1	161.317	7.167E+1	178.533	9.449E+1
139.032	4.589E+1	162.303	7.226E+1	179.527	9.485E+1
140.017	4.639E+1	163.285	7.286E+1	180.517	9.531E+1
141.002	4.694E+1	164.270	7.342E+1	181.508	9.574E+1
141.987	4.747E+1	165.253	7.398E+1	182.498	9.619E+1
142.973	4.803E+1	166.235	7.452E+1	183.484	9.685E+1
143.956	4.857E+1	167.218	7.508E+1	184.474	9.716E+1
144.938	4.912E+1	168.203	7.566E+1	185.463	9.771E+1
145.924	4.969E+1	169.184	7.623E+1	186.451	9.811E+1
146.910	5.021E+1	170.166	7.670E+1	187.438	9.852E+1
147.894	5.076E+1	171.148	7.733E+1	188.427	9.900E+1
148.883	5.129E+1	172.128	7.785E+1	189.412	9.943E+1
149.868	5.183E+1	173.114	7.831E+1	190.403	9.998E+1
150.765	5.230E+1	174.093	7.890E+1	191.385	1.003E+2
151.762	5.283E+1	175.075	7.948E+1	192.362	1.008E+2
152.748	5.337E+1	176.053	7.998E+1	193.343	1.012E+2
153.735	5.394E+1	177.036	8.055E+1	194.329	1.018E+2
154.721	5.445E+1	178.016	8.108E+1	195.318	1.022E+2
155.709	5.499E+1	178.995	8.163E+1	196.402	1.026E+2
156.694	5.554E+1	179.976	8.218E+1	197.380	1.031E+2
157.680	5.604E+1	180.953	8.267E+1	198.353	1.037E+2
158.665	5.659E+1	181.932	8.320E+1	199.329	1.040E+2

159.652	5.713E+1	182.912	8.370E+1	200.304	1.046E+2
160.638	5.760E+1	183.889	8.422E+1	201.279	1.050E+2
161.623	5.821E+1	184.869	8.469E+1	202.252	1.053E+2
162.610	5.871E+1	185.845	8.529E+1	203.228	1.056E+2
163.595	5.921E+1	186.822	8.580E+1	204.214	1.062E+2
164.579	5.977E+1	187.800	8.625E+1	205.192	1.066E+2
165.564	6.028E+1	188.776	8.680E+1	206.171	1.071E+2
166.551	6.081E+1	189.754	8.729E+1	207.160	1.074E+2
167.538	6.131E+1	190.733	8.782E+1	208.143	1.079E+2
168.526	6.186E+1	191.212	8.780E+1	209.121	1.083E+2
169.517	6.237E+1	192.181	8.821E+1	210.096	1.087E+2
170.504	6.291E+1	193.165	8.876E+1	210.751	1.091E+2
171.491	6.338E+1	194.134	8.924E+1	211.071	1.091E+2
172.477	6.396E+1	195.104	8.978E+1	212.286	1.095E+2
173.463	6.446E+1	196.073	9.025E+1	213.811	1.103E+2
174.450	6.491E+1	197.052	9.068E+1	214.757	1.107E+2
175.437	6.549E+1	198.026	9.119E+1	215.752	1.108E+2
176.422	6.601E+1	199.004	9.154E+1	216.738	1.114E+2
177.407	6.648E+1	199.980	9.217E+1	217.725	1.118E+2
178.394	6.702E+1	200.956	9.271E+1	218.709	1.120E+2
179.383	6.753E+1	201.930	9.314E+1	219.691	1.124E+2
180.373	6.805E+1	202.906	9.358E+1	220.677	1.131E+2
181.362	6.850E+1	203.884	9.411E+1	221.664	1.133E+2
182.355	6.897E+1	204.860	9.452E+1	222.649	1.135E+2
183.345	6.955E+1	205.835	9.508E+1	223.637	1.141E+2
184.332	7.006E+1	206.811	9.554E+1	224.622	1.144E+2
185.321	7.050E+1	207.796	9.592E+1	225.609	1.148E+2
186.313	7.104E+1	208.778	9.642E+1	226.598	1.153E+2
187.356	7.129E+1	209.765	9.681E+1	227.581	1.156E+2
188.396	7.199E+1	210.751	9.727E+1	228.566	1.161E+2
189.375	7.263E+1	211.735	9.773E+1	229.548	1.166E+2
190.346	7.312E+1	212.720	9.814E+1	230.531	1.166E+2
191.320	7.359E+1	213.705	9.865E+1	231.516	1.173E+2
192.305	7.400E+1	214.687	9.895E+1	232.497	1.176E+2
193.286	7.452E+1	215.672	9.955E+1	233.482	1.180E+2
194.273	7.502E+1	216.653	1.000E+2	234.462	1.185E+2
195.255	7.557E+1	217.638	1.005E+2	235.441	1.186E+2
196.240	7.599E+1	218.621	1.009E+2	236.424	1.192E+2
197.222	7.659E+1	219.602	1.014E+2	237.408	1.195E+2
198.203	7.698E+1	220.583	1.018E+2	238.389	1.197E+2
199.187	7.753E+1	221.564	1.023E+2	239.370	1.202E+2
200.167	7.797E+1	222.545	1.026E+2	240.353	1.203E+2
201.143	7.847E+1	223.528	1.030E+2	241.334	1.210E+2
202.123	7.892E+1	224.514	1.036E+2	242.315	1.214E+2
203.100	7.942E+1	225.494	1.040E+2	243.294	1.214E+2
204.082	7.992E+1	226.484	1.045E+2	244.274	1.216E+2
205.065	8.034E+1	227.470	1.048E+2	245.252	1.224E+2
206.046	8.089E+1	228.461	1.051E+2	246.230	1.226E+2
207.027	8.126E+1	229.443	1.056E+2	247.212	1.230E+2
208.007	8.182E+1	230.424	1.061E+2	248.193	1.232E+2
208.987	8.229E+1	231.401	1.066E+2	249.171	1.237E+2
209.963	8.276E+1	232.380	1.068E+2	250.149	1.235E+2
210.943	8.326E+1	233.359	1.073E+2	251.130	1.242E+2
211.921	8.370E+1	234.336	1.076E+2	252.112	1.247E+2
212.902	8.427E+1	235.318	1.080E+2	253.094	1.250E+2
213.881	8.478E+1	236.296	1.085E+2	254.076	1.249E+2
214.854	8.518E+1	237.275	1.090E+2	255.055	1.255E+2
215.829	8.566E+1	238.255	1.092E+2	256.034	1.259E+2
216.803	8.601E+1	239.237	1.098E+2	257.014	1.263E+2

217.777	8.646E+1	240.214	1.101E+2	257.996	1.264E+2
218.748	8.700E+1	241.196	1.106E+2	258.972	1.269E+2
219.721	8.743E+1	242.172	1.108E+2	259.953	1.273E+2
220.692	8.785E+1	243.150	1.111E+2	260.931	1.276E+2
221.666	8.811E+1	244.124	1.115E+2	261.910	1.276E+2
222.637	8.881E+1	245.101	1.120E+2	262.893	1.282E+2
223.608	8.912E+1	246.076	1.124E+2	263.877	1.282E+2
224.583	8.953E+1	247.051	1.127E+2	264.856	1.285E+2
225.559	9.000E+1	248.029	1.131E+2	265.835	1.288E+2
226.533	9.049E+1	249.000	1.135E+2	266.810	1.295E+2
227.508	9.089E+1	249.976	1.138E+2	267.788	1.295E+2
228.484	9.118E+1	250.954	1.143E+2	268.766	1.300E+2
229.458	9.149E+1	251.931	1.145E+2	269.743	1.303E+2
230.431	9.204E+1	252.911	1.149E+2	270.721	1.306E+2
231.404	9.243E+1	253.884	1.153E+2	271.697	1.312E+2
232.380	9.289E+1	254.861	1.156E+2	272.683	1.313E+2
233.354	9.325E+1	255.836	1.160E+2	273.662	1.314E+2
234.327	9.369E+1	256.813	1.164E+2	274.641	1.316E+2
235.298	9.399E+1	257.791	1.168E+2	275.621	1.319E+2
236.279	9.442E+1	258.765	1.170E+2	276.599	1.327E+2
237.258	9.482E+1	259.740	1.174E+2	277.617	1.330E+2
238.237	9.516E+1	260.716	1.178E+2	278.595	1.325E+2
239.214	9.552E+1	261.686	1.182E+2	279.576	1.328E+2
240.195	9.596E+1	262.662	1.185E+2	280.556	1.336E+2
241.172	9.615E+1	263.629	1.188E+2	281.536	1.337E+2
242.148	9.666E+1	264.604	1.191E+2	282.515	1.340E+2
243.126	9.692E+1	265.577	1.196E+2	283.494	1.340E+2
244.100	9.753E+1	266.549	1.199E+2	284.480	1.346E+2
245.072	9.791E+1	267.521	1.201E+2	285.460	1.348E+2
246.045	9.840E+1	268.492	1.205E+2	286.439	1.344E+2
247.022	9.869E+1	269.465	1.208E+2	287.420	1.351E+2
247.996	9.914E+1	270.434	1.211E+2	288.400	1.354E+2
248.967	9.962E+1	271.409	1.214E+2	289.382	1.352E+2
249.944	9.994E+1	272.384	1.217E+2	290.361	1.358E+2
250.921	1.004E+2	273.355	1.220E+2	291.342	1.362E+2
251.898	1.008E+2	274.323	1.223E+2	292.322	1.366E+2
252.876	1.013E+2	275.294	1.226E+2	293.304	1.371E+2
253.853	1.015E+2	276.265	1.231E+2	294.286	1.372E+2
254.831	1.021E+2	277.239	1.232E+2	295.267	1.378E+2
255.811	1.026E+2	278.210	1.235E+2	296.246	1.380E+2
256.787	1.029E+2	279.182	1.239E+2	297.233	1.382E+2
257.768	1.035E+2	280.155	1.241E+2	298.214	1.385E+2
258.745	1.038E+2	281.124	1.244E+2	299.196	1.385E+2
259.723	1.043E+2	282.096	1.248E+2	300.177	1.389E+2
260.700	1.047E+2	283.067	1.250E+2	300.287	1.390E+2
261.678	1.050E+2	284.037	1.252E+2	301.162	1.388E+2
262.657	1.054E+2	285.008	1.257E+2	301.267	1.395E+2
263.633	1.061E+2	285.977	1.258E+2	302.148	1.392E+2
264.616	1.065E+2	286.948	1.261E+2	302.218	1.398E+2
265.594	1.069E+2	287.918	1.263E+2	303.130	1.396E+2
266.571	1.075E+2	288.889	1.266E+2	303.171	1.397E+2
267.547	1.080E+2	289.859	1.269E+2	304.115	1.395E+2
268.522	1.082E+2	290.830	1.270E+2	304.134	1.401E+2
269.501	1.087E+2	291.805	1.272E+2	305.100	1.399E+2
270.478	1.094E+2	292.774	1.276E+2	305.101	1.404E+2
271.452	1.097E+2	293.746	1.279E+2	306.070	1.403E+2
272.430	1.102E+2	294.716	1.282E+2	306.104	1.407E+2
273.406	1.109E+2	295.689	1.284E+2	307.045	1.409E+2
274.379	1.112E+2	296.663	1.288E+2	308.027	1.407E+2

275.354	1.118E+2
276.328	1.122E+2
277.303	1.126E+2
278.278	1.132E+2
279.250	1.137E+2
280.224	1.141E+2
281.195	1.148E+2
282.169	1.151E+2
283.133	1.160E+2
284.106	1.164E+2
285.075	1.171E+2
286.045	1.172E+2
287.016	1.179E+2
287.988	1.184E+2
288.957	1.191E+2
289.926	1.198E+2
290.894	1.206E+2
291.866	1.211E+2
292.837	1.218E+2
293.808	1.227E+2
294.778	1.236E+2
295.747	1.241E+2
296.719	1.250E+2
297.688	1.261E+2
298.655	1.268E+2
299.624	1.278E+2
300.590	1.286E+2
301.159	1.295E+2
301.558	1.299E+2
302.409	1.312E+2
302.523	1.313E+2
302.724	1.312E+2
303.349	1.320E+2
303.489	1.328E+2
303.665	1.325E+2
304.313	1.339E+2
304.450	1.349E+2
304.957	1.354E+2
305.280	1.367E+2
305.413	1.371E+2
305.601	1.366E+2
305.926	1.358E+2
306.253	1.338E+2
306.392	1.318E+2
306.563	1.302E+2
306.860	1.271E+2
307.159	1.242E+2
307.412	1.233E+2
307.456	1.234E+2
307.746	1.218E+2
308.042	1.206E+2
308.333	1.203E+2
308.423	1.203E+2
308.623	1.200E+2
308.917	1.197E+2
309.210	1.190E+2
309.407	1.190E+2
310.087	1.183E+2
310.390	1.177E+2
297.636	1.289E+2
298.605	1.291E+2
299.578	1.292E+2
300.551	1.295E+2
301.529	1.297E+2
302.524	1.298E+2
303.504	1.302E+2
304.608	1.302E+2
305.466	1.306E+2
306.434	1.307E+2
307.403	1.308E+2
308.369	1.312E+2
309.340	1.314E+2
310.310	1.316E+2
311.283	1.319E+2
312.252	1.321E+2
313.221	1.323E+2
314.196	1.326E+2
315.166	1.327E+2
316.142	1.330E+2
317.114	1.334E+2
318.085	1.334E+2
319.059	1.336E+2
320.031	1.338E+2
321.000	1.340E+2
321.973	1.343E+2
322.949	1.344E+2
323.920	1.346E+2
324.896	1.349E+2
325.870	1.351E+2
326.852	1.354E+2
327.828	1.356E+2
328.803	1.357E+2
329.780	1.361E+2
330.753	1.363E+2
331.728	1.367E+2
332.706	1.367E+2
333.679	1.369E+2
334.654	1.372E+2
335.621	1.373E+2
336.598	1.376E+2
337.572	1.378E+2
338.542	1.380E+2
339.517	1.382E+2
309.009	1.412E+2
309.992	1.411E+2
310.975	1.417E+2
311.957	1.420E+2
312.937	1.429E+2
313.917	1.435E+2
314.902	1.434E+2
315.885	1.440E+2
316.871	1.439E+2
317.856	1.440E+2
318.837	1.445E+2
319.818	1.452E+2
320.799	1.460E+2
321.781	1.467E+2
322.766	1.470E+2
323.749	1.473E+2
324.732	1.480E+2
325.711	1.491E+2
326.692	1.498E+2
327.673	1.506E+2
328.653	1.514E+2
329.635	1.527E+2
330.618	1.527E+2
331.602	1.536E+2
332.588	1.540E+2
333.567	1.554E+2
334.554	1.558E+2
335.545	1.568E+2
336.527	1.573E+2
337.505	1.575E+2

310.395	1.175E+2
311.372	1.168E+2
312.349	1.158E+2
313.324	1.154E+2
314.302	1.147E+2
315.272	1.146E+2
316.247	1.141E+2
317.225	1.136E+2
318.195	1.136E+2
319.168	1.132E+2
320.143	1.131E+2
321.117	1.127E+2
322.095	1.124E+2
323.063	1.124E+2
324.035	1.121E+2
325.011	1.120E+2
325.987	1.119E+2
326.960	1.120E+2
327.936	1.117E+2
328.912	1.120E+2
329.889	1.119E+2
330.860	1.118E+2
331.834	1.120E+2
332.816	1.115E+2
333.790	1.117E+2
334.764	1.117E+2
335.742	1.112E+2
336.714	1.114E+2
337.690	1.112E+2
338.664	1.115E+2
339.638	1.117E+2

References

Adams GE, Bishop FC (1982) Experimental investigation of Ca-Mg exchange between olivine, orthopyroxene, and clinopyroxene: Potential for geobarometry. Earth Plan Sci Lett 57:241-250

Adams GE, Bishop FC (1986) The olivine-clinopyroxene geobarometer: experimental results in the CaO-FeO-MgO-SiO_2 system. Contr Mineral Petr 94:230-237

Ai Y (1992) PhD-thesis, Major and minor element systematics in the lherzolite system: A petrological and experimental study. University of Tasmania

Akella J (1976) Garnet pyroxene equilibria in the system $CaSiO_3$-$MgSiO_3$-Al_2O_3 and in a natural mineral mixture. Am Mineral 61:589-598

Allègre CJ, Hamelin B, Dupré B (1984) Statistical analysis of isotopic ratios in MORB: the mantle blob cluster model and the convective regime of the mantle. Earth Plan Sci Lett 71:71-84

Anastasiou P, Seifert F (1972) Solid solubility of Al_2O_3 in enstatite at high temperatures and 1-5 kb water pressure. Contr Mineral Petr 34:272-287

Anderson CT (1937) The heat capacities of chromium, chromic oxide, chromous oxide and chromic oxide at low temperatures. J Am Chem Soc 59:488-491

Asimov PD, Hirschmann MM, Ghiorso MS, O'Hara MJ, Stolper EM (1995) The effect of pressure induced solid-solid phase transitions on decompression melting of the mantle. Geoch Cosmoch Acta 59:4489-4506

Atlas L (1952) The polymorphism of MgSiO3 and solid-state equilibria in the system $MgSiO_3$-$CaMgSi_2O_6$. Journal of Geology 60:125-147

Baltzer PW, Wojtowicz PJ (1959) 4th Nat Congr Magnestism and Magnetic Materials (Philadelphia 1958). J Appl Phys 30:275

Barks RE, Roy DM (1967) Single-crystal growth of R_2O_3 (corundum structure) oxides by the flux method. In: Peiser HS (ed) Crystal growth. 497-504 Pergamon Press Oxford

Beattie P (1993a) The generation of uranium series disequilibria by partial melting of spinel peridotite: constraints from partitioning studies. Earth Plan Sci Lett 117:379-391

Beattie P (1993b) Uranium-thorium disequilibria and partitioning on melting of garnet peridotite. Nature 363:63-65

Berman RG (1988) Internally consistent thermodynamic data for minerals in the system Na_2O-K_2O-CaO-MgO-FeO-Fe_2O_3-Al_2O_3-SiO_2-TiO_2-H_2O-CO_2. J Petrol 29:445-552

Berman RG (1990) Mixing properties of Ca-Mg-Fe-Mn garnets. Am Mineral 75:328-344

Berman RG, Brown TH (1985) Heat capacity of minerals in the system Na_2O-K_2O-CaO-MgO-FeO-Fe_2O_3-Al_2O_3-SiO_2-TiO_2-H_2O-CO_2: representation, estimation, and high temperature extrapolation. Contr Mineral Petr 86:168-183

Bina CR (1998) Free energy minimization by simulated annealing with applications to lithospheric slabs and mantle plumes. Pure Appl Geophys 151:605-618

Blasse G, Fast JF (1963) Néel temperatures of some antiferromagnetic oxides with spinel structure. Philips Research Reports 18:393-399

Bohlen SR, Essene EJ, Boettcher AL (1980) Reinvestigation and application of olivine-quartz-orthopyroxene barometry. Earth Plan Sci Lett 47:1-10

Bonnikson KR (1955) High temperature heat contents of aluminates of calcium and magnesium. Journal of Physical Chemistry 59:220-221

Bose K, Ganguly J (1995) Quartz-coesite transition revisited: Reversed experimental determination at 500-1200°C and retrieved thermochemical properties. Am Mineral 80:231-238

Bosenick A, Geiger CA (1997) Powder X ray diffraction study of synthetic pyrope-grossular garnets between 20 and 295 K. J Geophy Res 102:22649-22657

Boyd FR, England JL (1960) Apparatus for phase-equilibrium measurements at pressures up to 50 kbar and temperatures up to 1750°C. J Geophy Res 65:741-748

Boyd FR, England JL (1961) Melting of silicates at high pressures. Carnegie Inst Wash Y Book 60:113-125

Boyd FR, England JL (1964) The system enstatite-pyrope. Carnegie Inst Wash Y Book 63:157-161

Brey G, Huth J (1984) The enstatite - diopside solvus to 60 kbar. Proc Third Int Kimb Conf 2:257-264

Brey GP, Doroshev AM, Girnis AV, Turkin AI (1998) Garnet-spinel-orthopyroxene equilibria in the FeO-MgO-Al_2O_3-SiO_2-Cr_2O_3 system: I. Composition and molar volumes of minerals. Eur J Min in press

Brey GP, Köhler T (1990) Geotherobarometry in four-phase lherzolites II. New thermobarometers, and practical assessment of existing thermobarometers. J Petrol 31:1353-1378

Brey GP, Nickel KG, Kogarko L (1986) Garnet-pyroxene equilibria in the system CaO-MgO-Al_2O_3-SiO_2 (CMAS): prospects for simplified (T'independent') lherzolite barometry and an eclogite-barometer. Contr Mineral Petr 92:448-455

Bruce RH, Cannell DS (1977) Specific heat of Cr_2O_3 near the Néel temperature. Physical Review B 15:4451-4459

Burns RG (1970) Crystal field spectra and evidence of cation ordering in olivine minerals. Am Mineral 55:1608-1632

Burns RG (1975) On the occurrence and stability of divalent chromium in olivines included in diamonds. Contr Mineral Petr 51:213-221

Burns VM, Burns RG (1975) Mineralogy of chromium. Geoch Cosmoch Acta 39:903-910

Callen HB, Harrison SE, Kriessman CJ (1956) Cation distributions in ferrospinels. Theroretical Phys Rev 103:851-856

Canil D, O'Neill HStC (1996) Distribution of ferric iron in some upper-mantle assemblages. J Petrol 37:609-635

Carlson WD, Lindsley DH (1988) Thermochemistry of pyroxenes on the join $Mg_2Si_2O_6$-$CaMgSi_2O_6$. Am Mineral 73:242-252

Caroll-Webb SA, Wood BJ (1986) Spinel-pyroxene-garnet relationships and their dependence on Cr/Al ratio. Contr Mineral Petr 92:471-480

Carswell DA, Griffin WL, Kresten P (1984) Peridotite nodules from the Ngopetsoeu and Lipelaneng kimberlites, Lesotho. Journal 167-178

Chamberlin L, Beckett JR, Stolper E (1995) Palladium oxide equilibration and the thermodynamic properties of $MgAl_2O_4$ spinel. Am Mineral 80:285-296

Chamberlin L, Beckett JR, Stolper E (1994) Pd-oxide equilibration: A new experimental method for the direct determination of oxide activities in melts and minerals. Contr Mineral Petr 116:169-181

Charlu TV, Newton RC, Kleppa OJ (1975) Enthalpies of formation at 970 K of compounds in the system MgO-Al_2O_3-SiO_2 by high-temperature solution calorimetry. Geoch Cosmoch Acta 39:1487-1497

Chase MW, Davies CA, Downey JR, Frurip DJ, McDonald RA, Syverud AN (1985) JANAF Thermochemical tables 3rd edition. J Phys Chem Ref Data 14:927-942

Chatterjee ND (1991) Applied Mineralogical Thermodynamics. Selected Topics. Springer Verlag Berlin

Chatterjee ND, Krüger R, Haller G, Olbricht W (1998) The Bayesian approach to an internally consistent thermodynamic database: theory, database, and generation of phase diagrams. Contr Mineral Petr 133:149-168

Chatterjee ND, Leistner H, Terhart L, Abraham K, Klaska R (1982) Thermodynamic mixing properties of corundum-eskolaite, α -$(Al,Cr^{3+})_2O_3$, crystalline solutions at high temperatures and pressures. Am Mineral 67:725-735

Chatterjee ND, Terhart L (1985) Thermodynamic calculation of peridotite phase relations in the system $MgO-Al_2O_3-SiO_2-Cr_2O_3$, with some geological applications. Contr Mineral Petr 89:273-284

Coey JMD (1988) Magnetic ordering and thermodynamics in silicates. In: Salje EKH (ed) Physical Properties and Thermodynamic Behaviour of Minerals. 225:459-499 D. Reidel Publishing Dordrecht

Danckwerth PA, Newton RC (1978) Experimental determination of the spinel peridotite to garnet peridotite reaction in the system $MgO-Al_2O_3-SiO_2$ in the range 900-1100°C and Al_2O_3 isopleths of enstatite in the spinel field. Contr Mineral Petr 66:189-201

Davidson PM, Lindsley DH (1989) Thermodynamic analysis of pyroxene-olivine-quartz equilibria in the system $CaO-MgO-FeO-SiO_2$. Am Mineral 74:18-30

Davidson PM, Mukhopadhyay DK (1984) Ca-Fe-Mg-olivines: Phase relations and a solid solution model. Contr Mineral Petr 86:256-263

Davis BTC, Boyd FR (1966) The join $Mg_2Si_2O_6-CaMgSi_2O_6$ at 30 kbars pressure and its application to pyroxenes from kimberlites. J Geophy Res 71:3567-3376

De Capitani C, Brown TH (1987) The computation of chemical equilibrium in complex systems containing non-ideal solutions. Geoch Cosmoch Acta 51:2639-2652

Deer WS, Howie RA, Zussman J (1992) An introduction to the rock-forming minerals. Longman Scientific & Technical Harlow

Dickey JSJr, Yoder HSJr (1971) Partitioning of chromium and aluminum between clinopyroxene and spinel. Carnegie Inst Wash Y Book 70:384-392

Doroshev AM, Brey GP, Girnis AV, Turkin AI, Kogarko LN (1997) Pyrope-knorringite garnets in the Earth's Mantle: Experiments in the $MgO-Al_2O_3-SiO_2-Cr_2O_3$ system. Russian Geology and Geophysics 38:559-586

Duke JM (1983) Ore deposit models 7, Magmatic segregation deposits of chromite. Geoscience Can 10:15-24

Dunitz D, Orgel LE (1957) Electronic properties of transition metal oxides II. J Phys Chem Solids 3:318-323

El-Shahat RM, White J (1966) Phase equilibrium relations in spinel-silicate systems. II. The pseudo-systems $MgAl_2O_4-MgCr_2O_4-CaMgSiO_4$,.... Trans Brit Ceram Soc 65:309-336

Fei Y (1995) Thermal Expansion. In: Ahrens TJ (ed) Mineral physics and crystallography: a handbook of physical constants. 2: American Geophysical Union Washington, DC

Fei Y, Saxena SK, Eriksson G (1986) Some binary and ternary silicate solution models. Contr Mineral Petr 94:221-229

Finnerty TA (1977) Exchange of Mn, Ca, Mg, and Al between synthetic garnet, orthopyroxene, clinopyroxene, and olivine. Carnegie Inst Wash Y Book 76:572-579

Frey FA, Prinz M (1978) Ultramafic inclusions from San Carlos, Arizona: petrologic and geochemical data bearing on their petrogenesis. Earth Plan Sci Lett 38:129-176

Frey FA, Shimizu N, Leinbach A, Obata M, Takazawa E (1991) Compositional variations within the lower layered zone of the Horoman peridotite, Hokkaido, Japan: constraints on models for melt-solid segregation. In: Menzies MA, Dupuy C and Nicolas A (eds) Journal of Petrology Special Issue: Orogenic Lherzolites and Mantle Processes:221-227

Fujii T (1977) Pyroxene equilibria in spinel lherzolite. Carnegie Inst Wash Y Book 76:569-572

Ganguly J, Cheng W, O'Neill HStC (1993) Syntheses, volume, and structural changes of garnets in the pyrope-grossular join: Implications for stability and mixing properties. Am Mineral 78:582-593

Ganguly J, Ghose S (1979) Aluminous orthopyroxene: Order-disorder, thermodynamic properties, and petrologic implications. Contr Mineral Petr 69:375-385

Gasparik T (1984) Experimental study of subsolidus phase relations and mixing properties of pyroxene in the system CaO-Al_2O_3-SiO_2. Geoch Cosmoch Acta 48:2537-2545

Gasparik T (1984) Two-pyroxene thermobarometry with new experimental data in the system CaO - MgO - Al_2O_3 - SiO_2. Contr Mineral Petr 87:87-97

Gasparik T, Lindsley DH (1980) Phase equilibria at high pressures of pyroxenes containing monovalent and trivalent ions. Rev Mineral 7:309-339

Gasparik T, Newton RC (1984) The reversed alumina contents of orthopyroxene in equilibrium with spinel and forsterite in the system MgO-Al_2O_3-SiO_2. Contr Mineral Petr 85:186-196

Ghiorso MS (1985) Chemical mass transfer in magmatic processes. 1. Thermodynamic relations and numerical algorithms. Contr Mineral Petr 90:107-120

Ghiorso MS, Sack RO (1995) Chemical mass transfer in magmatic processes IV. A revised and internally consistent thermodynamic model for the interpolation and

extrapolation of liquid-solid equilibria in magmatic systems at elevated temperatures and pressures. Contr Mineral Petr 119:197-212

Girnis AV, Brey GP (1998) Garnet-spinel-olivine-orthopyroxene equilibria in the FeO-MgO-Al_2O_3-SiO_2-Cr_2O_3 system: II. Thermodynamic analysis. Eur J Min in press

Gmelin E (1985) Low-temperature calorimetry: A particular branch of thermal analysis. Thermochimica Acta 92/53:1-38

Goldsmith JR (1980) The melting and breakdown reactions of anorthite at high pressures and temperatures. Am Mineral 65:272-284

Gottschalk M (1997) Internally consistent thermodynamic data for rock forming minerals. Eur J Min 9:175-223

Green DH (1964) The petrogenesis of the high-temperature peridotite intrusion in the Lizard area, Cornwall. J Petrol 5:134-188

Green DH, Falloon TJ (1998) Pyrolite: A Ringwood concept and its current expression. In: Jackson I (ed) The Earth's mantle: Composition, structure and evolution. 311-380 Cambridge University Press Cambridge

Green DH, Hibberson WO (1970) The instability of plagioclase in peridotite at high pressure. Lithos 3:209-221

Green DH, Ringwood AE (1967) The stability field of aluminous pyroxene peridotite and garnet peridotite and their relevance in upper mantle structure. Earth Plan Sci Lett 3:151-160

Green TH, Ringwood AE, Major A (1966) Friction effects and pressure calibration in a piston-cylinder high pressure-temperature apparatus. J Geophy Res 71:3589-3594

Gudfinnsson GH, Presnall DC (1996) Melting relations of model lherzolite in the system CaO-MgO-Al_2O_3-SiO_2 at 2.4-3.4 GPa and the generation of komatiites. J Geophy Res 101:27701-27709

Gudfinnsson GH, Wood BJ (1998) The effect of trace elements on the olivine-wadsleyite transformation. Am Mineral 83:1037-1044

Haas JL, Fisher JR (1976) Simultaneous evaluation and correlation of thermodynamic data. Am J Sci 276:525-545

Hansen B (1981) The transition from pyroxene granulite facies to garnet clinopyroxene granulite facies. Experiments in the system CaO-MgO-Al_2O_3-SiO_2. Contr Mineral Petr 76:234-242

Hariya Y, Kennedy GC (1968) Equilibrium study of anorthite under high pressure and high temperature. Am J Sci 266:193-203

Harley SL, Carswell DA (1990) Experimental studies on the stability of eclogite facies mineral paragenesis. In: Carswell DA (ed) Eclogite Facies Rocks. 53-82 Blackie and Son Ltd Glasgow

Harley SL, Green DH (1982) Garnet-orthopyroxene barometry for granulites and peridotites. Nature 300:697-701

Hartmann-Boutron F, Gérard A, Imbert P, Kleinberger R, Varret F (1969) Obsérvation d'une transition antiferro-paramagnétique du premier ordre dans les chromites de zinc et de magnésium. CR Acad Sc Paris 268 - B:906-908

Haselton HT, Newton RC (1980) Thermodynamics of pyrope-grossular garnets and their stabilities at high temperatures and high pressures. J Geophy Res 85:6973-6982

Hays JF (1966) Lime-alumina-silica. Carnegie Inst Wash Y Book 65:234-239

Helffrich G, Wood BJ (1989) Subregular model for multicomponent solutions. Am Mineral 74:1016-1022

Hemminger W, Höhne G (1979) Grundlagen der Kalorimetrie. Verlag Chemie Weinheim

Hensen BJ (1972) Phase relations involving pyrope, enstatite $_{ss}$ and sapphirine $_{ss}$ in the system MgO-Al_2O_3-SiO_2. Carnegie Inst Wash Y Book 71:421-427

Hensen BJ, Essene EJ (1971) Stability of pyrope-quartz in the system MgO-Al_2O_3-SiO_2. Contr Mineral Petr 30:72-83

Hensen BJ, Schmid R, Wood BJ (1975) Activity-composition relationships for pyrope-grossular garnets. Contr Mineral Petr 51:161-166

Herzberg CT (1976) The plagioclase spinel lherzolite facies boundary; its bearing on corona structure formation and tectonic history of the Norwegian caledonides. In: Progress in Experimental Petrology. D:233-235 Natural Enviromental Research Council Publications London

Herzberg CT (1978) Pyroxene geothermometry and geobarometry: experimental and thermodynamic evaluation of some subsolidus reactions involving pyroxenes in the system CaO-MgO-Al_2O_3-SiO_2. Geoch Cosmoch Acta 42:945-957

Herzberg CT, Chapman NA (1976) Clinopyroxene geothermometry of spinel lherzolites. Am Mineral 61:626-637

Hirschmann MM (1991) Thermodynamics of multicomponent olivines and the solution properties of $(Ni,Mg,Fe)_2SiO_4$ and $(Ca,Fe,Mg)_2SiO_4$ olivines. Am Mineral 76:1232-1248

Hirschmann MM, Stolper EM (1996) A possible role for garnet pyroxenite in the origin of the "garnet signature' in MORB. Contr Mineral Petr 124:185-208

Holland TJB, Powell R (1990) An enlarged and updated internally consistent thermodynamic dataset with uncertainties and correlations: the system K_2O-Na_2O-CaO-MgO-MnO-FeO-Fe_2O_3-Al_2O_3-TiO_2-SiO_2-C-H-O_2. J Metamorph Geol 8:89-124

Holland TJB, Powell R (1998) An internally consistent thermodynamic data set for phases of petrological interest. J Metamorph Geol 16:309

Holloway JR, Wood BJ (1988) Simulating the Earth. Unwin Hyman Ltd. London

Holzheid A, O'Neill HStC (1995) The Cr-Cr_2O_3 oxygen buffer and the free energy of formation of Cr_2O_3 from high-temperature electrochemical measurements. Geoch Cosmoch Acta 59:475-479

Howells S, O'Hara MJ (1978) Low solubility of alumina in enstatite and uncertainties in estimated paleogeotherms. Phil. Trans. R. Soc. Lond. 288:471-486

Huckenholz HG, Knittel D (1975) Uvarovite: Stability of uvarovite-grossularite solid solutions at low pressure. Contr Mineral Petr 49:211-232

Ionov DA, Ashchepkov IV, Stosch HG, Witt-Eickschen G, Seck HA (1993) Garnet peridotite xenoliths from the Vitim Volcanic field, Baikal region: the nature of the garnet-spinel peridotite transition zone in the continental mantle. J Petrol 34:1141-1175

Irifune T, Hariya Y (1983) Phase relationships in the system $Mg_3Al_2Si_3O_{12}$-$Mg_3Cr_2Si_3O_{12}$ at high pressure and some mineralogical properties of synthetic garnet solid solutions. Mineralogical Journal 11:269-281

Irifune T, Ohtani E, Kumazawa M (1982) Stability field of knorringite $Mg_3Cr_2Si_3O_{12}$ at high pressure and its implication to the occurrence of Cr-rich pyrope in the upper mantle. Physics of the Earth's Interior 27:263-272

Iwamori H, McKenzie D, Takahashi E (1995) Melt generation by isentropic upwelling. Earth Plan Sci Lett 134:253-266

Jacob KT (1978) Electrochemical determination of activities in Cr_2O_3-Al_2O_3 solid solution. J Electrochem Soc 125:175-179

Jacob KT (1977) Potentiometric determination of the Gibbs Free Energy of formation of cadmium and magnesium chromites. J Electrochem Soc 124:1827-1831

Jenkins DM, Newton RC (1979) Experimental determination of the spinel peridotite to garnet peridotite inversion at 900°C and 1000°C in the system CaO-MgO-Al_2O_3-SiO_2, and at 900°C with natural garnet and olivine. Contr Mineral Petr 68:407-419

Kay RW, Gast PW (1973) The rare earth content and origin of alkali-rich basalts. Journal Geol 81:653-682

King EG (1955) Heat capacities at low temperatures and entropies at 298.15 K of crystalline calcium and magnesium aluminates. Journal of Physical Chemistry 59:218-219

Kino Y, Lüthi B (1971) Magnetic and elastic properties of zinc-chromite. Solid State Communications 9:805-808

Klein EM, Langmuir CH (1987) Global correlations of ocean ridge basalt chemistry with axial depth and crustal thickness. J Geophy Res 92:8089-8115

Klemme S, O'Neill HStC (1997) The reaction $MgCr_2O_4 + SiO_2 = Cr_2O_3 + MgSiO_3$ and the free energy of formation of magnesiochromite ($MgCr_2O_4$). Contr Mineral Petr 130:59-65

Kleppa OJ (1982) Thermochemistry in mineralogy. In: Schreyer W (ed) High-pressure researches in geoscience. 461-473 Schweizerbart Stuttgart

Koch-Müller M, Cemic L, Langer K (1992) Experimental and thermodynamic study of Fe-Mg exchange between olivine and orthopyroxene in the system MgO-FeO-SiO_2. Eur J Min 4:115-135

Köhler TP, Brey GP (1990) Calcium exchange between olivine and clinopyroxene calibrated as a geothermobarometer for natural peridotites from 2 to 60 kb with applications. Geoch Cosmoch Acta 54:2375-2388

Kose K, Iida S (1984) Interacting phase transitions in $Fe_{1+x}Cr_{2-x}O_4 (O \leq x \leq 0.4)$. Journal of Applied Physics 55:2321-2323

Koziol AM, Newton RC (1988) Redetermination of the anorthite breakdown reaction and improvement of the plagiclase-garnet-Al_2SiO_5-quartz geobarometer. Am Mineral 73:216-223

Kushiro I, Yoder HSJr (1966) Anorthite-forsterite and anorthite-enstatite reactions and their bearing on the basalt-eclogite transformation. J Petrol 7:337-362

Lane DL, Ganguly J (1980) Al_2O_3 solubility in orthopyroxene in the system MgO-Al_2O_3-SiO_2: A re-evaluation, and mantle geotherm. J Geophy Res 85:6963-6972

LaTourette TK, Kennedy AK, Wasserburg GJ (1993) Thorium-uranium fractionation by garnet: evidence for a deep source and rapid rise of oceanic basalts. Science 261:739-742

Li J-P, O'Neill HStC, Seifert F (1995) Subsolidus phase relations in the system MgO-SiO_2-Cr-O in equilibrium with metallic Cr, and their significance for the petrochemistry of chromium. J Petrol 36:107-132

Liebermann RC, Ringwood AE, Major A (1976) Elasticity of polycrystalline stishovite. Earth Plan Sci Lett 32:127

Linares RC (1962) Growth of yttrium-iron garnet from molten barium borate. Journal of the American Ceramic Society 45:307-310

Lindsley DH, Dixon SA (1976) Diopside - enstatite equilibria at 850 to 1400°C, 5 to 35 kbars. Am J Sci 276:1285-1301

Lindsley DH, Grover JE, Davidson PM (1981) The thermodynamics of the $Mg_2Si_2O_6$ - $CaMgSi_2O_6$ join: A review and an improved model. In: Newton RC, Navrotsky A and Wood BJ (eds) Advances in Physical Geochemistry. 1:149-175 Springer Verlag New York

Maaloe S, Aoki K (1977) The major element composition of the upper mantle estimated from the composition of lherzolites. Contr Mineral Petr 63:161-173

MacGregor ID (1970) The effect of CaO, Cr_2O_3, Fe_2O_3, and Al_2O_3 on the stability of spinel and garnet peridotites. Phys. Earth Planet Int 3:372-377

MacGregor ID (1965) Stability fields of spinel and garnet peridotites in the synthetic system MgO-CaO-Al_2O_3-SiO_2. Carnegie Inst Wash Y Book 64:126-134

MacGregor ID (1974) The system MgO-Al_2O_3-SiO_2: solubility of Al_2O_3 in enstatite for spinel and garnet peridotite compositions. Am Mineral 59:110-119

Mah AD (1954) Heats of formation of chromium oxide and cadmium oxide from combustion calorimetry. J Am Chem Soc 76:3363-3365

Margules M (1895) Ueber die Zusammensetzungen der gesättigten Dämpfe von Mischungen. Sitzungsberichte Akad Wiss Wien 104:1243-1278

Matsui Y, Nimizawa O (1974) Iron (II)-magnesium exchange equilibrium between olivine and calcium-free pyroxene over a temperature range 800°C-1300°C. Bull Soc Fr Mineral Cristallogr 97:122-130

Mattioli GS, Bishop FC (1984) Experimental determination of the chromium-aluminum mixing parameter in garnet. Geoch Cosmoch Acta 48:1367-1371

McDonough WF, Sun S-S (1995) The Composition of the Earth. Chemical Geology 120:223-253

McGuire TR, Howard LN, Smart JS (1952) Magnetic properties of the chromites. Ceramic Age 60:22-24

McKenzie D, Bickle MJ (1988) The volume and composition of melt generated by extension of the lithosphere. J Petrol 29:625-629

Meyer HOA (1987) Inclusions in diamond. In: Nixon PH (ed) Mantle Xenoliths. 501-522 John Wiley & Sons Ltd Chichester

Milholland CS, Presnall DC (1998) Liquidus phase relations in the CaO-MgO-Al_2O_3-SiO_2 system at 3.0 GPa; the aluminous pyroxene thermal divide and high-pressure fractionation of picritic and komatiitic magmas. J Petrol 39:3-27

Millard RL, Peterson RC, Hunter BK (1992) Temperature dependence of cation disorder in $MgAl_2O_4$ spinel using 27Al and 17O magic-angle spinning NMR. Am Mineral 44-52

Mirwald PM, Kennedy GC (1979) The melting curve of gold, silver and copper to 60 kbar: a reinvestigation. J Geophy Res 84:6750-6756

Moore GE, Kelley KK (1944) High-temperature heat contents of the chromium carbides and of chromic oxide. US Bureau of Mines Technical Report 662

Mori T, Green DH (1975) Pyroxenes in the system $Mg_2Si_2O_6$-$CaMgSi_2O_6$ at high pressure. Earth Plan Sci Lett 26:277-286

Muan A, Hauck J, Löfall T (1972) Equilibrium studies with a bearing on lunar rocks. In: King EA (ed) Proc. Third Lunar Sci Conf. 1:185-196

Navrotsky A, Kleppa OJ (1967) The thermodynamics of cation distribution in simple spinels. J Inorg Nucl Chem 29:2201-2214

Naylor BF (1944) High-Temperature heat contents of ferrous and magnesium chromites. Industrial and Engineering Chemistry 36:933-934

Nehru CE, Wyllie PJ (1974) Electron microprobe measurements of pyroxenes coexisting with H_2O-undersaturated liquid in the join $CaMgSi_2O_6$-$Mg_2Si_2O_6$-H_2O at 30 kbars, with applications to geothermometry. Contr Mineral Petr 48:221-228

Newton RC (1987) Thermodynamic analysis of phase equilibria in simple mineral systems. In: Carmichael ISE and Eugster HP (eds) Thermodynamic modelling of geological materials: minerals, fluids and melts. 17:1-28 Mineralogical Society of America Washington D.C.

Newton RC, Charlu RV, Kleppa OJ (1977) Thermochemistry of high pressure garnets and clinopyroxenes in the system CaO-MgO-Al_2O_3-SiO_2. Geoch Cosmoch Acta 41:369-377

Newton RC, Charlu TV, Anderson PAM, Kleppa OJ (1979) Thermochemistry of diopside-structure clinopyroxenes on the join $CaMgSi_2O_6$-$Mg_2Si_2O_6$. Geoch Cosmoch Acta 43:55-60

Nickel K, Brey G (1984) Subsolidus orthopyroxene-clinopyroxene systematics in the system CaO-MgO-SiO_2 to 60 kb: a re-evaluation of the regular solution model. Contr Mineral Petr 87:35-42

Nickel K, Brey GP, Kogarko L (1985) Orthopyroxene-clinopyroxene equilibria in the system CaO-MgO-Al_2O_3-SiO_2. Contr Mineral Petr 91:44-53

Nickel KG (1983) PhD-thesis, Petrogenesis of garnet and spinel peridotites. A study with particular reference to the role of Chromium in geothermometry and geobarometry. University of Tasmania

Nickel KG (1986) Phase equilibria in the system SiO_2-MgO-Al_2O_3-CaO-Cr_2O_3 (SMACCR) and their bearing on spinel/garnet lherzolite relationships. Neues Jahrbuch für Mineralogie, Abhandlungen 155:259-287

Nickel KG, Green DH (1985) Empirical geothermobarometry for garnet peridotites and implications for the nature of the lithosphere, kimberlites and diamonds. Earth Plan Sci Lett 73:158-170

Nickel KG, Green DH (1984) The nature of the upper-most mantle beneath Victoria, Australia as deduced from ultramafic xenoliths. In: Kornprobst J (ed) Proc Third Int Kimb Conf. 161-178 Elsevier Amsterdam

Niida K, Green DH (1998) Stability and chemical composition of pargasitic amphibole in MORB pyrolite under upper mantle compositions. Contr Mineral Petr in press

O'Hara MJ, Richardson SW, Wilson G (1971) Garnet-peridotite stability and occurrence in crust and mantle. Contr Mineral Petr 32:48-68

O'Neill HStC (1997) Kinetics of the intersite cation exchange in $MgAl_2O_4$ spinel: The influence of nonstoichiometry. In: Proc Seventh Annual V.M. Goldschmidt Conf. Lunar and Planetary Institute LPI Contr. No. 921:153

O'Neill HStC (1981) The transition between spinel lherzolite and garnet lherzolite, and its use as a geobarometer. Contr Mineral Petr 77:185-194

O'Neill HStC, Dollase WA (1994) Crystal structures and cation distributions in simple spinels from powder XRD structural refinements: $MgCr_2O_4$, $ZnCr_2O_4$, Fe_3O_4 and the temperature dependence of the cation distribution in $ZnAl_2O_4$. Phys Chem Min 20:541-555

O'Neill HStC, Navrotsky A (1984) Cation distributions and thermodynamic properties of binary spinel solid solutions. Am Mineral 69:733-753

O'Neill HStC, Navrotsky A (1983) Simple spinels: Crystallographic parameters, cation radii, lattice energies, and cation distribution. Am Mineral 87:196-194

O'Neill HStC, Palme H (1998) Composition of the silicate Earth: Implications for accretion and core formation. In: Jackson I (ed) The Earths Mantle: Composition, Structure and Evolution. 3-126 Cambridge University Press Cambridge

Obata M (1976) The solubility of Al_2O_3 in orthopyroxenes in spinel and plagioclase peridotites and spinel pyroxenites. Am Mineral 61:804-816

Oka Y, Steinke P, Chatterjee ND (1984) Thermodynamic mixing properties of $Mg(Al,Cr)_2O_4$ spinel crystalline solutions at high pressures and temperatures. Contr Mineral Petr 87:196-204

Palme H, Nickel KG (1985) Ca/Al ratio and composition of the Earth's upper mantle. Geoch Cosmoch Acta 49:2123-2132

Panier ER, Tits AL (1993) On combining feasibility, descent and superlinear convergence in inequality constrained optimization. Mathematical Programming 59:261-276

Patera ES (1982) PhD-thesis, Phase equilibria of the upper martian mantle: calculations and experiments. Arizona State University

Pearce JA, Lippard SJ, Roberts S (1984) Characteristics and tectonic significance of supra-subduction zone ophiolites. In: Kokelaar BP and Howells MF (eds) Marginal Basin Geology. 77-94 Blackwell Scientific Publications Oxford

Perkins D (1983) The stability of Mg-rich garnet in the system $CaO-MgO-Al_2O_3-SiO_2$ at 1000-1300°C and high pressure. Am Mineral 68:355-364

Perkins D, Holland TJB, Newton RC (1981) The Al_2O_3 contents of enstatite in equilibrium with garnet in the system $MgO-Al_2O_3-SiO_2$ at 15-40 kbar and 900-1600°C. Contr Mineral Petr 78:99-109

Perkins D, Newton RC (1980) The composition of coexisting pyroxenes and garnets in the system $CaO-MgO-Al_2O_3-SiO_2$. Contr Mineral Petr 75:291-300

Plumier R (1968) Etude par diffraction des neutrons du composé spinelle normal $MgCr_2O_4$. CR Acad Sc Paris 267 B:98-101

Pownceby MI, O'Neill HStC (1994a) Thermodynamic data from redox reactions at high temperatures. III. Activity-composition relations in Ni-Pd alloys from EMF measurements at 850-1250 K, and calibration of the NiO+Ni-Pd assemblage as a redox sensor. Contr Mineral Petr 116:327-339

Pownceby MI, O'Neill HStC (1994b) Thermodynamic data from redox reactions at high temperatures. IV. Calibration of the $Re-ReO_2$ oxygen buffer from EMF and NiO + Ni-Pd redox sensor measurements. Contr Mineral Petr 118:130-137

Press S, Witt G, Seck HA, Ionov DA, Kovalenko VI (1986) Spinel peridotite xenoliths from the Tariat depression, Mongolia. I: Major element chemistry and mineralogy of a primitive mantle xenolith suite. Geoch Cosmoch Acta 50:2587-2599

Rampone E, Hofmann AW, Piccardo GB, Vannucci R, Bottazzi P, Ottolini L (1995) Petrology, Mineral and Isotope Geochemistry of the External Liguride Peridotites (Northern Appennines, Italy). J Petrol 36:81-105

Redlich O, Kister AT (1948) Thermodynamics of nonelectrolyte solutions. Algebraic representation of thermodynamic properties and the classification of solutions. Industr Engineer Chemis 40:345-348

Ringwood AE (1975) Composition and Petrology of the Earth's mantle. McGraw-Hill New York

Ringwood AE (1977) Synthesis of pyrope-knorringite solid-solution series. Earth Plan Sci Lett 36:443-448

Robie RA, Hemingway BS, Fisher JR (1979) Thermodynamic properties of minerals and related substances at 298.15 K and 1 bar (10^5 Pa) pressures and at higher temperatures. US Government Printing Office: Washington DC Vol. 1452, 1-456.

Roth WA, Wolf U (1940) Die Bildungswärme von Chromioxyd. Z Elektrochem 46:45-46

Roy DM, Barks RE (1972) Subsolidus phase equilibria in Al_2O_3-Cr_2O_3. Nature Physical Science 235:118-119

Sachtleben T, Seck HA (1981) Chemical control of Al-solubility in orthopyroxene and its implications on pyroxene geothermometry. Contr Mineral Petr 78:157-165

Sack RO, Ghiorso MS (1991a) Chromian spinels as petrogenetic indicators: Thermodynamics and petrological applications. Am Mineral 76:827-847

Sack RO, Ghiorso MS (1991b) An internally consistent model for the thermodynamic properties of Fe-Mg-titanomagnetite-aluminate spinels. Contr Mineral Petr 106:474-505

Salters VJM, Hart SR (1989) The hafnium paradox and the role of garnet in the source of mid-ocean-ridge basalts. Nature 342:420-422

Sautter V, Jaoul O, Abel F (1988) Aluminium diffusion in diopside using the 27Al-28Si nuclear reaction: preliminary results. Earth Plan Sci Lett 89:109-114

Schmid R, Cressey G, Wood BJ (1978) Experimental determination of univariant equilibria using divariant solid-solution assemblages. Am Mineral 63:511-515

Schnelle W, Gmelin E (1995) High-resolution adiabatic scanning calorimeter for small sample masses. Thermochim Acta 269:25-32

Schweitzer E (1982) The reaction pigeonite = diopside + enstatite at 15 kbars. Am Mineral 67:54-58

Sen G (1985) Experimental determination of pyroxene compositions in the system CaO-MgO-Al_2O_3-SiO_2 at 900-1200°C and 10-15 kbar using PbO and H_2O fluxes. Am Mineral 70:678-695

Shaked H, Hastings JM, Corliss LM (1970) Magnetic structure of magnesium chromite. Physical Review B 1:3316-3124

Shen Y, Forsyth DW (1995) Geochemical constraints on initial and final depths of melting beneath mid-ocean ridges. J Geophy Res 100:2211-2237

Shirane G, Cox D, Pickard S (1964) Magnetic structures in Fe-Cr_2S_4 and $FeCr_2O_4$. Journal of Applied Physics 35:954-955

Shomate CH (1944) Ferrous and magnesium chromites: Specific heats at low temperatures. Industrial and Engineering Chemistry 36:910-911

Spear FS (1993) Metamorphic phase equilibria and pressure-temperature-time paths. Mineralogical Society of America Washington D.C.

Staudigel H, Schreyer W (1977) The upper thermal stability of clinochlore, $Mg_5Al[AlSi_3O_{10}](OH)_8$, at 10-35 kb P H_2O. Contr Mineral Petr 61:187-198

Thompson JB (1967) Thermodynamic properties of simple solutions. In: Abelson PH (ed) Researches in geochemistry. 54:340-361 Wiley New York

Turkin AI, Doroshev AM, Malinovsky IY (1983) Study of the phase composition of garnet-bearing associations of the system MgO-Al_2O_3-SiO_2-Cr_2O_3 system at high temperatures and pressures. In: Silicate systems under high pressure [in Russian] Bull Inst Geol Geophys 5, Novosibirsk

Vickerman JC (1970) Magnetic properties of chromium ions in oxide matrices. Part 2. $MgCr_2O_4$ - $MgAl_2O_4$ solid solutions. Trans Faraday Soc 67:665-673

Volger J (1952) Anomalous specific heat of chromium oxide (Cr_2O_3) at the antiferromagnetic Curie temperature. Nature 170:1027

von Seckendorf V, O'Neill HStC (1993) Experimental determination of the partitioning of Mg and Fe^{2+} between olivine and orthopyroxene at 900°, 1000° and 1150°C and 1.6 GPa: constraints on activity-composition relations in binary Mg-Fe olivine and orthopyroxene solid solution. Contr Mineral Petr 113:196-207

Walter MJ, Presnall DC (1994) Melting behaviour of simplified lherzolite in the system CaO-MgO-Al_2O_3-SiO_2-Na_2O from 7 to 35 kbar. J Petrol 35:329-359

Ware NG (1991) Combined energy-dispersive-wavelenght-dispersive quantitative electron microprobe analysis. X-ray Spectrometry 20:73-79

Warner RD, Luth WC (1974) The diopside-orthoenstatite two-phase region in the system $CaMgSi_2O_6$ - $Mg_2Si_2O_6$. Am Mineral 59:98-109

Warshaw I, Keith ML (1954) Solid solutions and chromium oxide loss in part of the system MgO-Al_2O_3-Cr_2O_3-SiO_2. J Am Ceram Soc 37:161-168

White RS, McKenzie D, O'Nions RK (1992) Oceanic crustal thickness from seismic measurements and rare earth element inversions. J Geophy Res 97:19683-19715

Witt-Eickschen G, Seck HA (1991) Solubility of Ca and Al in orthopyroxene from spinel peridotite: an improved version of an empirical geothermometer. Contr Mineral Petr 106:431-439

Wood BJ (1988) Activity measurements and excess entropy-volume relationships for pyrope-grossular garnets. J Geol 96:721-729

Wood BJ (1978) The influence of Cr_2O_3 on the relationships between spinel- and garnet-peridotites. In: MacKenzie WS (ed) Progress in experimental petrology. D11:78-80 Natl Enviro Res Council Publ Manchester

Wood BJ (1978) Reactions involving anorthite and $CaAl_2SiO_6$ pyroxene at high pressures and temperatures. Am J Sci 278:930-942

Wood BJ (1974) The solubility of alumina in orthopyroxene coexisting with garnet. Contr Mineral Petr 46:1-15

Wood BJ, Banno S (1973) Garnet-orthopyroxene and orthopyroxene-clinopyroxene relationships in simple and complex systems. Contr Mineral Petr 42:109-124

Wood BJ, Blundy JD (1997) A predictive model for rare earth element partitioning between clinopyroxene and anhydrous silicate melt. Contr Mineral Petr 129:166-181

Wood BJ, Blundy JD, Robinson JAC (1998) Crystal chemical constraints on the partitioning of U-series elements during partial melting. Mineral Mag 62A:1664

Wood BJ, Holloway JR (1984) A thermodynamic model for subsolidus equilibria in the system CaO-MgO-Al_2O_3-SiO_2. 48:159-176

Wood BJ, Kirkpatrick RJ, Montez B (1986) Order- disorder phenomena in $MgAl_2O_4$ spinel. Am Mineral 71:999-1006

Wood BJ, Kleppa OJ (1984) Chromium and aluminum mixing in garnet: a thermochemical study. Geoch Cosmoch Acta 48:1373-1375

Wood BJ, Nicholls J (1978) The thermodynamic properties of reciprocal solid solutions. Contr Mineral Petr 66:389-400

Wood DA (1979) A variably veined suboceanic upper mantle - genetic significance for mid-ocean ridge basalts from geochemical evidence. Geology 7:499-503

Woodland AB, Droop G, O'Neill HStC (1995) Almandine-rich garnet from near Collobiieres, southern France, and its petrological significance. Eur J Min 7:187-194

Yaxley GM, Kamenetsky V, Green DH, Falloon TJ (1997) Glasses in mantle xenoliths from western Victoria, Australia, and their relevance to mantle processes. Earth Plan Sci Lett 148:433-446

Zhou JL, Tits AL, Lawrence CT (1998) User's Guide for FFSQP: A FORTRAN code for solving constrained nonlinear (Minimax) optimization problems, generating iterates satisfying all inequality and linear constraints. University of Maryland